3-AXIS AND 5-AXIS MACHINING WITH STEWART PLATFORM

NG CHEE CHUNG
(B. Eng. (Hons), NUS)

A THESIS SUBMITTED

FOR THE DEGREE OF DOCTOR OF PHILOSOPHY

DEPARTMENT OF MECHANICAL ENGINEERING

NATIONAL UNIVERSITY OF SINGAPORE

2012

Declaration

I hereby declare that this thesis is my original work and it has been written by me in its entirety. I have duly acknowledged all the sources of information which have been used in the thesis.

This thesis has also not been submitted for any degree in any university previously.

[illegible]

Ng Chee Chung
30 July 2012

Acknowledgements

The author would like to express his sincere gratitude to Prof. Andrew Nee Yeh Ching and Assoc. Prof. Ong Soh Khim for their assistance, inspiration and guidance throughout the duration of this research project.

The author is also grateful to his fellow postgraduate students, Mr. Vincensius Billy Saputra, Mr. Bernard Kee Buck Tong, Miss Wong Shek Yoon, Mr. Stanley Thian Chen Hai and professional officer, Mr. Neo Ken Soon and Mr. Tan Choon Huat for their constant encouragement and suggestions. Furthermore, he is also grateful to Laboratory Technologist Mr. Lee Chiang Soon, Mr. Au Siew Kong and Mr. Chua Choon Tye for their help in the fabrication of the components and their advice in the design of the research project.

In addition, the author would like to acknowledge the assistance given by the technical staff of the Advanced Manufacturing Laboratory, Mr. Wong Chian Long, Mr. Simon Tan Suan Beng, Mr. Ho Yan Chee and Mr. Lim Soon Cheong.

Last but not least, the author would also like to acknowledge the financial assistance received from National University of Singapore for the duration of the project, and to thank all those who, directly or indirectly, have helped him in one way or another.

Table of contents

Summary

There is an increasing trend of interest to implement the Parallel Kinematics Platforms (Stewart Platforms) in the fields of machining and manufacturing. This is due to the capability of the Stewart Platforms to perform six degrees-of-freedom (DOF) motions within a very compact environment, which cannot be achieved by traditional machining centers.

However, unlike CNC machining centers which axes of movements can be controlled individually, the movement of a Stewart Platform requires a simultaneous control of the six individual links to achieve the final position of the platform. Therefore, the available commercial CNC applications for the machining centers are not suitable for use to control a Stewart Platform. A specially defined postprocessor has to be developed to achieve automatic conversion of CNC codes, which have been generated from commercial CAM packages based on the CAD models, to control and manipulate a Stewart Platform to achieve the machining purposes. Furthermore, a sophisticated control interface has been developed so that users can perform machining with a Stewart Platform based on CNC codes.

Calibration of the accuracy of the developed NC postprocessor program has been performed based on actual 3-axis and 5-axis machining processes performed on the Stewart Platform. A machining frame with a spindle was designed and developed, and a feedback system was implemented based on wire sensors mounted linearly along the actuators of the platform. Thus, the position and orientation of the end-effector can be calibrated based on the feedback of the links of the platform. Experimental data was collected during the machining processes. The data was analyzed and improvement was made on the configuration of the system.

Alternate machining processes are reviewed with Parallel Kinematic Manipulators of different structural designs that have been used for the Stewart Platform. The structural characteristics associated with parallel manipulators are evaluated. A class of three DOF parallel manipulators is determined. Several types of parallel manipulators with translational movement and orientation have been identified. Based on the identification, a hybrid 3-.UPU (Universal Joint-Prismatic-Universal Joint) parallel manipulator was fabricated and studied.

List of Tables

List of Figures

List of Symbols

F_e	The effective DOF of the assembly or mechanism
λ	The DOF of the space in which the mechanism operates
L	Number of links
j	Number of joints
f_i	Degree-of Freedom of i-th joint
I_d	Idle or passive Degrees-Of-Freedom
X_p , Y_p , Z_P	The Origin of Platform
X_B , Y_B , Z_B	The Origin of Base
P_i	Platform attachment joints, spherical joints, i = 1, 2…, 6
B_i	Base attachment joints, universal joints, i = 1, 2…, 6
σ_i	The magnitude of the links vector, , i = 1, 2…, 6
W	The force that act on the platform
A	The area of the platform, m^2
Y	The Poisson’s Ratio
I	Inertia
$\vec{l}_i$	Leg vector
$\underline{R}$	Rotational matrix
S	Sine
C	Cosine
V	Matrix of Cartesian Velocities
W	Matrix of Joint Velocities
D, d	Euclidean distance between the two vectors

NaN	Not a Numerical number
Rot_{3x3}	3 x 3Rotation matrix of Stewart Platform
Tr_{3x1}	3 x 1Translational matrix of Stewart Platform
T	Homogeneous Coordinate
Ξ	Tolerance of Error
$\vec{t}$	Translational Vector
$\vec{X}_i$	Matrix of pose vector of Stewart Platform
G	Mapping function of length of actuators to the pose of the Stewart Platform
H	Differentiation of Mapping function G with the corresponding element of the pose vector of Stewart Platform
R_{xyz}	Rotation matrix around X-axis, Y-axis and Z-axis
$R_{z,\alpha}$	Rotation matrix around Z axis with rotational angle of α
$R_{y,\beta}$	Rotation matrix around Y axis with rotational angle of β
$R_{z,\gamma}$	Rotation matrix around Z axis with rotational angle of γ
A_z	Area of the workspace of Stewart Platform
V	Volume of Workspace
f_{bi}	Force acting on the spherical joint of the mobile platform
f_{ai}	Force acting on the universal joint of the base of Stewart Platform
ω_p	Angular velocity of the mobile platform
${}^{i}n_i$	Moment acting on the actuator
m_1	Mass of cylinder of actuator
m_2	Mass of piston of actuator

e_{1i}	Distance between the center of mass of the cylinder and the bottom of the cylinder
e_{2i}	Distance between the center of mass of the piston and the top of the piston
$v_{1,}v_2$	Velocity of the center of mass of the cylinder and piston
${}^{B}n_p$	Moment about the center of mass of the mobile platform
τ_i	Actuating force of the platform
X_platform, Y_platform, Z_platform	Coordinates of mobile platform in local coordinate system
X_CNC_Code, Y_CNC_Code, Z_CNC_Code	Coordinate of XYZ coordinates in NC program
X_{abs},Y_{abs},Z_{abs}	Absolute coordinate of X, Y and Z position of the mobile platform
X_{rel},Y_{rel},Z_{rel}	Relative coordinate of X, Y and Z position of the mobile platform
C	Vector between cutter contact point and normal N of the triangular faces of the freeform surface
N	Vector of normal to the face of the triangle in the freeform surface
α_c	Critical angle of Collision
α_1, α_2	Critical angle of gouging
V_{mw}	Vector from milling cutter to workpiece
N_R	Magnitude of vector of the normal to the triangle face of the freeform surface

Chapter 1 Introduction

Parallel manipulators can be found in many applications in the industry, such as vehicle and airplane simulators [Stewart, 1965], adjustable articulated trusses [Reinholtz and Gockhale, 1987], mining machines [Arai *et al*, 1991], positioning devices [Gosselin and Hamel, 1994], fine positioning devices, and off-shore drilling platforms. Recently, it has also been developed as high precision milling machines, namely, a hexapod machining center by Giddings and Lewis in 1995. A Stewart Platform is a form of manipulator with six degrees of freedoms (DOF), which allows one to provide a given position and orientation of the surface in the vicinity of any point of the platform on its three Cartesian coordinates and projection of the unit of normal vector [Alyushin, 2010].

The design of parallel manipulators can be dated back to 1962 when Gough and Whitehall [Gough, 1962] devised a six-linear jacking system for use as a universal tire testing machine. Stewart presented his platform manipulator for use as an aircraft simulator in 1965 [Stewart, 1965]. Hunt made a systematic study of the parallel manipulator structures [Hunt, 1983]. Since then, parallel manipulators have been studied extensively by many other researchers [Tsai, 1996].

However, greater interests in the application of these mechanisms in the metalworking field have only grown in the last decade. The first CNC-type hexapod machine tool prototype (Variax from Giddings & Lewis and the

Octahedral Hexapod from Ingersoll) was presented at the 1994 International Machine Tool Show in Chicago. These prototypes were enthusiastically welcomed as the new generation of machine tools due to their specific characteristics [Irene and Gloria, 2000]:

- Higher payload to weight ratio
- Non-cumulative joint error
- Higher structural rigidity
- Modularity
- Location of the motors close to the fixed base
- Simpler solution of the ‘inverse’ kinematics problem

However, there are still many disadvantages of the Stewart Platform as compared to the serial manipulators, such as a limited workspace and problems in singularity configuration. Furthermore, it also has complicated forward kinematics due to the closed loop configuration of the system.

Configuration and classification

Most of the robots being used in the industries today are serial robots or serial manipulators. Manipulators are basically mechanical motion devices, generally with two or more DOF. Serial manipulators are normally made up of between two to six rigid links with prismatic and/or revolute joints connecting the links in an open kinematics chain. Examples of this kind of robots include the PUMA 560 series of robot arm and the SCARA type Adept One robot arm [Yee 1993].

Serial manipulators are frequently applied in manufacturing due to their large workspace. The ability of the manipulator to stretch out the links and joints in a straight line creates an envelope to the shape of a sphere. The workspace is considered quite large compared to parallel manipulators, even though there are constraints of physical limits and problems of singularities.

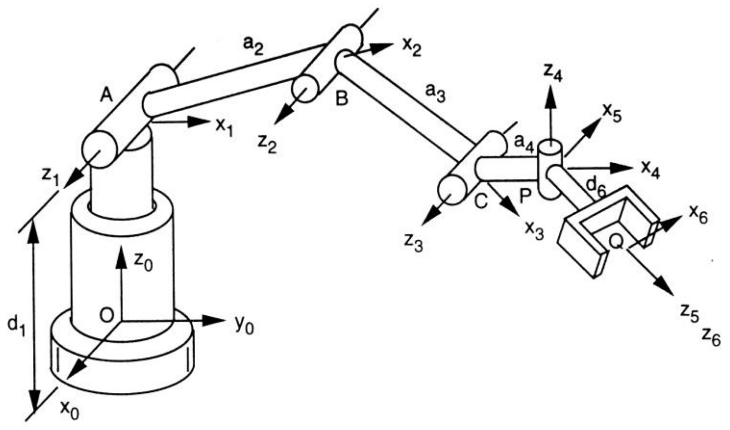

Figure 1.1 Serial kinematics chains [Irene and Gloria, 2000]

Furthermore, serial manipulators have fewer parts and present relatively straight-forward kinematics solutions. From the joint variables, the position and orientation of the end-effector can be defined easily based on the geometric relationships between the links and the joints of the manipulator as shown in Figure 1.1. However, the inverse kinematics is a multiple-solution problem which involves the solving of non-linear equations. Moreover, one of the shortcomings of a serial manipulator is its low payload to self weight ratio. The typical ratio for the payload is 20 kilograms of hardware for 1 kilogram load or 10 Newton forces. Hence, although most robots presently used in manufacturing applications are serial manipulators, parallel manipulators clearly excel in the aspects of stiffness, inertia, accuracy and payload [Vincent, 2001].

The parallel structures are classified according to the types of drives. This classification is not limited to the DOF, and hence the design of the joints is not restricted by the classification. As a result, rotary and translational drives can both be used [Reimund, 2002]. Among the types of drives used, rotary drives show a high degree of efficiency. With the installation of a gear system, the rotation motion can be converted to translation motion. Hence, ball screws are chosen for the gear conversion. Furthermore, other driver principles, such as pneumatic or hydraulic system can apply direct linear motion or indirect motion towards the parallel kinematics manipulator systems.

Independent of the drives installed in a system, the links can be divided into two major types, namely, the variable strut length and the constant strut length. The classification of the parallel kinematics manipulators (PKM) is shown in Figure 1.2. When a PKM is designed with constant strut length, the manipulation of the mobile platform is achieved by having a rotary drive such as in Figure 1.2(a) or a linear drive such as in Figure 1.2(c), and the constant strut is rotated by the drive to manipulate the platform. The other method is to have a linear or rotary drive to change the length of the variable length strut to perform a lifting movement of the mobile platform such as in Figure 1.2(b). This configuration is applied to the Stewart Platform in this project.

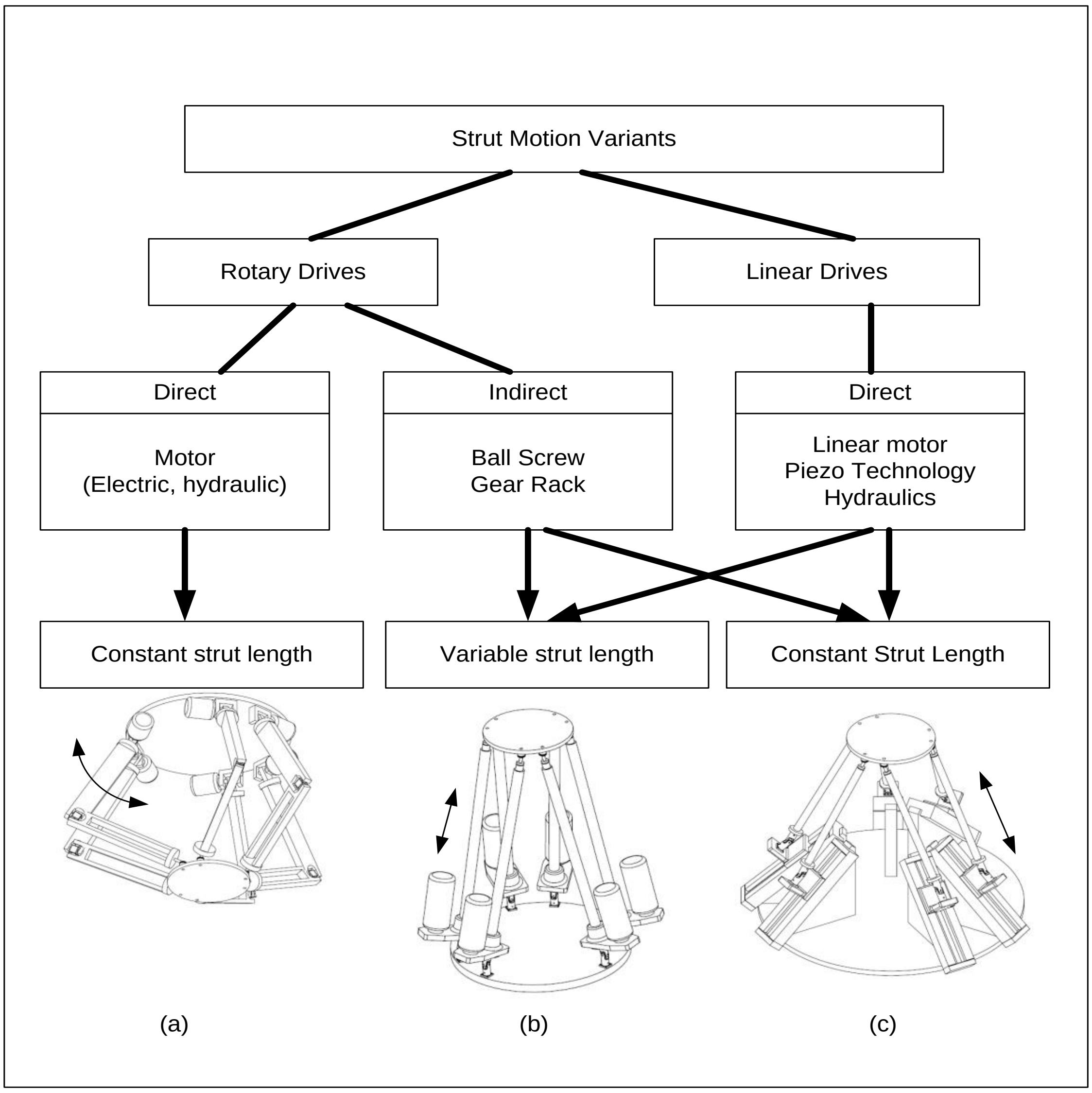

Figure 1.2 Parallel kinematics manipulator classifications

A Stewart Platform generally consists of a mobile platform and several links (normally six links) that connect the mobile platform to a fixed base as shown in Figure 1.3. Typically, the number of links is equal to the number of DOF for a parallel manipulator. Each link is driven by one actuator that is mounted at the base to reduce the inertia of the motors and to allow for lighter links. The end-points of these links are attached to three-DOF spherical joints on one end, and two-DOF universal joints on the other end. The position and orientation of the mobile platform are controlled by the lengths of the prismatic linear actuators. The Stewart mechanism depicts a closed loop alternative to the serial six-DOF manipulator [Craig, 1986]. The six DOF can be computed using the Grübler's formula in Equation (1.1)

$$F_e = \lambda(l - j - 1) + \sum_{i=1}^{j} f_i - I_d \tag{1.1}$$

where,

F_e = the effective DOF of the assembly or mechanism

λ = the DOF of the space in which the mechanism operates

l = number of links

j = number of joints

f_i = DOF of the i-th joint

I_d = idle or passive DOFs

The number of joints is 18 (six universal, six ball and socket, and six prismatic). The number of links is 14 (two for each actuator, the end-effector and the base). The sum of all the joint freedom is 36. Hence, based on Grübler's formula, the DOF is computed as $F = 6(14 - 18 - 1) + 36 = 6$.

The Stewart mechanism exhibits characteristics common to most closed loop mechanisms, *i.e.*, it can be very stiff, but the links have a much more limited range of motion than the serial manipulators. Hence, its workspace is relatively small. However, as the stiffness and the load are evenly distributed among several actuators, the Stewart mechanism can have both high payload and high stiffness. Since the actuator positional errors are not accumulated, the Stewart mechanism is also capable of achieving high precision.

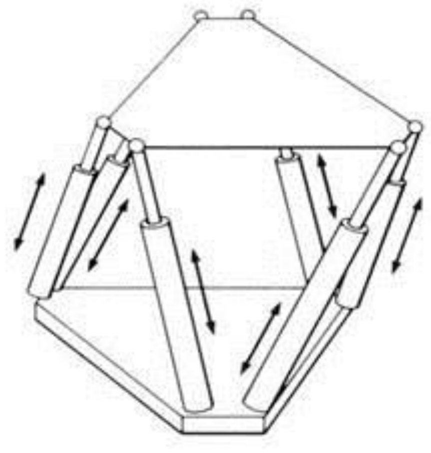

Figure 1.3 The standard Stewart Platform [Craig, 1986]

In short, the Stewart mechanism demonstrates interesting reversal characteristics to the serial manipulators. The inverse kinematics solution can be obtained easily since it can be calculated readily. The forward kinematics problem, on the other hand, requires the solution of a series of non-linear equations and has multiple solutions. In addition, complex design, complicated control, singularity problem and unstable configurations could cause the collapse or failed application of the manipulator. Most of the six-DOF manipulators studied to-date consists of six extensible limbs connecting a mobile platform to a fixed base by spherical joints. Other variations of the Stewart Platforms have also been proposed. An example is the Hexaglide parallel mechanism as shown in Figure 1.2(c), which has an improved workspace, and the locations of the attachment points on the base and on the mobile platform are not in a plane and are not symmetrical. There are advantages and disadvantages of the various types of Stewart Platform designs.

The Gough-Stewart Platform, which has the smallest workspace, was chosen as the design model because it has the most balanced performance [Huynh, 2001].

Currently, a Stewart Platform has been fabricated and assembled as shown in Figure 1.4. A simple control system was developed to manipulate the platform with a reasonable accuracy. The control interface software was developed such that the end-user is able to communicate with the Stewart Platform through the most common machining language, namely the NC programs. Automatic conversion of NC programs from a commercial CAM package based on a CAD model has been developed to control and manipulate the Stewart Platform to achieve the machining purposes. Moreover, verification of the accuracy of the software to convert the NC programs to the trajectory path of the Stewart Platform has been carried out by implementing a feedback system.

In this research, the tasks completed are as follows. Firstly, the workspace of the Stewart Platform was verified through performing simulations in MATLAB® to determine and evaluate the limitations of the machining dimensions. Literature review was performed to gain an understanding of the kinematics and dynamics of the Stewart Platform as well as NC codes programming, and to study the differences in the NC program control between serial and parallel manipulators. A sophisticated control interface was developed so that an end-user can communicate with the Stewart Platform based on NC programs and simulate the trajectory path of the movement of the Stewart Platform before actual machining.

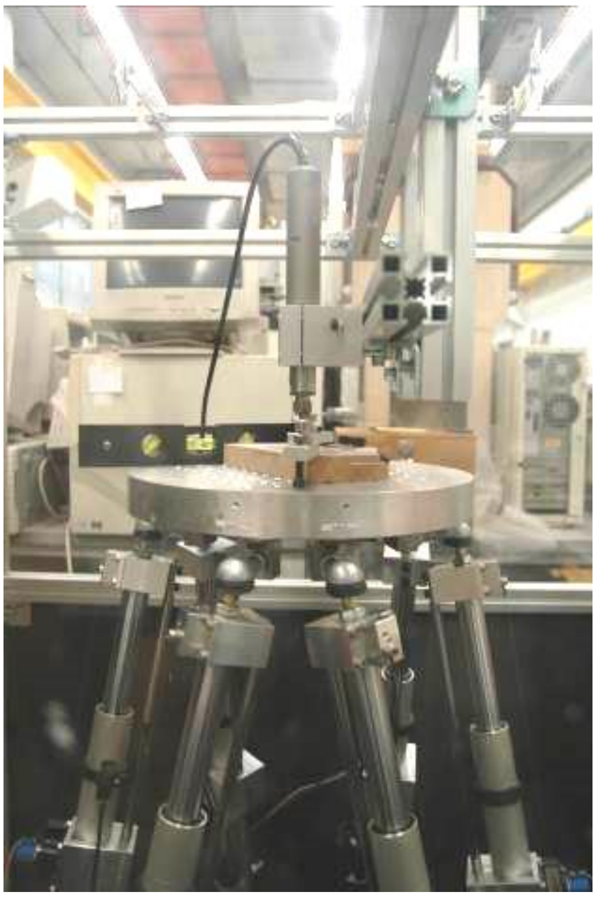

Figure 1.4 Stewart Platform machining center

In the last stage of the research, calibration of the accuracy of the developed NC program postprocessor was performed based on actual 3-axis and 5-axis machining tests that were performed on the Stewart Platform. A simple machining setup was configured for the machining tests. A frame with a spindle was designed and developed. A feedback system was applied based on wire sensors that are mounted linearly on the actuators of the Stewart Platform, so that the position and orientation of the end-effectors can be calibrated based on the feedback of the links of the Stewart Platform. Experimental data was collected during the machining tests. The data was analyzed and improvement was done on the configuration of the system.

The six-leg manipulator suffers from the disadvantages of the complex solution of direct kinematics, coupled problems of the position and orientation movement. Thus, further research is performed after investigation on the development of the PKM by reducing the 6-DOFs to 3-DOFs PKMs. The reduction of the DOF of the PKMs has advantages in workspace and cost reduction. However, the 3-DOF Parallel Kinematics Platform provides less rigidity and DOF. Recently, Tsai [Tsai, 1996] has introduced a novel 3-DOF translational platform that is made up of only revolute joints. The platform performs pure translational motion and has a closed-form solution for the direct and inverse kinematics. Hence, in terms of cost and complexity, 3-DOF 3-legged Micro Parallel Kinematic Manipulator is cost effective and the kinematics of the mechanism is further simplified for the purpose of control. However, the design algorithms either do not exist or are very complicated.

To further increase the flexibility and functionality of the self-fabricated Micro Stewart Platform, the concept of modular methodology is introduced. It helps to optimize the performance of the 3-leg 3 DOF Parallel Manipulator and the self-repair ability. Modular robots consist of many autonomous units or modules that can be reconfigured into a huge number of designs. Ideally, the modules will be uniform, and self-contained. The robot can be changed from one configuration to another manually or automatically.

In short the major contributions of the author in his thesis are shown as below. Further elaboration will be elaborated in the following chapters of the thesis:

1. The development of a "post-processor", or software routines, required to translate the motion codes in standard-format NC part programs into the required command joint coordinates for the control of Stewart Platform used for 3D machining. This involves detailed understanding of coordinate transformations, and transforming the required tool path, in NC part program coordinates to the required joint coordinates for the Stewart Platform. As part of the development of the post-processor, the workspace of the Stewart Platform used was determined and the correct performance of the post-processor demonstrated by actual machining on the Stewart Platform. The accuracy of the motion achieved through measurement of the actual lengths of the extensible legs of the Stewart Platform by attaching external wire position sensors to each leg. This is because the actuator of the Stewart Platform is belt driven by Stepper motor in open loop. Even though there is encoder count read by the controller card, it doesn't reflect the actual length of the actuators. Hence the wire sensor can be applied as the online position feedback system for the actual length of

the actuator. By using Newton-Raphson numerical method one is able to calculate the actual position of the moving platform.

2. The extension of the post-processor for 5D or 5-axis machining which involves significantly higher complexity. The correct performance of the post-processor was demonstrated by actual machining of the part on the platform.
3. The design and fabrication of a 3-DOF parallel manipulator intended for “micro-machining”. The proper working if this manipulator together with its own post-processor was also demonstrated

Chapter 2 Kinematics of Stewart Platform

2.1 Introduction

Kinematics is the study of motion. The study of kinematics analyses the motion of an object without considering the forces that cause the motion [Yee 1993]. Hence, only the position, velocity, acceleration and all the higher order derivatives of the position variables are considered. The kinematics of rigid mechanisms depends on the configuration of the joints.

Forward kinematics involves the calculation of the position and orientation of the end-effector from the joint positions. In short, forward kinematics is a mapping of the vectors of the joint coordinates to the vectors that indicate the position and orientation of the end-effector. The forward kinematics of a Stewart Platform is a complicated problem. The solution of the forward kinematics of Stewart Platforms is usually only possible with numerical techniques.

On the other hand, inverse kinematics is the reverse of the forward kinematics. It is the mapping of the possible sets of joint coordinates given the orientation and position. The inverse kinematics of a Stewart Platform is typically straightforward and simple. Comparatively, the solution of the inverse kinematics of a serial manipulator is more complicated.

As shown in Figure 2.1, the position and orientation of the mobile platform of the Gough-Stewart Platform are controlled by changes in the six links

l_i, which are connected in parallel between the mobile platform of diameter of 30 cm and the base with diameter of 60 cm. The six base attachment joints are universal joints and all the platform attachment joints are spherical joints. The joints at the base are universal joints because only two DOFs are needed, which are the rotation freedom about, and the rotational freedom to make an angle with the respective base sides. The spherical joints are used because extra DOFs are needed so that each link can rotate by itself.

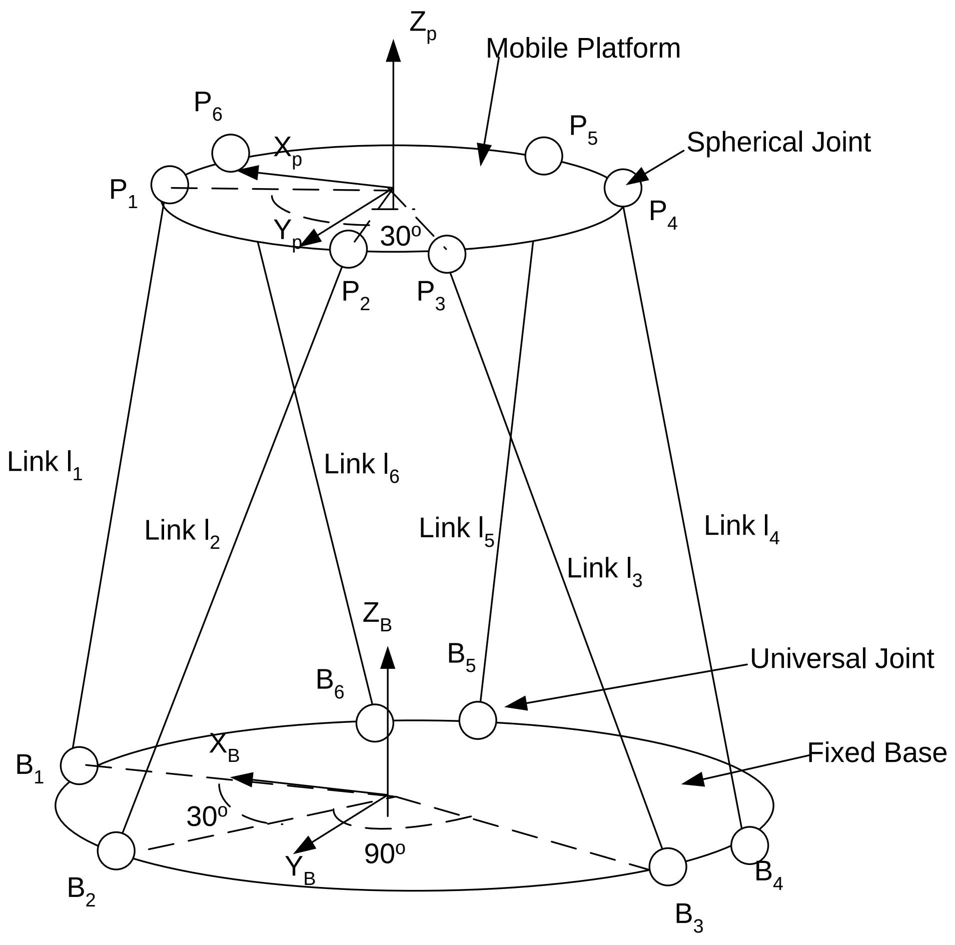

Figure 2.1 The Gough-Stewart Platform

The mobile platform and the base are split into six individual joints, which are allocated 15˚ symmetrically on both sides of each 120˚ line of the platform. The symmetrical allocation of the joints is to ensure more uniform loads distribution on the base and the platform. Each pair of adjacent platform joints p_i with 30˚ difference forms a triangle-like quadrilateral with two adjacent base joints b_i of 90˚ difference, such as p_1 and p_6 to b_1 and b_6, as shown in Figure 2.1.

The sides of the triangles are links of the platform. All the joints form inverted and forward triangles. The formation of the triangular shape strengthens the force to hold the load of the platform and the workpiece.

2.2 Inverse kinematics

The inverse kinematics problem is almost trivial for the Stewart Platform and is extensively used in many methods.

First, the Stewart Platform kinematics can be illustrated in many ways but the most common set of parameters includes the minimal and maximal link lengths ($\ell_{i_{\max}}, \ell_{i_{\min}}$), the radii of the platform and the base, the joint placement is determined as the angle between the closest joints for both the platform and the base, and the joint moving volume. Based on these common sets of parameters, $\vec{B}_i$ and $\vec{P}_i$ as shown in Equation (2.1) can be calculated. Inverse kinematics can be described with Equations (2.1) and (2.2).

$$\vec{P}_i = \vec{t} + \underline{R \cdot \vec{p}_i}\,, \tag{2.1}$$

$$\ell_i = d\left(\vec{P}_i, \vec{B}_i\right) \tag{2.2}$$

From geometry, P_i can be found as illustrated in Figure 2.2.

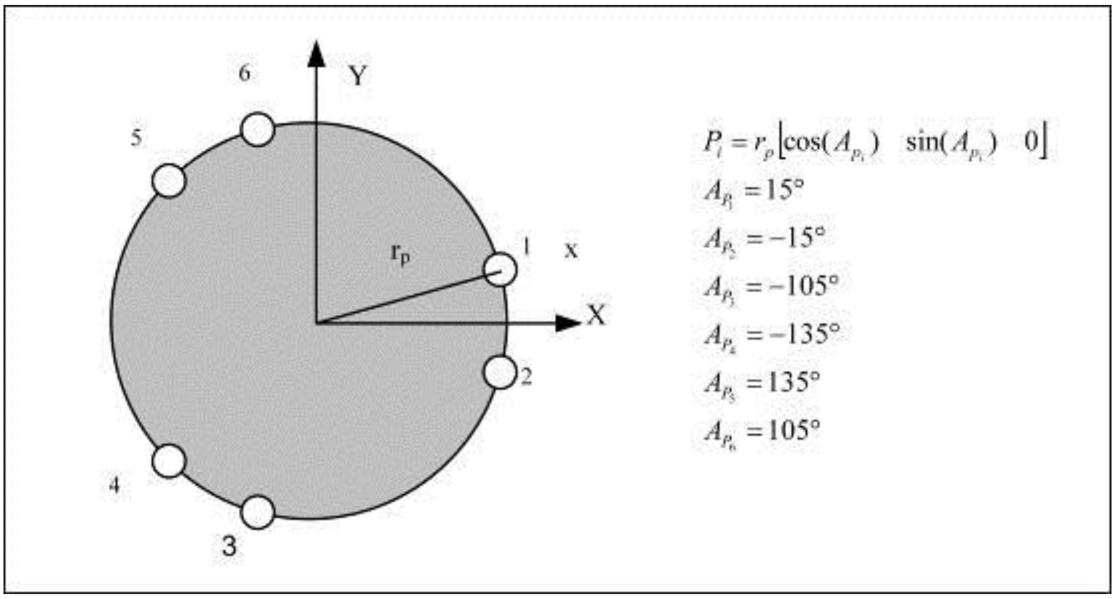

Figure 2.2 Locations of the joints of the platform

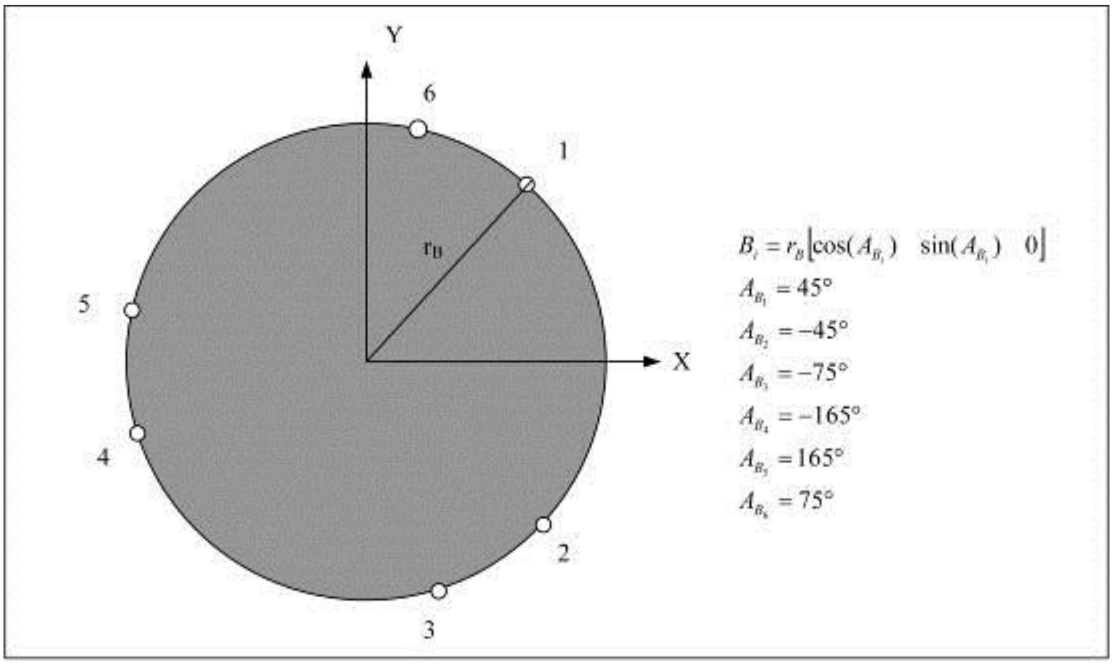

Figure 2.3 Locations of the joints of the base

As shown in Figures 2.2 and 2.3, a coordinate system is defined for the base and the platform respectively. Each of the six points on the base is described by a position vector, $\overrightarrow{B_i}$, which is defined with respect to the base coordinate system. Similarly, each of the six points on the platform is described by a position vector, $\overrightarrow{P_i}$, with respect to the platform coordinate system. The left superscript P denotes that the vector is referenced to the platform coordinate system while the superscript B denotes reference to the base coordinate system. This notation will be used in the following derivation of the inverse kinematics.

The matrix R shown in Equation (2.1) can be written in another form as shown in Equation (2.3) [Soh *et al*, 2002]:

$$\underline{R} = \begin{bmatrix} \alpha_x & \beta_x & \gamma_x \\ \alpha_y & \beta_y & \gamma_y \\ \alpha_z & \beta_z & \gamma_z \end{bmatrix} \tag{2.3}$$

Conversely, the orientation of the base with respect to the platform, ${}^{P}R$, is given by,

$$^{P}R = R^{-1} = R^{T} = \begin{bmatrix} \alpha_x & \alpha_y & \alpha_z \\ \beta_x & \beta_y & \beta_z \\ \gamma_x & \gamma_y & \gamma_z \end{bmatrix} \tag{2.4}$$

Having defined the position and orientation of the platform with respect to the base, the links ℓ_i are defined in Equation (2.5), which are the vectors of the i^{th} links from B_i to P_i vector algebra.

$$\ell_i = \vec{P_i} - \vec{B_i} \tag{2.5}$$

As shown in Equation (2.5), $\vec{P_i}$ is referenced to the base coordinate system. Hence, the transformation of the coordinates of a point on the platform to the base coordinate system can be determined using Equation (2.6).

$$\ell_i = \vec{t} + R \cdot \vec{P_i} - \vec{B_i} \tag{2.6}$$

As shown in Figure 2.3, B_i can be obtained by Equation (2.7).

$$\vec{B_i} = r_B[\cos(A_{B_i}) \quad \sin(A_{B_i}) \quad 0] \tag{2.7}$$

Similarly, P_i can be found and is given in Equation (2.8).

$$\vec{P_i} = r_p[\cos(A_{p_i}) \quad \sin(A_{p_i}) \quad 0] \tag{2.8}$$

Hence, the link ℓ_i can be written in its three-component scalar form as follows,

$$\ell_{ix} = r_P\left\lfloor \alpha_x \cdot \cos\left(A_{P_i}\right) + \beta_x \cdot \sin\left(A_{P_i}\right)\right\rfloor + T_x - r_B \cdot \cos\left(A_{B_i}\right) \tag{2.9}$$

$$\ell_{iy} = r_P\left\lfloor \alpha_y \cdot \cos\left(A_{P_i}\right) + \beta_y \cdot \sin\left(A_{P_i}\right)\right\rfloor + T_y - r_B \cdot \cos\left(A_{B_i}\right) \tag{2.10}$$

$$\ell_{iz} = r_P\left\lfloor \alpha_z \cdot \cos\left(A_{P_i}\right) + \beta_z \cdot \sin\left(A_{P_i}\right)\right\rfloor + T_z \tag{2.11}$$

The length of the link, σ_i is given by the magnitude of the links vector using Equation (2.12).

$$\sigma_i = \left|\ell_i\right| = \sqrt{\ell_{ix}^{\ 2} + \ell_{iy}^{\ 2} + \ell_{iz}^{\ 2}} \tag{2.12}$$

2.3 Forward kinematics

The forward kinematics for a Stewart Platform can be mathematically formulated in several ways. Every representation of the problem has its advantages and disadvantages, when a different optimization algorithm is applied [Jakobovic and Jelenkovic, 2002].

The configuration of the actual Stewart Platform has to be represented in order to define a forward kinematics problem [Jakobovic and Jelenkovic, 2002], *i.e.*, the actual position and orientation of the mobile platform have to be represented. The most commonly used approach utilizes the three positional coordinates of the center of the mobile platform and the three angles that define its orientation. The coordinates are represented by the vector:

$$\vec{t} = \begin{bmatrix} t_x \\ t_y \\ t_z \end{bmatrix} \qquad (2.13)$$

The three rotational angles are defined as the roll γ, pitch β and yaw angles α. The values of the angles represent the consecutive rotations about the X-, Y- and Z-axes respectively. From Figure 2.1, the Stewart Platform is defined with six vectors for the base and six vectors for the mobile platform, which define the six joint coordinates on each platform.

$$\vec{B}_i = \begin{bmatrix} B_{ix} \\ B_{iy} \\ 0 \end{bmatrix}, \vec{P}_i = \begin{bmatrix} P_{ix} \\ P_{iy} \\ 0 \end{bmatrix}, \text{i} = 1, \ldots, 6 \qquad (2.14)(2.15)$$

These vectors $\overrightarrow{B_i}$ and $\overrightarrow{P_i}$Pi shown in Figure 2.1 are constant values with respect to the local coordinate systems of the base $X_BY_BZ_B$ and the local coordinate systems of the mobile platform $X_PY_PZ_P$. The base and the mobile platform are assumed to be planar; therefore, it can be perceived that the Z-coordinate of the joint coordinate, B_i and P_i is zero. The link vector can be expressed as Equation (2.16) [Jakobovic and Jelenkovic, 2002].

$$\vec{l}_i = -\vec{B}_i + \vec{t} + \underline{R} \cdot \vec{P}_i \text{ , i = 1 ... 6} \qquad (2.16)$$

$\underline{R}$ is the rotational matrix that can be determined from the three rotational angles. The orientation of the mobile platform is rotated with respect to the mobile platform coordinate frame. In this research, the coordinate frame rotates about the reference X-axis (roll) by γ, followed by a rotation about the reference Y-axis (pitch) by an angle β before a rotation about the reference Z-axis (yaw) by an angle α. The resultant Eularian rotation is derived as below [Craig, 1986].

$$R_{XYZ}(\gamma,\beta,\alpha) = R_{Z,\alpha}R_{Y,\beta}R_{X,\gamma}$$

$$= \begin{bmatrix} c\alpha & -s\alpha & 0 \\ s\alpha & c\alpha & 0 \\ 0 & 0 & 1 \end{bmatrix} \begin{bmatrix} c\beta & 0 & s\beta \\ 0 & 1 & 0 \\ -s\beta & 0 & c\beta \end{bmatrix} \begin{bmatrix} 1 & 0 & 0 \\ 0 & c\gamma & -s\gamma \\ 0 & s\gamma & c\gamma \end{bmatrix}$$

$$= \begin{bmatrix} c\alpha c\beta & c\alpha s\beta s\gamma - s\alpha c\gamma & c\alpha s\beta c\gamma + s\alpha s\gamma \\ s\alpha c\beta & s\alpha s\beta s\gamma + c\alpha c\gamma & s\alpha s\beta c\gamma - c\alpha s\gamma \\ -s\beta & c\beta s\gamma & c\beta c\gamma \end{bmatrix} \qquad (2.17)$$

where $\begin{matrix} c \equiv \cos \\ s \equiv \sin \end{matrix}$

If the position and orientation of the mobile platform are known, the length of each link can be determined according to Equation (2.18).

$$\ell_i = D\left(\vec{b}_i, \vec{t} + \underline{R \cdot \vec{p}_i}\right), \text{ i = 1, 2,…, 6} \tag{2.18}$$

D represents the Euclidean distance between the two vectors. For an arbitrary solution to a forward kinematics problem, *i.e.*, an arbitrary position and orientation of the mobile platform, the error can be expressed as the sum of the squares of the differences between the calculated and the actual length values. Having stated the above relations, one can define the first optimization function and the related unknowns as

$$F_1 = \sum_{i=1}^{6} \left[D\left(\vec{b}_i, \vec{t} + \underline{R \cdot \vec{p}_i}\right)^2 - \ell_i^2 \right]^2 \tag{2.19}$$

$$\vec{X}_1 = \begin{bmatrix} t_x & t_y & t_z & \gamma & \beta & \alpha \end{bmatrix}^T \tag{2.20}$$

where $F_1$is the first optimization function, and $\overrightarrow{X_1}$are the translation and orientation parameters of the platform

The forward kinematics of a Stewart Platform determines the pose of the platform with respect to its base given the actuators lengths. The pose of the platform can be defined by Equation (2.21) as shown below:

$${}^{B}P_i = T \cdot P_i \tag{2.21}$$

where $T = \begin{bmatrix} Rot_{3\times3} & T_{r3\times1} \\ 0_{1\times3} & 1 \end{bmatrix}$.

T is the corresponding 4×4 homogeneous coordinate matrix. It consists of a 3×3 rotational matrix, $Rot_{3\times 3}$ which is defined by the rotational motions about the X-axis, Y-axis and Z-axis with respect to the platform coordinate system, and the translational matrix $T_{r3\times 1}$ which is defined by the translational motions along the X-axis, Y-axis and Z-axis with respect to the base coordinate system.

$$Rot_{3\times 3} = \begin{bmatrix} \cos\alpha\cos\beta & \cos\alpha\sin\beta\sin\gamma - \sin\alpha\cos\gamma & \cos\alpha\sin\beta\cos\gamma + \sin\alpha\sin\gamma \\ \sin\alpha\cos\beta & \sin\alpha\sin\beta\sin\gamma + \cos\alpha\cos\gamma & \sin\alpha\sin\beta\cos\gamma - \cos\alpha\sin\gamma \\ -\sin\beta & \cos\beta\sin\gamma & \cos\beta\cos\gamma \end{bmatrix} \tag{2.22}$$

$$T_{r3x1} = \begin{bmatrix} T_x \\ T_Y \\ T_Z \end{bmatrix} \tag{2.23}$$

The homogeneous translational matrix contains redundant information because its 4×4 elements can be solved uniquely from the six parameters that control the six DOFs, which are the three rotational parameters roll-pitch-yaw α, β and γ, and the three translation parameters T_x, T_y and T_z. These six parameters can be presented as Equation (2.24).

$$q = \begin{bmatrix} T_x & T_y & T_z & \alpha & \beta & \gamma \end{bmatrix}^T \tag{2.24}$$

$$S_i(q) = T(q) \times \vec{P}_i - \vec{B}_i = \begin{bmatrix} S_{xi} \\ S_{yi} \\ S_{zi} \end{bmatrix} \tag{2.25}$$

$$G(S_i) = \sqrt{S_{xi}^{\ 2} + S_{yi}^{\ 2} + S_{zi}^{\ 2}} = l_i \quad \text{where i = 1, 2, 3,…, 6} \tag{2.26}$$

Equations (2.25) and (2.26) define function (G:q→l); since G(S$_i$) cannot be inverted in a closed form, vector S can be estimated by linear function G(S(q)) around initial value of the actuator length l, with respect to vector q, using Newton's method [Jakobovic and Jelen 2002].

$$l_i = l_{0_i} + \frac{dG_i}{dq}\Delta q \Rightarrow l_i - l_{0_i} = \Delta l_i = \frac{dG_i}{dq}\Delta q \Rightarrow \Delta q = \left(\frac{dG_i}{dq}\right)^{-1}\Delta l_i \qquad (2.27)$$

$$\frac{dG_i}{dq} = \frac{dG_i}{ds_i}\frac{ds_i}{dq} = \frac{dG_i}{ds_i}\frac{d}{dq}\big(T(q)P_i - B_i\big) = \frac{dG_i}{ds_i}\frac{dT}{dq}P_i \qquad (2.28)$$

$$\frac{dG}{ds_i} = \begin{bmatrix} \frac{dG}{dS_x} \\ \frac{dG}{dS_y} \\ \frac{dG}{dS_z} \\ 1 \end{bmatrix} = \begin{bmatrix} \frac{d(\sqrt{S_{xi}^2 + S_{yi}^2 + S_{zi}^2})}{dS_x} \\ \frac{d(\sqrt{S_{xi}^2 + S_{yi}^2 + S_{zi}^2})}{dS_y} \\ \frac{d(\sqrt{S_{xi}^2 + S_{yi}^2 + S_{zi}^2})}{dS_z} \end{bmatrix} = \begin{bmatrix} \frac{1}{2}\times\frac{2\times S_{xi}}{\sqrt{S_{xi}^2 + S_{yi}^2 + S_{zi}^2}} \\ \frac{1}{2}\times\frac{2\times S_{yi}}{\sqrt{S_{xi}^2 + S_{yi}^2 + S_{zi}^2}} \\ \frac{1}{2}\times\frac{2\times S_{zi}}{\sqrt{S_{xi}^2 + S_{yi}^2 + S_{zi}^2}} \end{bmatrix} (2.29)$$

$$= \frac{1}{\sqrt{S_{xi}^2 + S_{yi}^2 + S_{zi}^2}}\begin{bmatrix} S_{xi} \\ S_{y_i} \\ S_{zi} \\ 1 \end{bmatrix}$$

Besides, dR/dq has to be defined. Since T is a 2-dimensional matrix, and q is a 1-dimensional vector, the derivative will be 3-dimentional. The first derivative is the derivative of the transformation matrix with respect to the first element of the vector q, dR/dq, the second is dR/dq$_2$, and so forth. The pose of the platform coordinate system {P} can be obtained based on the following sequence of fundamental rotations and translations about the base coordinate system {B}.

The resulting homogeneous transformation matrix is of the following form:

$$T = \begin{bmatrix} \cos\alpha\cos\beta & \cos\alpha\sin\beta\sin\gamma - \sin\alpha\cos\gamma & \cos\alpha\sin\beta\cos\gamma + \sin\alpha\sin\gamma & T_X \\ \sin\alpha\cos\beta & \sin\alpha\sin\beta\sin\gamma + \cos\alpha\cos\gamma & \sin\alpha\sin\beta\cos\gamma - \cos\alpha\sin\gamma & T_Y \\ -\sin\beta & \cos\beta\sin\gamma & \cos\beta\cos\gamma & T_Z \\ 0 & 0 & 0 & 1 \end{bmatrix} \tag{2.30}$$

The derivatives of the transformation matrix with respect to T_x, T_y, T_z, α, β and γ are given below:

$$\frac{dT}{dT_x} = \begin{bmatrix} 0 & 0 & 0 & 1 \\ 0 & 0 & 0 & 0 \\ 0 & 0 & 0 & 0 \\ 0 & 0 & 0 & 0 \end{bmatrix} \tag{2.31}$$

$$\frac{dT}{dT_y} = \begin{bmatrix} 0 & 0 & 0 & 0 \\ 0 & 0 & 0 & 1 \\ 0 & 0 & 0 & 0 \\ 0 & 0 & 0 & 0 \end{bmatrix} \tag{2.32}$$

$$\frac{dT}{dT_z} = \begin{bmatrix} 0 & 0 & 0 & 0 \\ 0 & 0 & 0 & 0 \\ 0 & 0 & 0 & 1 \\ 0 & 0 & 0 & 0 \end{bmatrix} \tag{2.33}$$

$$\frac{dT}{d\alpha} = \begin{bmatrix} -c\beta\cdot s\alpha & -c\gamma\cdot c\alpha - s\gamma\cdot s\beta\cdot s\alpha & c\alpha\cdot s\gamma - c\gamma\cdot s\beta\cdot s\alpha & 0 \\ c\beta\cdot c\alpha & c\alpha\cdot s\gamma\cdot s\beta + c\gamma\cdot s\alpha & c\gamma\cdot c\alpha\cdot s\beta + s\gamma\cdot s\alpha & 0 \\ 0 & 0 & 0 & 0 \\ 0 & 0 & 0 & 0 \end{bmatrix} \tag{2.34}$$

$$\frac{dT}{d\beta} = \begin{bmatrix} -c\alpha\cdot s\beta & c\beta\cdot c\alpha\cdot s\gamma & c\gamma\cdot c\beta\cdot c\alpha & 0 \\ -s\beta\cdot c\alpha & c\beta\cdot s\gamma\cdot s\alpha & c\gamma\cdot c\beta\cdot s\alpha & 0 \\ -c\beta & -s\gamma\cdot s\beta & -c\gamma\cdot s\beta & 0 \\ 0 & 0 & 0 & 0 \end{bmatrix} \tag{2.35}$$

$$\frac{dT}{d\gamma} = \begin{bmatrix} 0 & c\gamma \cdot c\alpha \cdot s\beta + s\gamma \cdot s\alpha & c\alpha \cdot s\gamma - c\gamma \cdot s\beta \cdot s\alpha & 0 \\ 0 & -c\alpha \cdot s\gamma + c\gamma \cdot s\beta \cdot s\alpha & -c\alpha \cdot c\gamma - s\alpha \cdot s\beta \cdot s\alpha & 0 \\ 0 & c\gamma \cdot c\beta & -s\gamma \cdot c\beta & 0 \\ 0 & 0 & 0 & 0 \end{bmatrix} \tag{2.36}$$

where *c* = cos, *s* = sin.

Hence, H = dG/dq is a 6x6 matrix which elements derived from Equation (2.29) to Equation (2.36) are:

$$H_{i,j} = \frac{dG(s_i)}{dq_j} = \frac{dG(s_i)}{ds}\left(\frac{dT}{dq_j}\right)_{4x4}(p_i)_{4x1} \tag{2.37}$$

The algorithm for forward kinematics is described below. It takes as input the model of the base B and the platform P, and the lengths of the actuators $l_{0.}$ The output S, which is the pose of the platform, is represented by the transformation matrix T or the pose vector q [Charles, 1991].

1. Select initial guess of the pose q
2. Compute the transformation matrix T=T(q), from Equation (2.30)
3. Calculate s = T ×P – B
4. Use inverse kinematics to find the actuator lengths: l = G(s) according to Equation (2.18)
5. Calculate the height errors : $\Delta l = l - l_0$
6. IF $|\Delta l|$ < ξ which is the error tolerance THEN STOP
7. Calculate matrix H from Equation (2.37)
8. Solve $\Delta h = H\Delta q$ for Δq
9. Update platform pose, $q = q + \Delta q$

10. GOTO step 2.

The forward kinematics algorithm performs iterations and calculates the increment in the platform pose and the link lengths for the new pose h. It terminates when the difference between the calculated and the desired actuator values drops below a predetermined iteration error, ξ. Step 8 involves an inversion of the matrix H. If the matrix is near singularity, it means the position is close to the singular position and special attention is necessary.

Equation (2.27) gives the relationship between the infinitesimal changes of actuator lengths and the changes in pose. Dividing both sides of this equation by an infinitesimal time period gives a relationship between the actuator velocities and the translational and rotational velocities of the platform. The inverse of matrix H is also called the Jacobian matrix.

$$J = H^{-1} \tag{2.38}$$

$$\dot{q} = J \cdot \dot{h} \tag{2.39}$$

In this method, all the joints of the platform or actuators on the base need not be in one plane. This is a useful fact when the joint coordinates are estimated after the manipulator has been manufactured, and newly re-calibrated values are used for the forward kinematics analysis. However, it is important to note that the solution for forward kinematics analysis is not unique. The actuator lengths feedback is not necessarily reliable when the feature space feedback is used and the approximate positions of the actuators are known. However, if the manipulator enters a singular position, the pose of the platform cannot be calculated with confidence from the actuator lengths.

2.4 Workspace

In general, the workspace of a Stewart Platform is the set of all pairs of position and orientation that the end-effector can reach. In short, the workspace is the space for which a kinematics solution exists. One of the difficulties in representing the workspace is that the workspace is described with the parameters of X, Y, Z, Roll, Pitch and Yaw. It is very difficult to be presented graphically. By making reference to the work of Bonev and Ryu [1999], the discretization method is applied for the computation of the workspace of a 6-DOF Stewart Platform.

For a Stewart Platform, the usable workspace is a subset of the reachable and dexterous workspace. The reachable workspace, taking into consideration the limits of the actuators, is the set of all the points an end-effector can reach for at least one orientation. A dexterous workspace is the set of all points that the end-effector can reach for an arbitrary orientation. Besides these workspaces, a workspace can also be defined as the directed workspace consisting of all the points an end-effector can reach for one given orientation, and the usable workspace is a connected portion of the workspace that does not contain singularities.

The main subset of the complete workspace that is defined in the 3-D rotation space is the orientation workspace. The 3-D orientation workspace is probably the most difficult workspace to determine and represent. However, as a six-DOF Stewart Platform is mainly used for 5-axis machining operations, only the set of all the attainable directions of the approach vector of the mobile platform are of interest, which is the unit vector along the axi-symmetric platform. This 2-D workspace is defined as the projected orientation workspace.

Using the discretization method, the 2-D subset of the orientation workspace of the Gough-Stewart Platform is calculated using MATLAB®. The possible directions of the approach vector are represented as the inside of a general conical surface. Furthermore, in the case of an axi-symmetric Gough-Stewart Platform, a close approximation of the projected orientation workspace can be found directly by fixing one of the modified Euler angles and finding an intersection of the orientation workspace.

To implement the 2-D discretization method for the calculation of the projected workspace, a few basic kinematics constraints that limit the workspace are considered. As shown in Figure 2.1, the base universal joints are denoted by B_i and the mobile platform spherical joints by P_i (I = 1, 2, … 6). Let the orientation of the mobile platform be represented by the rotation matrix R. Hence, by knowing the given position and orientation of the mobile platform, the length of each link can be calculated using the inverse kinematics methods as shown in Equation (2.40).

$$\vec{l}_i = -\vec{b}_i + \vec{t} + \underline{R} \cdot \vec{p}_i \text{ , i = 1, …. 6} \tag{2.40}$$

Instead of the inverse kinematics analysis, three main mechanical constraints that limit the workspace of a Gough-Stewart Platform would need to be considered in the determination of the workspace. These three constraints are presented as below:

The stroke of the actuators

The limited stroke of an actuator imposes a length constraint on link i, such that $\ell_{i,\min} \le \ell_i \le \ell_{i,\max}$, for *i* = 1, 2,….. 6 where $\ell_{i,\min}$ and $\ell_{i,\max}$ are the minimum and maximum lengths of the link *i* respectively.

The range of the passive joints

Each passive joint has a limited range of angular motions due to the characteristics of commercially available joints. Let j_{Ai} be the unit vector with respect to the base frame along the axis of symmetry of the universal joint at point A_i. Let the maximum misalignment angle of the universal joint be θ_i. Let the unit vector along link *i* be denoted by $n_i = \frac{A_i B_i}{\ell_i}$. Hence, the limit on the base joint *i* imposes a constraint, such that

$$\cos^{-1}\left(j_{Ai}^T n_i\right) \le \theta_i \; for i = 1,2\ldots6. \tag{2.41}$$

Similarly,

$$\cos^{-1}\left(j_{Bi}^T n_i\right) \le \phi_i \; for i = 1,2\ldots6. \tag{2.42}$$

where, j'_{Bi} is the unit vector with respect to the mobile frame that is along the axis of symmetry of the spherical joint at point $B_{i.}$ ϕ_i is the maximum misalignment angle of the spherical joint.

To simplify the calculation, a geometric model is implemented as a constraint where AB is the height difference of the center platform to the center of the base and ℓ_i is the length of the links. Hence, the formula can be derived as follows.

$$\sin^{-1}\left(\frac{AB}{l_i}\right) \leq \theta_i \; for i = 1,2,\ldots 6. \text{ for the universal joints} \qquad (2.43)$$

$$\cos^{-1}\left(\frac{AB}{l_i}\right) \leq \phi_i \; for i = 1,2,\ldots 6. \text{ for the spherical joints} \qquad (2.44)$$

The link interference

The links can be approximated by a cylinder of diameter D. This imposes a constraint on the relative position of the pairs of links, such that the distance between the two centers of the actuator must be larger than the diameter of the cylinder of the actuator.

$$dis\tan ce\left(A_i B_i, A_j B_j\right) \geq D \text{ for I = 1, 2,…6} \qquad (2.45)$$

Hence, the minimum distance between every two line segments corresponding to the links of the Stewart Platform should be greater than or equal to D.

2.5 Algorithm for workspace discretization calculation

The simulation is performed by applying all the mechanical kinematics constraints using MATLAB®. The first requirement sets for the Euler angles are defined by rotating the mobile frame about the base Z-axis by an angle, about the mobile Y-axis by an angle, and finally about the mobile X-axis by an angle. Hence, the rotation matrix can be defined as below:

$$R_{XYZ}(\gamma,\beta,\alpha) = R_{Z,\alpha} R_{Y,\beta} R_{X,\gamma} \tag{2.46}$$

Based on the characteristics of the passive joints in the assembly, the maximum misalignment angle of the spherical joint is set as ϕ_i = 20˚ and the maximum misalignment angle of the universal joint is set as θ_i = 45˚. It has been observed that the main constraint that is violated is usually the range of the platform joints. In fact, the link interference is never encountered. Hence, to reduce computation time, the interference check can be disabled. The result of the MATLAB® simulation to calculate the workspace is shown in Figure 2.4.

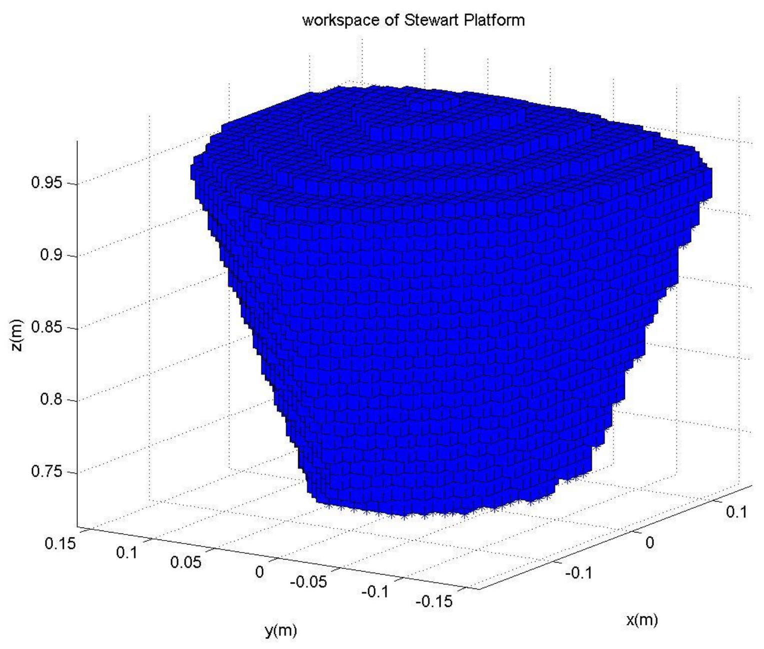

Figure 2.4 The workspace of Stewart Platform when $\gamma = 0, \beta = 0, \alpha = 0$

The area of the workspace tends to increase until a certain height before it decreases. Hence, the effective kinematics constraints have limited the workspace with respect to the height. The algorithm of the workspace calculation in MATLAB® is shown in Figure 2.5.

For a given Z height from Z_{min} to Z_{max} in ΔZ increments, the X-Y range of the area of the workspace A_Z is computed using the discretization method. The area A_Z is composed of $\mathbf{N_x}$ "slices" from X_{min} to X_{max} with $\Delta X = 0.01m$ throughout the workspace calculation. The length of the slice of each $\mathbf{N_x}$ is incremented until the boundary is obtained by solving the inverse kinematics to determine the link lengths. Thus

$$A_z = \sum_{X_{min}}^{X_{max}} Y_X \cdot \Delta X \text{ where } \Delta X = 0.01m \qquad (2.47)$$

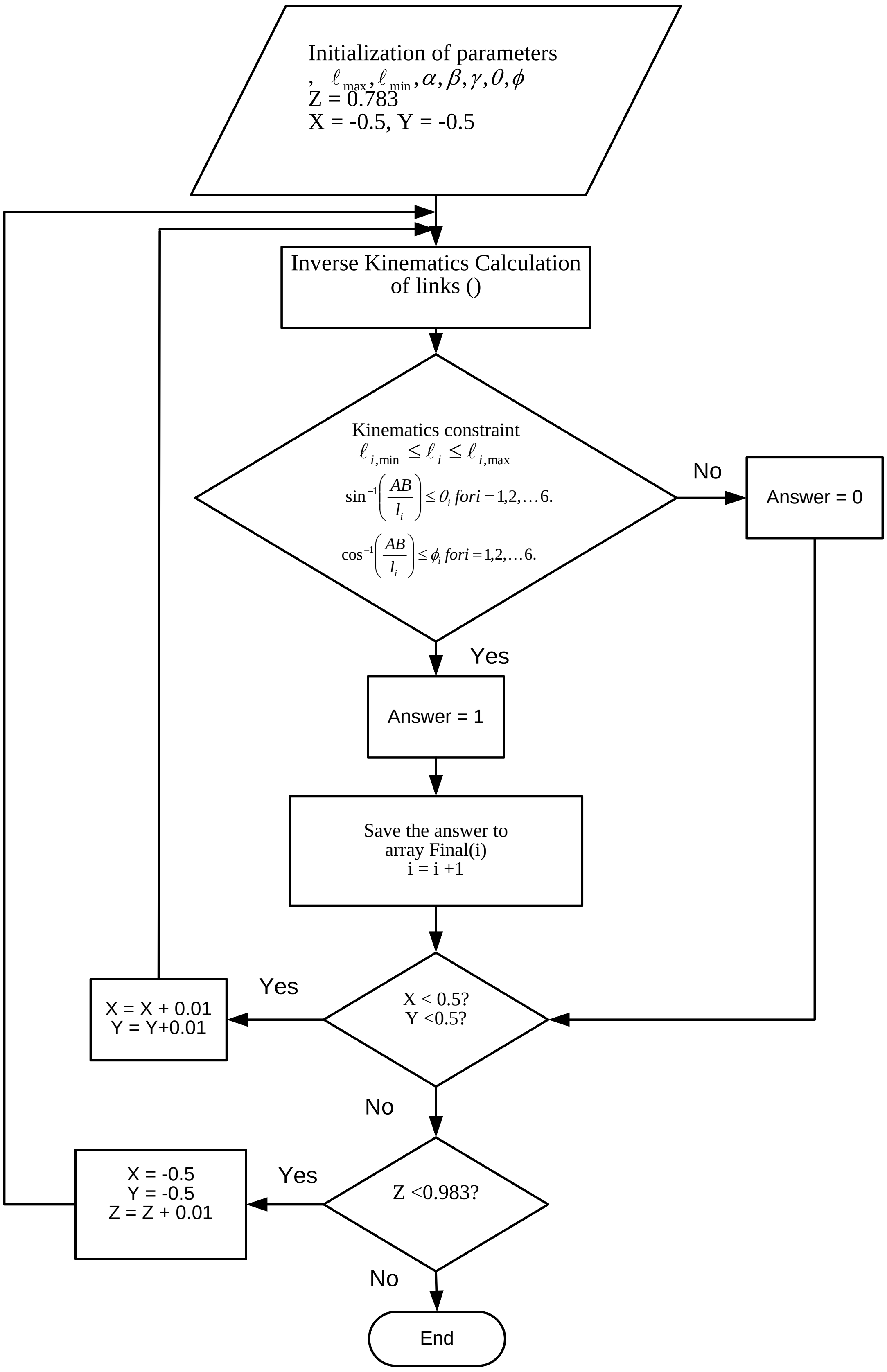
Initialization of parameters
, $\ell_{\max}, \ell_{\min}, \alpha, \beta, \gamma, \theta, \phi$
Z = 0.783
X = -0.5, Y = -0.5
Inverse Kinematics Calculation of links ()
Kinematics constraint
$\ell_{i,\min} \le \ell_i \le \ell_{i,\max}$
$\sin^{-1}\left(\frac{AB}{l_i}\right) \le \theta_i \; for\, i = 1,2,\ldots 6.$
$\cos^{-1}\left(\frac{AB}{l_i}\right) \le \phi_i \; for\, i = 1,2,\ldots 6.$
No
Answer = 0
Yes
Answer = 1
Save the answer to array Final(i) i = i +1
Yes
X = X + 0.01 Y = Y+0.01
X < 0.5? Y <0.5?
No
Yes
X = -0.5 Y = -0.5 Z = Z + 0.01
Z <0.983?
No
End

Figure 2.5 The algorithm of the workspace calculation

The total volume V is calculated as the sum of the incremental volumes of $A_z \cdot \Delta Z$.

Thus $$V = \sum_{Z_{\min}}^{Z_{\max}} A_z \cdot \Delta Z \text{ where } \Delta Z = 0.01m \qquad (2.48)$$

The calculation of the area of the workspace is performed by setting $\gamma = 0, \beta = 0, \alpha = 0$ and the Z-increments as 0.01m. Using the volume calculation method, the volume of the workspace can be obtained. The total volume of the workspace is 12179 cm^3 or 0.012179 m^3.

After obtaining the result of the workspace in Figure 2.5, the limitation of the position and orientation of the Stewart Platform can be verified. Hence, the motion of the platform can be operated safely within the allowance of the workspace. As a result, singularities can be avoided and the possible damage to the passive joints can be minimized.

2.6 Singular Position

The singularity configurations of a Stewart Platform introduce one or more extra DOF to the system. These additional DOFs are independent of the instantaneous velocities of the actuators and hence cannot be controlled by the motion of the links. This type of situation happens when there is no inverse solution for the Jacobian matrix, which occurs when the determinant of the matrix is equal to zero. Hence, if a linear transformation relating the velocity of the joint to the Cartesian velocity of mobile platform can be inverted for the calculation the joint velocity of actuator with a given Cartesian velocity [Craig, 1986], the matrix is non-singular.

As mentioned previously, the determinant for the inverse Jacobian is too complex to be solved. Hence, the effects of the singularities can only be felt when the control is performed using the dynamics equations and the Jacobian. Since both equations are not used, it would not be easy to identify these singularity problems [Yee, 1993].

All manipulators have singularities at the boundary of their workspaces, and most have loci of singularities inside their workspaces. Singularities are normally classified into two categories:

1. Workspace boundary singularities are those that happen when the platform is fully stretched out or folded back on itself such that the end-effector is near or at the boundary of the workspace.

2. Workspace interior singularities are those that occur away from the workspace boundary and are generally caused by two or more joints axes lining up.

Based on this classification of the singularities, for the particular Stewart Platform in this research, two kinds of singularity configurations have been identified according to the work of Fichter [1986].

The first type of singularity configurations can be observed from the physical structure of the Stewart Platform. When the plane of the surface of the mobile platform is parallel to any one of the planes of the links as shown in Figure 2.6, uncertainty exists due to the changes in the motion of the links to manipulate the end-effectors of the platform. Since the spherical joint acts as a pivot between the two surfaces of mobile platform and the respective link, the new corner between the surfaces at the new position could either point inwards or outwards, as shown in the Type 1 configuration of Figure 2.6.

The second type of singularity configurations is not easily observable. When the mobile platform is oriented at 90˚ either clockwise or anticlockwise about the Z-axis (Yaw), without any angular rotation about the X-axis (Roll) and the Y-axis (Pitch) as shown in Figure 2.6, Type 2 singularity happens when the mobile platform is parallel to the base. All the tangents of the spherical joints are perpendicular to the respective edge of the base. Thus, all the loci of the points at the mobile platform are tangential to the circular edge of the mobile platform. This will cause instability as stated in the earlier case [Yee, 1993].

However, the singularity problem does not occur at all times. When the mobile platform is co-planar with the plane of the link, and the moments caused by the motors of the links are greater than the effective moment of the load, the mobile platform will still be able to return to the real working space. However, if the loading effect is greater than the motor balancing weight, the platform will collapse. This applies to the Type 2 singularity configuration [Yee, 1993].

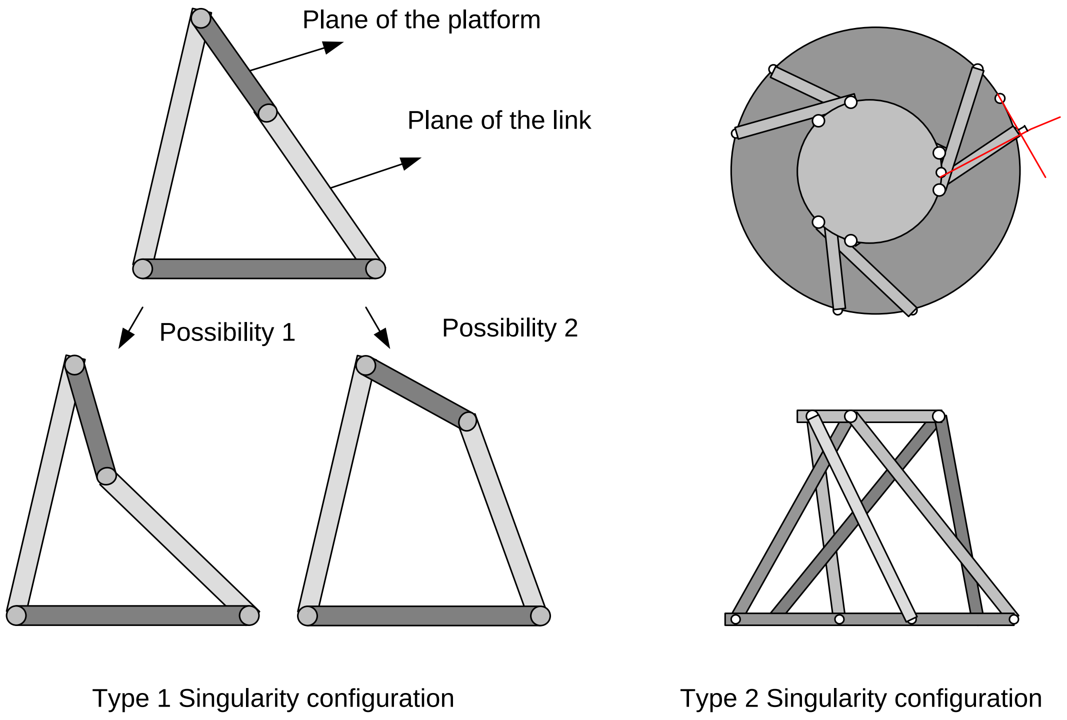
Plane of the platform
Plane of the link
Possibility 1
Possibility 2
Type 1 Singularity configuration
Type 2 Singularity configuration

Figure 2.6 The singularity configuration of Stewart Platform [Yee, 1993]

During the normal operation of a Stewart Platform, the singularity configurations should always be prevented to reduce the risk of uncertainty in the position and orientation, as well as to prevent overloading of the joints of the platform. Precautionary steps are taken through both the hardware and software aspects. A MATLAB® program has been developed to verify the singularity points by restricting the boundary of the movement through limiting the maximum rotation of the Z-axis to $\pm 60^\circ$ and the angle between the spherical joints and the platform to be less than $\pm 20^\circ$. Furthermore, the angular rotation between the universal joints and the base is restricted to $\pm 45^\circ$, which all are below the limits of the singularity configuration. Next, hardware precaution can be applied by installing a magnetic sensor to limit the movements of the links physically to prevent any possibility for singularity to occur due to the over traveling of the links.

Chapter 3 Fundamentals of Machining

3.1 Introduction

Computer Numerical Control (CNC) is a methodology of communicating with the machining centers through G-codes and M-codes instructions for manipulating the machine tool or workpiece. CNC performs according to numerically directed interpolation of the tool path of the cutting tool in the workspace of the machine center. The parameters of the CNC operations can be modified through the software within the controller.

The fundamental of CNC control is to move the machine tool along a path from one point to another. Certain machines can only perform planar motions, such as contouring along the X-axis and Y-axis while the Z-axis is controlled separately. In certain machines, additional two axes of rotation are implemented to control the orientation of the cutter or workpiece during the machining process. This can be achieved simultaneously along with the translation motion in the Cartesian workspace.

In modern manufacturing, 4-axis and 5-axis machines are becoming more popular due to their flexibility and capability to machine complex workpieces. Hence, a 3-axis machine can be used to move the tool head in the X, Y and Z-directions while the additional axes allow the workpieces to be rotated about the X-axis and Y-axis, similar to a lathe. These rotational axes are also called the A-

and B-axes in most cases. All motions can be built from linear motions between two adjacent machining points along the predefined trajectory path.

Intensive research has been conducted on parallel kinematics platforms, such as Stewart Platforms, due to their ability to achieve six DOF movements and they have pure linear force motion along the axis. Hence, these six DOF Stewart Platforms have the potential to be used as 5-axis machines with better stiffness and flexibility.

Lately, some controllers have achieved the ability to follow an arbitrary NURBS curve. However, these efforts have been met with skepticism since unlike circular arcs, their definitions are not natural and are too complicated to be set up manually. CAM software can already generate any motion using many short linear segments.

Computer-Aided Design and Computer-Aided Manufacturing (CAD/CAM) utilize computers to design drawings of part feature boundaries in order to develop cutting tool paths and CNC machine codes. The application of CAM allows the tools and methods to be defined for cutting purposes. Drawings in CAD are like constructing drawings using lines, arcs, circles and points, and positioning them relative to each other on the screen. One of the major advantages of CAD/CAM is the time saved. It is much more efficient than writing CNC codes line-by-line [Ken, 2001].

Presently, CAD/CAM is the conventional method of creating mechanical drawings and CNC programs for machine tools. CAD is the standard throughout the world for producing engineering drawings. Now, designers can convert the created drawings into other common file formats, such as Initial Graphics Exchange Specification (IGES) or Parasolids files. When using CAD/CAM software, such as MasterCam, the drawings may be created from scratch or imported from a CAD program. MasterCam can assign tools and their order of usage while creating the cutting tool path, as shown in Figure 3.1.

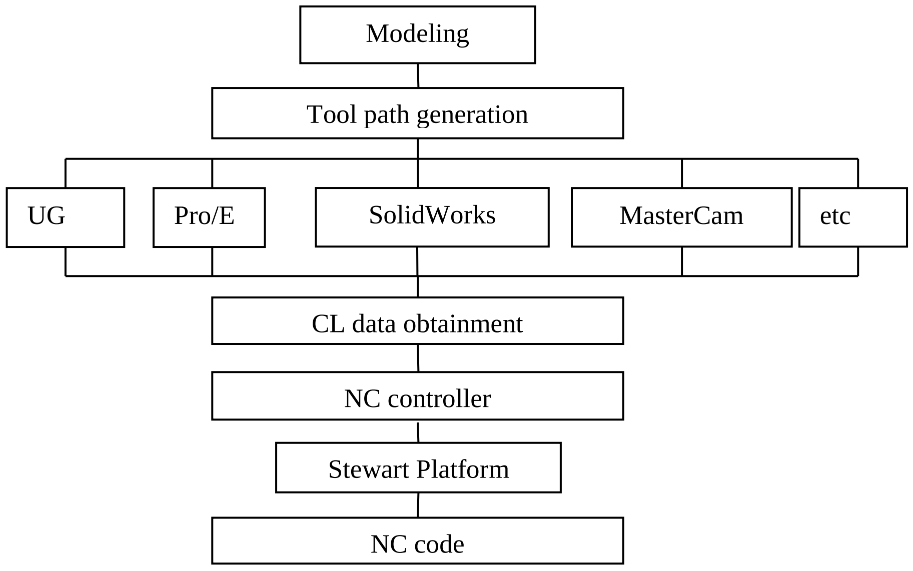

Figure 3.1 Standard postprocessor sequences

The overall purpose of the CAM software is to generate the tool path for a CNC machine, which in this research is the Stewart Platform. Hence, it is imperative to have a full understanding of the rectangular and polar coordinate systems. Furthermore, a few considerations need to be made, such as the cutting tool selection, speeds and feeds. Almost all the CAM software will automatically develop speeds and feeds data based on the tool selection. However, adjustments are frequently necessary for the machine tool, cutting parameters, workpiece and tool, which will affect the cutting condition and parameters during the machining process as shown in Figure 3.2.

In the process of constructing the geometry of a workpiece, the types of machining operations need to be considered. For instance, if the desired result is to drill a hole using a standard drill, only the construction of the point that represents the hole center location in the coordinate system is necessary [Ken, 2001].

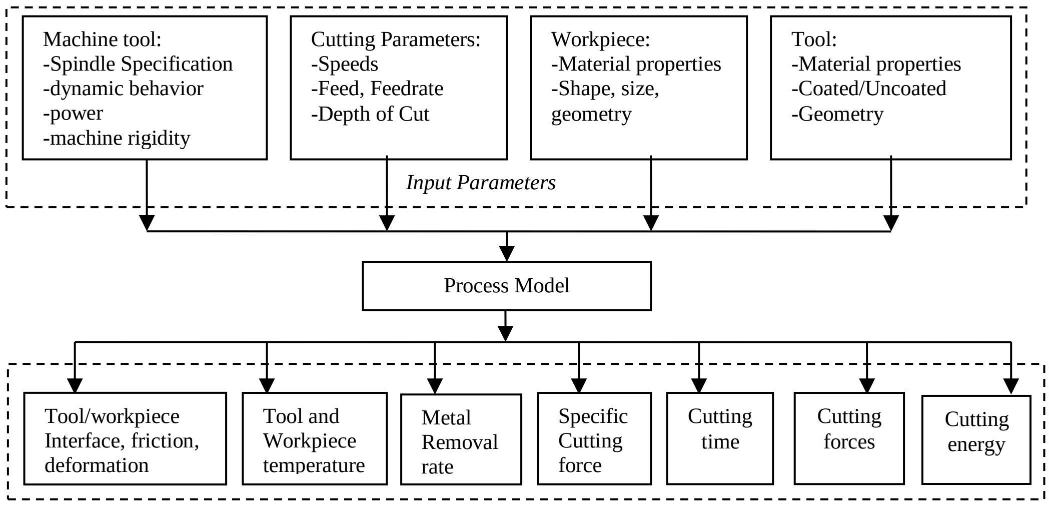

Figure 3.2 CNC model inputs/outputs schematic representation

3.2 Machine concept

Based on freeform surface machining, the kinematics requirement will be explained and various concepts with respect to kinematics, structure loading and stiffness will also be investigated [Reimund, 2000]. As reported by Reimund [2000], parallel kinematics manipulators are weak in inclination angle of rotary axes and the workspace dimension as shown in Table 3.1. However, parallel kinematics manipulators are favorable in the aspect of stiffness, repeatability and mechatronic properties as shown in Table 3.1. These outstanding characteristics of parallel kinematics manipulator have led to the interest in research of the machining process with Stewart Platforms.

Table 3.1 Characteristic of various structure concepts [Reimund, 2000]

Parameters	**Serial**	**Hybrid**	**Parallel**
Inclination of rotary axes (A-axis)	±95°	±95°	±15.45°
Feedrate of rotary axes	Unfavorable	Unfavorable	Favorable
Stiffness	Average	Unfavorable	Favorable
Masses to be moved	Unfavorable	Favorable	Very Favorable
Mechatronic Properties	Unfavorable	Average	Favorable
Dimensions	Favorable	Favorable	Unfavorable
Repeating parts	Unfavorable	Average	Favorable
Variation of number axes	Favorable	Average	Unfavorable
Collisions	Favorable	Average	Unfavorable

For a classical machining center, the workspace of the serial kinematics manipulator can be presented as a parallelepiped or a rectangle box as shown in the red lines in Figure 3.3. The axial stiffness of the rotary drive is constant over the entire workspace. Experiments were conducted and simulation was performed using MATLAB® so that the workspace of the system can be defined correctly. A comparison of the Stewart Platform and a CNC machine, which is available in the Workshop II of NUS, was made with respect to translation motions. The outcomes of the workspaces are compared as in Figure 3.3.

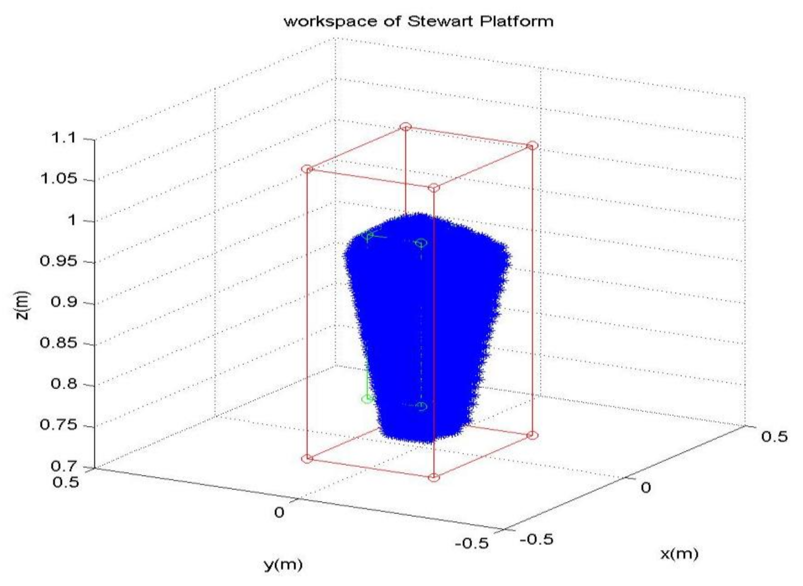

Figure 3.3 Comparison of the workspace of Stewart Platform (blue color dots) and CNC machine (red color lines)

In terms of the motion of the Stewart Platform, the workspace can be defined as the dexterous workspace and the reachable workspace. As shown in Figure 3.3, the workspace area varies with respect to the translation motion along the Z-axis. As shown in the result in Table 3.2, the reachable workspace is bigger than the dexterous workspace, and it will cause confusion to the end-user since the workspace will be changing along with the movement of the mobile platform. Thus, a singularity is foreseeable if the machining path is defined according to the reachable workspace of the Stewart Platform as there is a risk of reaching the boundary of the workspace easily.

Therefore, to increase safety of the machining processes and to reduce the risk of damaging the Stewart Platform during the machining processes, the machining path is defined with respect to the dexterous workspace of the Stewart

Platform, as shown in Figure 3.4(a) and Figure 3.4(b). As a result, the final volume of the workspace in the Cartesian coordinate system is shown in Table 3.2.

Table 3.2 Comparison of workspace of CNC machine and Stewart Platform

Movement	CNC Machine	Stewart Platform (Reachable Workspace)	Stewart Platform (Dexterous Workspace)
X (mm)	410	Different Height has different Workspace Area	130
Y (mm)	310		130
Z (mm)	300		200
Total Workspace	$38.13 \times 10^6 mm^3$	$13.62 \times 10^6 mm^3$	$3.38 \times 10^6 mm^3$

Stewart Platforms exhibit the lowest inclination of the mobile platform as compared with serial and hybrid kinematics manipulators in Table 3.1. Nevertheless, since the low setting angles are good enough for die and mold making, the limitation of the orientation workspace of the Stewart Platform is still acceptable. Although there is a possibility of collisions based on the designed structure, this issue can be solved through modifying the structure of the parallel kinematics manipulators. In addition, the path velocity also plays an important role with regards to the productivity in die and mold making as the speed performance is defined by the slowest individual axis in the serial and parallel manipulator. Since the Stewart Platform possesses the characteristics of better feed rate of rotary axes as shown in Table 3.1, it exhibits the most favorable dynamic parameters (velocity and acceleration) and has advantages as compared with the serial kinematics manipulator.

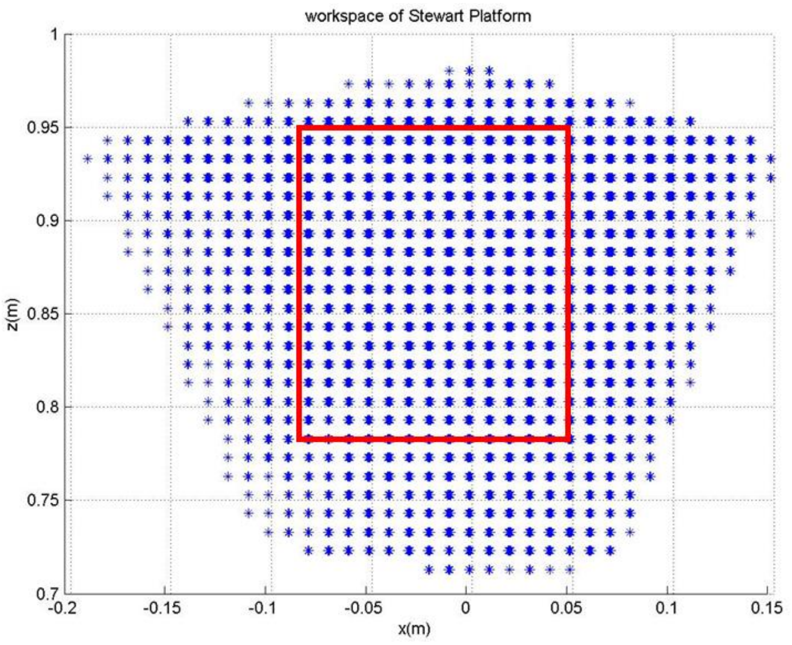

Figure 3.4(a) Dexterous workspace (red color box) of the Stewart Platform (Front)

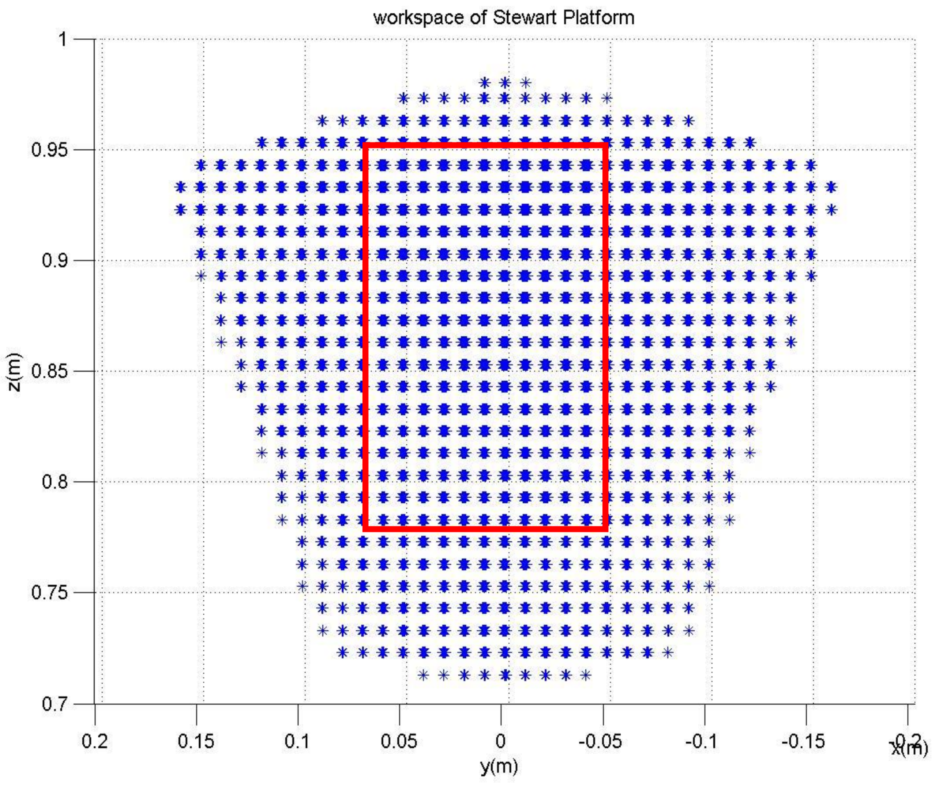

Figure 3.4(b) Dexterous workspace (red color box) of the Stewart Platform (Side)

In the literature review of [Reimund, 2000], a stiffness comparison was done with different design principles, such as Hexaglide which is a parallel kinematics manipulator with constant strut length while Stewart Platform is a parallel kinematics manipulator with variable strut length. The comparison indicates that the Stewart Platform is very homogeneous in the working area as compared with the Hexaglide. For the parallel kinematics system, no other values can be specified for an inclination of 30° due to the occurrence of singularities in this range, whereby the loads approach infinity and the stiffness converges to zero.

As a result, the loads in the structure with constant strut length are greater than the structure with variable strut length. This is due to the arrangement of the pivot planes and the center of motion, which imposes limitation on the rotational motions of the mobile platform.

In term of static stiffness of the tool cutting point, the major cause is the arrangement of the pivot points. The investigations are based on the position of the pivot points. The limited workspace of a Stewart Platform introduces difficulty of achieving accurate motion. Furthermore, gravitation introduces sag of the platform which is relatively large and inconsistent throughout the workspace when it is under the weight of the spindle or the workpiece. Even though the ball-screw actuator is loaded by a pure linear force of tension or compression, the overall stiffness of the strut is still limited by the stiffness in the ball-screw/nut contacts, the thrust bearings and the spherical joints at each end of the strut. As a result, the effective stiffness will be changing throughout the workspace. This will cause a prominent issue of accuracy and induce difficulty in the compensation of the dynamics of the platform.

During machining processes, stability against chatter is defined by the stiffness, damping and natural frequency of the most flexible mode of the vibration of the machining system. The spindle, holder and tool assembly is the least stiff element in the structure for most machines. For a Stewart Platform, the ball-screw-driven actuator assembly represents not only the axis drives but also the entire support structure. In addition, each ball-screw assembly must be supported at each end by spherical joints at the top and universal joints at the bottom. The effect of this flexibility causes a very significant reduction in the overall stiffness. Moreover, each actuator drives the platform at an angle to its motion, and this causes an unfavorable transmission ratio. The result is that the stiffness at the platform is rather low as compared to the stiffness of the individual actuators.

Hence, by applying the ball-screw drive as a classical machining center, the Stewart Platform is not capable of providing sufficient tool point stiffness to be useful for high speed milling. The low stiffness together with the variation of the workspace has led to the problems of deflections under cutting forces, sag due to the weight of the spindle or workpiece, problems with chatter, overshoot, general dynamics of the drives and the control system. Nevertheless, a Stewart Platform can still be designed to be of high stiffness by implementing further kinematics constraints which it will generate sufficiently for the purpose of high speed machining. With the same basic drive elements implemented, a Stewart Platform is capable of higher flexibility due to its ability to be manipulated in six DOF as compared with a classical serial kinematics manipulator.

Chapter 4 Three-Axis Machining

4.1 Introduction

Since the mobile platform of a Stewart Platform is a rigid body, the cutter coordinate system can be converted directly to form the machining coordinate system on a Stewart Platform easily. Currently, the coordinate system used is defined with reference to the base of the Stewart Platform, as shown in Figure 4.1.

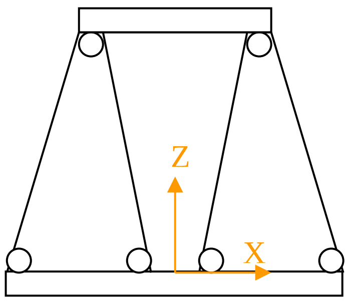

Figure 4.1 The coordinate system of a Stewart Platform

All the coordinates in the NC programs are either expressed in absolute position or incremental position. They are redefined with respect to one reference point at the datum plane of the base surface, which is the origin of the Stewart Platform coordinate system shown in Figure 4.1. However, the origin of the coordinate system may vary in different situations. Hence, prior to the start of a machining process, the first priority is to define the origin of the coordinate system. However, unlike a normal Cartesian CNC machine, there is a concern of workspace limitation when setting up the origin of the coordinate system. In addition, there is a limitation on the working area of XY-coordinate system with different Z-coordinate.

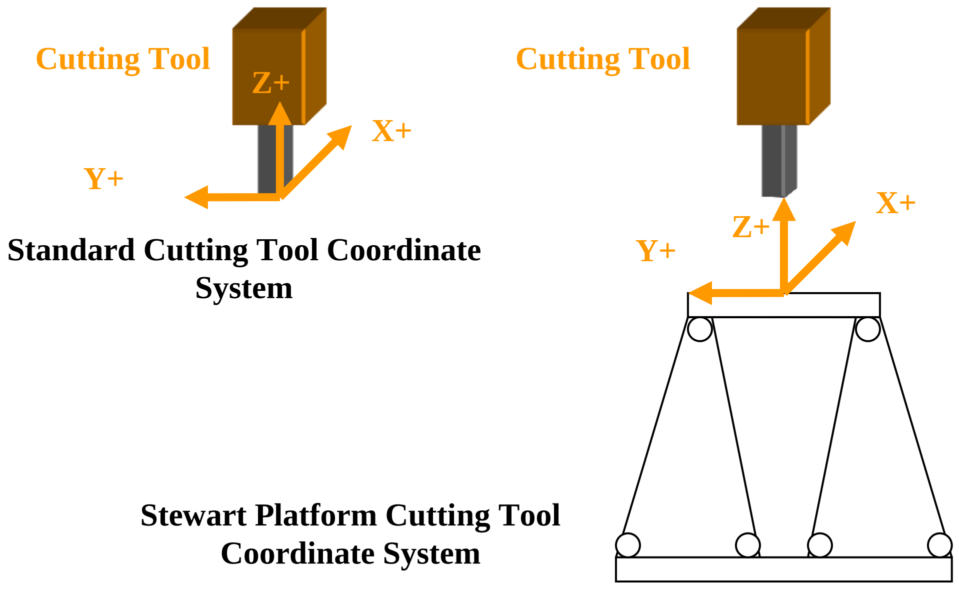
Cutting Tool
Z+
X+
Y+
Standard Cutting Tool Coordinate System
Cutting Tool
Z+
X+
Y+
Stewart Platform Cutting Tool Coordinate System

Figure 4.2 Comparison of the coordinate systems of the cutting tool and the Stewart Platform

From Figure 4.2, the X- , Y- as well as Z-axis of the coordinate systems of a CNC machine and a Stewart Platform are almost the same. However, when a cutting tool is moving, the platform moves in a direction opposite to the feed of the cutting tool in the standard cutting tool coordinate system. In a Stewart Platform, the workpiece is moved towards the cutting tool as shown in Figure 4.3.

From Figure 4.3, since the NC program is written with the coordinate system defined at the tip of the cutting tool, when the coordinate system of the Stewart Platform is known, the NC program can be converted and defined with referred to the coordinate system of the Stewart Platform. All the values of the coordinates in the Stewart Platform will move in opposite directions of the coordinates in the NC program. Thus, the value would be as follows:

X_platform = -X_CNC_code;

Y_platform = -Y_CNC_code;

Z_platform = -Z_CNC_code.

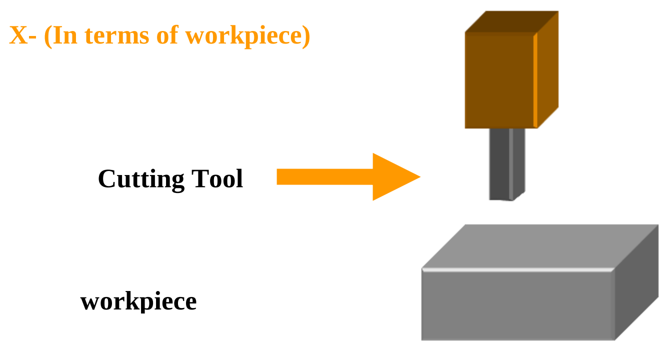

In a Stewart Platform, to follow the NC code of X+, which is the cutting tool moves towards the workpiece, the platform that holds the workpiece will move in the X-direction toward the cutting tool.

Figure 4.3 Cutting tool and platform movements during the machining process for Stewart Platform

There are normally three coordinate systems in a standard CNC machine. They are given in Table 4.1.

Table 4.1 Coordinate systems

Absolute Coordinate	Incremental Coordinate	Machine Coordinate	Distance to travel
X_{abs} Y_{abs} Z_{abs}	X_{rel} Y_{rel} Z_{rel}	$X_{machine}$ $Y_{machine}$ $Z_{machine}$	ΔX ΔY ΔZ
$X_{abs} = X_{abs} + X_{rel}$ $Y_{abs} = Y_{abs} + Y_{rel}$ $Z_{abs} = Z_{abs} + Z_{rel}$		$X_{machine} = X_{machine} + X_{abs}$ $Y_{machine} = Y_{machine} + Y_{abs}$ $Z_{machine} = Z_{machine} + Z_{abs}$	

4.2 Input format

NC machining simulation is completed by using MATLAB® in this study. CNC machines allow input values in units of millimeters and degrees with a decimal point and significant zeros in front of (leading) or at the end (trailing) of the values. The language used for controlling a machine tool is identified as the "G-code" or "M-code". The advantage of an NC code is that the program created for machining a particular part on one machine may be used on other machines with minimal changes required. Table A1 in Appendix A is a list for all of the address characters applicable for programming along with a brief explanation.

The address characters in Table A1 are standard address characters used in the NC programs. The G and M codes are the most commonly used characters in an NC program, which serve as the instruction to control the tool path. An NC program normally consists of blocks of information separated by the semicolon symbol (;). This symbol (;) is used as the end of a block character (EOB), and it indicates the end of a command line. Thus, a standard NC code can be expressed in the example below.

Word	Word	Word	Word	Word
N01	G00	X24	Y45	F40

Each word contains an address, followed by specific data, as illustrated in the example below which was translated from the previous shown NC code.

Address	Data	Address	Data	Address	Data	Address	Data	Address	Data
N	01	G	00	X	24	Y	45	F	40

Through an analysis of the address and the respective data, a machining path can be generated based on the instructions provided by the address.

G codes are the preparatory functions which provide instruction on a machining path and identifying activities execution activities by the machine. In NC code, normally there is more than one G-Codes in a program block. Specific G-codes work as the communication between the machine controller and the machine tool especially when the machine is performing specific machining operations. In a G-code, the modal commands remain in effect for multi blocks until the next new G-code is called to replace the commands from the same group. In addition there are non-modal G-code commands that are only used once in a single block.

There are different groups of modal G-codes. One code from each group may be specified in an individual block. However, if two codes of the same group appear in the same block, the former one will be ignored and the latter will be applied in the program. A safety block is a block of G codes which is used as a code to overwrite any remaining G code from the previous program. Hence, it is a good habit to implement a safety block after changing a tool or when there is a need to rerun a single operation within the program. This implementation can help prevent some unwanted effects left by the previous G-codes.

A few G-codes are active when a machine is started. The items marked with an * before the G value of Code column, as shown in G-codes chart of Table

A2 in Appendix A, are active upon the startup of a machine. G00, G01, G90 and G91, are the active initial code that is determined by a parameter setting. Normally, during a start-up condition, the program is set at G01 and G90.

Besides G-codes, M codes also play an important role in an NC program. M codes serve as the miscellaneous functions that control the working components, such as the activation of the coolant flow, spindle rotation, direction of the spindle rotation, etc. Table A3 in Appendix A shows the commonly used M codes in NC programs.

Based on these guidelines, a post-processor for a Stewart Platform has been developed to implement an NC program as the trajectory path for 3-axis machining. All the basic G-codes are translated in the post-processor such that by inputting the NC program into the post-processor, an appropriate trajectory path can be generated for the Stewart Platform to perform the required machining process.

Firstly, a model is created using a CAD software, such as SolidWorks, and exported as a Parasolids file. This file is imported into CAM software, such as MasterCam, to generate the required NC program to machine out the model. The generated NC program will be imported into the post-processor that has been developed in MATLAB® to produce the required trajectory path that will be used for the actual machining on the Stewart Platform. The format of an NC program is shown in Figure 4.4.

```
%
O0000
G21
G0 G17 G40 G49 G80 G90
T2 M6
G0 G90 G54 X45.302 Y125.453 A0. S800 M3
G43 H2 Z10.
Z2.
G1 Z-10. F32.
G3 X42.013 Y139.208 R10.
G2 X63.987 Y175. R21.
```

Figure 4.4 Format of an NC program

After the NC program has been imported into the post-processor, it is first converted into ASCII format. Next, an identification algorithm is executed to evaluate the address characters and the respective values of the address characters. The algorithm is shown in the flow chart of Figure 4.5.

The address characters and their respective values are assigned into the 2D array of matrix, named as Newmatrix as shown in Figure 4.5. Furthermore, as a zero, a space or a semi-colon is needed to trigger the record of a numerical value, an additional column has to be added so that a zero can be added to the end of each line to indicate that it is the end of a line. Hence, the row of the matrix can be determined with this function in the flow chart of Figure 4.5.

```
NC Program Conversion Algorithm

Input:
NC program

Output:
N(Sequence)
G(Code)
```

X(Position)
Y(Position)
Z(Position)
I(Circular Position)
J(Circular Position)
K(Circular Position)
F(Feed Rate)
R(Radius or Retract)
S(Speed)
T(Tool)
M(Miscellaneous)

After obtaining the ASCII values of the NC program, determine the size of the ASCII array of the NC program.

inputmatrix = ASCII Array of the NC program
[row_max column_max] = size of the inputmatrix

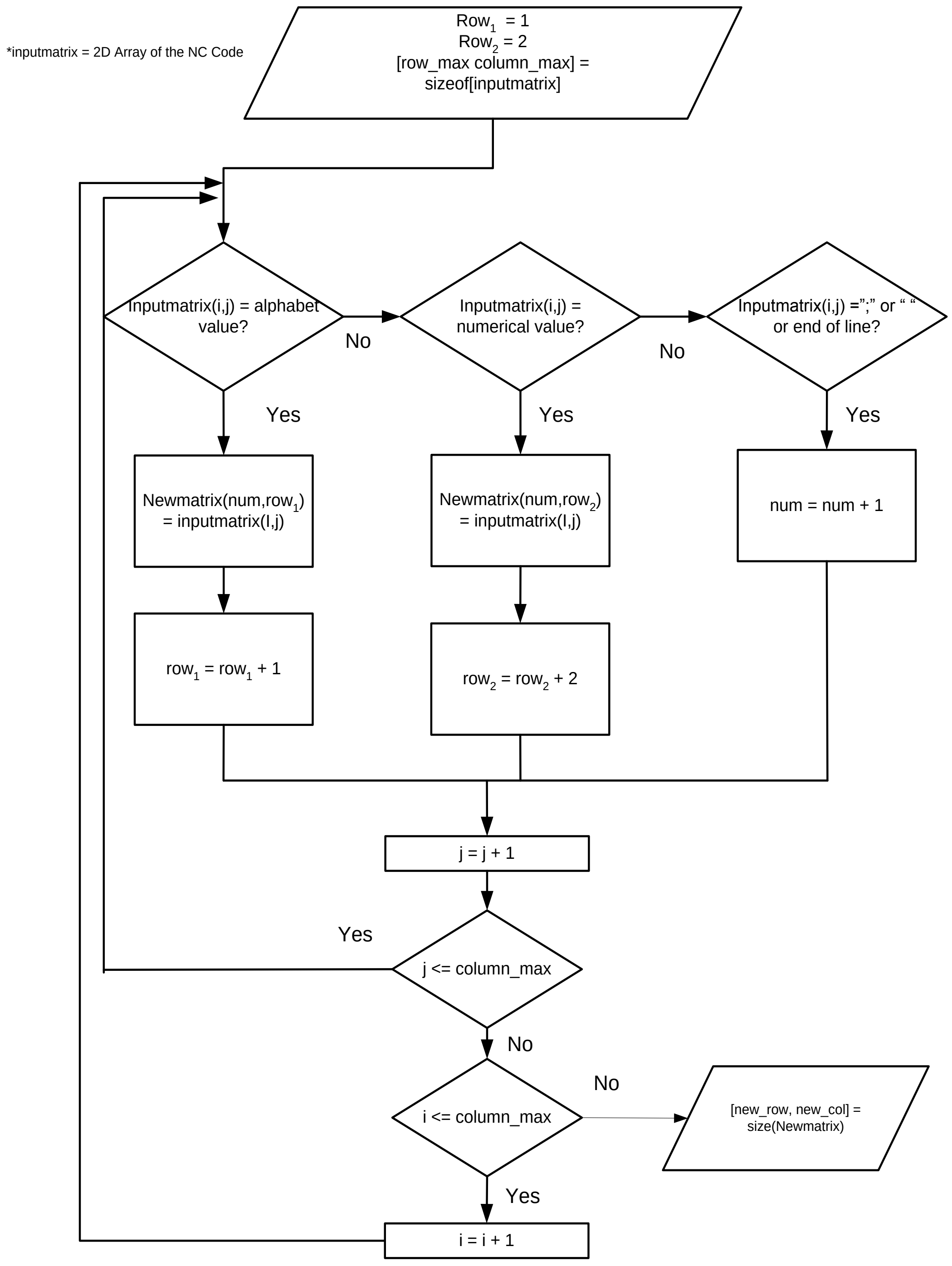
*inputmatrix = 2D Array of the NC Code
$Row_1 = 1$
$Row_2 = 2$
[row_max column_max] = sizeof[inputmatrix]
Inputmatrix(i,j) = alphabet value?
No
Inputmatrix(i,j) = numerical value?
No
Inputmatrix(i,j) =";" or " " or end of line?
Yes
Yes
Yes
$Newmatrix(num,row_1) = inputmatrix(I,j)$
$Newmatrix(num,row_2) = inputmatrix(I,j)$
num = num + 1
$row_1 = row_1 + 1$
$row_2 = row_2 + 2$
j = j + 1
Yes
j <= column_max
No
No
i <= column_max
[new_row, new_col] = size(Newmatrix)
Yes
i = i + 1

Figure 4.5 Flow chart of identification algorithm to evaluate address characters and the respective values

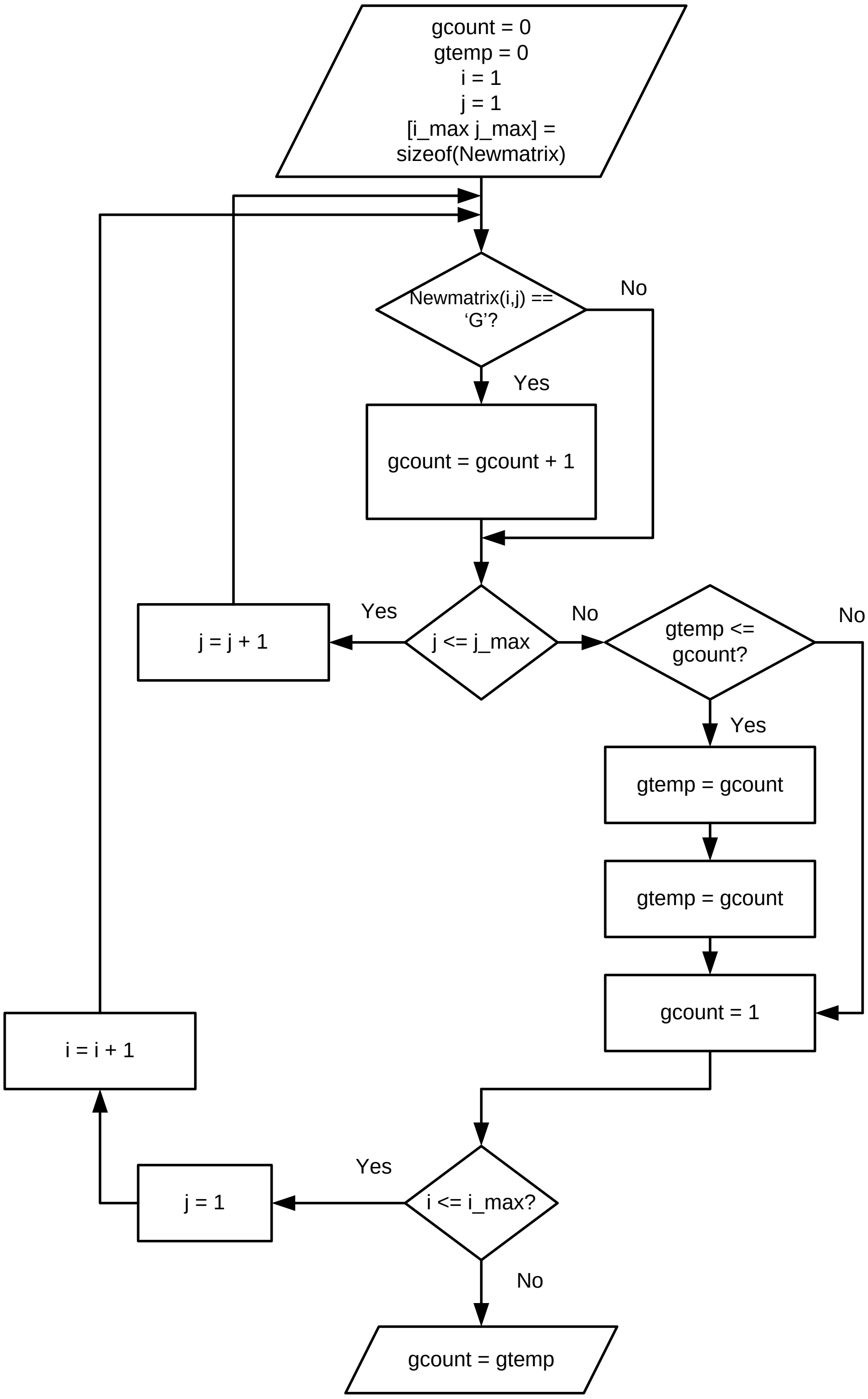

Figure 4.6(a) Flow chart of algorithm to determine maximum number of G code

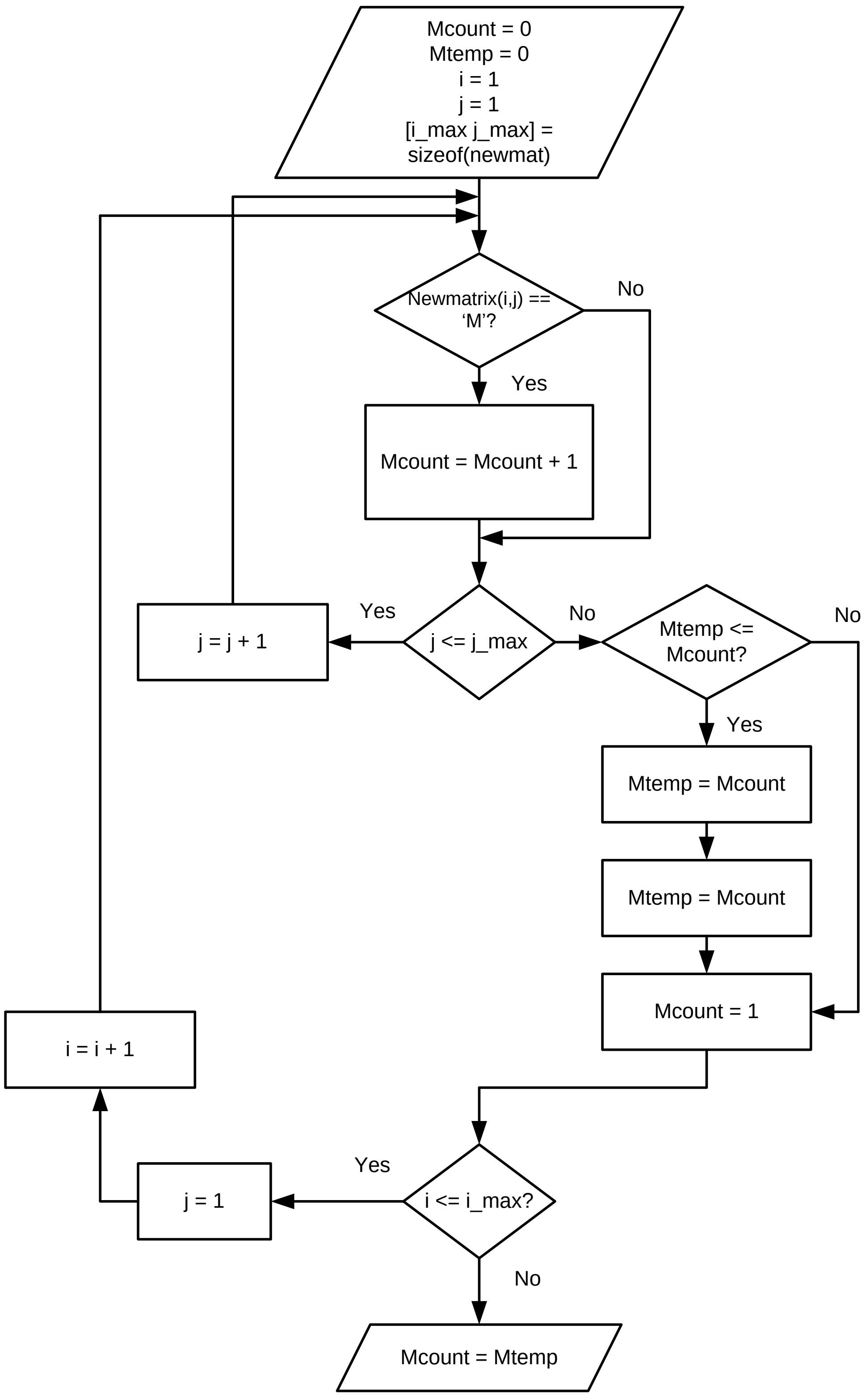

Figure 4.6(b) Flow chart of algorithm to determine maximum number of M code

The matrix, Newmatrix is further categorized into 1D array matrix of the corresponding address characters code such as X, Y and Z code. However, since G and M codes can appear more than once in each single line of NC program, an algorithm is developed to detect the maximum number of G and M code appearance in each line of the NC program as shown in Figure 4.6(a) and Figure 4.6(b). The flow of the algorithm to assign the matrix size of the respective character address can be expressed in the flow chart as shown in Figure 4.7.

Therefore, each command block consists of only one specific character except for characters 'M' and 'G', the arrays of the respective characters can be determined. The maximum number of G and M characters that appear in an NC program can also be defined.

As a result, the output of the corresponding character addresses matrix is obtained for further development of the conversion of the NC program to the trajectory path recognized by the Stewart Platform. The flow chart of the algorithm that assigns the NC program character address to the respective matrix is shown in Figure 4.8.

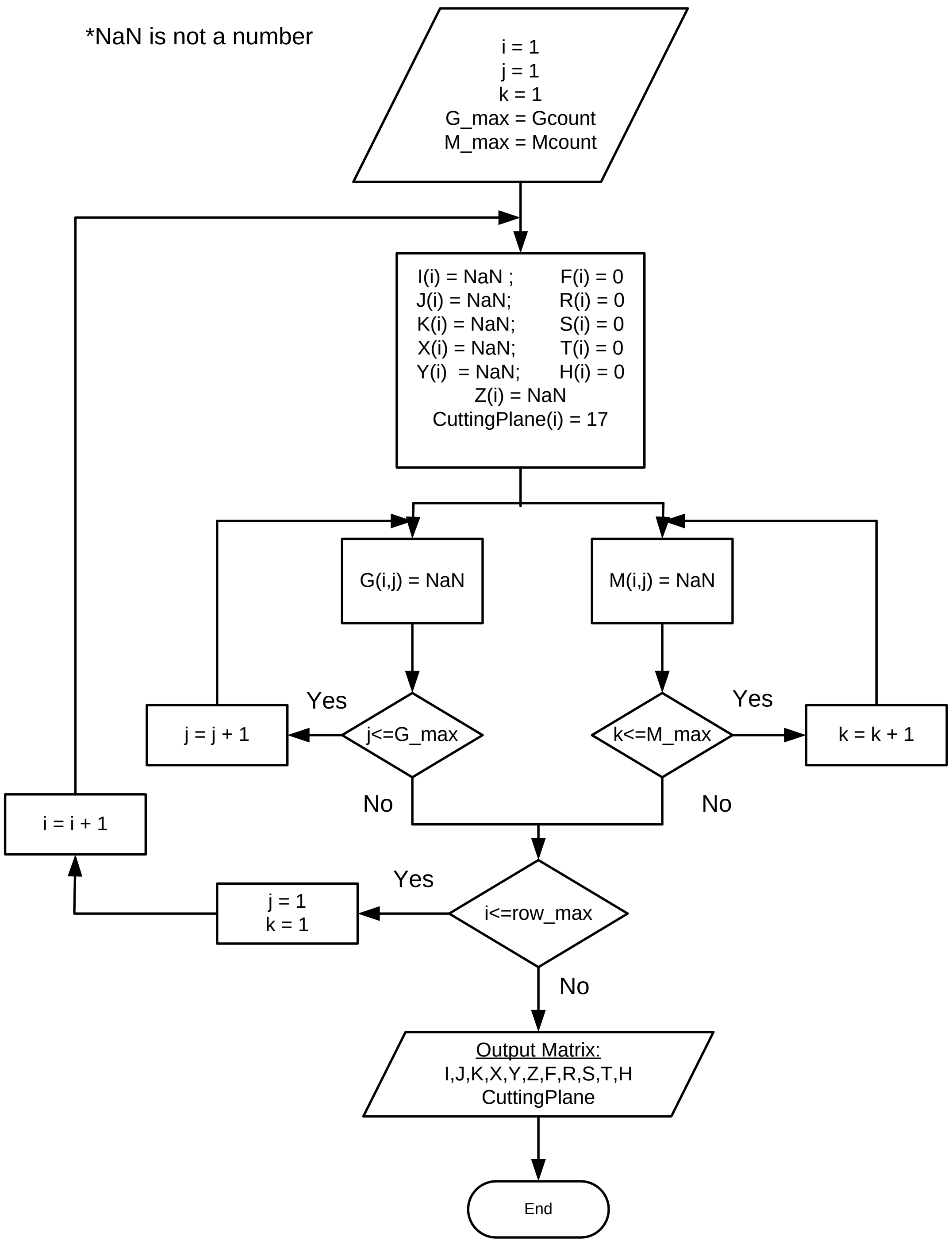

Figure 4.7 Flow chart of matrix preparation for the corresponding character address of an NC program

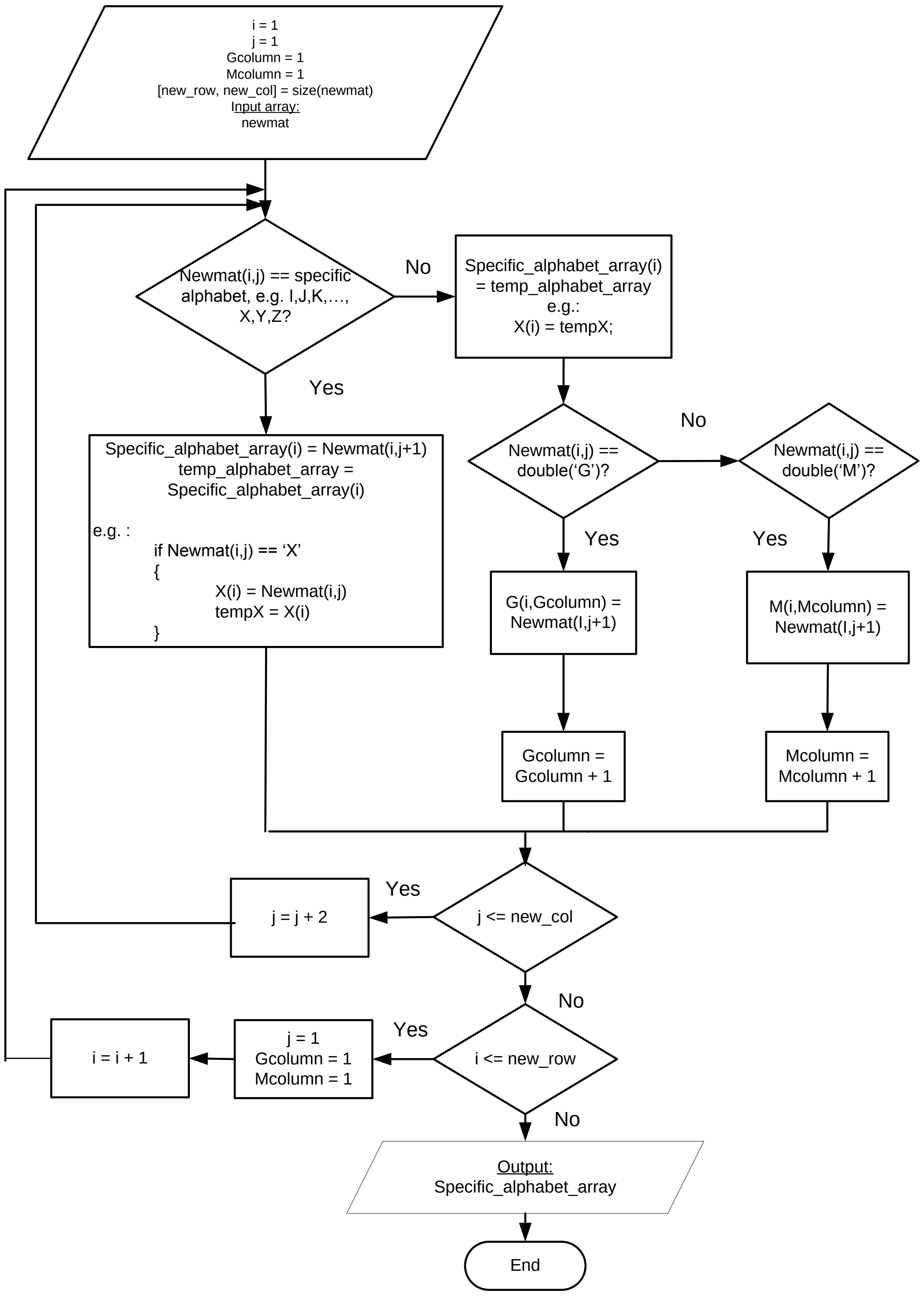
i = 1
j = 1
Gcolumn = 1
Mcolumn = 1
[new_row, new_col] = size(newmat)
Input array:
newmat
Newmat(i,j) == specific alphabet, e.g. I,J,K,…, X,Y,Z?
No
Specific_alphabet_array(i) = temp_alphabet_array e.g.: X(i) = tempX;
Yes
Specific_alphabet_array(i) = Newmat(i,j+1)
temp_alphabet_array = Specific_alphabet_array(i)
e.g. :
if Newmat(i,j) == 'X'
{
X(i) = Newmat(i,j)
tempX = X(i)
}
Newmat(i,j) == double('G')?
No
Newmat(i,j) == double('M')?
Yes
Yes
G(i,Gcolumn) = Newmat(I,j+1)
M(i,Mcolumn) = Newmat(I,j+1)
Gcolumn = Gcolumn + 1
Mcolumn = Mcolumn + 1
Yes
j = j + 2
j <= new_col
No
Yes
i = i + 1
j = 1
Gcolumn = 1
Mcolumn = 1
i <= new_row
No
Output:
Specific_alphabet_array
End

Figure 4.8 Flow chart of algorithm to assign the value of character addresses of an NC program to the respective character addresses matrix array

The purpose of the identification algorithm is to ensure that the post-processor can recognize important G-codes, namely, G17, G18 and G19. G17 is the selection of the X-Y plane as the machining plane, which is the default setting. G18 is the selection of the X-Z plane as the main machining plane for circular interpolation movements and/or cutter compensation. This G18 code changes the default machining plane to the X-Z plane where Y-axis is the secondary axis and it works perpendicularly to the X-Z plane. In the X-Z plane, it is possible to cut convex or concave surfaces using the G02 and G03 circular interpolation commands. It should be noted that since the X- and Z-axes are the primary axes instead of the X- and Y-axes, the radius is no longer expressed in terms of I and J (distance from the start-point to the center-point; refer to G02 and G03 in Table 5.3) but in terms of I and K. In addition, the determination of the direction of travel of the tool is based on the view of the user towards the two axes from the Y+ direction, in the same way as the user looks at the X- and Y-axes from the Z+ axis in the G17 plane. When using the G02 and G03 commands, the primary and secondary axes are reversed. This means that G02 will look like a counterclockwise arc and G03 will look like a clockwise arc.

After arranging the values corresponding to the characters, the machining coordinates can be arranged according to the instructions provided by the 'G' and 'M' codes. Firstly, the post-processor determines the presence of G90 (absolute coordinates) or G91 (incremental coordinates), by scanning through the array of the G-codes line-by-line. It helps to determine whether a block command is defined as absolute or incremental coordinate as shown in the flow chart of Figure 5.9. G90 is the default setting.

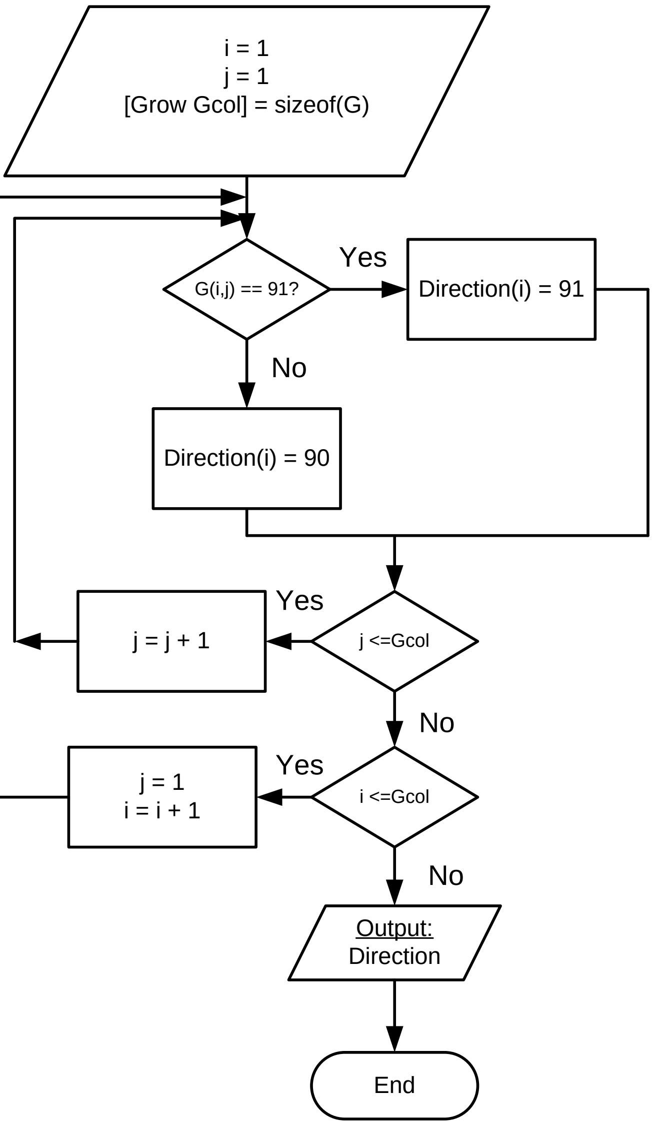

Figure 4.9 Flow chart of algorithm to determine the characteristics of the coordinate system

Thus, by knowing the coordinate system of the NC program, the values of the Cartesian coordinate system of NC program can be determined with respect to

X-coordinate, Y-coordinate and Z-coordinate absolutely or relatively as shown in the flow chart in Figure 4.10.

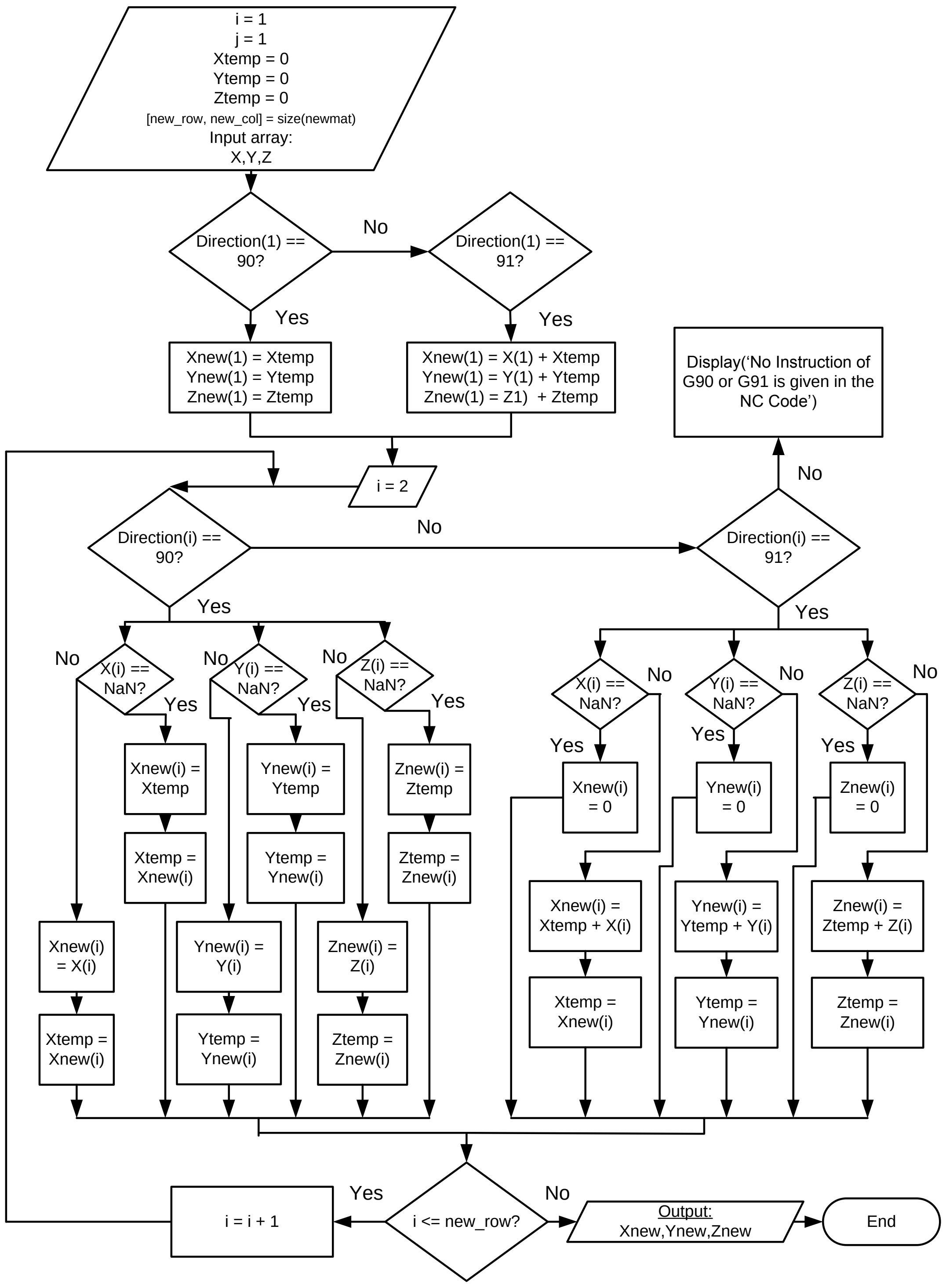

Figure 4.10 Flow chart of algorithm to determine the values of X-, Y- and Z-coordinates

After determining the coordinate system and values of X, Y and Z-coordinates of the NC program, the machining plane is verified. In G-codes, G17, G18 and G19 represent machining on the X-Y plane, Z-X plane and Y-Z plane respectively. Hence, an array with respect to a block command is created to record the cutting plane for each line of NC program. The next step is to determine the style of cutting path of the cutter. This depends on the specified G-code. G0 is rapid transverse positioning, G01 is for linear interpolation, G02 is clockwise circular path and G03 is counter-clockwise circular path. The flow chart of Figure 4.11 illustrates this algorithm.

After the circular arc values are calculated according to the flow chart in Figure 4.12, the X-, Y- and Z-coordinates of the NC path will be determined according to the G0, G1 and G2 instructions. Since the pseudo algorithm is too lengthy, only certain commands are shown below, and the entire pseudo codes are provided in **Appendix B**. A few conditions need to be evaluated before determining the coordinates of the tool path. As shown in Figure 4.13, the corresponding new X-, Y- and Z-coordinates are obtained through the provided condition of the machining plane and the circular value determined through the G-code of the NC program.

In addition, the values processed through the algorithm of the flow chart in Figure 4.13 are read into a new matrix array named Trajectory as shown in Figure 4.13. The Trajectory matrix consists of the information of the coordinates for 3D machining, X-, Y- and Z-coordinates, feed rate, Spindle speed, I, J and K values as well as the R values.

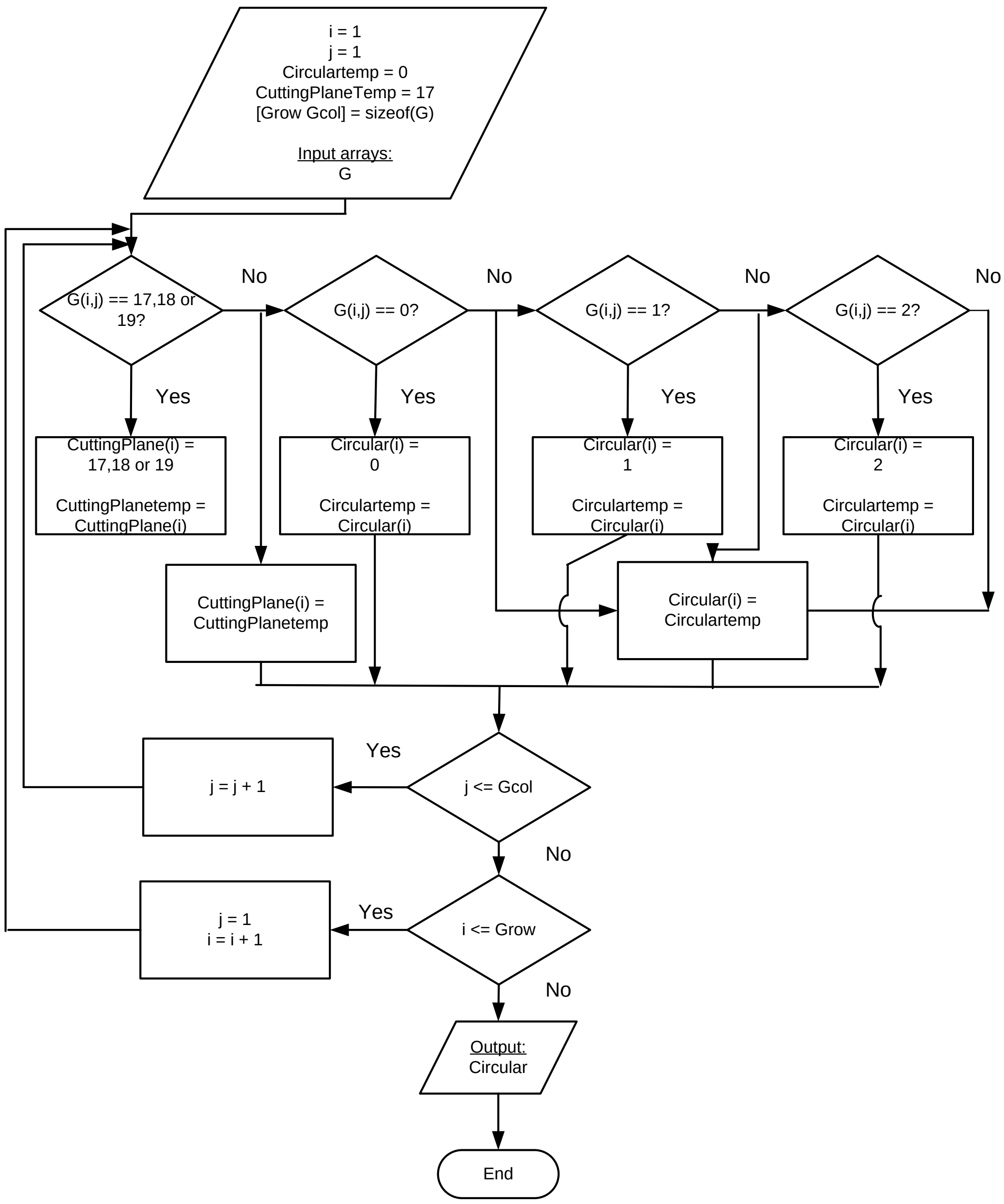

Figure 4.11 Flow chart of algorithm to determine the cutting plane and the style of the cutting path

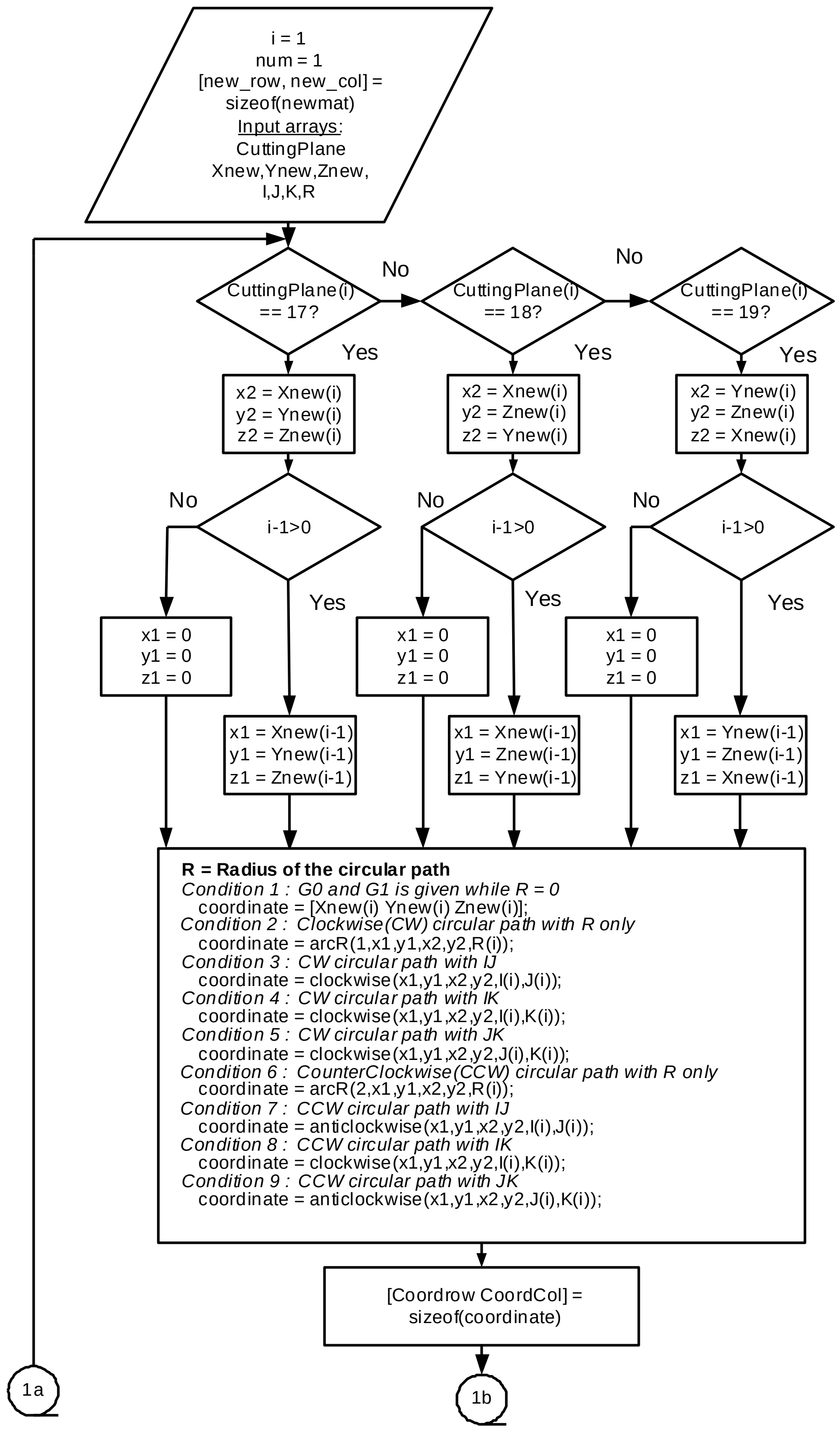

R = Radius of the circular path
Condition 1 : G0 and G1 is given while R = 0
coordinate = [Xnew(i) Ynew(i) Znew(i)];
Condition 2 : Clockwise(CW) circular path with R only
coordinate = arcR(1,x1,y1,x2,y2,R(i));
Condition 3 : CW circular path with IJ
coordinate = clockwise(x1,y1,x2,y2,I(i),J(i));
Condition 4 : CW circular path with IK
coordinate = clockwise(x1,y1,x2,y2,I(i),K(i));
Condition 5 : CW circular path with JK
coordinate = clockwise(x1,y1,x2,y2,J(i),K(i));
Condition 6 : CounterClockwise(CCW) circular path with R only
coordinate = arcR(2,x1,y1,x2,y2,R(i));
Condition 7 : CCW circular path with IJ
coordinate = anticlockwise(x1,y1,x2,y2,I(i),J(i));
Condition 8 : CCW circular path with IK
coordinate = clockwise(x1,y1,x2,y2,I(i),K(i));
Condition 9 : CCW circular path with JK
coordinate = anticlockwise(x1,y1,x2,y2,J(i),K(i));

Figure 4.12(a) Flow chart of algorithm to convert NC program to machine trajectory

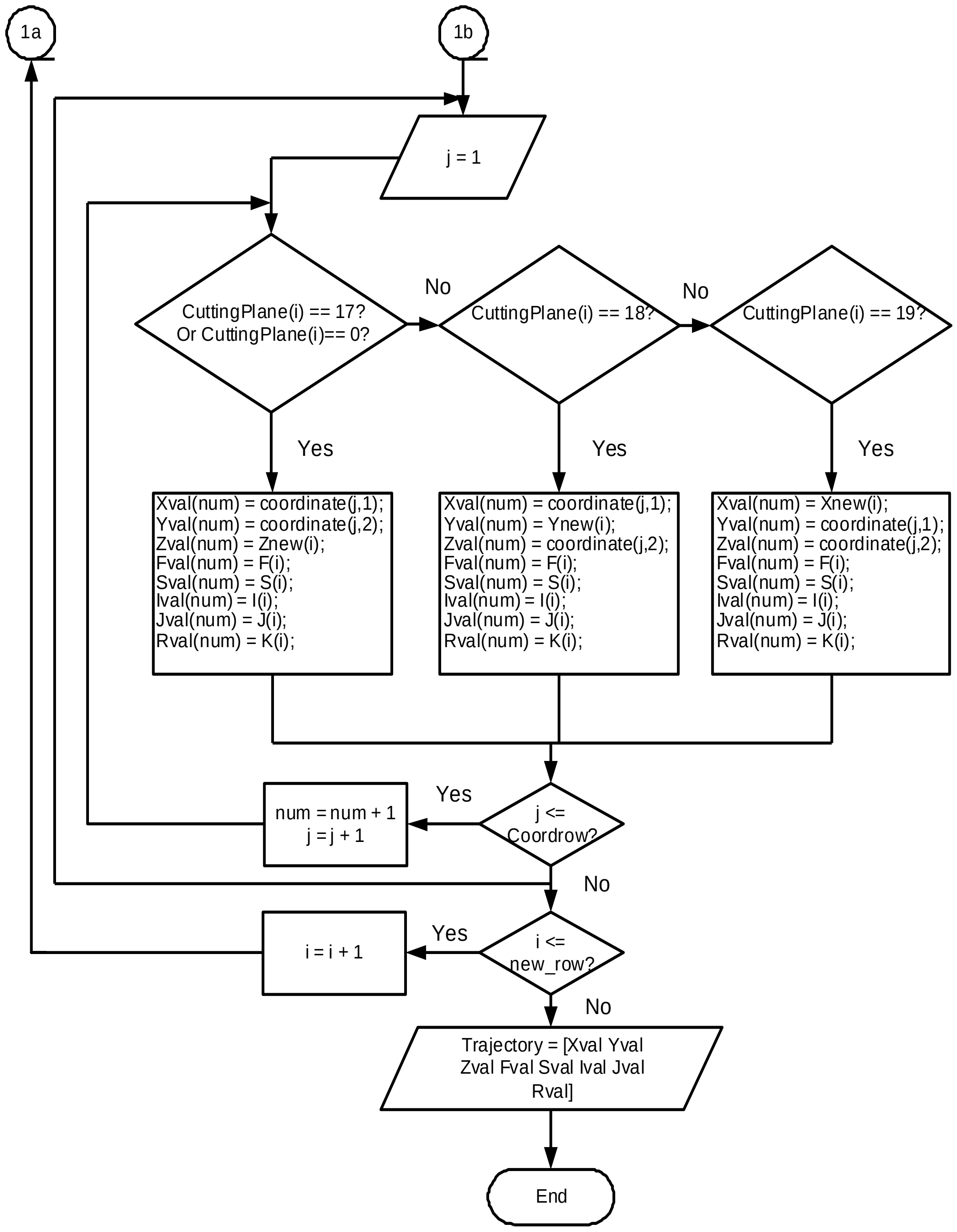
1a
1b
j = 1
CuttingPlane(i) == 17? Or CuttingPlane(i)== 0?
No
CuttingPlane(i) == 18?
No
CuttingPlane(i) == 19?
Yes
Yes
Yes
Xval(num) = coordinate(j,1); Yval(num) = coordinate(j,2); Zval(num) = Znew(i); Fval(num) = F(i); Sval(num) = S(i); Ival(num) = I(i); Jval(num) = J(i); Rval(num) = K(i);
Xval(num) = coordinate(j,1); Yval(num) = Ynew(i); Zval(num) = coordinate(j,2); Fval(num) = F(i); Sval(num) = S(i); Ival(num) = I(i); Jval(num) = J(i); Rval(num) = K(i);
Xval(num) = Xnew(i); Yval(num) = coordinate(j,1); Zval(num) = coordinate(j,2); Fval(num) = F(i); Sval(num) = S(i); Ival(num) = I(i); Jval(num) = J(i); Rval(num) = K(i);
num = num + 1 j = j + 1
Yes
j <= Coordrow?
No
i = i + 1
Yes
i <= new_row?
No
Trajectory = [Xval Yval Zval Fval Sval Ival Jval Rval]
End

Figure 4.12(b) Flow chart of algorithm to convert NC program to the machine trajectory

Subsequently, a trajectory path of the Stewart Platform can be obtained according to the machine trajectory generated by following the instructions in an

NC program as shown in the flow chart of Figure 4.12. Since only 3-axis machining is considered in this conversion algorithm, the rotational angle around X-, Y- and Z-axes can be ignored and assumed to be zero while the X-, Y- and Z-coordinates of the manipulation of the Stewart Platform can follow the machining trajectory path, as shown in Figure 4.13.

X	Y	Z	Roll	Pitch	Yaw	Feedrate
0	0	0	0	0	0	32.0000
0	0	0	0	0	0	32.0000
0	0	0	0	0	0	32.0000
0	0	0	0	0	0	32.0000
0	0	0	0	0	0	32.0000
45.3020	125.4530	0	0	0	0	32.0000
45.3020	125.4530	10.0000	0	0	0	32.0000
45.3020	125.4530	2.0000	0	0	0	32.0000

Figure 4.13 Trajectory path of a Stewart Platform translated from an NC program

4.3 Case study: pocketing process

The post-processor was tested and verified based on actual machining operations performed on the Stewart Platform. A pocketing path was first modeled using MasterCam and the required NC program was generated. The NC program was converted into the trajectory path of the Stewart Platform using the post-processor developed using MATLAB®. The trajectory path was executed on the Stewart Platform. Although the resulting trajectory path consists of more than 500 lines of commands, the platform is able to move smoothly. The pocketing process is shown in Figure 4.14. Firstly, the workpiece outline can be either imported from CAD model generated from SolidWorks or plotted directly in MasterCam. Next, MasterCam can be used to generate the tool cutting path. The simulation of the cutting path was run in MasterCam and a NC program was generated through the

MasterCam. By obtaining the NC program through the post-processor of MasterCam, the Stewart Platform trajectory path can be generated using MATLAB®. After the trajectory path was generated, it was implemented and the Stewart Platform was manipulated to machine the workpiece based on the contouring process. The sequences of the conversion of the NC codes of CAD/CAM software to the trajectory path recognized by Stewart Platform are shown in Figure 4.14(a-e).

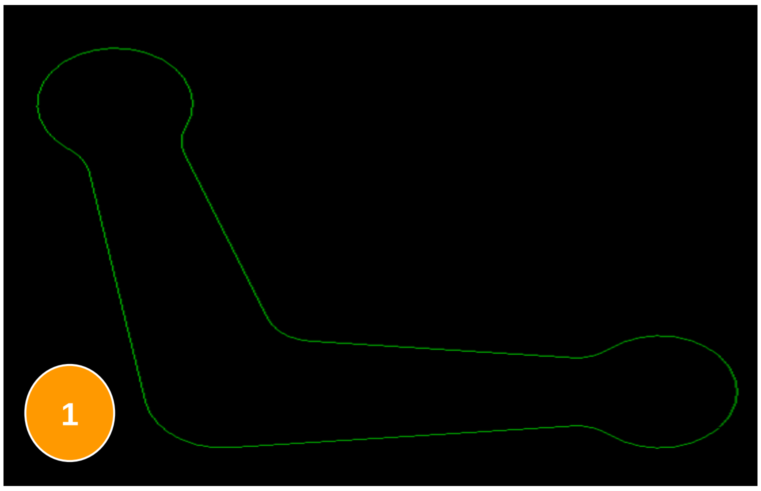

Figure 4.14(a) The pocketing machining process: plot outline in MasterCam

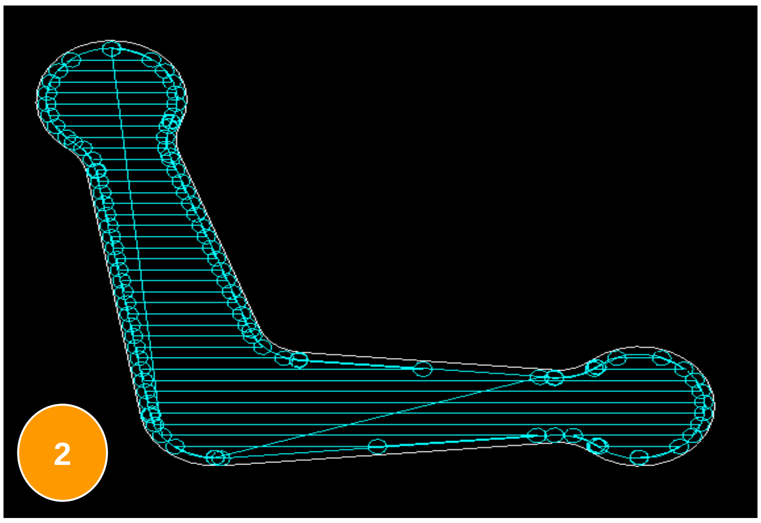

Figure 4.14(b) The pocketing process: MasterCam generate the tool cutting path

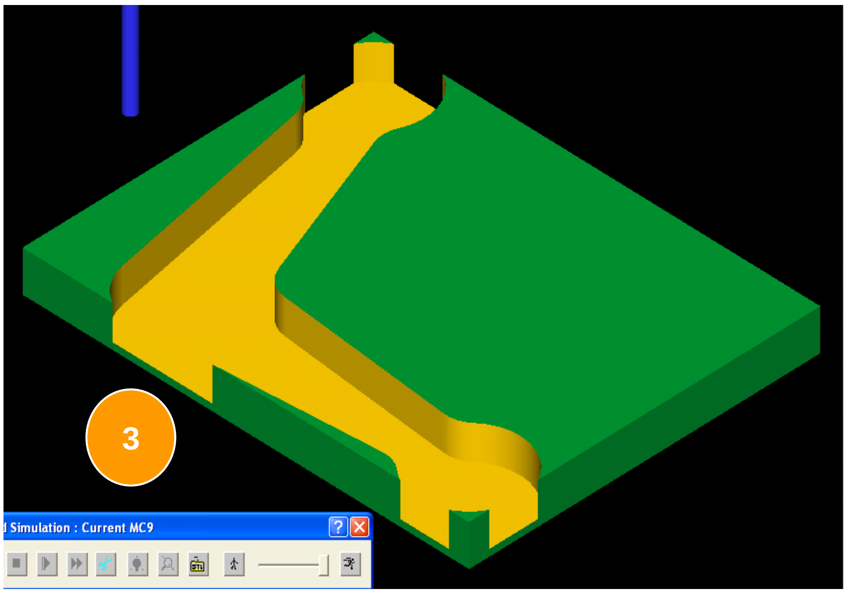

Figure 4.14(c) The pocketing process: Simulation of cutting path in MasterCam

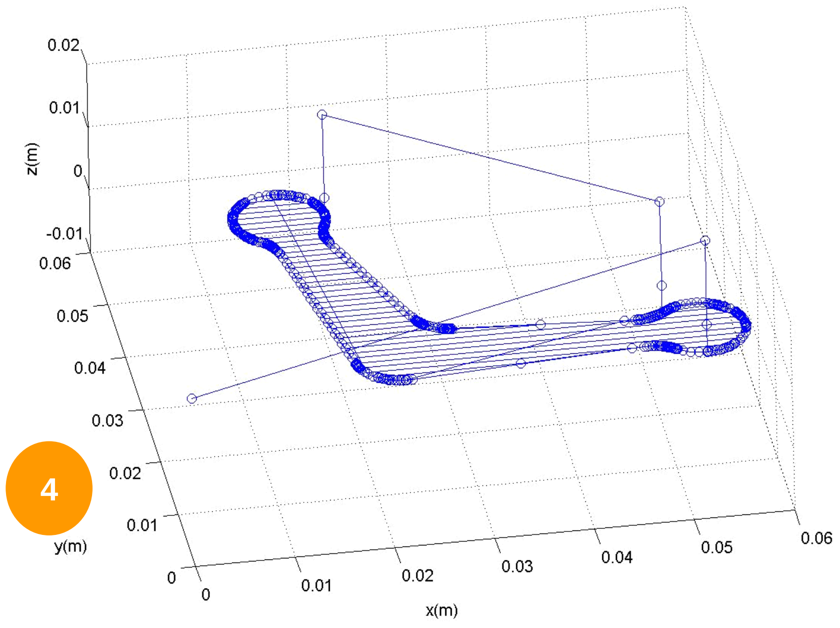

Figure4.14(d) The pocketing process: Generate trajectory path

through MATLAB®

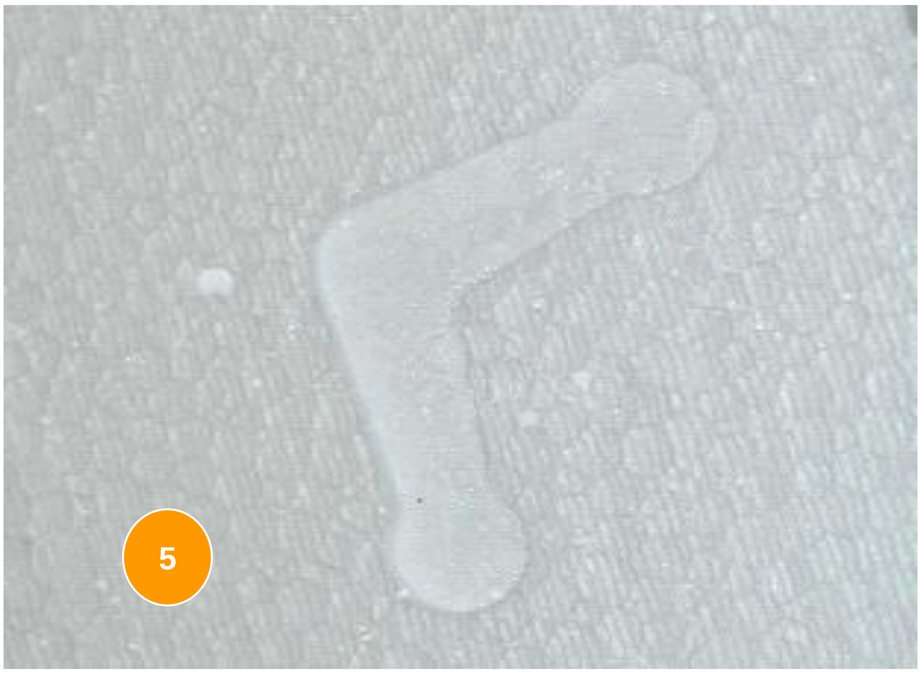

Figure 4.14(e) The pocketing process: Machine workpiece through the contouring process

4.4 Case study: three-axis machining

NC program conversion for 3D machining paths was also developed using MATLAB®. As shown in Figure 4.15, a 3D hemi-sphere milling path was generated for a 3D NC program generated from the MasterCam.

A trajectory path for the rough cut was first generated to machine the outline of the surface of the workpiece using a flat end milling cutter. Next, a trajectory path for the finishing cut was generated for machining the surface of the workpiece using a ball-end milling cutter. Figure 4.16 shows the outcome of the machining performed on a Stewart Platform.

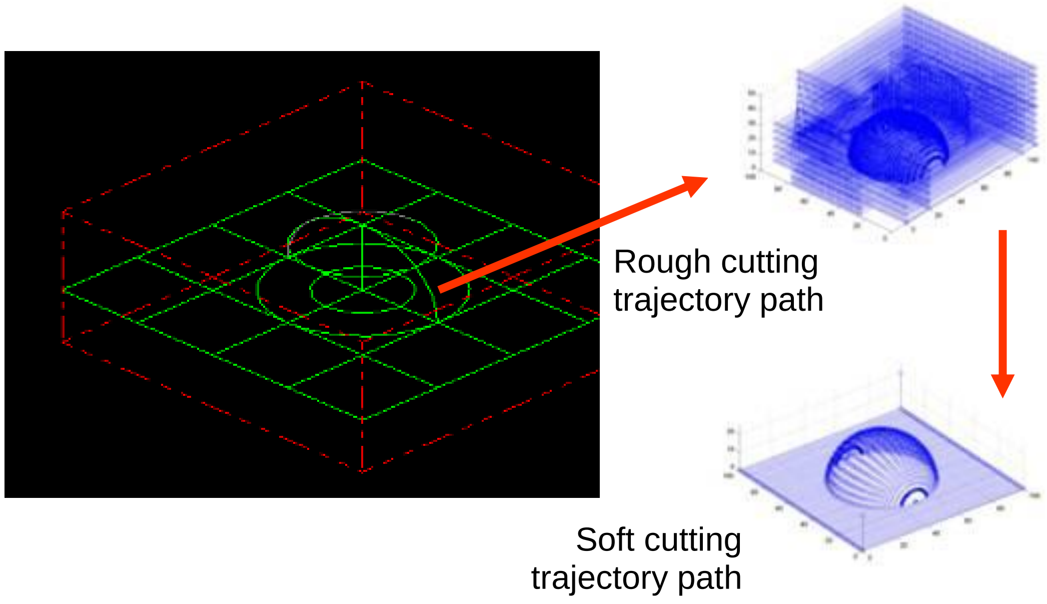

Figure 4.15 3D cutting path generated from the NC program created from model in MasterCam

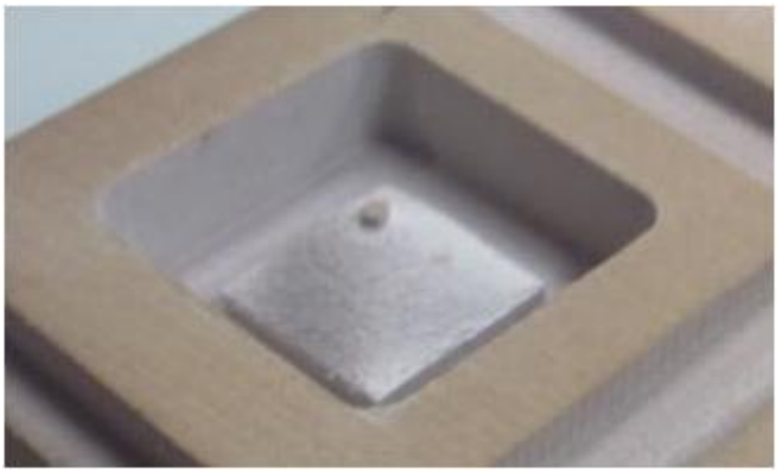

Figure 4.16 Outcome of machining on a Stewart Platform

Chapter 5 Five-axis machining

5.1 Introduction

As described in Chapter 4, 3-axis machining can be performed easily on a Stewart Platform due to the common characteristics shared by parallel kinematics manipulators and CNC machines. Hence, minimum effort is required to convert an NC program from a SolidWorks file to the trajectory path of the Stewart Platform. Stewart Platforms can be manipulated to perform translation motion for 3-axis machining in the same manner as a serial manipulator since the end-effectors of both systems are rigid bodies.

However, many considerations need to be looked into due to the fundamental mechanical design differences between 5-axis CNC machines and Stewart Platforms, especially when there are rotational movements. This is due to the fact that the joint errors of the serial manipulators are accumulated and amplified from joints between links because all joints are dependent on each other and they are open loop chains. Hence, rotational motions of the joints will give rise to complicated coordinates of the end-effector. Similarly, Stewart Platforms can provide very straight-forward joint manipulation because the rotation and translation of the end-effector can be converted to the joint movement of the actuator easily using the inverse kinematics algorithm. As a result, Stewart Platforms have greater advantages over serial manipulators and they can be controlled easily for 5-axis machining. However, there are some disadvantages of

Stewart Platforms, such as a limited workspace and limited working angles of the joints. The limited working angles of the joints can be avoided if it is used for mold machining.

In most CAD systems, 3D freeform surfaces are usually described by parametric surface patches, such as NURBS (Non-Uniform Rational B-Splines), B-spline and Bézier types [Mortenson, 1985; Piegl, 1991; Faux and Pratt, 1979]. However, these mathematical methods are not suitable for NC machining since in NC machining, a sequence of straight lines is implemented to approximate the freeform surfaces with various curvatures, as shown in Figure 5.1 [Liang, 2002].

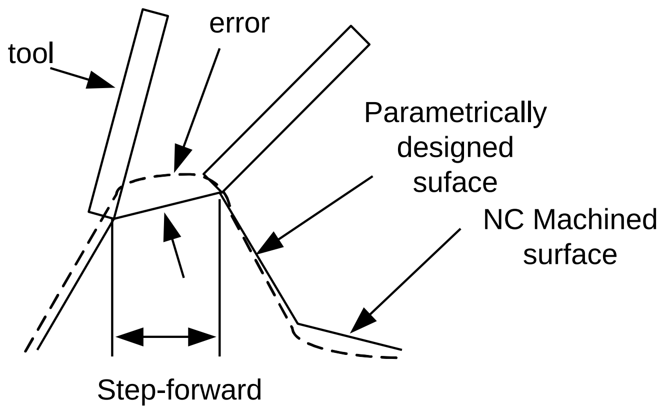

Figure 5.1 Geometric error associated with tolerance between freeform surface and designed surface

As shown in Figure 5.1, the geometric error between the parametric surface and the machine surface is dependent on the step forward distance and the surface curvature. Although a freeform surface can be defined using the iso-parametric method, it is difficult to determine the step over distance between adjacent tool paths, as a constant step over distance in the parametric space does not generally generate a constant step over distance in the Cartesian space (Figure 5.2). As a result, unpredictable cusp heights between the adjacent tool paths will generate missing cutting area which will affect the quality of the machined surface. The iso-parametric method will divide the cutting surface into numerous patches. The non-continuity between two adjacent patches will lose necessary surface parameter information through the constant step over cutting path.

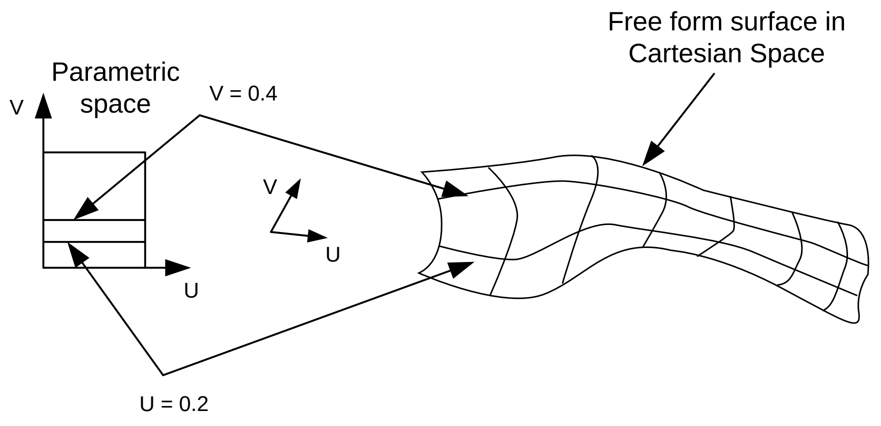

Figure 5.2 A constant step over distance in the parametric space does not generally yield a constant step over in the Cartesian space [Liang, 2002]

The triangular tessellation method is a promising approximation method that can solve these drawbacks. This method was first proposed by Drysdale and Ozair [1991].

As shown in Figure 5.3, using the triangular tessellation method can provide more details of the curvature surface of the designed CAD surface with higher resolution of triangular nodes of the workpiece. Thus, the machining error can be minimized as long as the cutting tool moves on the triangles. Based on the model presented in CAD/CAM systems, the deviation of each surface can be set as a very small value, such as 0.3-2 μm. A common file format for 3D tessellated models is the STL format. An STL file is a triangular representation of a 3D surface. It is suitable for communicating the geometry data for NC programming.

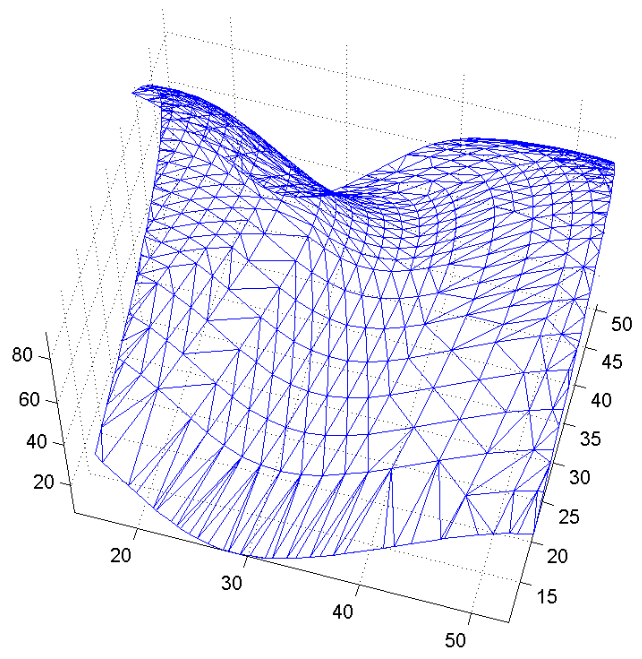

Figure 5.3 Triangular tessellated freeform surface

The surface of the model is tessellated into a series of small triangles (faces). Each triangle is defined by a normal of unit length and three vertices, as shown in Figure 5.4.

The corners are described by the [X_1 Y_1 Z_1 1], [X_2 Y_2 Z_2 1] and [X_3 Y_3 Z_3 1] coordinates. The determination of the normal of the triangle can be achieved by first determining the vectors of the triangle from P1 to P2 and from P1 to P3, which are $[V_{x1}\ V_{y1}\ V_{z1}\ 0] = [X_2\text{-}X_1\ Y_2\text{-}Y_1\ Z_2\text{-}Z_1\ 0]$ and $[V_{x2}\ V_{y2}\ V_{z2}\ 0] = [X_3\text{-}X_1\ Y_3\text{-}Y_1\ Z_3\text{-}Z_1\ 0]$. Thus, the normal of the triangle is $V_n = [X_n\ Y_n\ Z_n\ 0] = [V_{x1}\ V_{y1}\ V_{z1}\ 0] \times [V_{x2}\ V_{y2}\ V_{z2}\ 0]$. The length of the normal of the triangle is $L_n = \sqrt{X_n^{\,2} + Y_n^{\,2} + Z_n^{\,2}}$. Hence, the unit vector of the normal is V_n/L_n. The orientation of the triangle is based on the right hand rule which direction of the unit vector of the triangle is always pointing outwards while the vertices are defined in the counterclockwise direction.

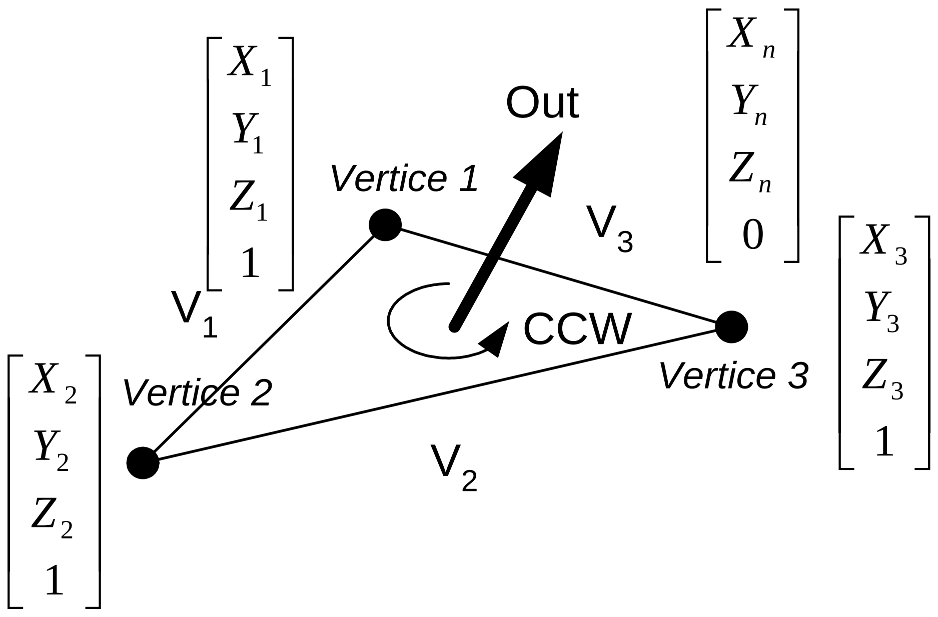

$\begin{bmatrix} X_1 \\ Y_1 \\ Z_1 \\ 1 \end{bmatrix}$
Out
$\begin{bmatrix} X_n \\ Y_n \\ Z_n \\ 0 \end{bmatrix}$
Vertice 1
V_3
$\begin{bmatrix} X_3 \\ Y_3 \\ Z_3 \\ 1 \end{bmatrix}$
V_1
CCW
$\begin{bmatrix} X_2 \\ Y_2 \\ Z_2 \\ 1 \end{bmatrix}$
Vertice 2
Vertice 3
V_2

Figure 5.4 Standard triangular representation of STL model

However, there are disadvantages associated with tessellated surfaces, such as accuracy and resolution. Accuracy is an issue since a tessellated surface is an approximation of the original surface such that the curve surfaces are uneven as they are formed by a collection of lines and points. In NC machining, the contouring movements are composed of linear movements. Hence, the triangular dimension resolution of the tessellated surfaces can be improved to 0.001mm to reduce the unevenness.

The number of triangles and the resolution applied to the original surfaces will determine the size of an STL file. Normally, the size of the file is inversely proportional to the resolution level and proportional to the number of triangles. STL files can be generated in two formats, namely, the ASCII and binary formats. In this research project, the ASCII format is chosen because this format can be easily read with any text editor and errors can be spotted easily. In addition, the ASCII format of the STL file can be easily interpreted by the MATLAB® and converted into an array of vertices of the tessellated triangles and translated into the suitable trajectory path.

Another issue needs to be considered is the edit-ability of the STL files. This is due to the fact that when the STL files are exported from the CAD/CAM system, it is very hard to perform any further modification. Thus, the CAM system must rely on the CAD system to produce a good quality STL representation and suitable tolerance. The tolerance of the tessellated surfaces must be chosen in anticipation of the tightest machining tolerance under a particular specification.

5.2 Planar tool paths

Since the step over distance using iso-parametric method is hard to apply in the generation of tool paths, parallel cutting planes can be used to generate tool paths instead. The advantages of implementing planar movement are that it can overcome the topological inconsistencies such as overlapping of surface patches, small gaps between surface patches.

Data from the STL model are used by an algorithm to slice the tessellated surface by perpendicular cutting planes with predefined interval. The intercepted coordinates between the tessellated surface and the cutting plane will determine the 2D cross-sections of the 3D STL models. It could readily be turned into a physical prototype for Rapid Prototyping (RP) machines. Since these slicing planes are quite similar to that of a NC milling tool path, the cutting plane principles used in RP can be applied to the construction of planar tool paths on the STL freeform surfaces.

In this research, a flat-end milling cutter is used instead of a ball-end milling cutter for 5-axis machining since the focus is on the milling of surfaces with limited curvature profiles due to the limited working angle of the Stewart Platform. The flat-end milling cutter has a more effective radius and a larger cutting area so that more materials can be removed than using a ball-end milling cutter. Hence, it can provide a higher productivity. A flat-end milling cutter is also more suitable for producing large and complex parts, such as turbines. However, a flat-end cutter has the potential problem of accidentally cutting an adjacent feature due to tool collision. Thus, in this study the experiment is focused on dealing with less intricate features.

5.3 Cutter contact point generation

Cutter contact points (CC Points) are the intersection points between the planar cutting planes and the triangular face edges. The intersections can happen at the edges or at the vertices of the triangles as shown in Figure 5.5. Hence, the cutting tool will be touching the surfaces of the workpiece where the CC points are allocated along the tool paths.

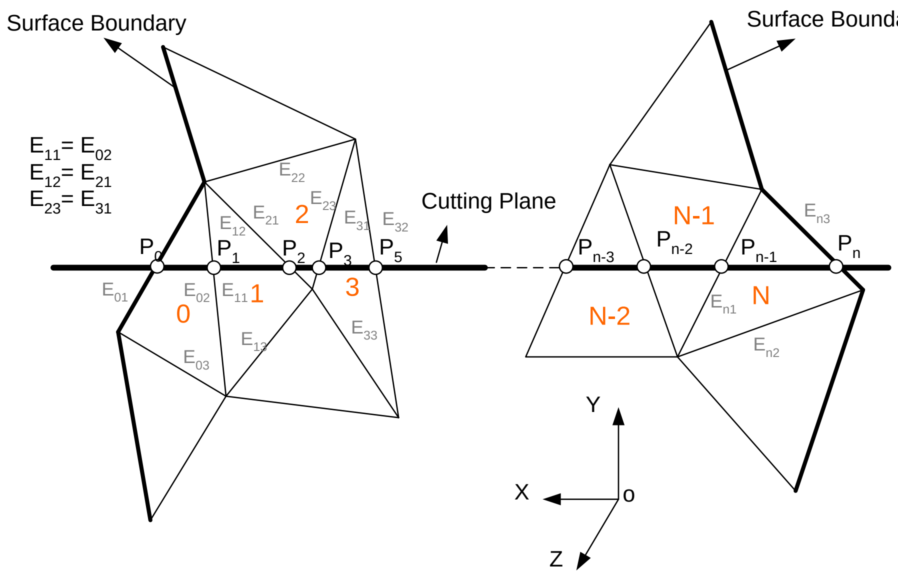

Figure 5.5 Generation of CC points

During the process of generation of the CC points, the cutting plane direction is first chosen. In this algorithm, the cutting plane is chosen to be parallel to the X-Z plane of the machine coordinate system. The bold lines in Figure 5.5 indicate the boundary of the surface of the workpiece. Triangles 0 to N represent the triangles on the surface that intersect with the cutting plane. CC points are denoted as P_0 to P_n, which are the intersection points of the cutting plane with the edges of the triangles along the cutting plane. When P_0 lies on the edge E_{01} of Triangle 0 as shown in Figure 5.5, the next CC point P_1 should lie on the one of the remaining two edges E_{02} or E_{03} of Triangle 0. If P_1 is found on E_{03}, the next step would be to determine whether there is another face sharing the same edge as Triangle 0. Assuming that Triangle 1 shares edge E_{03} with Triangle 0, and that edge is E_{11}, the search continues with the remaining two edges of Triangle 1, E_{12} and E_{13} to check for intersection with the cutting plane. Suppose that E_{12} contains the third CC point P_2, the search goes on to find the triangle that shares E_{12} with Triangle 1. For the last CC point, P_n which is located at the boundary of the surface, there would be no adjacent triangle that shares E_{n3}. Hence, the search will end at $P_{n.}$ The tool path is finally obtained by connecting all the CC points, from P_0 to P_n.

The identification of the intersecting coordinates of the faces and the planes can be illustrated in the simple algorithm as shown in Figure 5.6. Normally in the tessellated triangles of the freeform surface as shown in Figure 5.6, certain faces will intersect with the specific cutting plane. The intersected face has maximum three edges contact with the cutting plane in three intersected points. The intersected point can be verified by the factor α. Factor α can be defined by knowing the cutting plane and vertices of the intersected triangle. By using simple vector geometry calculation, as long as $\alpha >= -1$ and $\alpha <= 0$, the intersected points will stay within the length of the edge of the triangle. Similarly, the intersected points will be located at the coordinate which is not within the edge length of the triangle as shown by IP_1 in the diagram.

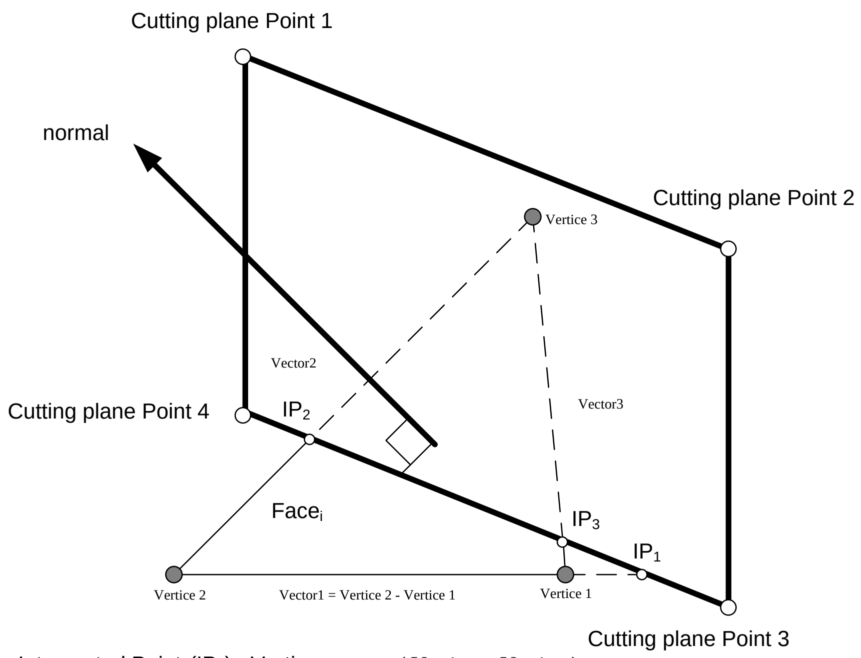

Intersected Point$_1$(IP$_1$)= Vertice$_1$ + α_1 x (Vertice$_2$ - Vertice$_1$)

Intersected Point$_2$(IP$_2$)= Vertice$_2$ + α_2 x (Vertice$_3$ - Vertice$_2$)

Intersected Point$_3$(IP$_3$)= Vertice$_3$ + α_3 x (Vertice$_3$ - Vertice$_1$)

Figure 5.6 Determination of the intersection points between the cutting plane and the face on the freeform surface

Based on the described principles, the CC points can be determined by knowing the arrays of the faces and vertices of the tessellated triangles on the freeform surface. Furthermore, the cutting plane is defined by obtaining points parallel to the X-Z plane that are intersected with the freeform surface while the step-over distances are noted. Hence, through the determination of the intersected points of the faces with the corresponding cutting planes, a cutting trajectory of specific coordinates can be retrieved as shown in the flow chart in Figure 5.7. Hence, using this method, the coordinates and orientation of the intersected points can be verified with respect to the cutting plane.

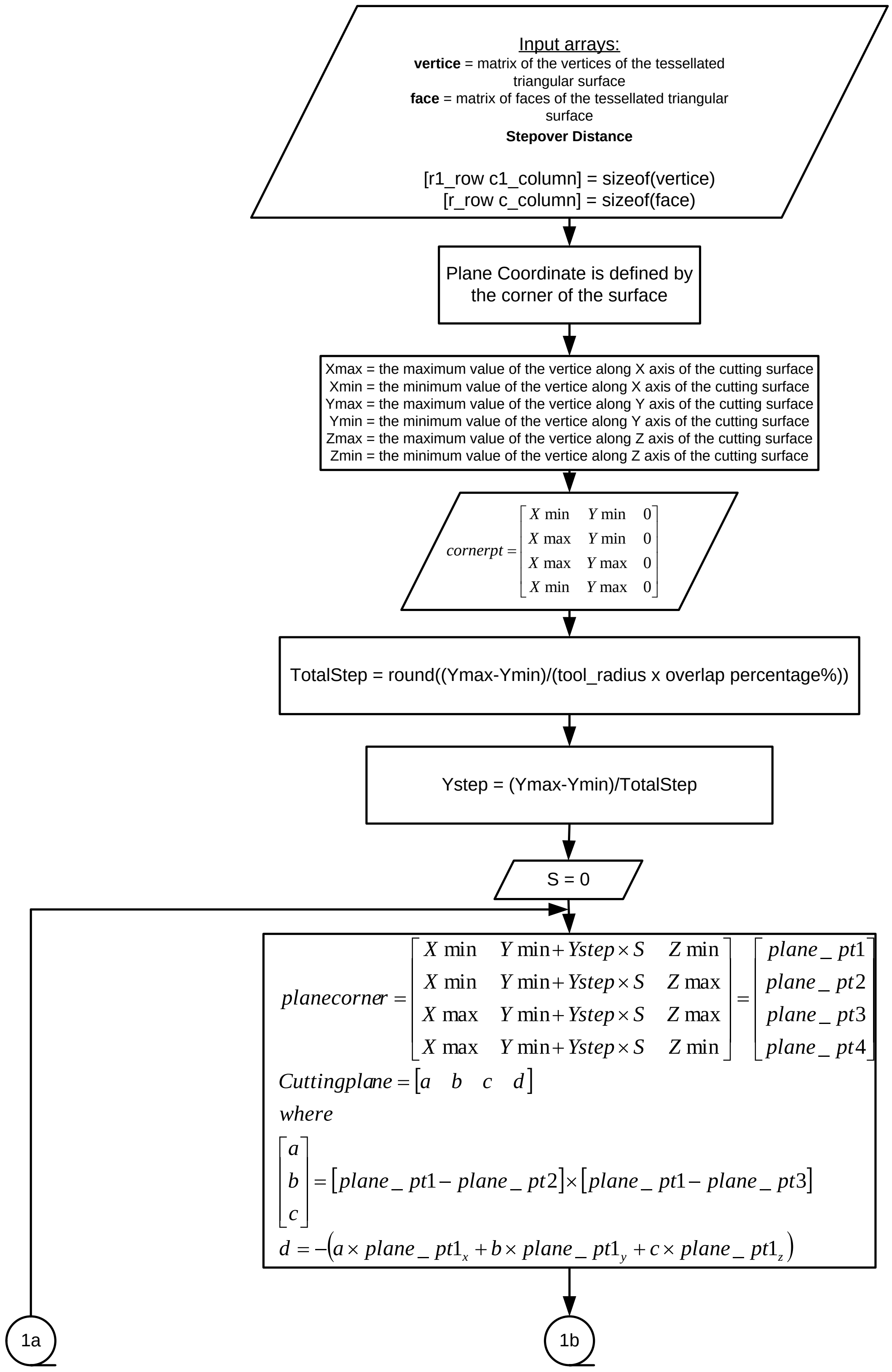
Input arrays:
vertice = matrix of the vertices of the tessellated triangular surface
face = matrix of faces of the tessellated triangular surface
Stepover Distance
[r1_row c1_column] = sizeof(vertice)
[r_row c_column] = sizeof(face)
Plane Coordinate is defined by the corner of the surface
Xmax = the maximum value of the vertice along X axis of the cutting surface
Xmin = the minimum value of the vertice along X axis of the cutting surface
Ymax = the maximum value of the vertice along Y axis of the cutting surface
Ymin = the minimum value of the vertice along Y axis of the cutting surface
Zmax = the maximum value of the vertice along Z axis of the cutting surface
Zmin = the minimum value of the vertice along Z axis of the cutting surface
$cornerpt = \begin{bmatrix} X\min & Y\min & 0 \\ X\max & Y\min & 0 \\ X\max & Y\max & 0 \\ X\min & Y\max & 0 \end{bmatrix}$
TotalStep = round((Ymax-Ymin)/(tool_radius x overlap percentage%))
Ystep = (Ymax-Ymin)/TotalStep
S = 0
$planecorner = \begin{bmatrix} X\min & Y\min + Ystep \times S & Z\min \\ X\min & Y\min + Ystep \times S & Z\max \\ X\max & Y\min + Ystep \times S & Z\max \\ X\max & Y\min + Ystep \times S & Z\min \end{bmatrix} = \begin{bmatrix} plane\_pt1 \\ plane\_pt2 \\ plane\_pt3 \\ plane\_pt4 \end{bmatrix}$
$Cuttingplane = [a \quad b \quad c \quad d]$
where
$\begin{bmatrix} a \\ b \\ c \end{bmatrix} = [plane\_pt1 - plane\_pt2] \times [plane\_pt1 - plane\_pt3]$
$d = -(a \times plane\_pt1_x + b \times plane\_pt1_y + c \times plane\_pt1_z)$
1a
1b

Figure 5.7(a) Flow chart for the generation of CC points

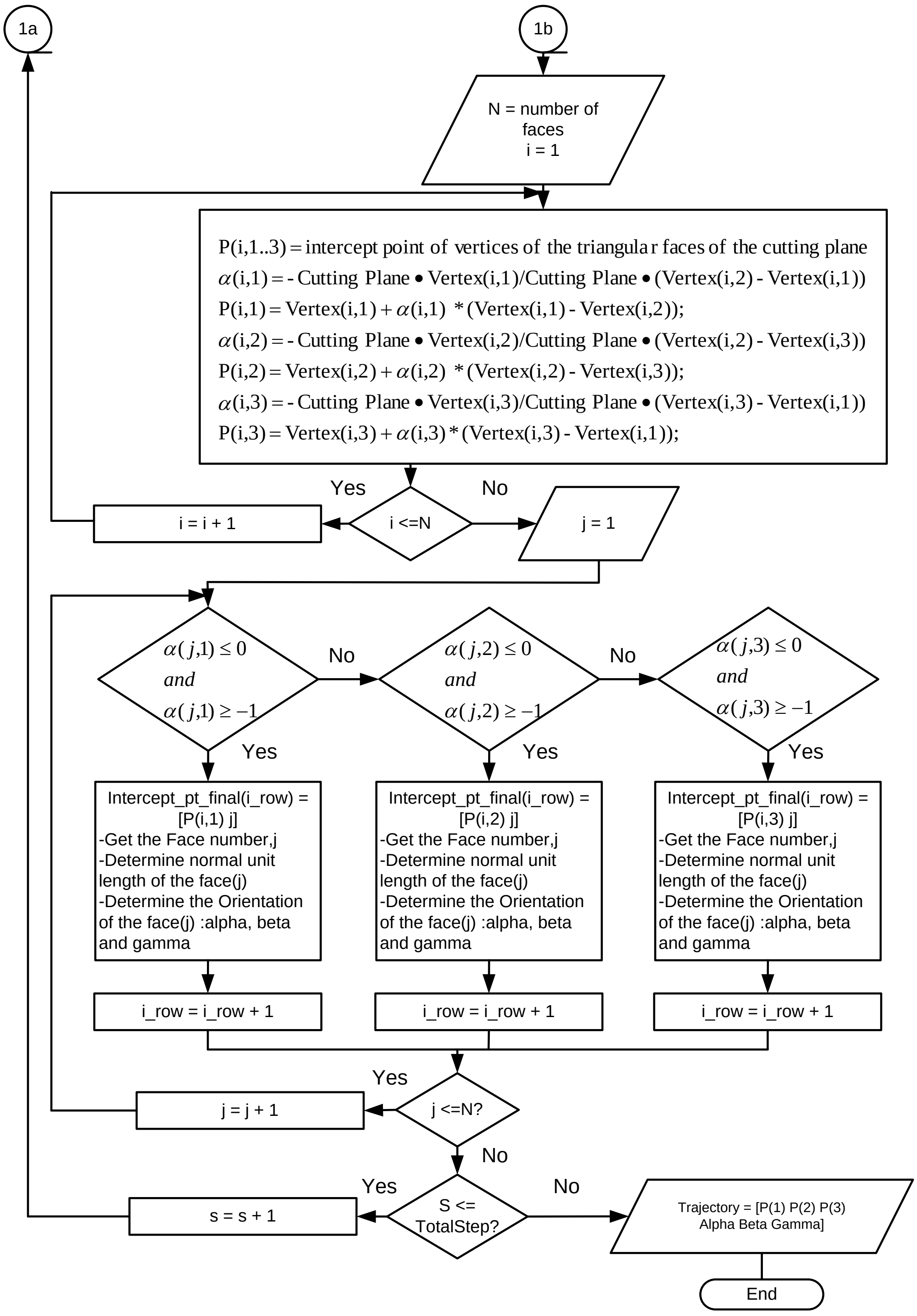
1a
1b
N = number of faces
i = 1
P(i,1..3) = intercept point of vertices of the triangular faces of the cutting plane
α(i,1) = - Cutting Plane • Vertex(i,1)/Cutting Plane • (Vertex(i,2) - Vertex(i,1))
P(i,1) = Vertex(i,1) + α(i,1) * (Vertex(i,1) - Vertex(i,2));
α(i,2) = - Cutting Plane • Vertex(i,2)/Cutting Plane • (Vertex(i,2) - Vertex(i,3))
P(i,2) = Vertex(i,2) + α(i,2) * (Vertex(i,2) - Vertex(i,3));
α(i,3) = - Cutting Plane • Vertex(i,3)/Cutting Plane • (Vertex(i,3) - Vertex(i,1))
P(i,3) = Vertex(i,3) + α(i,3) * (Vertex(i,3) - Vertex(i,1));
Yes
No
i = i + 1
i <=N
j = 1
$\alpha(j,1) \le 0$ and $\alpha(j,1) \ge -1$
No
$\alpha(j,2) \le 0$ and $\alpha(j,2) \ge -1$
No
$\alpha(j,3) \le 0$ and $\alpha(j,3) \ge -1$
Yes
Yes
Yes
Intercept_pt_final(i_row) = [P(i,1) j] -Get the Face number,j -Determine normal unit length of the face(j) -Determine the Orientation of the face(j) :alpha, beta and gamma
Intercept_pt_final(i_row) = [P(i,2) j] -Get the Face number,j -Determine normal unit length of the face(j) -Determine the Orientation of the face(j) :alpha, beta and gamma
Intercept_pt_final(i_row) = [P(i,3) j] -Get the Face number,j -Determine normal unit length of the face(j) -Determine the Orientation of the face(j) :alpha, beta and gamma
i_row = i_row + 1
i_row = i_row + 1
i_row = i_row + 1
Yes
j = j + 1
j <=N?
No
Yes
No
s = s + 1
S <= TotalStep?
Trajectory = [P(1) P(2) P(3) Alpha Beta Gamma]
End

Figure 5.7(b) Flow chart for the generation of CC points

5.4 Local Coordinate System (LCS) Setup

The definition of the tool position in the machine coordinate system (MCS) is complicated especially for 5-axis machining. Hence, a local coordinate system (LCS) is set up at each CC point. Figure 5.8 shows the configuration of the local coordinate system, H(**f**, **t**, **n**) at a CC point. The origin of LCS coincides with a CC point on the freeform surface. **f** is the unit vector that defines the feed direction of the tool from the current CC point to the next CC point on a planar tool path. **n** is the normal of the triangular face which the current CC point lies. The unit surface tangent **t** is defined as the cross product of **t** and **n**. Figure 5.8 shows the two rotational DOFs provided by 5-axis machining. **α** (tilting angle) and **β** (rotational angle) are the cutting tool rotational angles about **t** and **n** respectively.

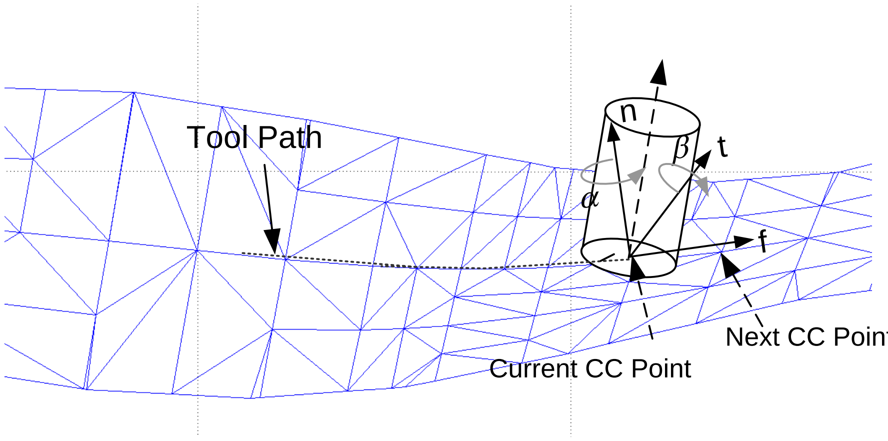

Figure 5.8 Local Coordinate System (LCS) Setup

There are a total of four coordinate systems to be considered when transforming the LCS of the freeform surface to the MCS of the Stewart Platform, and they are, *viz*., the local coordinate system, freeform surface coordinate system, workpiece coordinate system and the machine coordinate system.

5.5 Interference in 5-axis machining

Collision and gouging are the interference factors in 5-axis machining of a freeform surface. The trajectory path of the Stewart Platform for 5-axis machining needs to be generated such that interference is prevented.

Collision

Collision can occur during the machining of a freeform surface. Collision is defined as an unintentional and undesirable "crash" of the cutting tool shaft or tool holder with the workpiece surroundings. One of the ways to avoid collision is to define a collision range. The faces within the collision range are faces that have been determined to have a possibility of collision, and the geometrical data of these faces are used in the generation of a collision-free cutting location domain. This checking operation is performed for each CC point along the tool path.

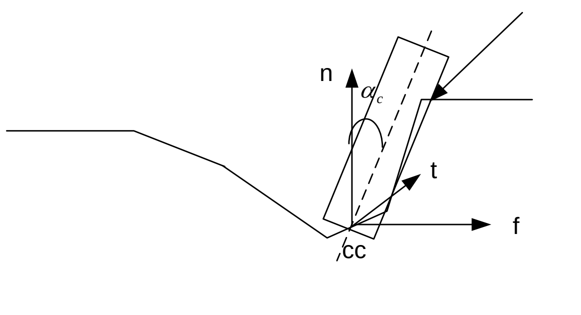

Figure 5.9 Collision between tool and freedom surface

Gouging

Gouging will occur during 5-axis machining operations when the bottom of the cutting tool cuts the surface around the CC point unintentionally, as shown in Figure 5.10. Normally any triangles or vertices that are within the ¼ torus traced out by the bottom of the cutting tool will cause gouging, as shown in Figure 5.10.

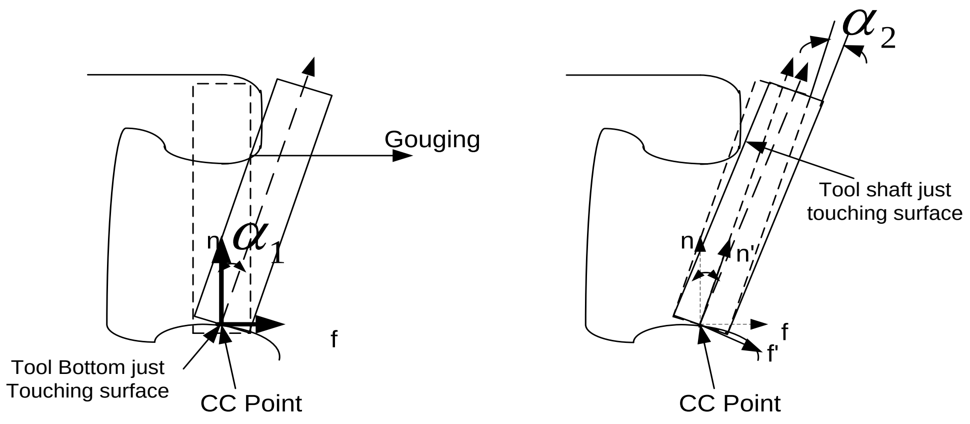

Figure 5.10 Gouging

This collision and gouging detection method can be implemented to improve the trajectory path so as to reduce the risk of damaging the tool and the workpiece. Thus, 5-axis machining on a Stewart Platform can be achieved in a more systematic manner.

Chapter 6 Five-axis machining post-processor

6.1 Introduction

Before the collision-free and gouging-free CL data can be applied to machine a particular workpiece on the Stewart Platform, the Cutter Location (CL) data in the Local Coordinate System (LCS) of the freeform surface has to be first translated to the Machine Coordinate System (MCS) of the Stewart Platform using the post-processor. The post-processor acts as the data conversion interface between the CAD/CAM systems and the NC machine tools. The generation of the CL data in the MCS for the trajectory path is dependent on the geometric structure of the NC machine tool. Hence, the post-processor is the developed software in the computer to translate tool motion data from an NC programming system into a trajectory path programming for the numerically controlled Stewart Platform. However, each post-processor is developed for a specific machining system in the aspect of kinematics and structures of the machining system. Thus, the post-processor expresses machining trajectory path in a homogenous coordinate transformation matrix with respect to kinematics for specific 5-axis machines.

Unlike a normal 5-axis machining center, the Stewart Platform has one advantage, *i.e.*, the inverse kinematics solution of the end-effector of the Stewart Platform is much simpler than a common 5-axis machining center. The common 5-axis machining center is a serial kinematics manipulator which joints are located between two adjacent links. Hence, the rotational axes of a 5-axis machine center are not aligned at the same point as shown in Figure 6.1(a), and this will cause complexity in the mapping of the joint coordinates from the known Cartesian coordinates of the end-effector to the machine coordinate system of the machining center.

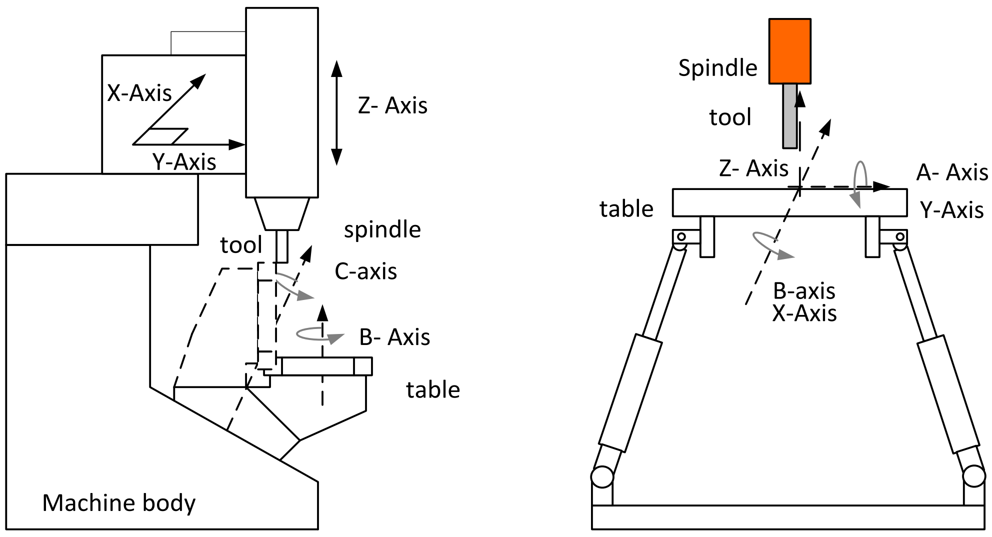

Figure 6.1 Comparison of (a) 5-axis machining center and (b) Stewart Platform

However, since a Stewart Platform is a parallel kinematics manipulator with close loop form, all the rotational axes co-align in the same point at the end effector of the mobile platform which is shown in Figure 6.1(b). This characteristic makes the solution of the inverse kinematics of the platform more straight forward. Thus, the coordinates of the joints and actuators of the platform can be determined easily from the known Cartesian coordinates of the end-effector, as shown in Figure 6.2. However, there is limitation of workspace of the Stewart Platform due to the limited working angles of the installed spherical and universal joints.

To have better understanding of the kinematics of the Stewart Platform under the condition of the machining process, several coordinate systems are assigned along the Stewart Platform. This assignment of the series of coordinate systems is to map the coordinates in the local coordinate system of the workpiece to the coordinate system with respect to the base frame. Firstly, there is a global coordinate system assigned at the base frame as shown in Figure 6.2. A frame is the entity defined by four vectors of the position and orientation information of the particular position of the Stewart Platform.

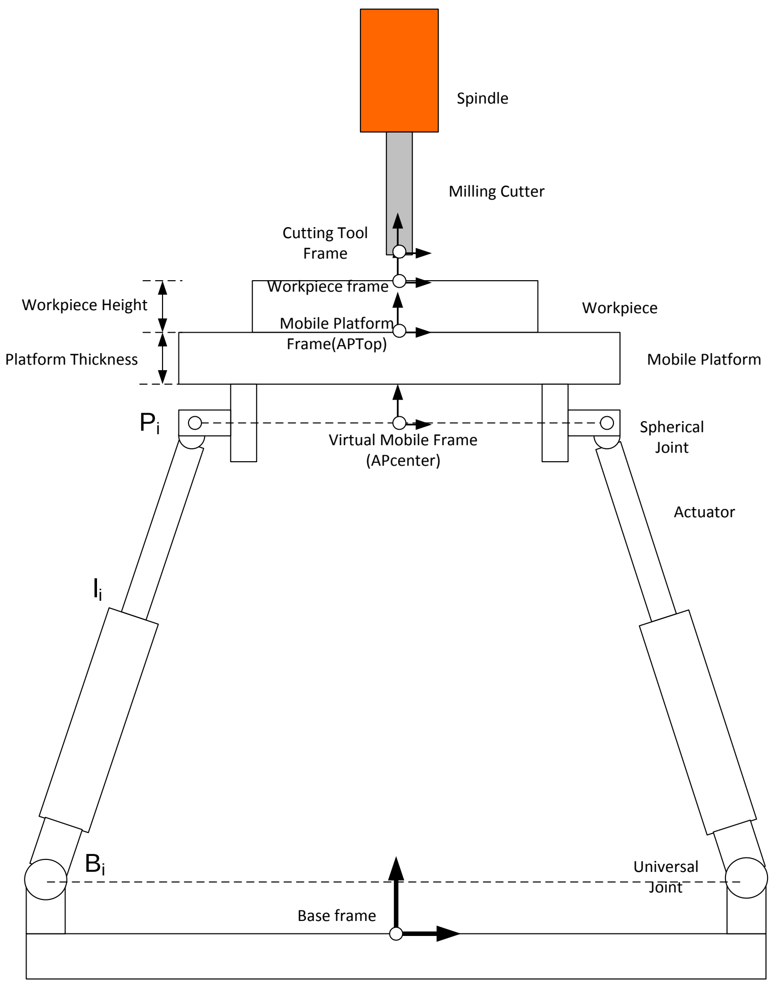

Figure 6.2 Various coordinate systems defined in the Stewart Platform

In addition, a few local coordinate systems are assigned along the mobile platform. A virtual mobile platform coordinate system is assigned virtually at the center point where it is coplanar with the coordinates of the spherical joints as shown in Figure 6.2. Next, the mobile platform coordinate system is assigned at the center of the top surface of the mobile platform while the workpiece coordinate system is also assigned on the top surface of the workpiece. Lastly, a cutting tool coordinate system is assigned at the bottom center of the cutting tool tip. All the parameters of the local coordinate systems are referred to the global coordinate system at the base frame. Since the mobile platform is a rigid body, the local coordinate systems, such as the mobile platform coordinate system and the virtual mobile coordinate system share the same translation vectors in term of X-, Y- and Z-coordinates.

A post-processor is developed in this research to generate the appropriate machining trajectory path of the Stewart Platform based on the local coordinates of a freeform surface. Based on the equations in Chapter 2, the joint coordinates of an actuator can be determined using Equation (6.1),

$$P_{newi} = R \times P_i + T, i = 1,2...,6 \tag{6.1}$$

$$l_i = R \times P_i + T - B_i, i = 1,2...,6 \tag{6.2}$$

where R is the rotational matrix.

$$Rot_{3\times3} = \begin{bmatrix} \cos\alpha\cos\beta & \cos\alpha\sin\beta\sin\gamma - \sin\alpha\cos\gamma & \cos\alpha\sin\beta\cos\gamma + \sin\alpha\sin\gamma \\ \sin\alpha\cos\beta & \sin\alpha\sin\beta\sin\gamma + \cos\alpha\cos\gamma & \sin\alpha\sin\beta\cos\gamma - \cos\alpha\sin\gamma \\ -\sin\beta & \cos\beta\sin\gamma & \cos\beta\cos\gamma \end{bmatrix} \tag{6.3}$$

and T is the translational movement of the end effector of the mobile platform.

$$T = \begin{bmatrix} T_x \\ T_y \\ T_z \end{bmatrix} \tag{6.4}$$

All these coordinates are determined based on the local coordinate system of the virtual mobile platform frame with respect to the base coordinate system at the base frame as shown in Figure 6.3. As stated in Equation (6.1), $\mathbf{P_i}$ is the coordinate of the spherical joint with respect to the center of the virtual mobile frame and $\mathbf{B_i}$ is the coordinate of the rotational center of universal joints with respect to the base frame as illustrated in Figure 6.3. Based on the inverse kinematics analysis, the prismatic joint coordinates, $\mathbf{l_i}$ can be determined based on the known Cartesian coordinates of the end-effector as shown in Equation (6.2). However, a few conditions need to be taken into consideration when applying the postprocessor for the Stewart Platform to obtain the machining coordinates.

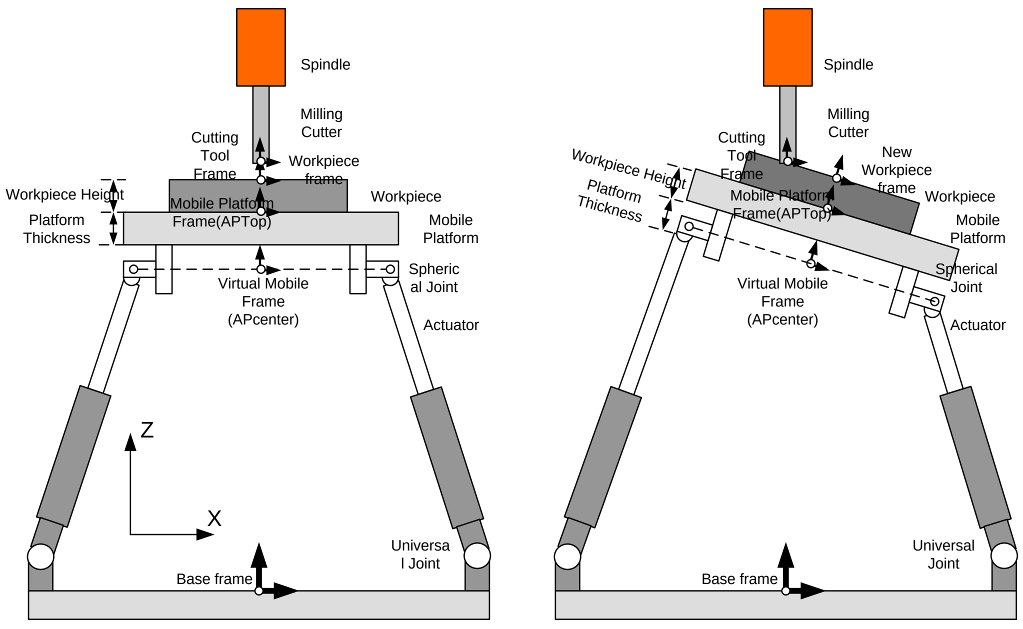

Figure 6.3 Orientation of mobile platform around Y-axis

When the machining trajectory path of the Stewart Platform is used in 3-axis machining, the orientation angle of the mobile platform is negligible since only translation movement is concerned in the machining process. In addition, the workpiece and the mobile platform can be considered as one single rigid body. Hence, as long as the local coordinates of the workpiece are known, the machining coordinates can be evaluated easily by implementing the translational motion **T** of the Stewart Platform. However, when the Stewart Platform is performing 5-axis machining, the rotational angles around **A** and **B** axes as shown in Figure 6.1 will introduce different challenges to define the center coordinates of orientation. It is because the lengths of the actuators are defined based on the orientation and translation of the mobile platform. However, in 5-axis machining, the respective machining coordinates are defined based on the orientation and translation of the center of the mobile platform; now it is defined based on the orientation and translation of the contact point between the freeform machined workpiece and the center of the bottom point of the cutting tool.

As shown in Figure 6.3, five local coordinate systems (LCS) are defined which can affect the joint coordinates during the movement of the Stewart Platform in five axis machining, namely, the base frame LCS, virtual mobile frame LCS, mobile platform frame LCS, workpiece frame LCS and the cutting tool frame LCS. Normally, the joint coordinates of the prismatic actuators can be determined based on the difference between the coordinates in the base frame LCS and the coordinates in the virtual mobile frame LCS. However, in 5-axis machining, the point center where the rotational axes of the workpiece are located will vary depending on the intersection point between the bottom center of the cutting tool and the workpiece as shown in Figure 6.4.

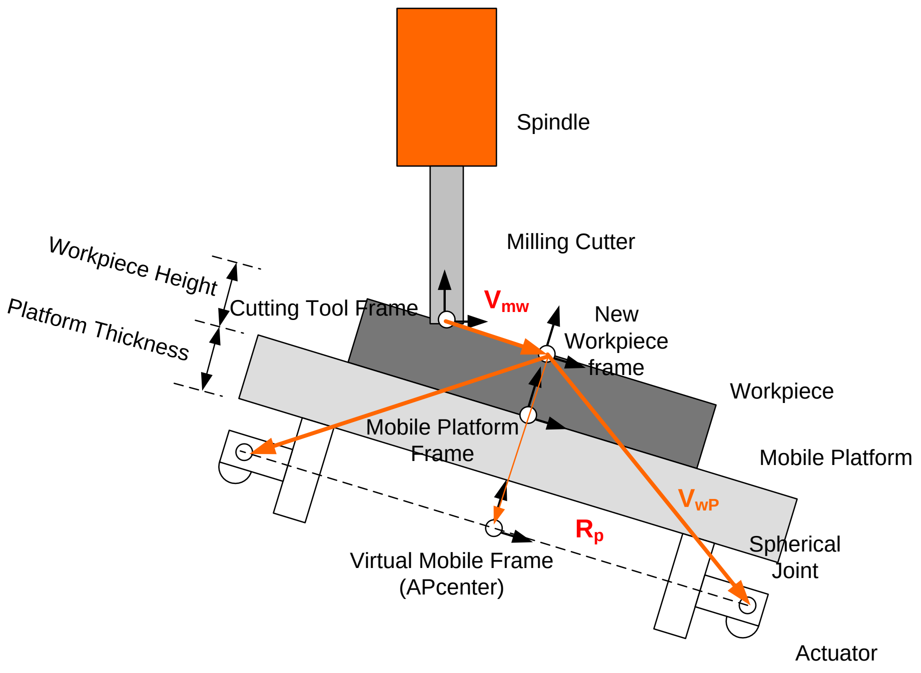

Figure 6.4 Relationship between the cutting tool frame LCS and the workpiece frame LCS

Hence, the origin of the workpiece frame LCS is used as the center of the end-effector. The coordinates of the spherical joint will be defined with respect to the workpiece frame LCS through the following vector in Equation (6.5).

V_{wP} = Center of Workpiece + P_i

$$\text{where } P_i = \begin{bmatrix} R_p \cos\theta_i \\ R_p \sin\theta_i \\ -Workpiece\_Height - Platform\_Thickness \\ 1 \end{bmatrix} \qquad (6.5)$$

By knowing the orientation of the intersection points between the center of the cutting tool and the workpiece, the new rotational center of the workpiece frame can be derived based on the vectors between the centers of the bottom of the flat end milling cutter and the original center of the workpiece frame LCS as show in Equation (6.6). The original center of the workpiece corresponds to the Cartesian coordinates of the freeform surface. Since the orientation angles are known for each point on the freeform surface, the new center of the workpiece can be determined using Equation (6.7). Hence, by determining the new center of the workpiece frame, the machining coordinate system can be determined. As a result, the joint coordinates of the actuators can be determined using the inverse kinematics algorithm.

$$V_{mw} = \text{Center of the workpiece frame} - \text{Center of the bottom of the milling cutter} \quad (6.6)$$

where V_{mw} is the vector between the milling cutter center and the workpiece center as shown in Figure 6.4.

$$\text{new center of workpiece frame} = \text{center of the bottom of the cutter} + R \times V_{mw} \quad (6.7)$$

where R is the rotational matrix

From the LCS of the freeform surface, the orientation of each face is defined with respect to the angle of rotation about Y-axis and Z-axis of the local coordinate system. However, due to the limitation of the orientation workspace of the Stewart Platform, rotational angles γ and β which rotate around X- and Y-axes respectively are used for the machining coordinate system (MCS) of the platform.

Therefore, an algorithm is developed for the mapping of the orientation angles of the intersected faces in the freeform surface LCS to the orientation angles of the trajectory path in the machining coordinate system of the Stewart Platform. The mapping process is illustrated in Figure 6.5.

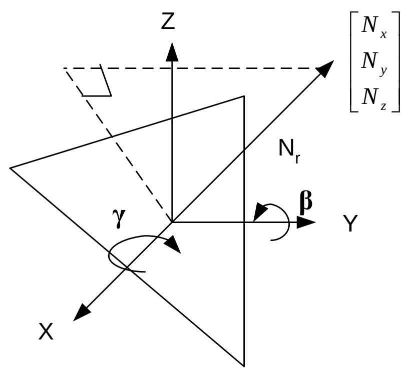

Figure 6.5 Normal Vector of Face intersected with the Cutting Plane

As shown in Figure 6.5, the vectors [N_x N_y N_z] and the magnitude $N_R = \sqrt{N_x^{\ 2} + N_y^{\ 2} + N_z^{\ 2}}$ of the normal vector of the faces intersect with the cutting plane at the freeform surface LCS are known. Since the orientation of the Stewart Platform is limited to rotation about the X- and Y-axes, the rotational matrix can be further simplified as in Equation (6.8).

$$Rot_{xy} = \begin{bmatrix} \cos\beta & \sin\beta\sin\gamma & \sin\beta\cos\gamma \\ 0 & \cos\gamma & -\sin\gamma \\ -\sin\beta & \cos\beta\sin\gamma & \cos\beta\cos\gamma \end{bmatrix} \tag{6.8}$$

Hence, mapping of the angles of rotation of the machining coordinate of the Stewart Platform to the angles of rotation of the faces in the freeform surface LCS can be defined as below.

$$\begin{bmatrix} \cos\beta & \sin\beta\sin\gamma & \sin\beta\cos\gamma \\ 0 & \cos\gamma & -\sin\gamma \\ -\sin\beta & \cos\beta\sin\gamma & \cos\beta\cos\gamma \end{bmatrix} \begin{bmatrix} 0 \\ 0 \\ N_r \end{bmatrix} = \begin{bmatrix} N_x \\ N_y \\ N_z \end{bmatrix}$$

$$\begin{aligned} &\textit{where} \\ &N_r \times \sin\beta\cos\gamma = N_x \\ &-N_r \times \sin\gamma = N_y \\ &N_r \times \cos\beta\cos\gamma = N_z \end{aligned} \tag{6.9}$$

By rearranging Equation (6.9), the angle of rotation can be determined using Equations (6.10) and (6.11). Thus, the machining coordinates can be obtained based on the local coordinate system of the freeform surface. Hence, the lengths of each link can be verified and the trajectory path of the Stewart Platform can be defined for 5-axis machining.

$$\gamma = \sin^{-1}\left(\frac{-N_y}{N_r}\right) \tag{6.10}$$

$$\beta = \tan^{-1}\left(\frac{N_x}{N_z}\right) \tag{6.11}$$

6.2 Case Study: 5-axis surface machining

The postprocessor for converting the NC programs for 5-axis machining to the trajectory paths for the Stewart Platform was developed in MATLAB®. Firstly, a part to be machined is modeled using SolidWorks, and the drawing file exported as an ASCII STL file, for example, as shown in Figure 6.6. After an STL file has been generated, this text file is imported into MATLAB® to convert into the corresponding faces, vertices and colors, which are recognized by MATLAB®, to generate a model in MATLAB®, as shown in Figure 6.7. The imported model can also be expressed as tessellated triangles as shown in Figure 6.8.

```
solid name_of_object
    facet normal $n_i,n_j,n_k$
        outer loop
            vertex $x_1,y_1,z_1$
            vertex $x_2,y_2,z_2$
            vertex $x_3,y_3,z_3$
        endloop
    endfacet
endsolid name_of_object
```

Figure 6.6 ASCII STL text format

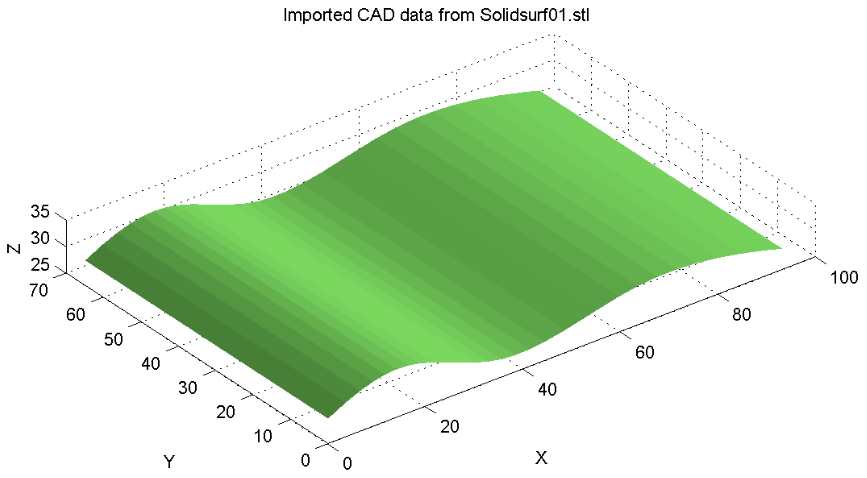

Figure 6.7 The surface model derived from the vertices and faces

After retrieving the data of the faces and the vertices of the triangles of the freeform surface, cutting planes (red) are defined by the step over parameters in MATLAB® function as shown in Figure 6.9. A cutting plane is basically a plane where the cutting path of the cutting tool mills through the freeform surface with the pattern of parallel cutting. The cutting plane is defined as a rectangular plane along the XZ plane while the cutting surface is resting on the XY plane. Thus, by knowing the dimension of the freeform surface area projected onto the XY plane, the total distance along the Y-axis can be determined for which maximum value of the Y-axis is defined as Ymax and the minimum value of the Y-axis defined as Ymin. In addition, the step-over should be 75% to 80% of the cutter's diameter in normal tool path planning. Hence, the percentage of overlapping of the diameter of the cutting tool along the machining path is defined through the MATLAB® function; the interval distance between the two adjacent cutting planes along the Y-axis can be defined as:

Interval parameter along Y axis = Total distance length of Y Coordinate / (Diameter of the Cutting Tool-(Percentage% of overlap × Diameter of the Cutting Tool).

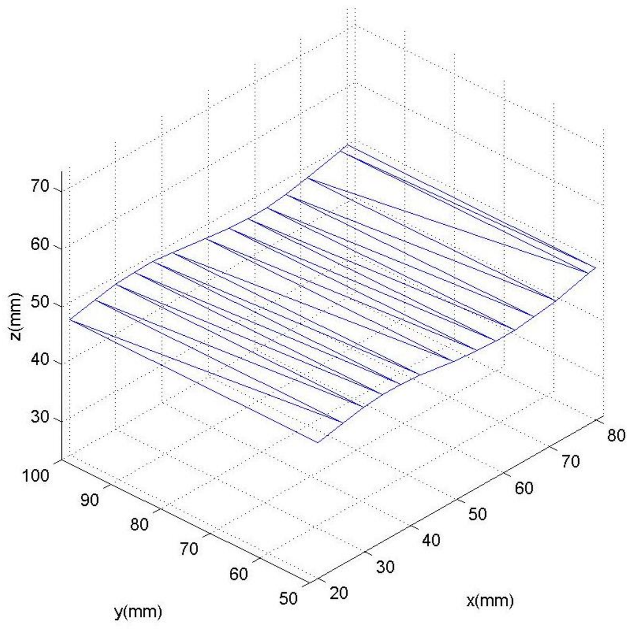

Figure 6.8 Tessellated triangular surfaces of the freeform surface

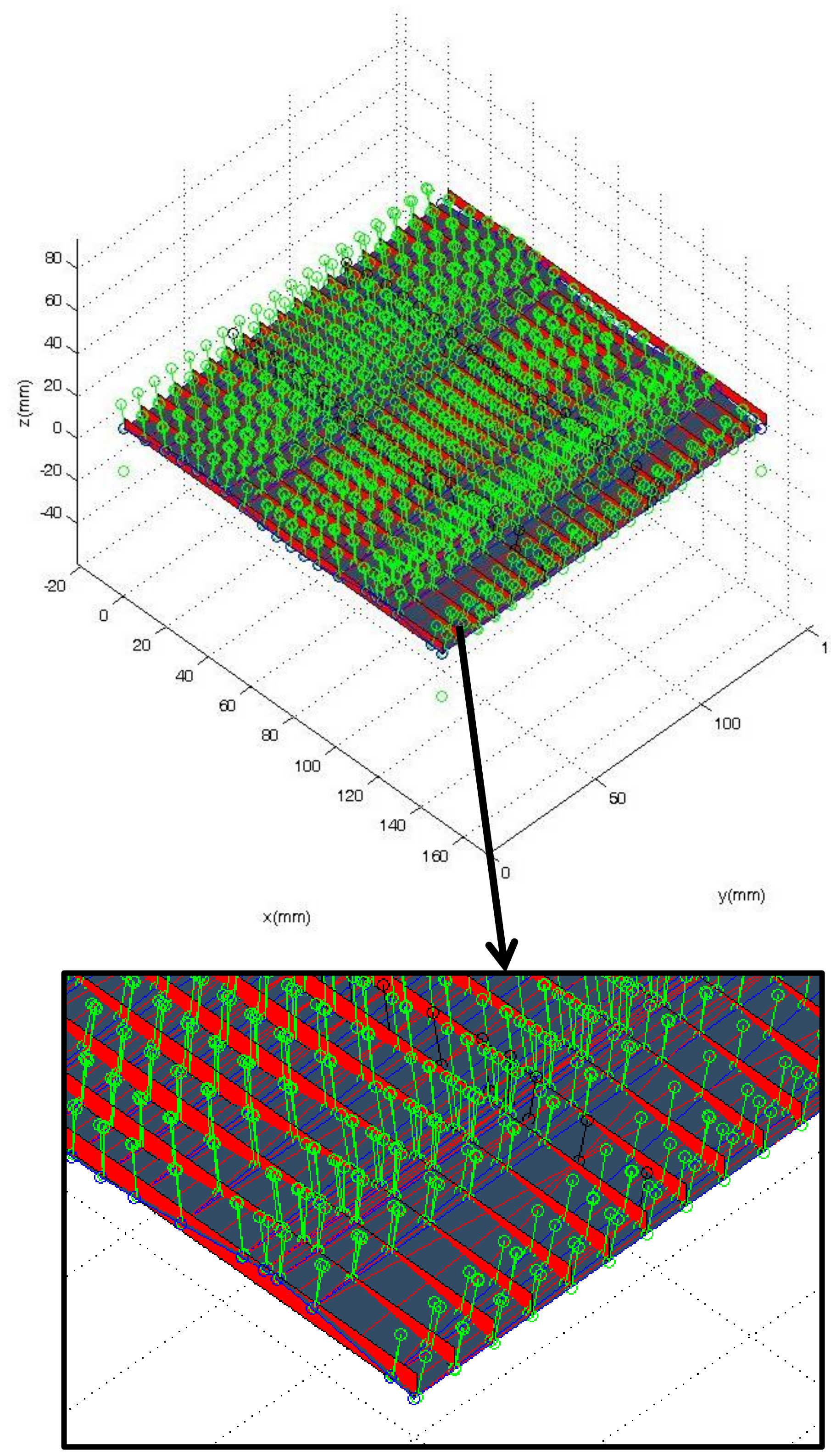

Figure 6.9 Intersected points with norm (green dot line) along the cutting plane

The cutting plane is perpendicular to the cutting surface so that each cutting plane will intersect with the freeform surface and form a series of points where the edge of the triangles intersect with the respective cutting plane, as shown in Figure 6.9. By knowing the intersected points, the orientation of the intersected points can be defined easily since the corresponding intersected faces and normal of the faces are known as shown in Figure 6.10.

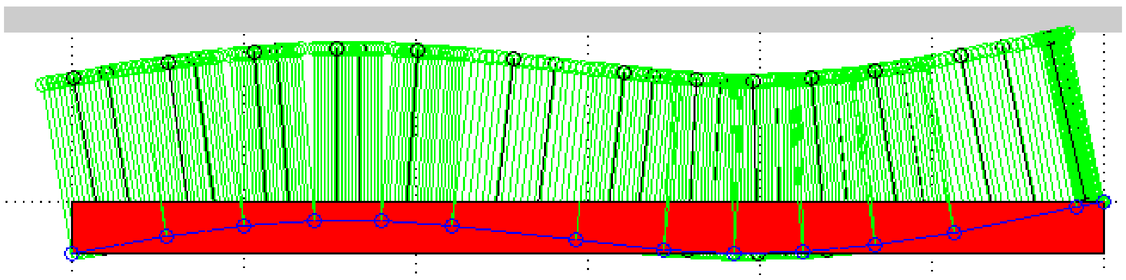

Figure 6.10 Intersected points of the freeform surface with one cutting plane and perpendicular lines (green) are the normal of the intersected points

Normally in the tessellated triangular surface, certain faces will interact with the specific cutting plane as shown in Figure 6.11. The intersected triangular plane has at most three edges in contact with the cutting plane at the intersected point. The intersected point can be verified by the factor α. As long as α <= -1, the intercepted point will be located within the length of the edge, otherwise the intercepted point will be located at the coordinate which is longer than its edge length shown as IP3 in the diagram. Hence, using this method, the intercepted points can be verified with respect to the cutting plane. The edge of circle which has direct intercepted points can be found. Since the normal of the tessellated triangular plane is determined by two edge vectors of the tessellated triangular plane. Hence all the intercepted coordinates can be used to determine the normal vectors and thus the rotational angles α and β in equation 6.10 and equation 6.11.

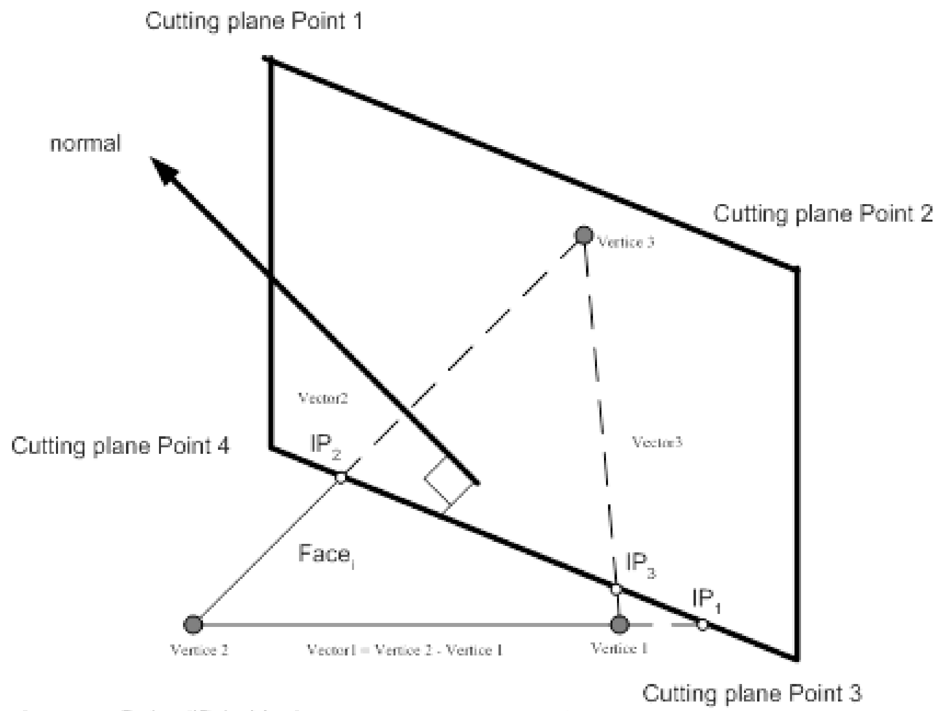

$$\text{Intercept Point}_1(IP_1) = \text{Vertice}_1 + \alpha_1 \text{ x } (\text{Vertice}_2 - \text{Vertice}_1)$$

$$\text{Intercept Point}_2(IP_2) = \text{Vertice}_2 + \alpha_2 \text{ x } (\text{Vertice}_3 - \text{Vertice}_2)$$

$$\text{Intercept Point}_3(IP_3) = \text{Vertice}_3 + \alpha_3 \text{ x } (\text{Vertice}_3 - \text{Vertice}_1)$$

Figure 6.11 Generation of the intersected points with a series of cutting planes

Since the cutting path is defined as parallel milling on the surface, it is moved along the Y-axis incrementally from Ymin to Ymax with interval parameter along the Y-axis as shown in Figure 6.12.

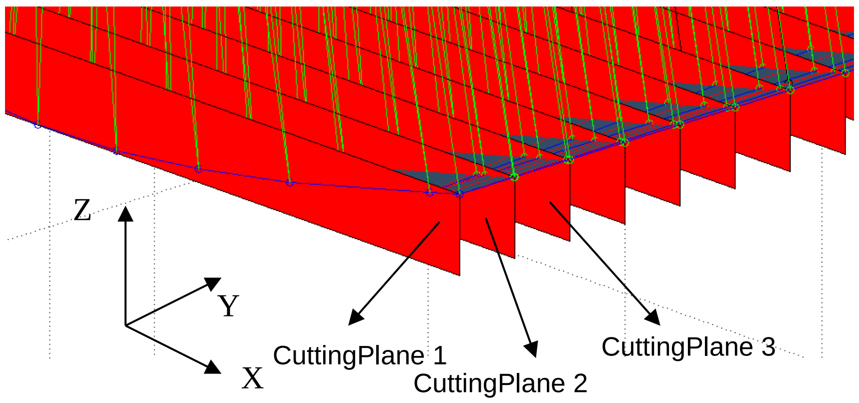

Figure 6.12 Generation of the intersected points with a series of cutting planes

The intersected points with the normal of the freeform surface will be converted into the Stewart Platform machining coordinates using the post-processor that has been developed in this research. Hence, the data of the intersected points are collected with respect to the cutting plane. The trajectory is represented as the format of [X Y Z Roll Pitch 0]. The trajectory values can be illustrated as shown in Figure 6.13. The blue lines represent the trajectory of the intersected points while the green lines indicate the orientation of the corresponding intersected point. Since it is 5-axis machining, the rotational angles are limited to be rotated around X- and Y-axes while the rotation around Z-axis will remain as zero for the Stewart Platform. Subsequently, a trajectory path for the Stewart Platform to achieve the required machining in the NC program can be generated and saved in the text format that can be read by the controller of the Stewart Platform.

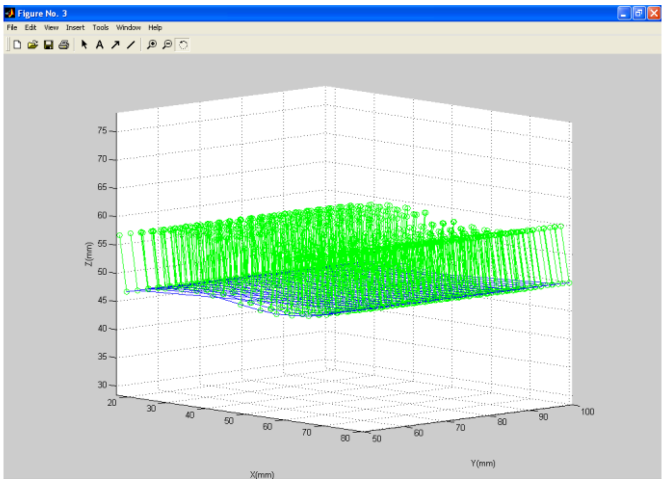

Figure 6.13 Trajectory path of the Stewart Platform generated based on the LCS of the freeform surface

The trajectory path is further enhanced by implementing the retracted points so that it can be used to machine smoothly on the Stewart Platform as shown in Figure 6.14.

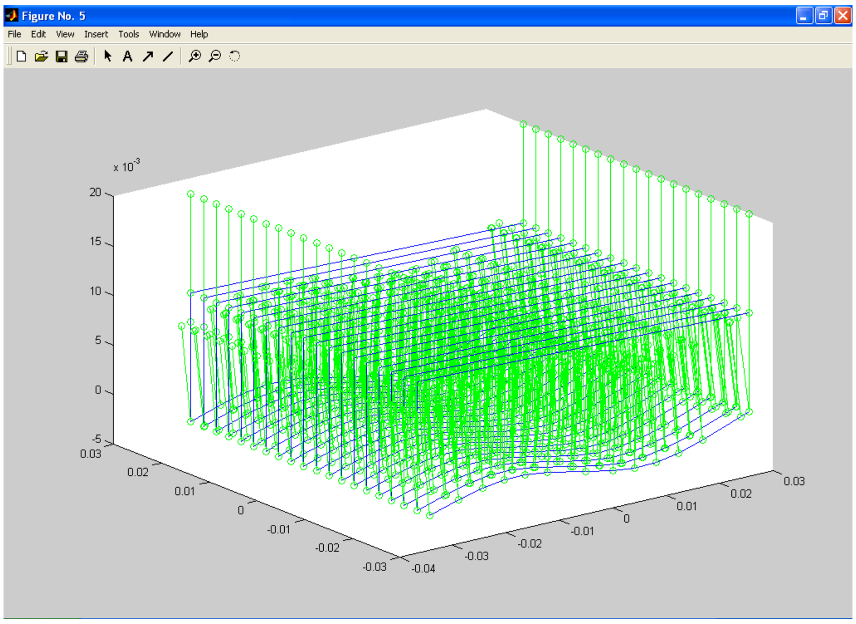

Figure 6.14 Trajectory path of the Stewart Platform with retracted points

Hence, the 5-axis machining specified in the NC program can be performed on the Stewart Platform based on this trajectory path. In addition, a simulation has been developed in MATLAB® to verify the accuracy of the orientation and translation of the Stewart Platform, as shown in Figure 6.14.

Due to safety consideration as the machining environment is not completely enclosed, workpieces made of Styrofoam were used to verify the postprocessor developed. Machining results are shown in Figure 6.15.

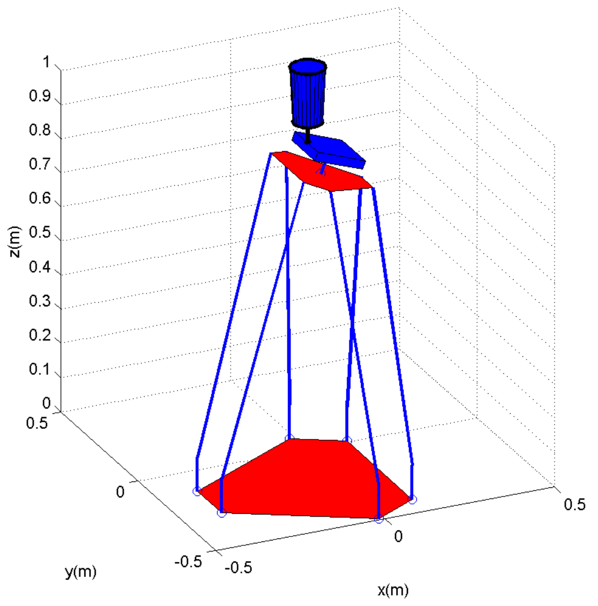

Figure 6.15 Simulation of 5-axis machining in MATLAB®

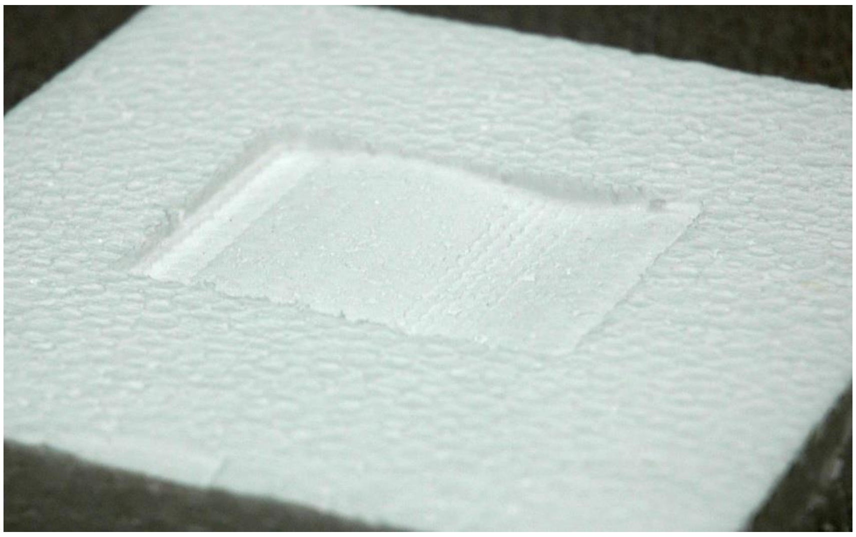

Figure 6.16 5-axis machining result

From the results, it has been observed that the postprocessor that has been developed is able to convert the LCS of a freeform surface into the MCS of the Stewart Platform successfully. The trajectory path generated can also be implemented to achieve actual 5-axis machining processes.

Chapter 7 Calibration of Stewart Platform

7.1 Sensors Feedback System

Several calibrations methods of the Stewart Platform are proposed in **Appendix C.** Among the proposed methods, a forward kinematics algorithm using Newton-Raphson method is chosen for the calibration purpose.

The WPS-750-MK30-P draw-wire displacement sensors from Micro-Epsilon^{TM} were installed along the actuators for the calibration purpose. Sensor holders for the actuators are fabricated in the workshop and installed onto the links of the Stewart Platform as shown in Figure 7.1. Each sensor holder is also installed with a round rod to serve as a guide track to ensure that the steel wires of the sensors extend linearly and parallel with the extraction of the links. The round rod not only prevents the tangling of the wires of the sensor due to the rotation of the piston of actuator around its own axis, the accuracy of the reading from the sensors can also be further improved. To measure the displacement of the wires of the sensors, a set of calibration system is developed.

The forward kinematics algorithm is implemented to calibrate the final position of the mobile platform. Based on the collected data, a position compensation algorithm is developed to increase the accuracy of the manipulation of the platform.

In addition, an offline monitoring program is developed to calibrate the end-effector of the Stewart Platform by collecting a set of feedback data from the wire sensors which are attached to the actuators. The collected data is used to predict the final position of the Stewart Platform through the calculation of the forward kinematics algorithm. Based on the result of the calibration, it is able to calibrate the end-effector of the Stewart Platform. The forward kinematics calibration method is better than the other calibration methods. It is able to verify not only the position of the end-effector but also the orientation of the end-effector (**Appendix C**). However, the accuracy of the result is limited by the resolution of the wire sensor which is 0.15mm. Moreover, the fluctuation of the measured values with wire sensors also affects the accuracy. An example is shown on the calibration sequence of the end-effector with wire sensors in the subsequent section.

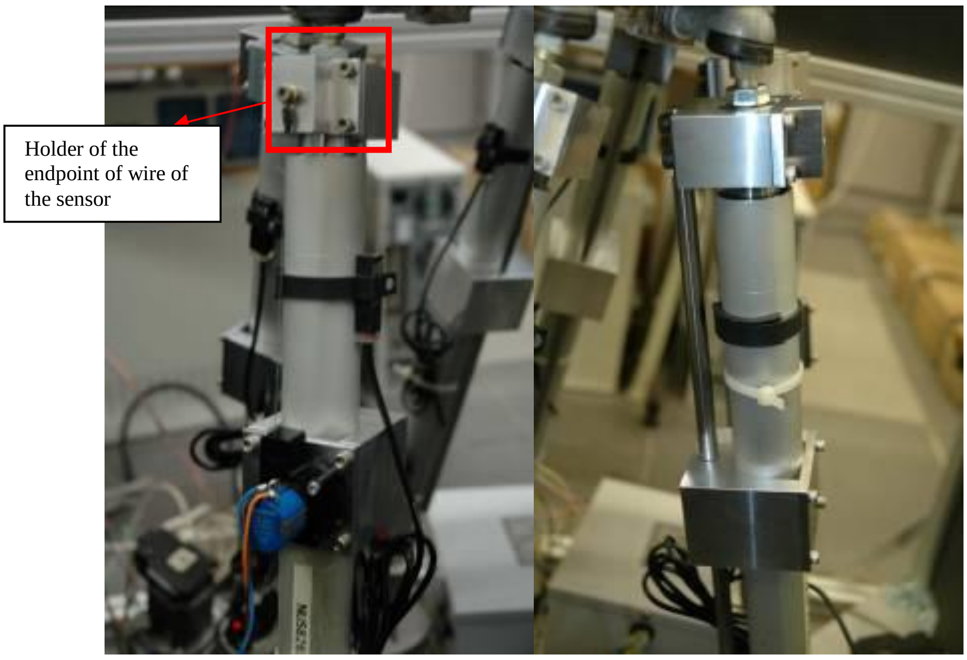

Figure 7.1 The mounting of the sensors to the sensor holder

Firstly, modeling of the motion of the platform is carried out when it is moving along the Z-axis. The respective data in the modeling of the end effector of the platform is collected through the actuation of the respective links of the platform with wire sensors. The platform is manipulated from 796.6 mm to 856.6 mm along the Z-axis. The data of the actuators is then processed through forward kinematics algorithm. The calibrated model of the trajectory of the end-effector is presented as a triangle surface in Figure 7.2 so that the orientation and translation of the end-effector can be illustrated clearly. The result is compared with the theoretical trajectory manipulation path in terms of translation and orientation movement.

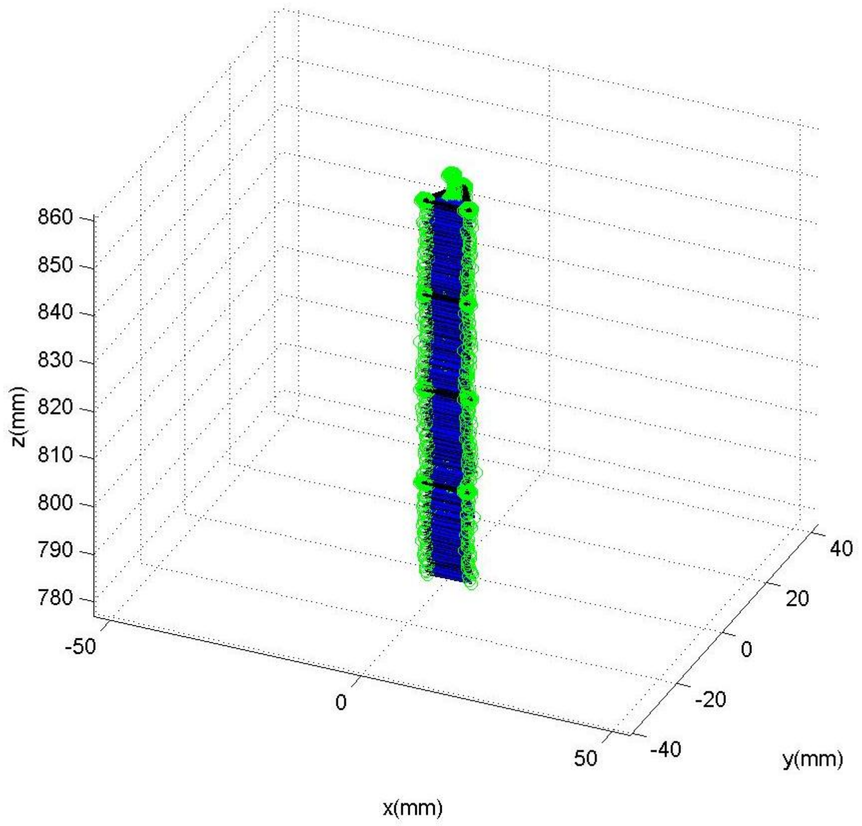

Figure 7.2 The model of the trajectory path of the end-effector based on the feedback of the wire sensors while the platform was moving along the Z-axis

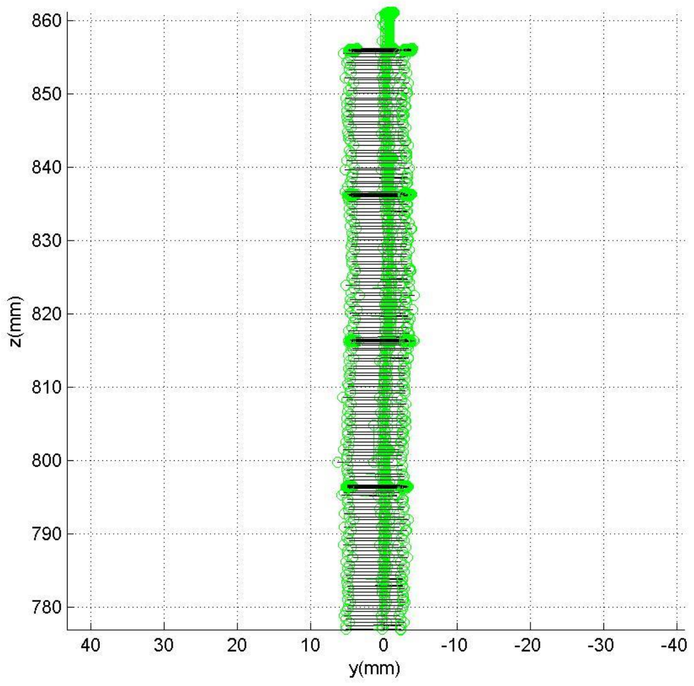

Figure 7.3 The model of the trajectory path of the end-effector based on the feedback of the wire sensors while the platform was moving along the Z-axis (front view)

Through the calibration experiment, it is found that the actual manipulation is not linear along the Z-axis as shown in Figure 7.3. The errors can be identified when they are compared with the ideal trajectory path of moving along the Z-axis as shown below:

Table 7.1 Average Error verification along Z-axis

Position X (mm)	Position Y (mm)	Position Z (mm)	Roll (deg)	Pitch (deg)	Yaw (deg)
0.1248	-0.5017	0	-0.0176	-0.0483	0.1765

Besides comparing the errors between the actual and ideal trajectory paths along the Z-axis, error verifications are also performed along the X- and Y-axes. The Stewart Platform is manipulated to move along the X-axis from 0 to 50 mm while other parameters are set as constant theoretically, such as Z = 856 mm and Y = 0 mm as illustrated in Figure 7.4.

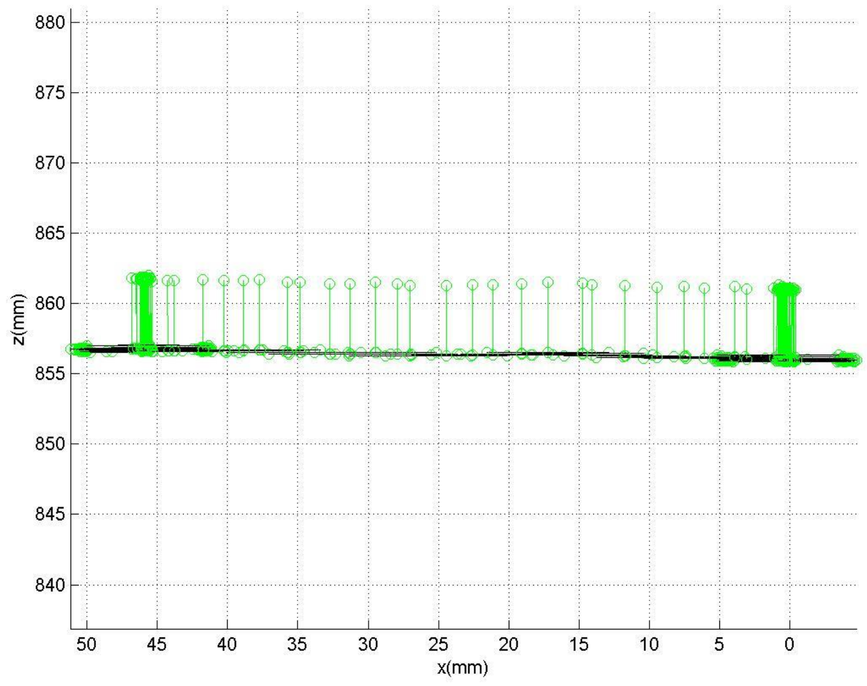

Figure 7.4 The model of the trajectory path of the end-effector based on the feedback of the wire sensors while the platform was moving along the X-axis

Through feedback of the wire sensors, the actual position of the Stewart Platform is determined. It is found that the motion is not even and tends to move in a curved shape as shown in Figure 7.4. The errors can be identified as shown in Table 7.2.

Table 7.2 Average Error verification along X-axis

Position X (mm)	Position Y (mm)	Position Z (mm)	Roll (deg)	Pitch (deg)	Yaw (deg)
0	-1.168	0.465	0.059	0.027	0.471

The same method is applied to measure the error of the actual manipulation of the Stewart Platform along the Y-axis. The Stewart Platform is manipulated to move along Y-axis from 0 to 50 mm and back to -50 mm while other parameters are set as constant, such as Z = 826 mm and X = 0 mm. The actual motion of the Stewart Platform which is derived from the feedback values of the wire sensors is shown in Figure 7.5.

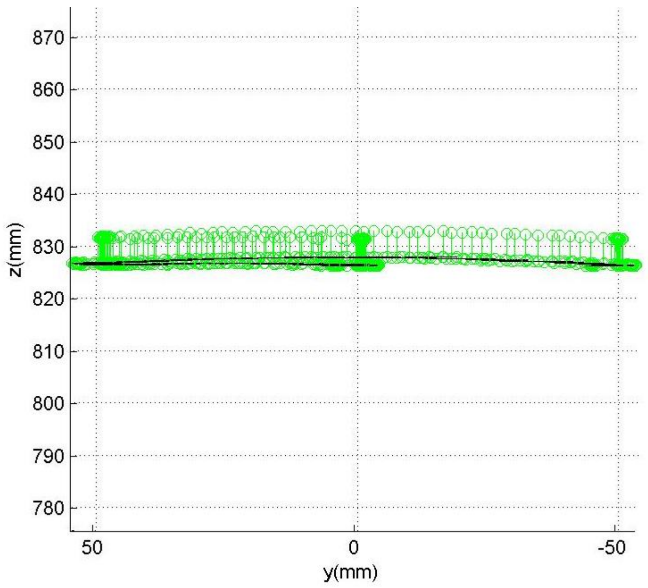

Figure 7.5 The model of the trajectory path of the end-effector based on the feedback of the wire sensors while the platform was moving along the Y-axis

As illustrated in Figure 7.5, the actual motion of the Stewart Platform generates a motion of a curved profile. Errors are verified through the comparison of the actual and theoretical positions of the manipulated Stewart Platform. The errors are shown in Table 7.3.

Table 7.3 Average Error verification along the Y-axis

Position X (mm)	Position Y (mm)	Position Z (mm)	Roll (deg)	Pitch (deg)	Yaw (deg)
-0.315	0	0.767	-0.048	0.019	0.167

From the error result of the trajectory path, the feedback of the position and orientation of the mobile platform is reasonable as the errors of the translation and orientation of the Stewart Platform are bounded within ±0.6 mm and ±0.2°. However, the feedback position error is found to be higher when dealing with pure motion along the X-axis which the position error can increase until ±1.2 mm and ±0.5 °. In short, the error is still quite high, a further fine tuning of the motion of the actuators needs to be done. Furthermore, the stability of the wire sensors needs to be further improved to increase the accuracy of the feedback. Figure 7.6 shows the MATLAB$^{®}$ model of continuous feedback of the respective actuators while the parameters of the actuator used to derive the continuous trajectory path of the translation and orientation of mobile platform are varied. It is manipulated freely in the Cartesian coordinate system as shown in Figure 7.7.

In short, the offline forward kinematics programming helps to predict and visualize the actual position and orientation of the platform with the feedback from the wire sensors. It also helps to calibrate the errors of the position and orientation in a more reliable manner.

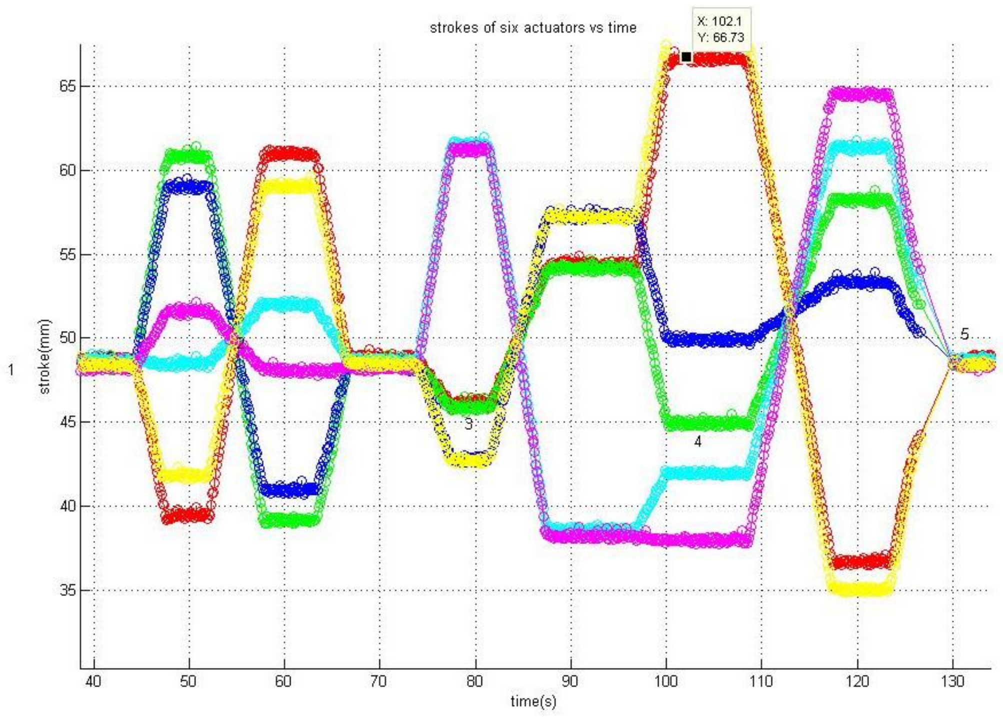

Figure 7.6 Feedback of actuators stroke position while the platform is being manipulated.

After the offline program of the forward kinematics algorithm has been successfully developed, a real time forward kinematics algorithm is implemented on the current Stewart Platform controller with VC++ (Figure 7.8). By manipulating the Stewart Platform, the feedback from the wire sensors enables one to calibrate the position and orientation of the end-effector of the mobile platform immediately. The real time feedback is able to help further improve the accuracy of the Stewart Platform because an immediate correction can be done to reduce the positioning error. However, there are still some disadvantages of this calibration system. It is because by using the forward kinematics algorithm with the Newton-Raphson numerical method, it will take a longer time to complete the iterations before the final calibration can be retrieved. Furthermore, the resolution of the wire sensors is limited to 0.15 mm but the resolution of the actuator is 0.1 mm. Thus, the retrieved data will fluctuate and are not reliable when the actuator is commanded to be moved in interval of less than 0.1 mm. A sampling averaging is performed which will delay the output of the position and orientation of the platform. Hence, the current calibration system can only be considered as a near real time calibration system.

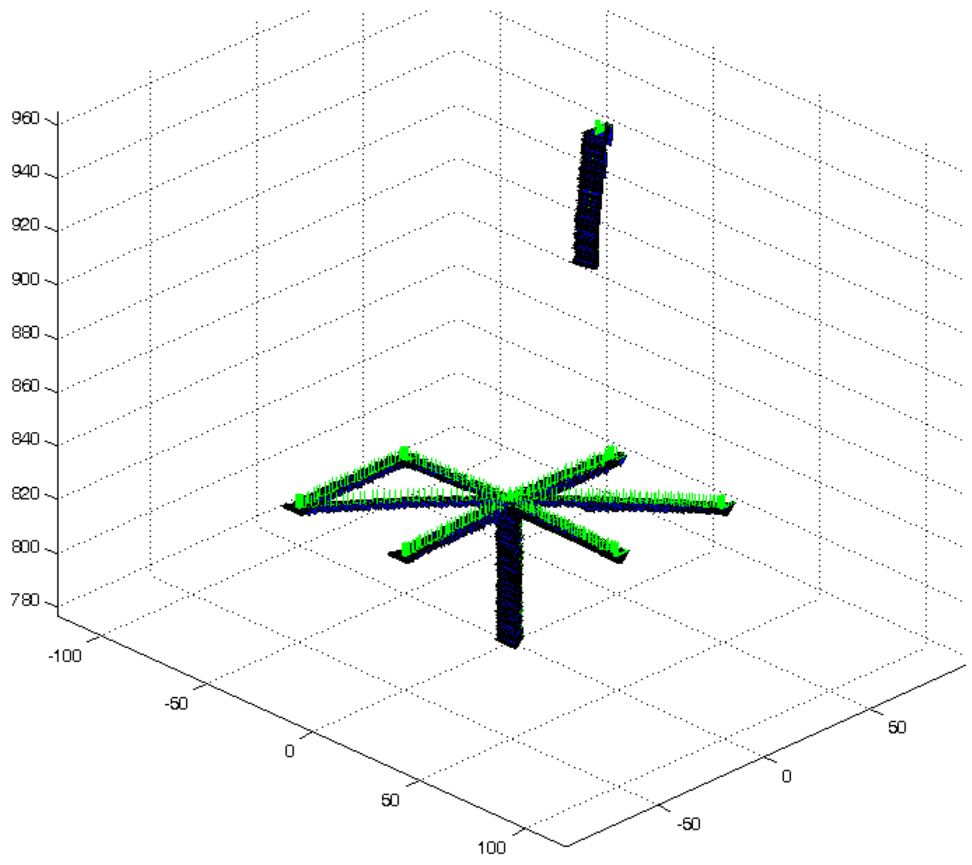

Figure 7.7 The corresponding position and orientation of the platform end-effector with respect to the strokes of the actuators

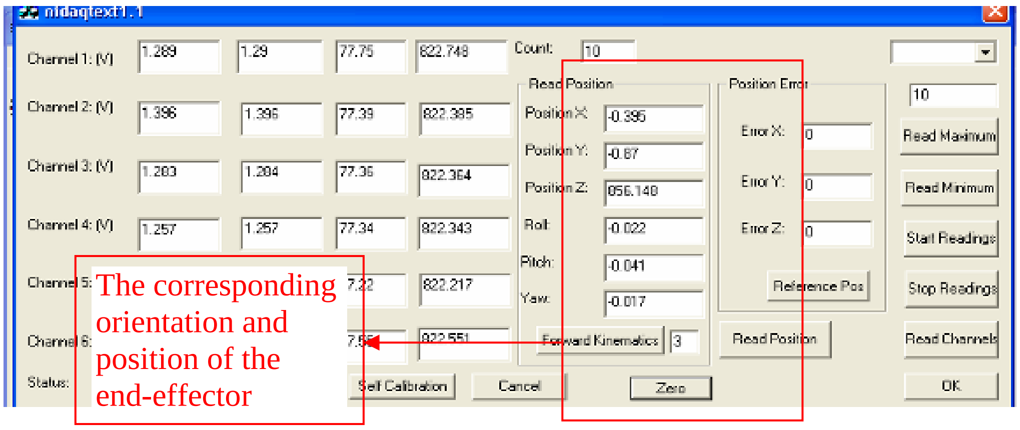
nidaqtext1.1

Channel 1: (V)	1.289	1.29	77.75	822.748
Channel 2: (V)	1.396	1.396	77.39	822.385
Channel 3: (V)	1.283	1.284	77.36	822.364
Channel 4: (V)	1.257	1.257	77.34	822.343
Channel 5:			7.22	822.217
Channel 6:			7.55	822.551

Count: 10

Read Position
Position X: -0.395
Position Y: -0.87
Position Z: 956.140
Roll: -0.022
Pitch: -0.041
Yaw: -0.017

Position Error
Error X: 0
Error Y: 0
Error Z: 0

10

Forward Kinematics 3

Status:

Figure 7.8 The Stewart Platform position and orientation feedback interface

7.2 Real Time Feedback Interface

The implementation of the real time feedback system allows more accurate prediction and calibration of the position and orientation of the platform as shown in Figure 7.9. Through a series of calibration and positioning experiments, the errors of the position and orientation of the platform are evaluated. Figure 7.10 shows a tool path generated from real time position feedback.

The errors of the positioning and orientation of the platform when the platform is moved theoretically to X = 0 mm, Y = 0 mm and Z = 966.36 mm:

- X-axis = 0.0005 mm
- Y-axis = -0.004 mm
- Z-axis = 0.36 mm
- Roll = 0 deg
- Pitch = -0.6 deg
- Yaw = 3 deg

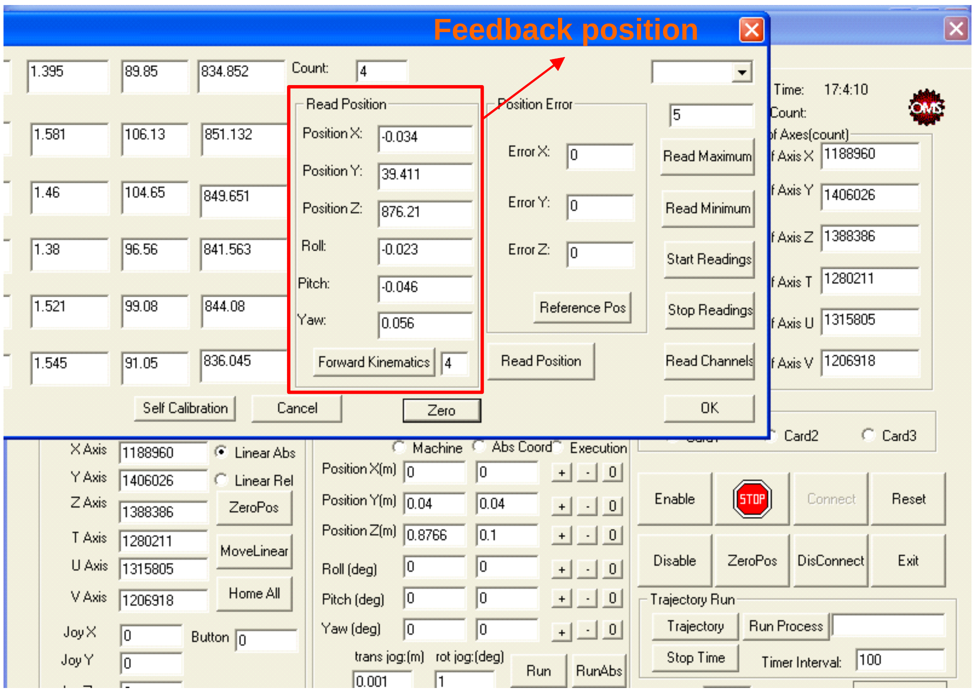

1.395	89.85	834.852
1.581	106.13	851.132
1.46	104.65	849.651
1.38	96.56	841.563
1.521	99.08	844.08
1.545	91.05	836.045

Count: 4

Read Position
Position X: -0.034
Position Y: 39.411
Position Z: 876.21
Roll: -0.023
Pitch: -0.046
Yaw: 0.056
Forward Kinematics 4

Position Error
Error X: 0
Error Y: 0
Error Z: 0
Reference Pos
Read Position

5
Read Maximum
Read Minimum
Start Readings
Stop Readings
Read Channels

Self Calibration Cancel Zero OK

Time: 17:4:10
Count:
f Axes(count)
f Axis X 1188960
f Axis Y 1406026
f Axis Z 1388386
f Axis T 1280211
f Axis U 1315805
f Axis V 1206918

X Axis 1188960
Y Axis 1406026
Z Axis 1388386
T Axis 1280211
U Axis 1315805
V Axis 1206918
[✓ Linear Abs] Linear Rel
ZeroPos
MoveLinear
Home All
Joy X 0
Joy Y 0
Button 0

Machine Abs Coord Execution
Position X(m) 0 0
Position Y(m) 0.04 0.04
Position Z(m) 0.8766 0.1
Roll (deg) 0 0
Pitch (deg) 0 0
Yaw (deg) 0 0
trans jog:(m) 0.001
rot jog:(deg) 1
Run RunAbs

Card2 Card3
Enable STOP Connect Reset
Disable ZeroPos DisConnect Exit
Trajectory Run
Trajectory Run Process
Stop Time Timer Interval: 100

Figure 7.9 The real time feedback interface of the wire sensor when the platform is being manipulated

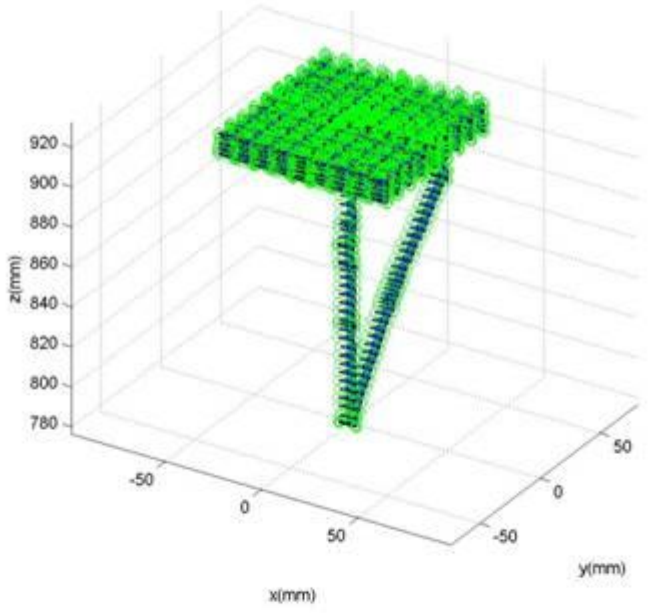

Figure 7.10 The tool path generated from the real time position feedback

All the error values are determined based on a specified calibration workpiece as shown in Figure 7.11. Hence, the accuracy of the platform can be compensated by considering the errors during the manipulation of the platform.

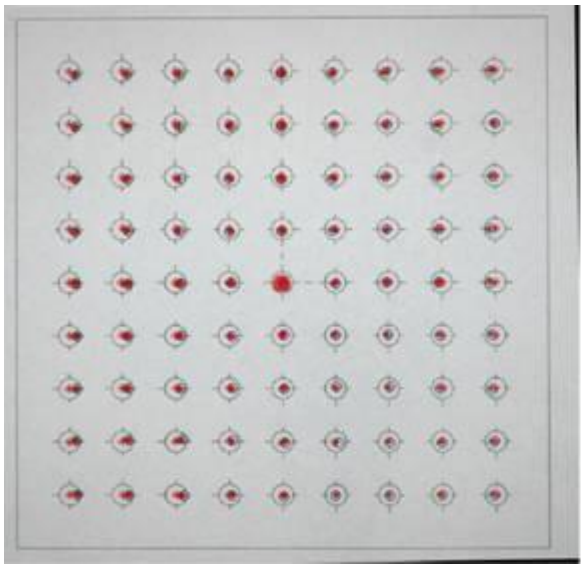

Figure 7.11 Calibration of workpiece

After the errors have been compensated, the accuracy of the platform is improved significantly and the repeatability of the platform is also improved. Calibration experiments are conducted to verify the accuracy of the platform after the positioning errors are compensated.

7.3 Result of Calibration Experiments

Calibration tests on the specific workpiece as shown in Figure 7.12 are repeated on the new calibrated platform with the real time monitoring system. The calibration results are satisfactory and are shown below:

- Angle tilted around the Y-axis = -0.49 deg
- Average error along the X-axis of the calibrated point with the original point = -0.27 mm
- Average error along the Y-axis of the calibrated point with the original point = -0.2 mm
- Mean value of distance between two adjacent points along the X-axis = 9.74 mm
- Mean value of distance between two adjacent points along the Y-axis = 9.95 mm

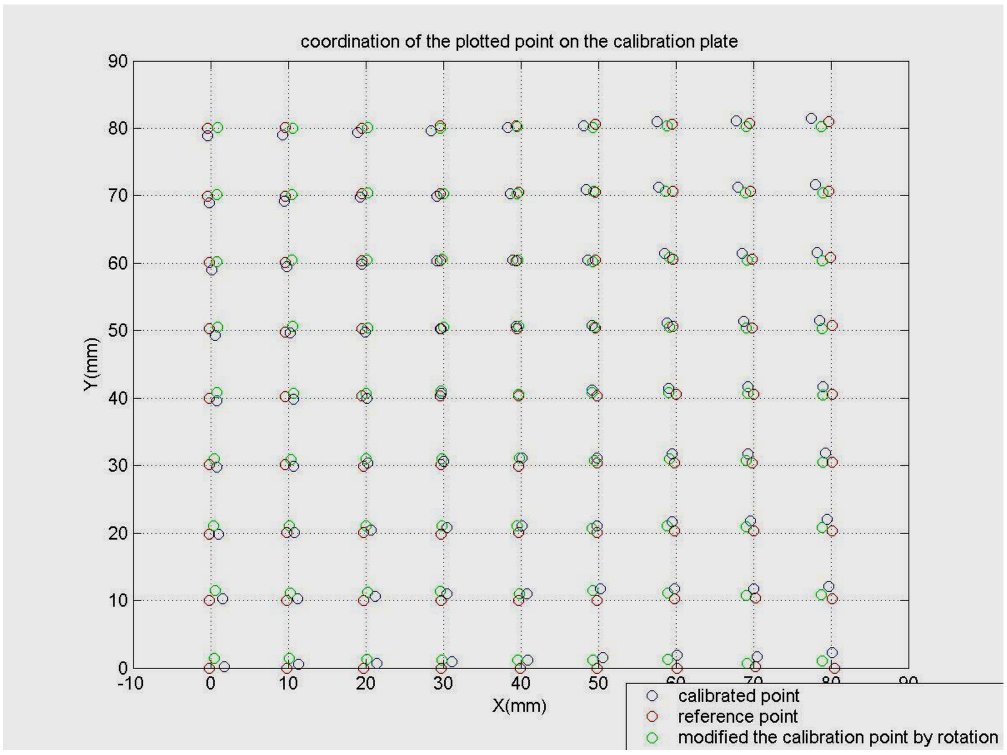

Figure 7.12 Comparison of calibrated result of the plotted point (Blue) and the ideal point (Red) and the coordinate of the plotted points on the calibration plate

From the calibration results shown in **Appendix D**, the accuracy has been improved significantly but there are still errors in terms of the X- and Y-axes. From the trend of the errors, it is observed to be a linear error. Basic image processing is developed to improve the error as shown in Appendix D. However, the accuracy of the calibration is also limited by the resolution of the wire sensors as discussed before.

Chapter 8 Control interface

After all the relevant algorithms have been developed in the study; different modular programs are developed and implemented on one single graphic user interface (GUI) written in Visual C++. Hence, the user now can control and monitor the motion of the Stewart Platform under one user environment. There are in total five main control modules in the Stewart Platform control interface.

8.1 Motion control interface

The actuators of the platform can be controlled by providing the orientation and translation parameters of the end-effector of the platform through the inverse kinematics algorithm. It can also be controlled by the parameters of the extension of each individual actuator. All the speeds and accelerations of the platform can also be controlled. Furthermore, a real time feedback of the position, velocity and acceleration of the actuators can be viewed from the same interface through the feedback from the encoder of the actuator as shown in Figure 8.1. A forward kinematics calculation is performed so that the position and orientation of the end-effector of the platform can also be retrieved.

Furthermore, a trajectory path planning function is also implemented in the control interface. When a trajectory path file is imported on the Stewart Platform, the mobile platform will be manipulated according to the trajectory path with the controlled interval time (**Appendix E**). Hence a machining process can be performed through this interface.

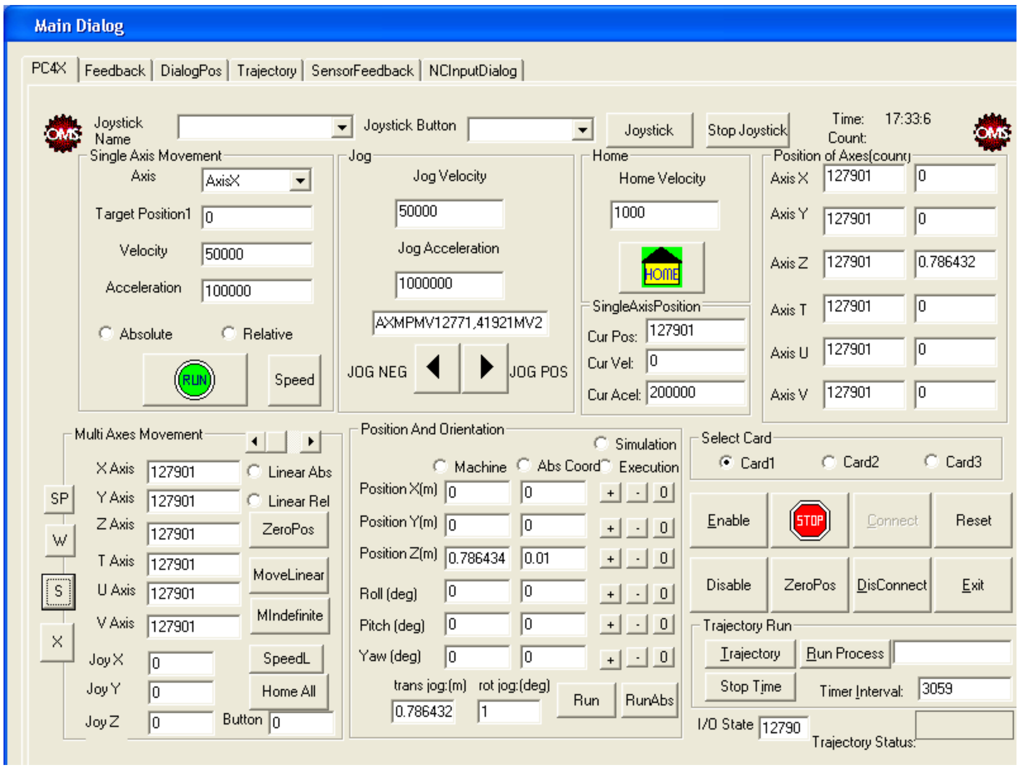
Main Dialog

Joystick Name:
Joystick Button:
Time: 17:33:6
Count:

Single Axis Movement
Axis: AxisX
Target Position1: 0
Velocity: 50000
Acceleration: 100000
Absolute / Relative

Jog
Jog Velocity: 50000
Jog Acceleration: 1000000
AXMPMV12771,41921MV2

Home
Home Velocity: 1000

SingleAxisPosition
Cur Pos: 127901
Cur Vel: 0
Cur Acel: 200000

Position of Axes(count)
Axis X: 127901 | 0
Axis Y: 127901 | 0
Axis Z: 127901 | 0.786432
Axis T: 127901 | 0
Axis U: 127901 | 0
Axis V: 127901 | 0

Multi Axes Movement
X Axis: 127901
Y Axis: 127901
Z Axis: 127901
T Axis: 127901
U Axis: 127901
V Axis: 127901
Joy X: 0
Joy Y: 0
Joy Z: 0
Button: 0
Linear Abs / Linear Rel

Position And Orientation
Machine / Abs Coord / Simulation Execution
Position X(m): 0 | 0
Position Y(m): 0 | 0
Position Z(m): 0.786434 | 0.01
Roll (deg): 0 | 0
Pitch (deg): 0 | 0
Yaw (deg): 0 | 0
trans jog:(m): 0.786432
rot jog:(deg): 1

Select Card
[✓ Card1] Card2 Card3

Trajectory Run
Timer Interval: 3059
I/O State: 12790
Trajectory Status:

Figure 8.1 Motion control interface

8.2 Motion control feedback

All the feedback positions, velocities and accelerations of the encoder can be read through another control interface module. In addition, a low level ASCII code command window is also developed in this module so that the user can communicate directly with the Stewart Platform through the basic command codes provided by the controller card as shown in Figure 8.2. Hence it is efficient to be used when only simple motion is needed to be performed by the Stewart

Platform. In addition, this direct communication is also able to reduce the communication time between the user and the Stewart Platform.

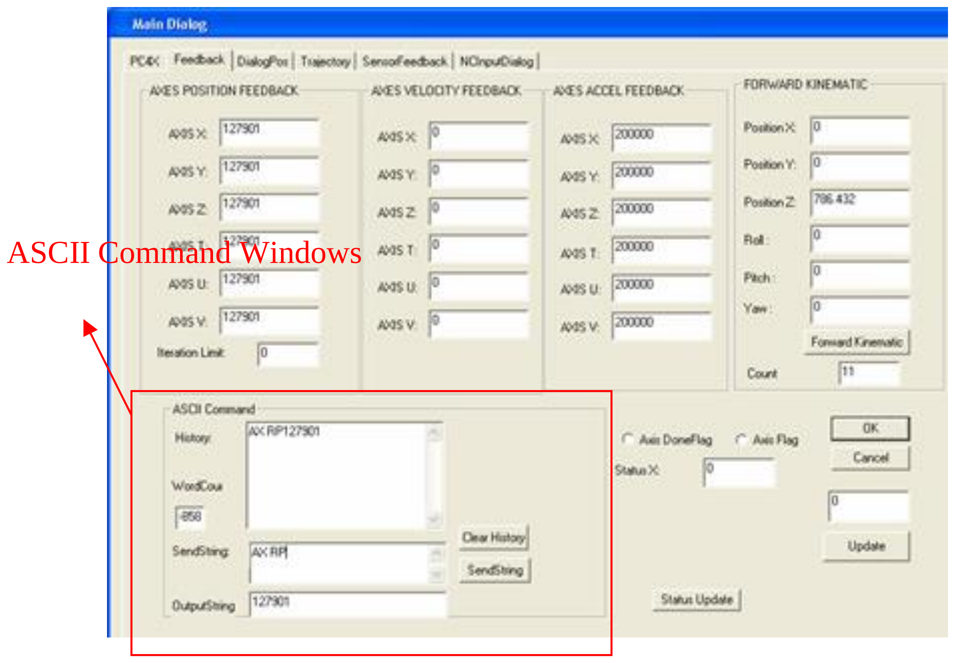

AXES POSITION FEEDBACK

AXIS X:	127901
AXIS Y:	127901
AXIS Z:	127901
AXIS T:	127901
AXIS U:	127901
AXIS V:	127901
Iteration Limit	0

AXES VELOCITY FEEDBACK

AXIS X:	0
AXIS Y:	0
AXIS Z:	0
AXIS T:	0
AXIS U:	0
AXIS V:	0

AXES ACCEL FEEDBACK

AXIS X:	200000
AXIS Y:	200000
AXIS Z:	200000
AXIS T:	200000
AXIS U:	200000
AXIS V:	200000

FORWARD KINEMATIC

Position X:	0
Position Y:	0
Position Z:	786.432
Roll :	0
Pitch :	0
Yaw :	0
Count	11

ASCII Command

History:	AX RP127901
WordCou	-858
SendString:	AX RP
OutputString	127901

( ) Axis DoneFlag ( ) Axis Flag

Status X:	0
	0

Figure 8.2 Motion control feedback

8.3 Wire sensor interface

By implementing the wire sensors interface in the GUI as shown in Figure 8.3, external sensors can be used to measure the linear motion of the actuators of the platform which could provide a more reliable feedback. Through the feedback of the length of the stroke of the actuator, reliable feedback of the position and orientation of the mobile platform can be calculated through the forward kinematics algorithm. Hence, this interface is created in the GUI to read the data generated by the external sensors transferred in real time.

Firstly, the data are obtained from National Instrument DAQ card. The analog value of the extension of the wire is converted into digital values using the DAQ card. The digital value is expressed in terms of voltage which is proportional to the extended length of the wire sensors. The voltage value of each sensor is converted to the measurement unit of millimeter with the calibrated gain value. The values are further stabilized using root mean square with a sampling time.

Next, the feedback values can be used to calculate the position and orientation of the platform through forward kinematics. The voltage value and the measured extension length as well as the position and orientation of the mobile platform are shown on the wire sensor interface in Figure 8.3.

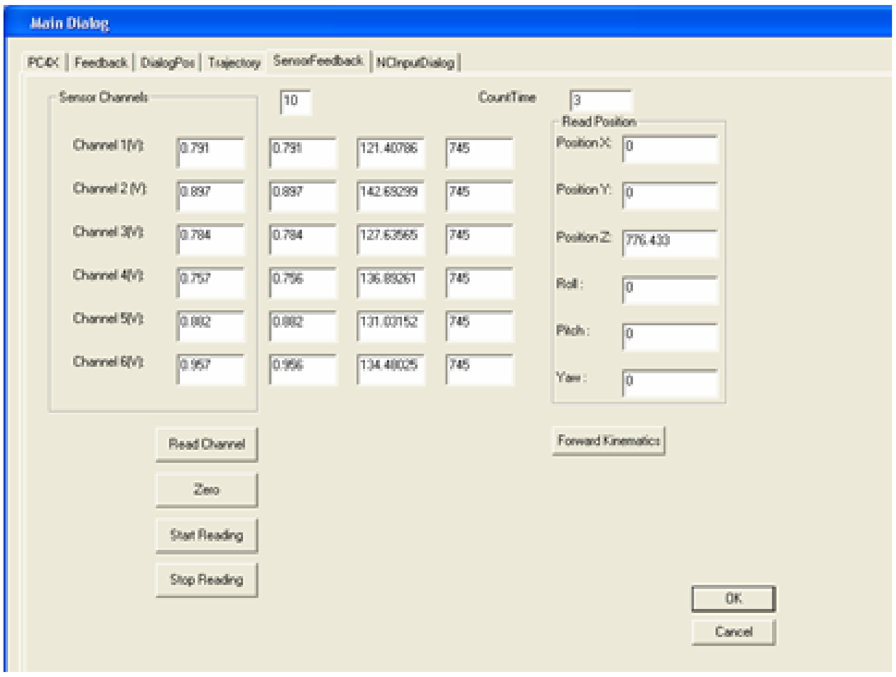

Sensor Channels: 10

CountTime: 3

Channel 1(V):	0.791	0.791	121.40786	745
Channel 2 (V):	0.897	0.897	142.69299	745
Channel 3(V):	0.784	0.784	127.63565	745
Channel 4(V):	0.757	0.756	136.89261	745
Channel 5(V):	0.882	0.882	131.03152	745
Channel 6(V):	0.957	0.956	134.48025	745

Read Position

Position X:	0
Position Y:	0
Position Z:	776.433
Roll :	0
Pitch :	0
Yaw :	0

Figure 8.3 Wire sensor interface

8.4 NC program interface

An NC program interface is developed so that the user can communicate with the Stewart Platform by writing the command in NC codes. The NC program can be generated through the postprocessor of the MasterCam and imported to the NC program interface as shown in Figure 8.4. The interface can help translate the NC program into multi lines of command which can be understood by the Stewart Platform. It will generate the trajectory path that can be used to manipulate the platform to the defined position and orientation with the specific velocity.

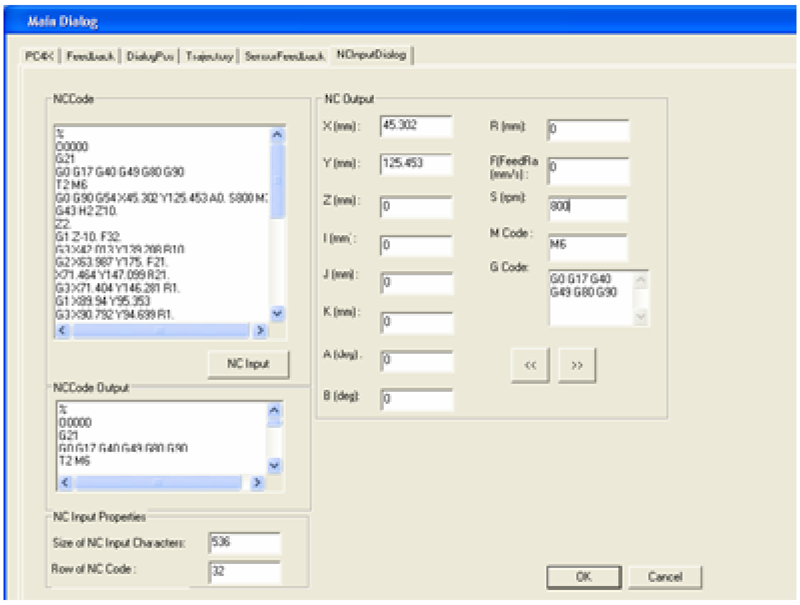
Main Dialog
PC4K | Feedback | DialogPos | Trajectory | SensorFeedback | NCInputDialog
NC Input
<<
>>
OK
Cancel

NCCode

```
%
O0000
G21
G0 G17 G40 G49 G80 G90
T2 M6
G0 G90 G54 X45.302 Y125.453 A0. S800 M
G43 H2 Z10.
Z2.
G1 Z-10. F32.
G3 X42.013 Y139.208 R10.
G2 X63.987 Y175. F21.
X71.464 Y147.099 R21.
G3 X71.404 Y146.281 R1.
G1 X89.94 Y95.353
G3 X90.792 Y94.639 R1.
```

NCCode Output

```
%
O0000
G21
G0 G17 G40 G49 G80 G90
T2 M6
```

NC Input Properties

Size of NC Input Characters: 536

Row of NC Code: 32

NC Output

X (mm): 45.302

Y (mm): 125.453

Z (mm): 0

I (mm): 0

J (mm): 0

K (mm): 0

A (deg): 0

B (deg): 0

R (mm): 0

F(FeedRa (mm/s): 0

S (rpm): 800

M Code: M6

G Code: G0 G17 G40 G49 G80 G90

Figure 8.4 NC program Interface

8.5 OpenGL interface

A basic OpenGL interface is also developed so that the user can visualize the cutting path based on the provided NC program generated through MasterCam.

Hence when the NC programs are imported to the NC program interface, the conversion to the Stewart Platform machining path, the coordinates of the trajectory path will be visualized on the window in the OpenGL interface as shown in Figure 8.5. This function can help the user identify the error of the trajectory path through the illustrated diagram of the platform.

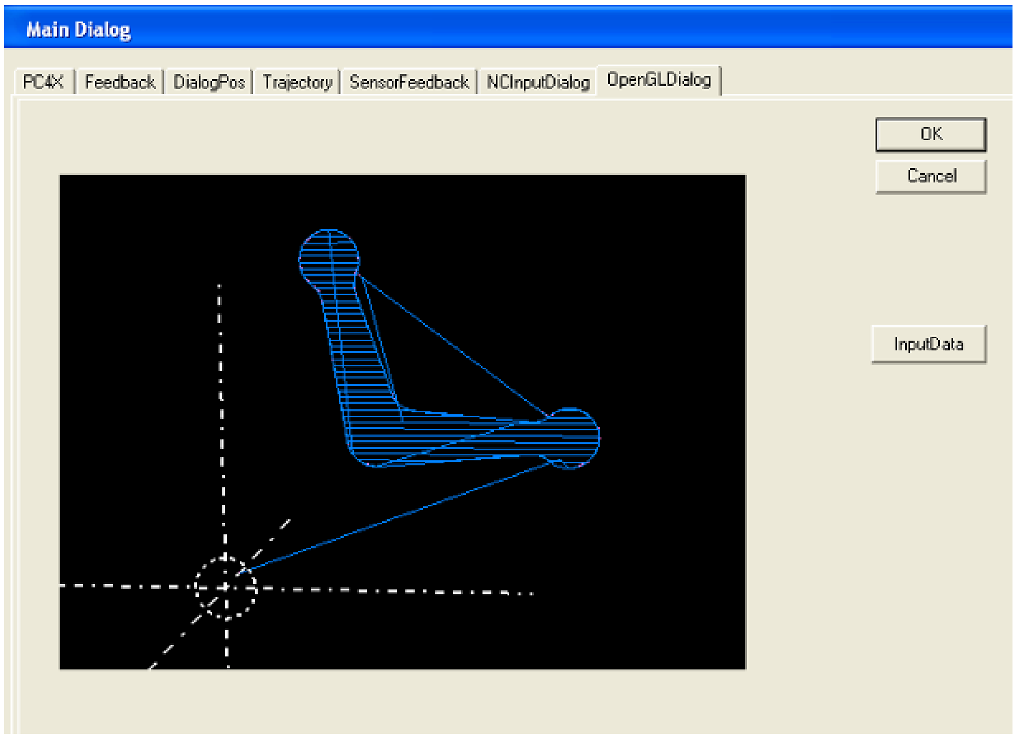

Figure 8.5 OpenGL Interface

In short, the development of the graphic user interface (GUI) is able to help the users have a friendlier working environment to control and manipulate the Stewart Platform in machining processes. A real time feedback system developed for the platform also helps to improve the accuracy of the system in the aspect of translation and orientation of the mobile platform.

Chapter 9 3-DOF modular micro Parallel Kinematic Manipulator for machining

9.1 Introduction

The increasing demand of product quality, reducing product cost and shortening the product development cycle results in a continuing need to achieve improvements in speed, versatility and accuracy in machining operations especially high speed machining. Hence, the recent trends towards high speed machining have driven the motivation in the research and development of new novel types of parallel kinematics machines (PKMs) [Sameer, 2003].

In the process of research and development, there are still some disadvantages of the Stewart Platform. This six-legged manipulator suffers the disadvantages of the complex solution of direct kinematics, coupled problems of the position and orientation movement as well as the expensive cost to manufacture high precision spherical joint [Tsai, 1996]. Thus, further research was performed after investigating the present Stewart Platform. A new trend of development of the Parallel Kinematics Manipulator tends to reduce the 6-DOFs to 3-DOFs PKMs. The reducing of DOF of the PKMs has advantages in workspace and cost reduction. It is because 6-DOFs are not often required in machine tools and other applications. However, the 3-DOF Parallel Kinematics Platform provides less rigidity and degrees of freedom.

To overcome the above shortcomings, parallel manipulators with fewer than six DOFs have been investigated. For examples, Clavel [Clavel, 1988] and Sternheim [Sternheim, 1987] studied a 4-DOF high speed robot called Delta Robot. Lee and Shah [Lee, 1987] analyzed a 3-DOF parallel manipulator. Although, these two robots possess closed-form direct kinematics solutions, the Delta robot contains twelve spherical joints while Lee and Shah’s manipulator contains three spherical joints. In addition, the position and orientation of Lee and Shah’s manipulator are coupled. Some 3-DOF parallel manipulator architectures provide pure relative rotation of the moving platform about a fixed point and are used as pointing devices, wrists of manipulators and orienting devices [Asada, 1985], [Gosselin, 1994]. Tsai [Tsai, 1996] introduced a novel 3-DOF translational platform that is made up of only revolute joints. It performs pure translational motion and has a closed-form solution for the direct and inverse kinematics.

Hence, a study of running 3-axis machining with the multi-axis robots reported that it is highly unjustified as several of the axes remain under-utilized because of the redundancy in DOF thus increases the complexity and cost. It is because a pure 3-DOF translational or orientation motion would require the activation of all the six-module legs, which means increase in energy consumption [Mircea, 2002]. Hence, in terms of cost and complexity, 3-DOF 3-legged Micro Parallel Kinematic Manipulator is cost effective and the kinematics of the mechanism is further simplified for the purpose of control. However, if the new system is decided to be constructed, the design algorithms either do not exist or are very complicated.

To further increase the flexibility and functionality of the self-fabricated Micro Stewart Platform, the concept of modular methodology is introduced. In recent years, modular robots were increasingly proposed as means to develop reconfigurable and self-repairable robotic systems [Mckee, 1999]. To further optimize the performance of the 3-legged 3-DOF Parallel Manipulator and the self-repair ability, the manipulation systems need to incorporate modularity and self-reconfiguration capabilities. Modular robots develop many autonomous units or modules that can be reconfigured into a huge number of designs. Ideally, the modules will be uniform, and self-contained. The robot can change from one configuration to another manually or automatically. Hence, a modular manipulator can be reconfigured or modified in shape to adapt to a new environment. Modules must interact with one another and cooperate in order to realize self-configuration. In addition, modular Micro Parallel Kinematic Manipulators can repair themselves by removing and replacing failed modules. Since one self-reconfigurable modular robot can provide the functionality of many traditional mechanisms, they will especially suit high variety tasks, such as the high speed machining [Sameer, 2003] in the precision engineering industry.

Basically the direction of the development of the Micro Parallel Kinematic Manipulator (MSP) is set to emphasize on the minimization of the dimensions of the system and the portability of the system on the CNC machine.

Due to the minimization of the dimensions of the MSP, the number of links of the Stewart Platform is reduced to three instead of six. The DOF for a closed-loop Parallel Kinematic Manipulator is examined by the Grübler's formula in Equation (9.1).

$$F_e = \lambda(l - j - 1) + \sum_{i=1}^{j} f_i - I_d \tag{9.1}$$

The number of joints is 9 (6 universal joints and 3 prismatic). The number of links is 8 (2 parts for each actuator, the end effector and the base) .The sum of all the joint freedom is 15. Hence, by using Grübler's formula as shown in Equation (9.1), the DOF is computed as $F = 6(8-9-1)+15=3$. By using a systematic enumeration methodology developed by Tsai [Tsai, 2002], the search domain can be further conjugated in Table 9.1.

Table 9.1 Feasible limb configurations for spatial 3-DOF manipulators [Tsai, 2000]

Type	Kind
120	UPU, RUU, PUU
201	RRS,RSR,RPS,RSP,PSR,PRS,SPR,PPS,PSP,SPP

U = Universal Joint, R = Rotational Joint, S = Spherical Joint, P = Prismatic Joint

Based on Table 9.1, a comparison study on each configuration is performed to justify the configuration method that meets the requirement of the parallel kinematics system that need to be constructed.

Furthermore, the PKM needs to achieve an accuracy of 1 micron. Thus, good quality components need to be searched for the required high level performance to achieve the requisite accuracy. The selection of the relevant parts needs to be carefully performed since the Platform is used for micromachining, which requires higher rigidity than the previously completed Stewart Platform.

A micron precision Micro Parallel Kinematic Manipulator is built which can take loads up to 3 kg for the purpose of micro machining and assembly. Therefore, based on the previous study of the fabricated Stewart Platform, various designs of Parallel Manipulator were simulated in micro scale in MATLAB® such as the 6-legged Stewart Platform, 3-legged Parallel Kinematic Manipulator and PUS (Prismatic, Universal and Spherical Joint Configuration) Stewart Platform. The workspaces of the respective platforms were simulated and compared such that the most suitable design will be chosen.

Besides, the relationship between the workspace and the radii of the mobile platform and the fixed base is also studied. It is to define the radii of the base and platform so that the workspace can be optimized. The maximum angle of the platform which can be oriented is also being deliberated based on the stroke of the actuators, in order that it can be a reference for the selection of the actuators.

9.2 Simulation of Various Parallel Kinematic Manipulators

Mathematical models of the various Stewart Platforms are investigated by performing simulation using MATLAB®. The workspaces of the Stewart

Platforms are compared to verify the suitable kinematics model. 6-legged Stewart Platform, 3-legged Parallel Kinematic Manipulator and PSU Stewart Platform are simulated in MATLAB®. These kinematics models are chosen because they have higher payload and are simpler to be controlled. All the three models are shown in Figure 9.1.

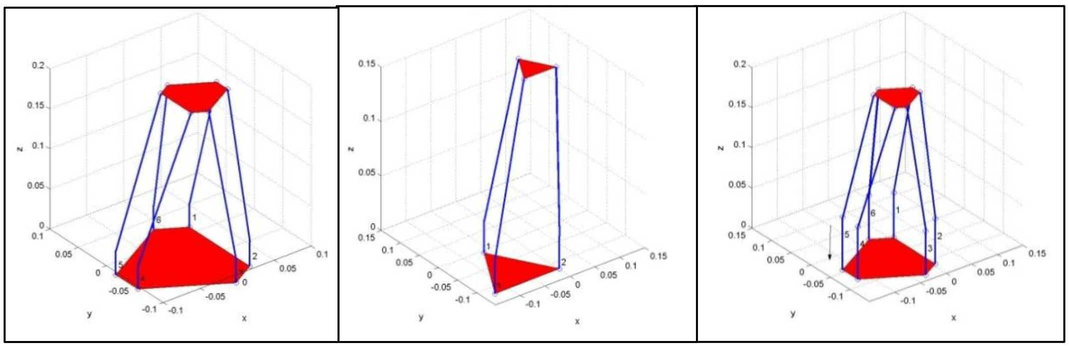

Figure 9.1(a)(b) 6-Legged Micro Stewart Platform and 3-Legged Micro Stewart Platform (c) PSU Micro Stewart Platform

Simulation is performed to determine the optimized workspace of the PKMs with suitable radii of the base and the platform as well as passive spherical joints. In the simulation, certain parameters are set constant, such as the length of the link is set as 0.22 m with a stroke of 0.05 m. Besides, the tilting angle of the universal joint is set as ±45º**.**

Using MATLAB® to simulate the motion of the Manipulator, each 3D-space position that the Platform can reach is recorded and compared in the same graph in Figure 9.2. From Figure 9.2, it can be seen that the workspace of the 6-

legged Parallel Manipulator can reach a higher position. However, the volume of the workspace of the 3-legged Parallel Manipulator is larger.

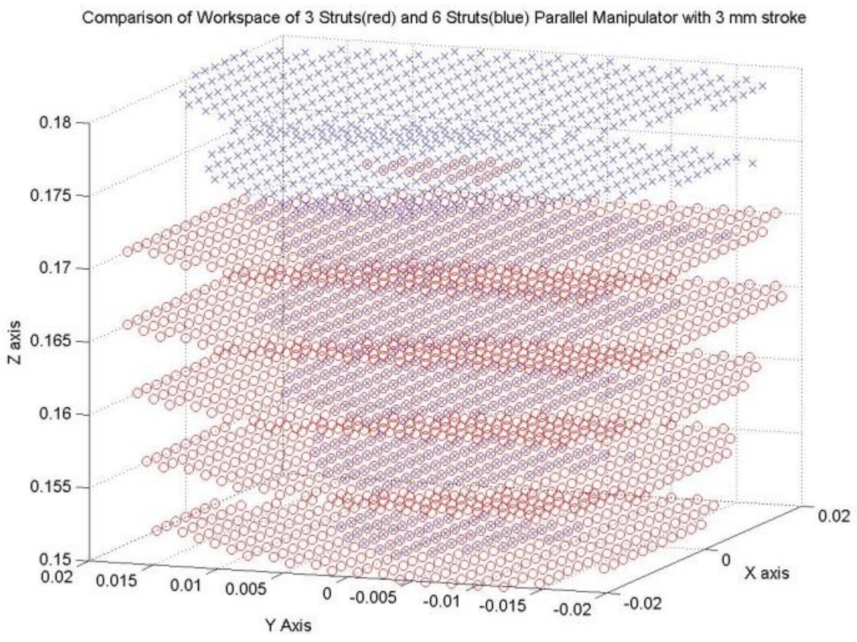

Figure 9.2 Comparison of Workspace of 3-legged (red) and 6-legged (blue) Parallel Manipulator

9.3 Simulation Result

In this simulation, the radius of the base of the PKM is set as 0.075 m. By setting different radii of the mobile platform of the PKM through the workspace simulation, various workspaces are found. Based on the analysis, as shown in Table 9.2 and Figure 9.3, the workspace of the PKM is affected by the radius of the mobile platform. Thus, the bigger the radius of the mobile platform, the bigger is the workspace that can be achieved. However, a potential problem can be foreseen if the radius of the mobile platform is equal to the radius of the base.

Singularity might happen at the point when the radii of mobile platform and the base are the same. The stiffness of the MSP might be reduced because all the joints are vertically upward, hence the tension force of the struts between the mobile platform and the base may be reduced. Thus, the problem has to be further studied and a complete solution is needed if a larger mobile platform is used.

Table 9.2 Workspace of mobile platforms with various radii

The radius of the Micro SP, r	Workspace x $10^{-4}m^3$
0.035	3.0032
0.04	3.2810
0.05	5.7313
0.06	6.7163
0.07	9.9988
0.075	11

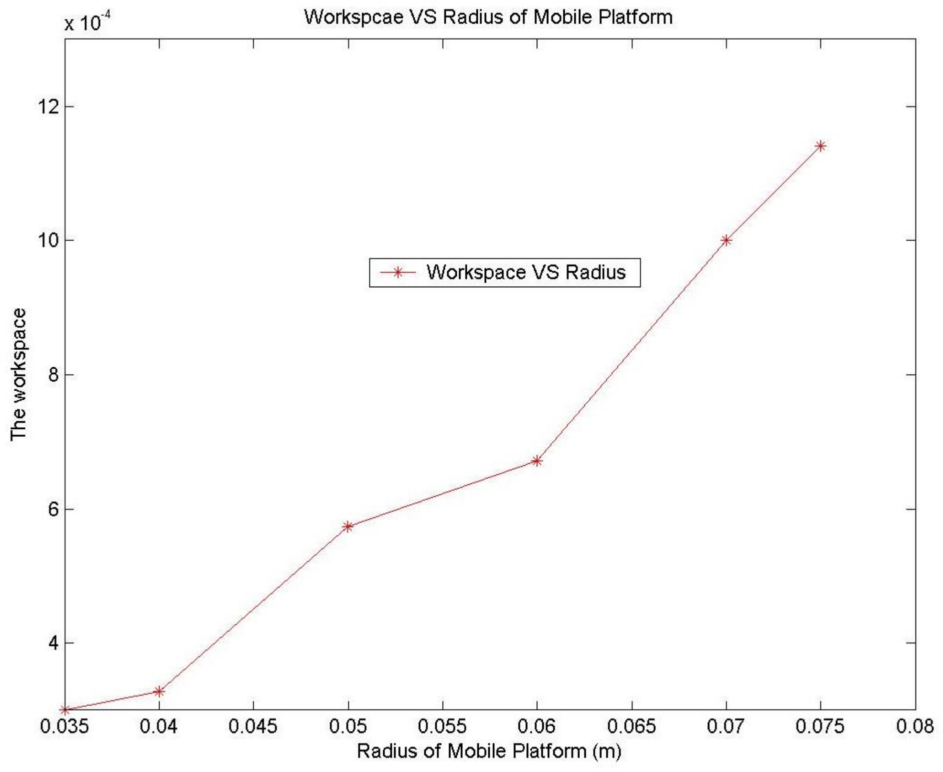

Figure 9.3 Workspace VS radius of Mobile Platform

In addition, the height of the PKM is affected by the radius of the mobile platform. Since the length of the struts is fixed, with a smaller mobile platform, the struts can be tilted to a certain angle, which can reduce the height of the platform. In contrast to the relationship between the radius of the platform and the workspace, the workspace of the MSP decreases while the radius of the base is increased, as shown in Table 9.3 and Figure 9.4. In this simulation, the radius of the platform is set to be 0.04 m.

Table 9.3 Workspace of the base with various radii

The radius of the Base, r	Workspace x $10^{-3}m^3$
0.075	0.4126
0.085	0.2760
0.095	0.1665
0.105	0.0826

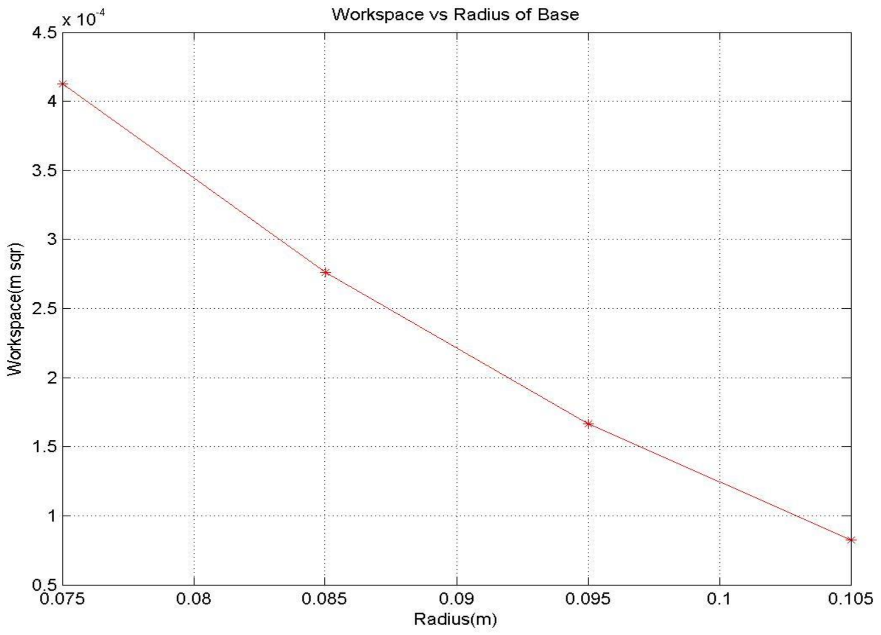

Figure 9.4 Workspace vs Radius of Base

Based on the analysis of the results of both simulations, when the difference between the size of the base and the platform becomes bigger, the workspace of the platform will become smaller. Hence, to utilize the workspace of the platform, the base of the MSP is suggested to be 0.075 m and the platform to be 0.05m. Thus, a ratio of 2:3 is suggested for the design of the radius of mobile platform and the base.

In short, the functional features of the Micro Parallel Kinematic Platform are very important. The required functional feature of the platform will affect future development directions of the platform, whether it will be designed for stiffness or for smaller sizes for portability purposes.

The results of the workspace simulated (Figure 9.5) are obtained by setting the platform with a base radius of 0.075 m and the platform radius as 0.05m with various passive spherical joint angles of 20º and 45º. From the results, the workspace of the MSP increases drastically when the tilting angle of the spherical joint changes from ±20 º to ±45º. By installing a 45º spherical joint, the volume of the workspace can reach up to 0.0014 m^3 instead of 4.1263 x 10^{-4} m^3 when a spherical joint of 20 º is installed.

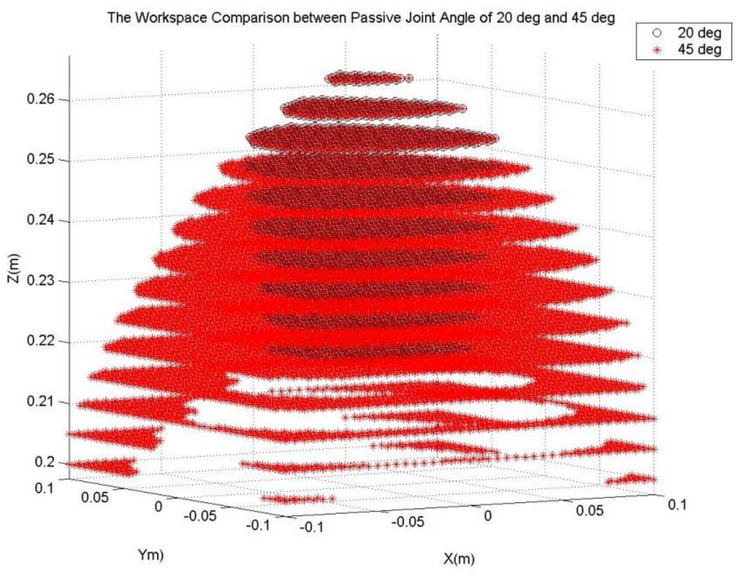

Figure 9.5 The workspace comparison between Passive Joint angle of 20º and 45º

Simulation is also done to search for the maximum stroke that the actuator needs to achieve the largest orientation angle. Different actuators with various strokes are simulated to obtain the respective angle it can rotate. In the end, to achieve 45º angle of rotation of the mobile platform, the stroke of the actuators must be 50 mm.

Based on the study on the feasibility of the 3-legged Micro PKM, it was found that the DOF is limited by the availability of the active joints. Thus, the 3-legged Micro Stewart Platform only possesses 3 DOF by having three prismatic actuators. The DOF of the system can be increased by installing extra active joints such as revolute motors or extra prismatic legs are installed. Vice versa, the DOF of each link can be reduced by replacing the passive joints such as spherical joints with universal Joints or install some constraint components such as a rigid link.

A 3-DOF Parallel Kinematic Manipulator can be manipulated either purely in translational or rotational movement. The hybrid of both motions is feasible but the complexity will be increased. Another method was suggested in [Sameer, 2003], a cooperating hybrid kinematics machine can be constructed by installing a 3-legged orientation mechanism parallel manipulator and a 3-legged translational mechanism parallel manipulator, a 6-DOF Parallel Kinematic Manipulator system can be achieved.

In short, based on the result of simulation, a 3-DOF Micro Parallel Kinematic Manipulator will be constructed with the installation of a 50 mm stroke actuator and 125 mm diameter platform and 250 mm diameter base to achieve the requirements of the workspace and functions of the platform.

9.4 Selection of Actuator and Joints

Based on all the previous studies of the Parallel Platform, a M-235.5DG actuator from PI company is chosen. It has higher loads of 120 N and 100 N of lateral force; theoretically the three legs can hold literally up to 360 N of load vertically. It can also achieve micron accuracy in linear motion.

To further increase the degree of orientation mechanism as suggested in literature study, a Hephaist Spherical Joint from Hephaist Seiko Co. is selected as shown in Figure 9.6. A Hephaist Spherical Joint is unlike other available spherical joints in the market. It has a working angle of 40º and can take higher torque.

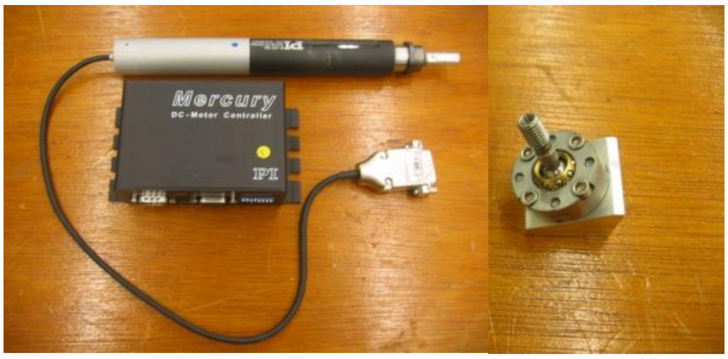

Figure 9.6 The M-235.5 DG Actuator and Hephaist Seiko Spherical Joint Designs of the Micro Parallel Manipulator

Basically, a modular parallel robot consists of a set of independently designed modules, such as actuators, passive joints, rigid links (connectors), mobile platforms and end-effectors that can be assembled rapidly into various configurations with different kinematics characteristics and dynamic behaviors. There are many configurations for a modular platform. Therefore, the development of a methodology for the type and dimensional synthesis of a parallel robot system for a particular task is a basic and important requirement [Anjan, 2003].

Based on the research in [Anjan, 2003], a modular parallel robot may have unlimited configurations depending on the inventory of modules. Principally, the modules to assemble a modular micro Stewart Platform can be divided into two sections:

a) Fixed Dimension Modules:

   This includes actuator modules, passive joint modules, such as rotary, pivot and spherical joints and end-effector joints.

b) Variable-Dimension Modules:

This gives the end-user the ability to fine-tune the kinematic and dynamic performance of the manipulators rapidly. A set of links and a mobile platform have been designed and fabricated.

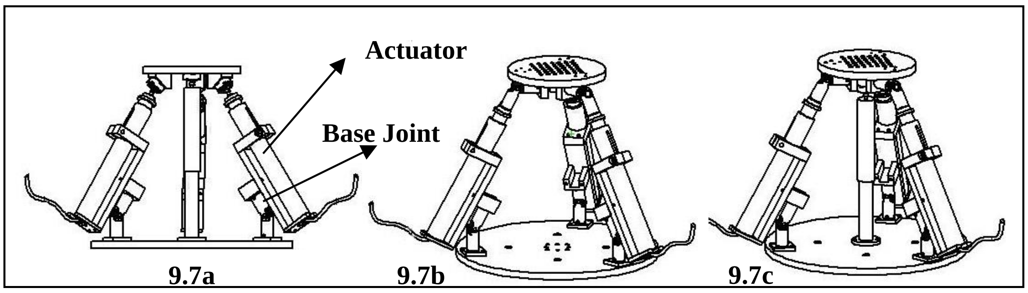

Figure 9.7 Parallel Manipulator system fabricated using the same modular components (Prismatic Actuator, Spherical Joints, Universal Joints and Variable Links)

By combining the modules, different kinds of Modular Parallel Kinematic Manipulators can be assembled based on the functionality and purpose of the system. As shown in Figure 9.7(a), a pure orientation mechanism platform, a pure translational mechanism platform as well as a hybrid UPU platform can be assembled by interchanging the spherical joints and universal joints or adding extra rigid links.

Therefore, based on the principles of the system, three designs of the Parallel Kinematic Platform drawn using SolidWorks are shown in Figure 9.7. To maintain the high rigidity of the Platform, the DOF of the system needs to be constrained by installing some extra joints or reduce the DOF of the joints. For the

4-legged orientation mechanism platform as shown in Figure 9.7(a), a rigid leg with a spherical joint is installed in the middle of the platform, in order that the motion of the KPM is limited to angle rotation; thus it can perform pure orientation movement. Another design of 3 UPU System is shown in Figure 9.7(b), the spherical joint of the MSP is replaced by Universal Joints. Hence, the platform system is limited to translational movement by properly orienting the axes of universal joints. Besides, another 3-DOF Parallel Kinematic Manipulator is set up as shown in Figure 9.7(c). It is a hybrid 3-DOF platform which consists of translation movement along Z-axis and orientation around X- and Y-axes. However, due to the length of the actuator which is 218 mm for 50 mm stroke, it is quite hard to assemble the whole system inclusive of the joints in the 150 mm x 150 mm x150 mm dimensions. The minimum height that can be achieved with this system is 250 mm as shown in Figure 9.7. As shown in Figure 9.7(a), by installing the actuator parallel to the base joint instead of the usual way of installing the actuator on top of the base joint, the height of the platform can be reduced to 250 mm. However, the kinematics calculation of the stroke of the actuator will be more complicated since the actuator is not in-line with the base joint and spherical joint. A new method of calculation will be shown in the next section.

Nevertheless, there are certain advantages of installing a 3-DOF micro parallel platform. The post-processing will be less complex and the stiffness of the systems can be increased. Furthermore, the modular design concept can be introduced to the 3-DOF platform. By fabricating interchangeable parts for the system, the 3-DOF Parallel Kinematic Manipulator can be modified from a translational platform to a rotational platform. In future, extra legs or active joints can be bought to increase the DOF of the Micro Parallel Kinematic Manipulator.

A few configurations of the 3 DOF of Stewart Platform were assembled in the lab as shown in Figure 9.8, such as a pure translational Parallel Kinematic Manipulator and a pure orientation movement Parallel Kinematic Manipulator.

Translational singularities were detected in the calibration of the pure translational MSP while it is in the static form. It is verified that in the static position, extra DOFs are introduced. It is because some geometry conditions are not met, such as all the revolute pair axes at the leg endings do not converge towards a single point and every leg has two intermediate resolute pair axes which are not parallel to one another and are perpendicular to the straight line through the universal joint center [Gregorio, 2001]. Hence, a careful assembly of the modular unit of the 3-UPU platform with certain geometry condition is needed to attain controllable pure translational motion.

Calibrations and various tests were performed on the modular configured. For the Orientation-Movement Parallel Kinematics Platform, the platform is able to perform 3-DOF rotational movements in roll, pitch and yaw angles. As all the links are installed with 2-DOF universal joints, prismatic links and 3-DOF spherical joints, by installing a fixed link in the middle with a spherical joint, the motion of the platform will be limited to purely orientation movement around a fixed point. The major disadvantage of this type of configuration is that the platform cannot perform Z axis movement which is a crucial requirement for micro machining. The over constrained design of the platform by installing a fixed middle link will cause the high risk of damaging the platform if it is manipulated out of the defined workspace.

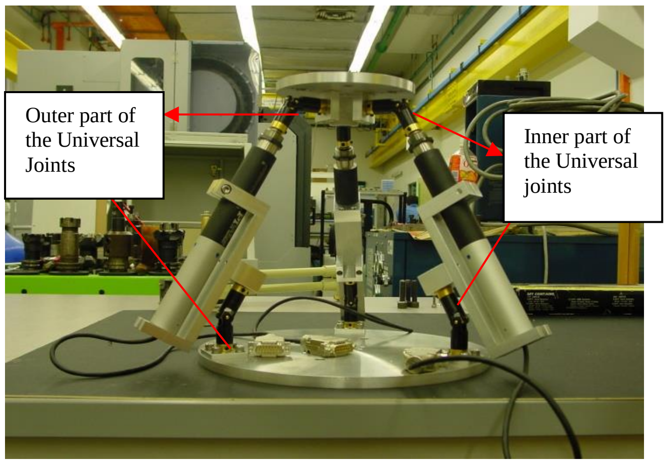
Outer part of the Universal Joints
Inner part of the Universal joints

(a)

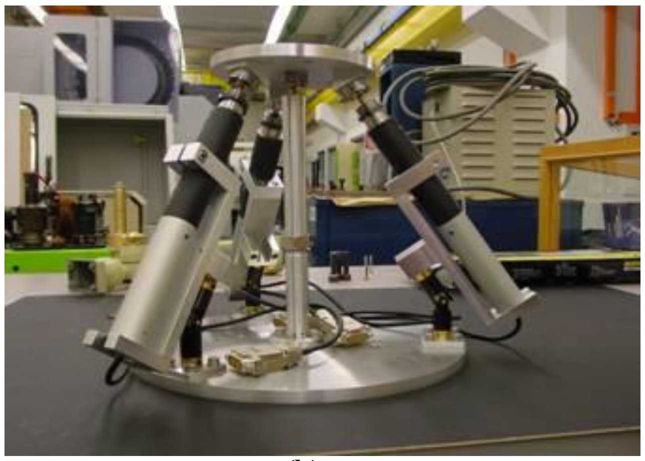

(b)

Figure 9.8 (a) Pure Translational Platform, (b) Pure Rotational Platform

A hybrid Parallel Kinematic Manipulator is assembled by installing a passive prismatic link in the middle of the pure translational platform as shown in Figure 9.9. The problem of the singularity problem can be solved. By installing the passive prismatic joint with a spherical joint attached to the platform, the extra degree of freedom incurred by the universal joints of the links is constrained. Thus, the hybrid Parallel Kinematic Manipulator is able to performed movements along Z-axis and rotation around X-axis and Y-axis. Among the three parallel kinematic manipulator architectures, the hybrid platform is further elaborated because it is planned to be used as a micro manipulator for the tool holder to perform machining jobs on the workpiece which is located on the large Stewart Platform. Calibration of the hybrid UPU Parallel Kinematic Manipulator is performed and the results are very decent where the accuracy of the movement is up to 0.5 mm and 0.02 deg. Further elaboration of the mathematical model of the manipulators will be discussed in the later section of this chapter.

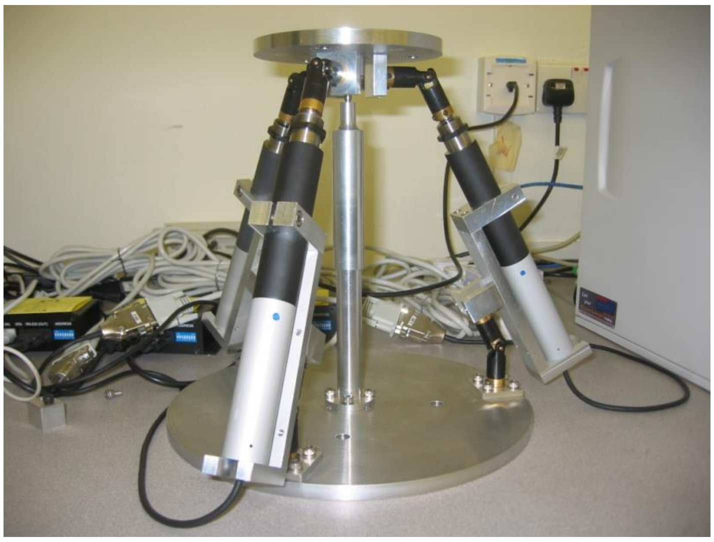

Figure 9.9 Hybrid UPU Parallel Kinematic Manipulator

9.5 Mathematical Models of Hybrid Parallel Kinematic Manipulator

Due to the height limitation of 250 mm, the actuator is not located in-line with the joints but parallel to the joints as shown in Figure 9.10.

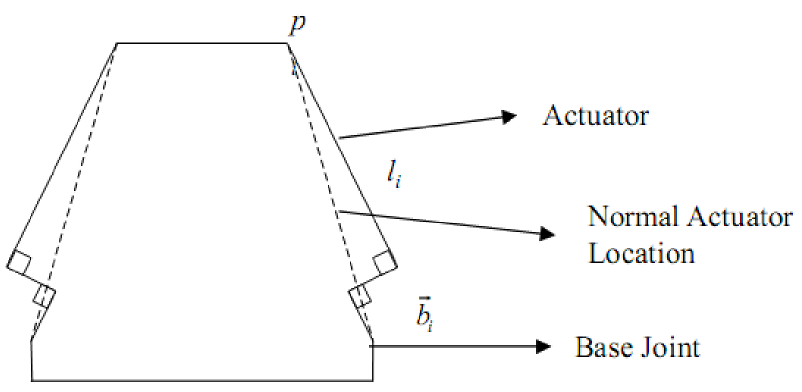

Figure 9.10 Schematic Diagram of the Parallel Kinematics Platform (PKM)

Thus, the calculation of the length of the link is different from the normal PKM actuator length as shown:

$$\vec{l}_i = -\vec{b}_i + \vec{t} + \underline{R} \cdot \vec{p}_i \text{ , i = 1 ... 3} \tag{9.2}$$

where l_i is the dotted link length and $\vec{t}$ and R are the translation and orientation of p_i with respect to [X_P Y_P Z_P]^T. However, for this hybrid PKM, extra calculation steps need to be performed as shown in Figure 9.11.

$$x^2 + a^2 = y^2 \tag{9.3}$$

$$\frac{k-x}{x} = \frac{z}{a} = \frac{L-y}{y} \Rightarrow y = \frac{xL}{k} \tag{9.4}$$

$$(10.3) \Rightarrow (10.4) \Rightarrow x = \sqrt{\frac{a^2}{(\frac{L^2}{k^2})-1}} \tag{9.5}$$

$$(9.5) \Rightarrow (9.4) \Rightarrow z = a \times \frac{k-x}{x} = \left(\frac{k - \sqrt{\frac{a^2}{\frac{L^2}{k^2}-1}}}{\sqrt{\frac{a^2}{\frac{L^2}{k^2}-1}}} \right) \times a \qquad (9.6)$$

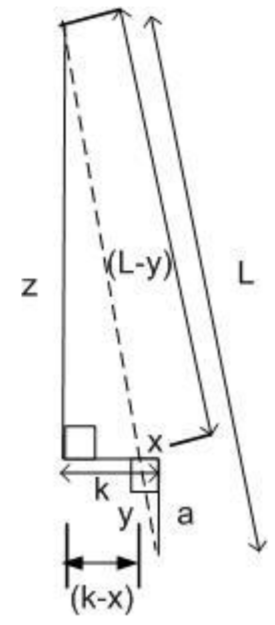

Figure 9.11 Calculation of the actual stroke of the link

By knowing the length of the dotted link L using inverse kinematics, the length of Z can be measured using the similarity triangular theory. Hence, the strokes of the links are found indirectly by knowing the motion of the platform. However, the stroke of the links would need to be further affirmed by requiring the orientation of each link to the desired position and orientation of the platform by using forward kinematics as shown in Fig.9.12.

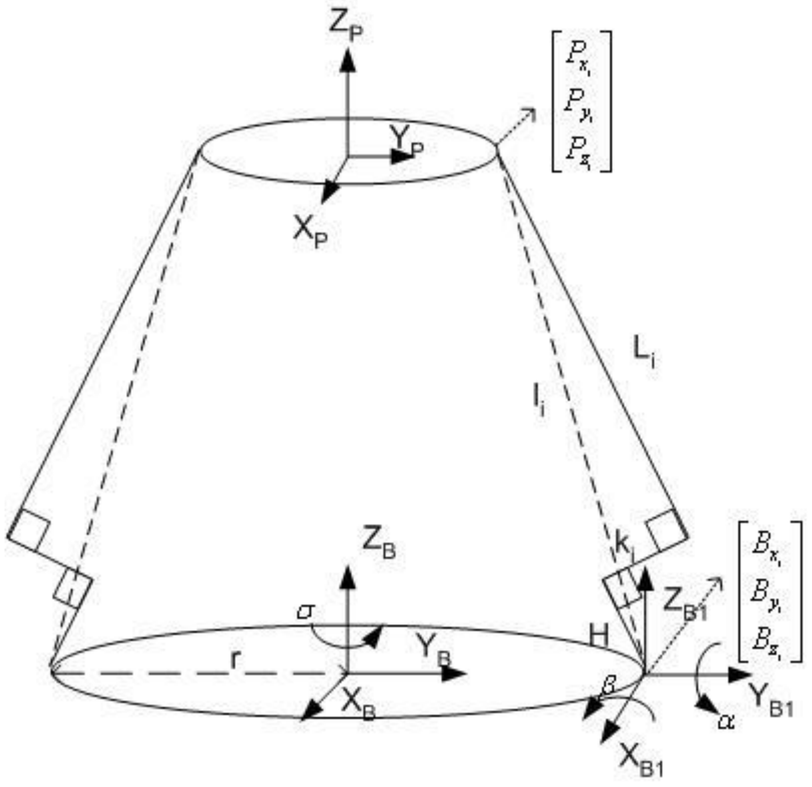

Figure 9.12 Denavit-Hartenberg Representation

Let $X = \alpha, Y = \beta, Z = \sigma$, let L_i+H = M_i, because L_i is known from the similarity triangle equation. Since by inverse kinematics of the platform, one should be able to know the point $\begin{bmatrix} P_{x_i} \\ P_{y_i} \\ P_{z_i} \end{bmatrix}$, i = 1, 2, 3. Thus from the known platform point, it is possible to calculate the rotational angles of X and Y by the known actuator stroke lengths as shown in Equation (9.7).

$$\therefore R_z \times R_{xy} \times \begin{bmatrix} 0 \\ k_i \\ Mi \end{bmatrix} + \begin{bmatrix} r_{xi} \\ r_{yi} \\ 0 \end{bmatrix} = \begin{bmatrix} P_{x_i} \\ P_{y_i} \\ P_{z_i} \end{bmatrix} \tag{9.7}$$

$$\begin{bmatrix} \cos Z & -\sin Z & 0 \\ \sin Z & \cos Z & 0 \\ 0 & 0 & 1 \end{bmatrix} \times \begin{bmatrix} \cos Y & \sin Y \sin X & \sin Y \cos X \\ 0 & \cos X & -\sin X \\ -\sin Y & \cos Y \sin X & \cos Y \cos X \end{bmatrix} \times \begin{bmatrix} 0 \\ k_i \\ M_i \end{bmatrix} + \begin{bmatrix} r_{x_i} \\ r_{y_i} \\ 0 \end{bmatrix} = \begin{bmatrix} P_{x_i} \\ P_{y_i} \\ P_{z_i} \end{bmatrix} \quad (9.8)$$

Hence, by knowing the rotational angle of each universal joint of the respective links, the stroke length of the actuators can be confirmed. The known rotational angle is also used as a constraint to determine the workspace of the platform. By implementing the algorithm of the inverse and forward kinematics of this hybrid Parallel Kinematic Manipulator with MATLAB®, the simulation of the movements of the platform is shown in Fig.9.13:

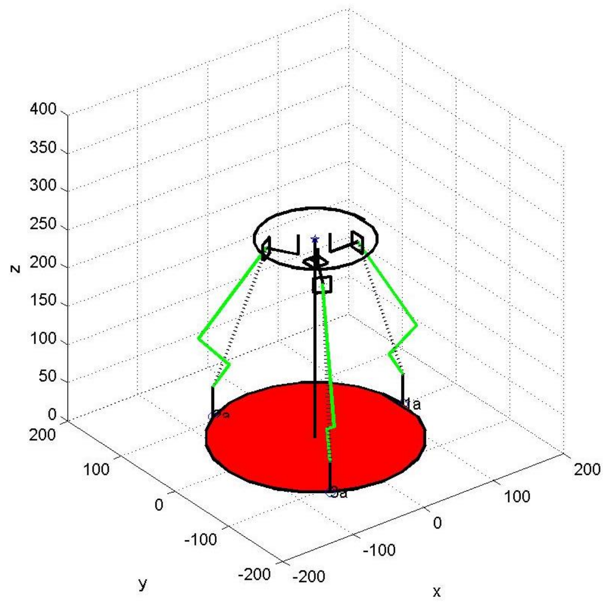

Figure 9.13 The UPU Modified Stewart Platform with a passive prismatic middle link

As shown in Figure 9.13, a passive middle link is installed with a spherical joint attached to the platform. The passive middle link acts as a constraint of an extra degree of freedom of the platform from translational movements along X- and Y-axes.

The workspace of the platform is also determined by measuring the surface point in the middle of the top platform with respect to the middle spherical joint. Due to the fact that the spherical joint is not directly attached beneath the platform, by rotating the platform with respect to the spherical joint, there is some movement of the surface point which will form a spherical locus that could depict the movement of the surface point in the Cartesian coordinate (Figure 9.14).

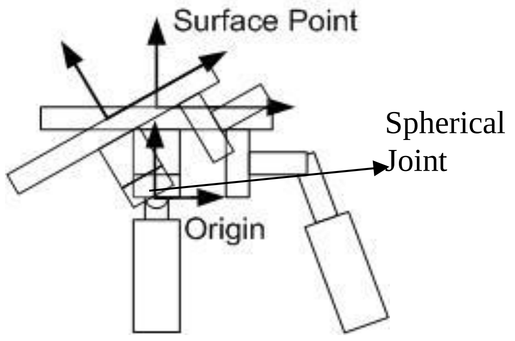

Figure 9.14 The Relationship between the Surface Point and the spherical joint

With the constraint of the middle link, the limitation of the actuator stroke and the known limitations of the rotation of the joint angle help to perform a more reliable simulation of the workspace as shown in Figure 9.15.

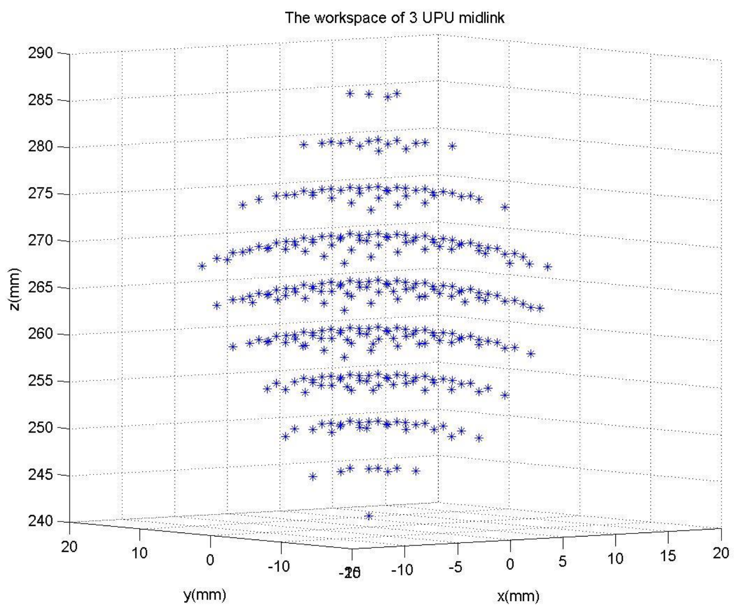

Figure 9.15 Workspace of the Surface Point of the Hybrid PKM

The workspace of the platform is relative small compared to other modular PKM configurations. However, this hybrid Micro Parallel Kinematic Manipulator is set to serve as a fine movement platform for micro machining in Z-direction as well as the rotation angle of the coordinates along the Z axis. Hence, by knowing the simulated working workspace, it can be incorporated into the post-processor checking to identify any motion outside of the workspace taking into account the physical travel limits of each individual link and joint. It is able to limit the platform from over travel and cause damage to the system. However, this system has limited Cartesian workspace; in terms of orientation workspace, it is able to perform up to ±20° around X- and Y-axes and 450 mm travel range along the Z-axis. Eventually, the well-developed algorithm of the platform is implemented using visual C++ interface to interact and manipulate the platform.

After all the simulation and interface programs have been completed, calibration was conducted using the CMM. The accuracy and repeatability of the measured platform can be up to 100 micron. The setup of the CMM is shown in Figure 9.16.

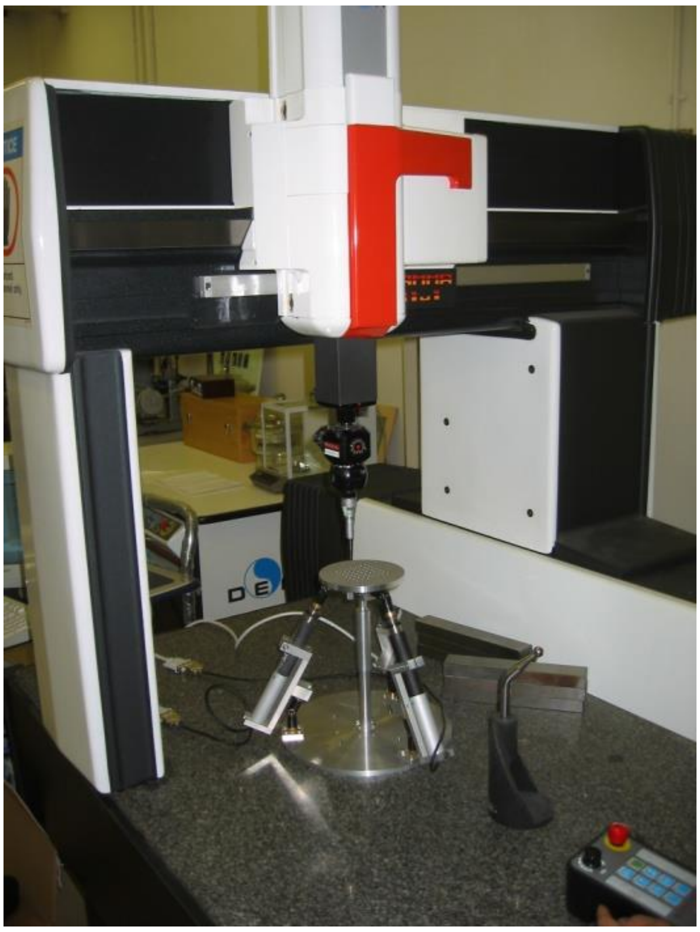

Figure 9.16 Accuracy Calibration of the Micro Stewart Platform with CMM

The calibration is performed by manipulating the platform to the theoretical position and orientation through the visual C++ interface. After the movement is performed, the calibration probe collects coordination data from the surface of the platform to calculate the actual surface plane of the platform. By using the CMM, the measurement variation of the actual angle and position to the theoretical angle and position are compared with respect to the surface of the table which has been predetermined as the reference plane. Hence, the result of the calibration is shown in Table 9.4.

Table 9.4 Calibration Result of the Micro Stewart Platform with the CMM

Theoretical Position and Orientation			Actual Position and Orientation			Position and Orientation Error		
Rotation X(deg)	Rotation Y(deg)	Position Z(mm)	Z - 10.426(mm)	Actual X(deg)	Actual Y(deg)	Z error (mm)	Angle X error(deg)	Angle Y error(deg)
0	0	279	278.850	-0.045	-0.365	-0.150	0.045	0.365
0	0	304	304.157	-0.040	-0.373	0.157	0.040	0.373
0	0	279	278.887	-0.055	-0.368	-0.113	0.055	0.368
0	0	304	304.153	-0.039	-0.378	0.153	0.039	0.378
0	0	279	278.851	-0.045	-0.370	-0.149	0.045	0.370
0	0	328	328.415	-0.047	-0.395	0.415	0.047	0.395
0	0	279	278.800	-0.049	-0.372	-0.200	0.049	0.372
0	0	314	314.258	-0.055	-0.382	0.258	0.055	0.382
5	0	314	314.407	4.957	-0.479	0.407	0.043	0.479
10	0	314	314.109	10.005	-0.709	0.109	-0.005	0.709
15	0	314	313.180	15.051	-1.092	-0.820	-0.051	1.092
20	0	310	309.027	20.088	-1.563	-0.973	-0.088	1.563
-5	0	310	309.747	-5.020	0.375	-0.253	0.020	-0.375
-10	0	310	309.146	-10.025	-0.128	-0.854	-0.025	-0.128
-15	0	310	307.820	-15.027	0.850	-2.180	-0.027	0.850
-20	0	310	307.390	-19.909	2.146	-2.610	0.091	2.146
0	5	310	309.952	0.310	4.527	-0.048	0.310	-0.473
0	10	310	309.527	0.565	9.535	-0.473	0.565	-0.465
0	15	310	309.195	0.866	14.536	-0.805	0.866	-0.464
0	20	310	306.751	1.171	19.495	-3.249	1.171	-0.505
0	-5	310	309.815	-0.027	-5.481	-0.186	-0.027	-0.481
0	-10	310	310.054	-0.085	-10.512	0.054	-0.085	-0.512
0	-15	310	310.990	-0.257	-15.545	0.990	-0.257	-0.545
5	5	310	309.900	5.133	4.438	-0.100	0.133	-0.562
10	10	310	310.200	9.886	9.636	0.200	-0.114	-0.364
-5	-5	310	310.331	-5.061	-5.387	0.331	-0.061	-0.387
-10	-10	310	310.073	-10.365	-10.035	0.073	-0.365	-0.035
-15	-15	310	308.015	-15.678	-14.331	-1.986	-0.678	0.669

□ **=Maximum Error**

From the graph in Figure 9.17, the maximum roll angle error is 1.17°, the maximum pitch angle error is 2.16°, while the maximum error in the Z-axis displacement is -3.25 mm. All the maximum errors occur while at least two errors are in the same data input, which is when the platform is translating and rotating simultaneously to the permitted maximum angle of rotation. However, while the platform is in a pure translational movement, the error of displacement is within ±0.42 mm.

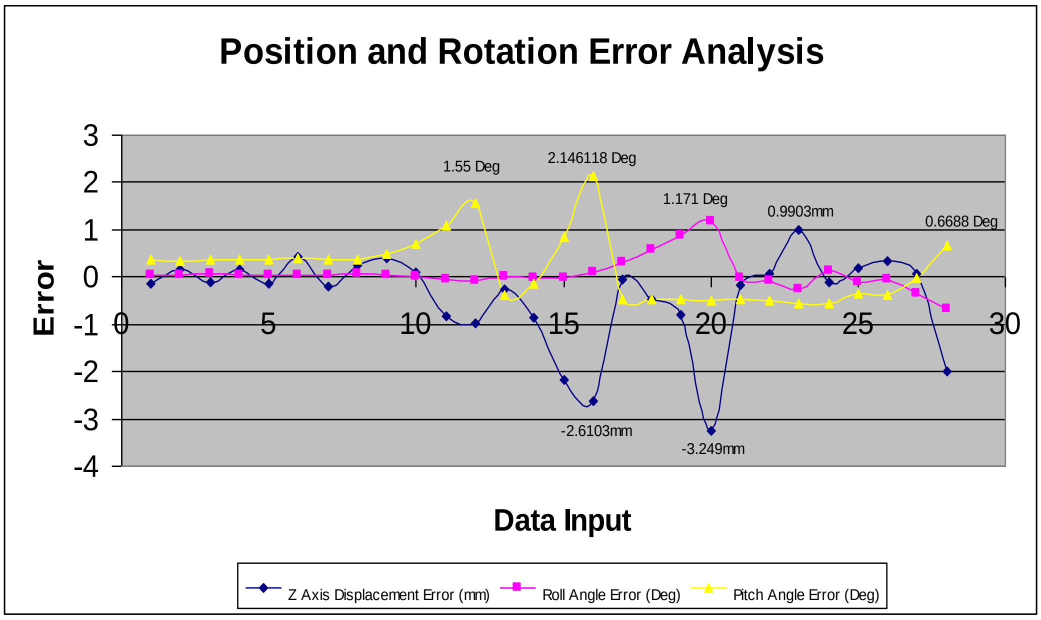

Figure 9.17 Displacement and Rotational Error Analysis

On the whole, the variation of angle orientation and the translation movement of the Z-axis are acceptable. The overall average errors of the angle of rotation and the error of translation are 0.064° for Roll Rotation and 0.18° for Pitch Rotation as well as 0.429 mm for the Z-axis movement. From the result of the calibration, the error of the rotational angle and position increases while it reaches the maximum rotational angle which is the boundary of the calculated workspace. Hence, the result has implicitly indicated the accuracy of the simulated workspace.

So if the platform travels within the boundary of the workspace, the overall errors of the angle rotation and translation can be improved to 0.064^{o} for Roll Rotation and 0.09^{o} for Pitch Rotation as well as -0.163 mm for the Z-axis movement as shown in Table 9.5

Table 9.5 Calibration Result of the Micro Stewart Platform with the CMM when the Platform travels within boundary workspace

Theoretical Position and Orientation			Actual Position and Orientation			Position and Orientation Error		
Rotation X(deg)	Rotation Y(deg)	Position Z(mm)	Z - 10.426(mm)	Actual X(deg)	Actual Y(deg)	Z error (mm)	Angle X error(deg)	Angle Y error(deg)
0	0	279	278.85	-0.045	-0.365	-0.15	0.045	0.365
0	0	304	304.157	-0.04	-0.373	0.157	0.04	0.373
0	0	279	278.887	-0.055	-0.368	-0.113	0.055	0.368
0	0	304	304.153	-0.039	-0.378	0.153	0.039	0.378
0	0	279	278.851	-0.045	-0.37	-0.149	0.045	0.37
0	0	314	314.258	-0.055	-0.382	0.258	0.055	0.382
-5	0	310	309.747	-5.02	0.375	-0.253	0.02	-0.375
-10	0	310	309.146	-10.03	-0.128	-0.854	-0.025	-0.128
-15	0	310	307.82	-15.03	0.85	-2.18	-0.027	0.85
0	5	310	309.952	0.31	4.527	-0.048	0.31	-0.473
0	10	310	309.527	0.565	9.535	-0.473	0.565	-0.465
0	15	310	309.195	0.866	14.536	-0.805	0.866	-0.464
0	-5	310	309.815	-0.027	-5.481	-0.186	-0.027	-0.481
0	-10	310	310.054	-0.085	-10.512	0.054	-0.085	-0.512
0	-15	310	310.99	-0.257	-15.545	0.99	-0.257	-0.545
5	5	310	309.9	5.133	4.438	-0.1	0.133	-0.562
10	10	310	310.2	9.886	9.636	0.2	-0.114	-0.364
-5	-5	310	310.331	-5.061	-5.387	0.331	-0.061	-0.387
-10	-10	310	310.073	-10.37	-10.035	0.073	-0.365	-0.035
					Average	-0.163	0.064	-0.090

9.6 Summary

This chapter addresses the kinematics analysis of the hybrid parallel mechanism of a hybrid 3-UPU Parallel Mechanism assembled to obtain translation along the Z-axis and Orientation movements around X- and Y-axes. The modular configuration of various kinds of parallel kinematics platforms were successfully assembled with the same modular unit of the respective actuators and joints. The Hybrid UPU Micro Parallel Kinematics Platform was further studied and the accuracy of the movement of the platform was calibrated using the CMM based on the simulated workspace. The errors are acceptable and are limited within 0.2 deg and 0.5 mm.

The developed inverse kinematic algorithm of the Parallel Kinematic Manipulator can be applied generally to the same kind of modular configuration platform by giving a different constraint setting. The algorithm has been successfully implemented in the control of the hybrid parallel kinematic platform. The platform is able to travel to the specific position and orientation smoothly and accurately after calibration with the CMM. The platform is also integrated into a 3-axis machine center to perform machining as shown in Figure 9.18. A designed workpiece is milled through the integration system as shown in Figure 9.19

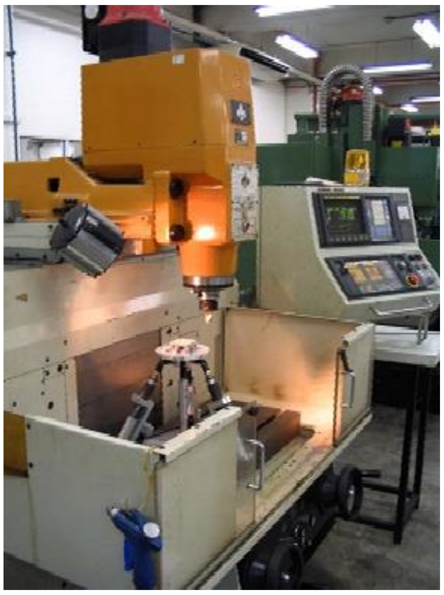

Figure 9.18 Integration of the hybrid 3-DOF PKM into 3-axis machining center

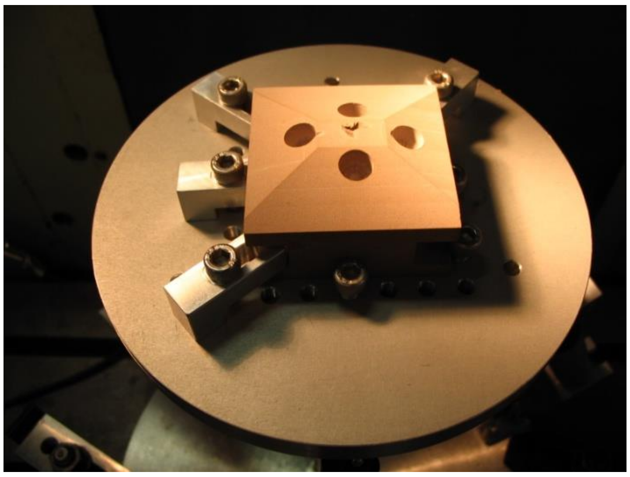

Figure 9.19 The machined workpiece

In conclusion, it has been shown that the performance of the platform is limited by the workspace of the platform. The constraint of the workspace is contributed by the limited length of the actual actuators and working angle of the joints. Hence the modular configuration system is able to solve the problem by designing the specified configuration.

Chapter 10 Conclusions and Recommendations

10.1 Conclusions

A Gough-Stewart Platform has been fabricated and developed in this research. Software development was completed on the Stewart Platform for this study so that users can communicate with the controller of the Stewart Platform with standard NC codes through building models using commercial CAD/CAM systems.

In this research, the kinematics of the system was studied. The forward kinematics problem cannot be solved easily compared to the case of a serial manipulator. However, the inverse kinematics of the parallel manipulator is found to have a direct solution. Nevertheless, the forward kinematics can be solved by using the Newton Raphson numerical method. The developed forward kinematics can also help develop a proper feedback system for the Stewart Platform. The installation of the wire sensors helps to predict the final position and orientation of the end-effector of the mobile platform by knowing the length of the actuators. In addition, the dynamics of the system was investigated and simulation was done by using MATLAB® SimMechanics in the study.

The kinematics analysis of the hybrid parallel mechanism was also studied. A hybrid 3-UPU Parallel Mechanism was assembled to obtain the motion of translation along the Z-axis and Orientation movement around X- and Y-axes. Modular configurations of various kinds of parallel kinematics platforms were successfully assembled with the same modular units of the respective actuators and joints. A Hybrid UPU Micro Parallel Kinematics Platform was further elaborated and the accuracy of the movement of the platform was calibrated using the CMM based on the simulated workspace.

The developed inverse kinematic algorithm of the Parallel Kinematic Manipulator can be used generally for the same kind of modular configuration platform by having a different constraint setting. The platform is able to travel to the specified position and orientation smoothly and accurately after calibration with the CMM.

Furthermore, the accuracy of the Stewart Platform was calibrated using the encoder of the motors and wire sensors which were installed along the actuators. A calibration workpiece was used to verify the translation movement of the Stewart Platform and improvement of the controlling software was achieved by referring to the calibrated results.

NC programs for 3-Axis machining were developed in this study based on the mechanistic principle of the Stewart Platform. The software was first developed in MATLAB® to verify the accuracy of the machining trajectory through simulation. The program was further developed in Visual C++ and implemented with the graphic user interface of the controller of the Stewart Platform. Contour machining experiments were carried out based on the machining trajectory path generated from the NC program. The experimental results were quite accurate but unevenness of the motion of the platform was detected during the machining process.

After 3-Axis machining has been successfully implemented with the control system of the Stewart Platform, 5-axis machining was further developed. The 5-axis machining trajectory path was developed using MATLAB® by performing conversion of the local coordinate system of the freeform surface to the trajectory path based on the machining coordinate system. In addition, the Stewart Platform is found to have advantages over 5-axis CNC machine in terms of mechanical design and the simplicity of the inverse kinematics towards orientation and translation of the end-effector of the mobile platform to achieve 5-axis motion.

At the completion of the project, all the developed programs and algorithms were integrated into one single user interface to manipulate the motion of the Stewart Platform. Thus, users can control the movement of the Stewart Platform by issuing parameters either in terms of the orientation and position of the mobile platform or the extracted length of the actuator. The machining process of the Stewart Platform can also be achieved by using the input of the NC program. In conclusion, the study of 3D and 5D machining of the Stewart Platform has been achieved in this research.

10.2 Recommendations for Future Work

Even though the objectives of the project have been achieved, further study can be carried out to improve the quality of the machining process on the Stewart Platform. Some future work can be focused on the following aspects.

Workspace

The Parallel Kinematic Manipulator is well known for its workspace limitation. Hence, to improve the workspace of the Stewart Platform, two methods are suggested. One method is to replace the existent spherical joints with larger working angle spherical joints. Another method is the collaboration of two Stewart Platforms to form a single system to perform the machining task. However, several challenges would need to be overcome, such as the synchronization of the motion of the Stewart Platforms to achieve the same position at the same time. There will also be problems to assure the allocation of the two Stewart Platforms is within the working workspace concurrently such that the platforms can have the same stiffness and rigidity.

Accuracy of the Platform

There are some limitations of the accuracy of the platform since the current Stewart Platform was driven by stepper motors. Hence, a servomotor system Stewart Platform is currently being developed in the Advanced Manufacturing Lab. By using a servomotor system, the Stewart Platform can be manipulated with higher accuracy and smoother motion for machining processes. Furthermore, the resolution of the wire sensors currently installed for the feedback system is too low to achieve high accuracy measurement. Instead of applying contact measurement devices like wire sensors to obtain indirect calibration of the position of the platform through the forward kinematics algorithm, a non-contact measurement device, such as the Theodolite as shown in Figure 10.1 or a CCD camera, are suggested for measuring the end-effector position of the Stewart Platform. Hence, a direct measurement method can be used to calibrate the position and orientation of the platform in the machining environment without disrupting the machining process.

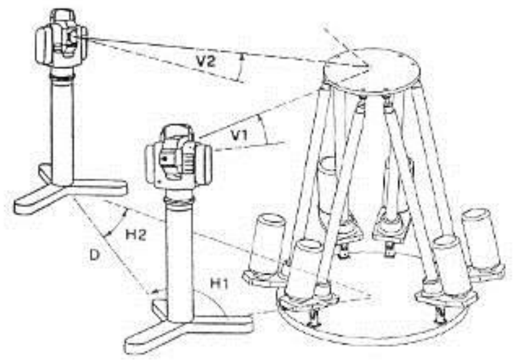

Figure 10.1 The theodolites system based on the principle of triangulation

<u>Manipulation of the Stewart Platform</u>

The velocity of the adjacent stroke of the actuators can be calculated and implemented with the trajectory path of the platform. As a result, errors caused by the constant velocity of the actuator can be compensated. Hence, instead of controlling the platform to move from point to point, the platform can now be controlled using the velocity profile. The most popular way to control the Stewart Platform is using a linear (PID-like) control law at the joint level and a simple inverse kinematics algorithm on top of the control loop.

In short, better and more reliable calibration experiments must be developed to further improve the accuracy of motion of the Stewart Platform, so that it can be optimized for machining tasks. These mentioned issues will be the challenges for future Stewart Platform research.

References

1. **[Alyushin, 2010]** Alyushin, Y.A., and Elenev, S.A., “Mathematical Model of Stewart Platform Motion”, Journal of Machinery Manufacture and Reliability, 2010, Vol. 39, No 4, pp 305-312
2. **[Anjan, 2003]** Dash, A.K., Chen, I.M., Yeo, S.H., and Yang, G.L., “Task-Based Configuration Design for 3-Legged Modular Parallel Robots Using Simplex Methods” Computational Intelligence in Robotics and Automation, 2003. Proceedings. 2003 IEEE International Symposium, vol.2 998 - 1003
3. **[Arai, 1991]** Arai, T., Cleary, K., Homma, K., Adachi, H. and Nakamura, T., 1991, “Development of Parallel Link Manipulator for Underground Excavation Task,” 1991 International Symposium on Advanced Robot Technology, pp.541-548.
4. **[Asada, 1985]** Asada, H., and Cro Granito, J.A., 1985, “Kinematic and Static Characterization of Wrist Joints and Their Optimal Design” Proceedings of IEEE International Conference on Robotics and Automation, St. Louis, pp. 91-100.
5. **[Badescu, 2002]** Badescu, M., Morman, J., and Mavroidis, C., 2002, “Workspace Optimization of Orientational 3-Legged UPS Parallel Platforms”, Proceedings of DETC’02 ASME 2002 Design Engineering Technical Conferences and Computers and Information in Engineering Conference.
6. **[Bonev, 1999]** Bonev, I.A. and Ryu, J., 1999, “Orientation Workspace Analysis of 6-DOF Parallel Manipulators”, Proceedings of the 1999 ASME

Design Engineering Technical Conferences September 12-15, 1999, Las Vegas, Nevada, USA.

7. **[Chan, 2001]** Chan, V., 2001, "Singularity Analysis and Redundant Actuation of Parallel Manipulators" M Eng Thesis, The Ohio State University , pp. 5-50
8. **[Charles, 1991]** Nguyen, C.C., Zhou, Z.-L., Antrazi, S.S., and Campbell, C.E., Jr., 1991, **"**Efficient computation of forward kinematics and Jacobian matrix of a Stewart platform-based manipulator", IEEE Proceedings of Southeast conference '91, 7-10 April 1991, vol.2 , pp 869 - 874
9. **[Clavel, 1988]** Clavel, R., 1988 "DELTA, A Fast Robot With Parallel Geometry," 18th International Symposium on Industrial Robots, pp. 91 -100, April.
10. **[Craig, 1986]** Craig, J.J., 1986, "Introduction To Robotic Mechanics and Control", 2nd Edition, Addison Wesley Publishing Company Inc, pp.278-279
11. **[Eric, 1996]** Eric, P. and Reymond, C., 1996, "Parallel Robots And Microbotics", Volume 6, Robotics and manufacturing: Recent Trends in Research and Applications edited by M. Jamshid, F. Pin and P. Dauchez, ASME Press, pp 35.
12. **[Fassi, 2000]** Fasssi, I. and Weins, G.J., 2000, "Multi Axis Machining : PKMs and Traditional Machining Centers", Journal of Manufacturing Processes; 2000; 2,1: ABI/INFORM Global pp.1
13. **[Faux, 1979]** Faux, I.D. and Pratt, M.J.,1979, "Computational Geometry for Design and Manufacture, Ellis Horwood
14. **[Gregorio, 2001]** Gregorio, R.D., 2001, "Statics and Singularity Loci of the 3-UPU Wrist", 2001 IEEE/ASME International Conference on Advanced

Intelligent Mechatronics Proceedings 8-12 July 2001, Como, Italy. Pp 470-475

15. **[Gosselin, 1989]** Gosselin, C. and Angeles, J., 1989, "The Optimum Kinematics Design of a Spherical Three-Degree-Freedom Camera – Orientation Device," IEEE Int. Conference on Robotics and Automation, pp. 781-786.
16. **[Gough, 1962]** Gough V.E. and Whitehall, S.G., 1962, "Universal Tyre Test Machine," Proc. 9th Int'l Tech. Congress, F.I.S.I.T.A, 177 (Institution of Mechanical Engineers).
17. **[Gosselin, 1994]** Gosselin, C., and Hamel, J., 1994, "The Agile Eye: Agile Performance Three-Degree-of Freedom Camera-Orienting Device," IEEE International Conference on Robotics and Automation, pp. 781-786.
18. **[Hunt, 1983]** Hunt, K.H., 1983, "Structural Kinematics of In-Parallel-Actuated Robot-Arms," ASME Journal of Mechanisms, Transmissions, and Automation in Design, Vol. 105, pp. 705-712.
19. **[Huynh, 2001]** Huynh, P., 2001, "Kinematics Performance Comparison of Linear Type Parallel Mechanisms Application To The Design And Control of A Hexaslide", 5th International Conference on Mechatronics Technology, June 6-8, 2001, National University of Singapore. pp. 1-8
20. **[Jakobovic, 2002]** Jakobovic, D. and Jelenkovic, L. 2002, "The Forward and Inverse Kinematics Problems for Stewart Parallel Mechanisms" Proc. 8th Int. Scientific Conference on Production Engineering CIM 2002, Brijuni, June 13-14.

21. **[Joshi, 2003]** Joshi, S.A., and Tsai, L.W., 2003, "The Kinematics of a Class of 3-DOF, 4-Legged Parallel Manipulators", Transactions of the ASME Vl125, March 2003.

22. **[Ken, 2001]** Ken E., 2001, Programming of Computer Numerically Controlled Machines, 2nd Edition, 2001, pp 321 - 341

23. **[Lebret, 1992]** Lebret, G., Liu, K. and Lewis, F.L., 1993, "Dynamic Analysis and Control of a Stewart Manipulator", Journal of Robotics Systems 10(5), 629-655.

24. **[Lee, 1987]** Lee, K., and Shah, D.K., 1987, "Kinematic Analysis of a Three Degrees of Freedom In-Parallel Actuated Manipulator", Proc. IEEE International Conf. On Robotics and Automation, 1, pp. 345-350.

25. **[Liang, 2002]** Liang, X.H., 2002, "Computer Aided Tool Path Generation For 5-axis Machining of freeform surface", Master thesis, 2002 , National University of Singapore , pp 17- 59, 2002

26. **[Lim, 2002]** Lim, A.K., 2002, "A Window-Based System for Five Axis CNC Milling Tool Path Planning", Bachelor Thesis, 2002, National University of Singapore, pp 10, 29 – 30, 2002

27. **[Masory, 1995]** Masory O., and Yan J.H., 1995, "Measurement of Pose Repeatability of Stewart Platform", Robotic Center Florida Atlantic University, Boc Raton, Journal of Robotics Systems, Vol. 12, No. 12, pp. 821-832

28. **[MATLAB® Exchange, 2003]** http://www.mathworks.com/MATLAB central/fileexchange/loadFile.do?objectId=3642&objectType=file

29. **[Mckee, 1999]** Mckee, G. and Schenker, P., Editors, 1999, sensor Fusion and Decentralized control in Robotic Systems II, SPIE Proceeding Series, Vol. 3839.
30. **[Mortenson, 1985]** Mortenson M.E. 1985, Geometric Modeling, John Wiley
31. **[Neugebauer, 2000]** Neugebauer, R., Wieland, F., and Ihlenfeldt, S., 2000, “Comparison of parallel structure concepts for five-axis machining”, Journal of Manufacturing Processes; 2000; 2, 1; ABI/INFORM Global pp 59-66
32. **[Neugebauer, 2000]** Neugebauer, R., Wieland, F., and Ihlenfeldt, S., 2002, “Comparison of parallel structure concepts for five-axis Machining”, Journal of Manufacturing Processes , 1, ABI/INFORM Global pp. 59
33. **[Piegl, 1991]** Piegl L., 1991 “On NURBS: a survey, IEEE Computer Graphics and Application”, Jan 1991
34. **[Reinholz, 1987]** Reinholz, C. and Gokhale D., 1987,”Design and Analysis of Variable Geometry Truss Robot,” Proc. 9th Applied Mechanism Conference, Oklahoma State University.
35. **[Shih, 2003]** Shih, C.Y., 2003, “An Impedance Control Design and Simulation of Stewart Platform with Fuzzy Neural Network Compensator”, Master Thesis, Chung Yuan Christian University, pp 20 – 26
36. **[Sternheim, 1987]** Sternheim, F., 1987, “Computation of the Direct and Inverse Kinematics Model of the Delta 4 Parallel Robot,” Robotersysteme, 3, pp. 199-203.
37. **[Stewart, 1965]** Stewart, D., 1965, “A Platform with Six Degrees of Freedom,” Proc. Institute of Mechanical Engr., London, England, Vol. 180, pp.371-386.

38. **[Tlusty, 2000]** Tlusty, J., Ziegert, J.C., and Ridgeway, S., 2000, 'A Comparison of Stiffness Characteristics of Serial and Parallel Machine Tools', Journal of Manufacturing Processes; 2000; 2,1; ABI/INFORM Global , pp 67 – 76
39. **[Tsai, 1996]** Tsai, L.W., 1996, "Kinematics of a Three-DOF Platform With Three Extensible Limbs", Recent Advances in Robot Kinematics, 401-410, Kluwer Academic Publishers pp.401-402
40. **[Tsai, 1996]** Tsai, L.W., Walsh, G.C., and Stamper, R.E., 1996, "Kinematics of a Novel Three DOF Translational Platform", Proceedings of the 1996 IEEE International Conference on Robotics and Automation Minneapolis, Minnesota – April 1996.
41. **[Tsai, 1999]**Tsai, L.W., 1999, "Robot analysis, "The Mechanics of Serial and Parallel Manipulators", John Wiley & Sons, INC, pp169 – 433
42. **[Tsai, 2000]**Tsai, L.W., 2000, Mechanism Design: Enumeration of Kinematic Structures According to Function, ISBN 0-8493-0901-8, CRC Press, Boca Raton, FL.
43. **[Tsai, 2002]** Tsai, L.W., and Joshi, S., "Kinematic Analysis of 3-DOF Position Mechanisms for Use in Hybrid Kinematic Machines", Journal of Mechanical Design, June 2002, Vol 124, Pp 245-253
44. **[Yang, 2003]** Yang, G.L., Chen, I.M., Chen, W.H., and Yeo, S.H., 2003, "Design and Analysis of a 3-RPRS Modular Parallel Manipulator for Rapid Deployment", Proceedings of the 2003 IEEE/ASME International Conference on Advanced Intelligent Mechatronics (AIM 2003), pp 1250-1255

Appendices

Appendix A: NC Code tables

Table A1 Address characters [Ken, 2001]

Character	Meaning
A	Additional rotary axis parallel and around the X-axis
B	Additional rotary axis parallel and around the Y-axis
C	Additional rotary axis parallel and around the Z-axis
D	Tool radius offset number, depth of cut for multiple repetitive cycles
E	User macro character, precise designation of thread lead
F	Feed rate, precise designation of thread lead
G	Preparatory function
H	Tool length offset number
I	Incremental X-coordinate of circle center or parameter of fixed cycle
J	Incremental Y-coordinate of circle center
K	Incremental Z-coordinate of circle center or parameter of fixed cycle
L	Number of repetition
M	Miscellaneous function
N	Sequence or block number
O	Program number
P	Dwell time, program number, and sequence number designation in subprogram; Sequence number for multiple repetitive cycles
Q	Depth of cut, shift of canned cycles; Sequence number for multiple repetitive cycles
R	Point R for canned cycles, as a reference return value; Radius designation of a cycle arc
S	Spindle-speed function
T	Tool-function
U	Additional linear axis parallel to X-axis
V	Additional linear axis parallel to Y-axis
W	Additional linear axis parallel to Z-axis
X	X-coordinate
Y	Y-coordinate
Z	Z-coordinate

Table A2 G-codes chart [Ken, 2001]

Code	Group	Function
*G00	01	Rapid traverse positioning
*G01	01	Linear interpolation
G02	01	Circular and helical interpolation CW (clockwise)
G03	01	Circular and helical interpolation CCW (counterclockwise)
G04	00	Dwell
G09	00	Exact stop
*G15	17	Polar coordinates cancellation
G16	17	Polar coordinates system
*G17	02	XY plane selection
G18	02	ZX plane selection
G19	02	YZ plane selection
G20	06	Input in inches
G21	06	Input in millimeters
*G22	04	Store stroke limit ON
G23	04	Store stroke limit OFF
G27	00	Reference point return check
G28	00	Reference point return
G29	00	Return from reference point
G30	00	Return to second, third, and fourth reference point
G33	01	Thread Cutting
G37	00	Automatic tool length measurement
*G40	07	Cutter compensation cancel
G41	07	Cutter compensation left side
G42	07	Cutter compensation right side
G43	08	Tool length offset compensation positive (+) direction
G44	08	Tool length offset compensation negative (-) direction
G45	00	Tool offset increase
G46	00	Tool offset decrease
G47	00	Tool offset double increase
G48	00	Tool offset double decrease
*G49	08	Tool length offset compensation cancel
*G50	11	Scaling cancel
G51	11	Scaling
G52	00	Local coordinate system
G53	00	Machine coordinate system
*G54	14	Work coordinate system 1
G55	14	Work coordinate system 2
G56	14	Work coordinate system 3
G57	14	Work coordinate system 4
G58	14	Work coordinate system 5
G59	14	Work coordinate system 6
G60	00	Single direction positioning
G63	15	Tapping mode
G68	16	Rotation of coordinate system
*G69	16	Cancellation of coordinate system
G73	09	High speed peck drilling cycle
G74	09	Reverse tapping cycle
G76	09	Fine boring cycle
*G80	09	Canned cycle cancel
G81	09	Drilling cycle, spot drilling
G82	09	Drilling cycle, counter boring “chip break”
G83	09	Deep hole drilling cycle
G84	09	Tapping cycle
G85	09	Boring cycle
G86	09	Boring cycle
G87	09	Back boring cycle
G88	09	Boring cycle
G89	09	Boring cycle
*G90	03	Absolute programming command
*G91	03	Incremental programming command
G92	00	Setting for the work coordinate system for maximum spindle RPM
*G94	05	Feed per minute
G95	05	Feed per revolution
G96	13	Constant surface speed control
*G97	13	Constant surface speed control cancel

*G98	10	Canned cycle initial level return
G99	10	Canned cycle initial R-level return

Table A3 Miscellaneous functions (M functions) [Ken, 2001]

Code	Function
M00	Program stop
M01	Optional Stop
M02	Program end without rewind
M03	Spindle ON clockwise (CW) rotation
M04	Spindle ON counterclockwise (CCW) rotation
M05	Spindle OFF rotation stop
M06	Tool Change
M07	Mist coolant ON
M08	Flood coolant ON
M09	Coolant OFF
M10	Work table rotation locked
M11	Work table rotation unlocked
M13	Spindle ON clockwise and coolant ON, dual command
M14	Spindle On counterclockwise and coolant ON, dual command
M16	Change of heave tools
M19	Spindle orientation
M21	Mirror image in the direction of the X-axis
M22	Mirror Image in the direction of the Y-axis
M23	Cancellation of the mirror image
M30	Program end with rewind
M98	Subprogram call
M99	Return to main program from subprogram

Appendix B: Coordinate of circular arc in NC program

Article on how to determine the points of radius in an NC program

An algorithm is described in pseudo codes to explain the methodology to determine the coordinates of the machining point passing through when it is moved in the circular motion. There are a few conditions which need to be considered, such as whether the cutting tool moves in the path of circular arcs in clockwise or anticlockwise direction. There are also a few methods of NC codes which can be used to determine the arc direction and the coordinates of the starting point and end point of the circular arc motion. Besides referring to G codes, such as G01, G02, G03, to determine the direction of the arc circle, the coordinates of the machining points can be defined based on parameters, such as X, Y and Z coordinates, or R radius of the arc as well as I, J and K, the direction coordinates which are the incremental distances to the center along X-, Y- and Z-axes. All the definitions of the parameters are defined at the start of the pseudo code as shown below:

```
function clockwise1(x,y,x1,y1,i,j)

Input
x,y = starting point
x1,y1 = ending point
i,j = relative vector of center point from starting
point
```

Firstly, the center of the circle is needed to be defined:

```
centerX = x+i;
centerY = y+j;
```

Secondly, the vector of the starting point, the end point and one reference vector and the lengths of the point to the center of the circle are determined.

```
vector1 = [x-centerX y-centerY];
vector2 = [x1-centerX y1-centerY];
vector3 = [x1-x y1-y];
length1 = (vector1(1).^2+vector1(2).^2).^0.5;
length2 = (vector2(1).^2+vector2(2).^2).^0.5;
length3 = (vector3(1).^2+vector3(2).^2).^0.5;
```

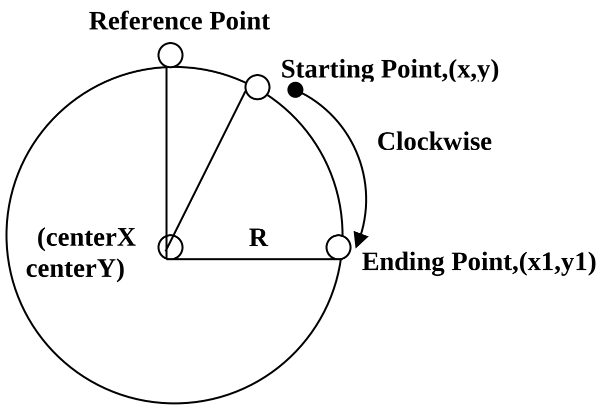

Figure B1 Generic circular arc motion of the machining point in one plane

```
R = length1;
vectorref = [(centerX+R*sin(0))-centerX
(centerY+R*cos(0))-centerY];
lengthref = (vectorref(1).^2+vectorref(2).^2).^0.5;
```

The angle between vector 1 and vector ref, vector 2 and vector ref as well as vector 1 and vector 2 can be defined as shown below.

Example to determine the generic angle:

We know that $\theta = \cos^{-1}\left(\frac{vectorref(1)\times vector1(1) + vectorref(2)\times vector1(2)}{lengthref \times length1}\right)$

$lengthref = \sqrt{(vectorref(1)^2 + vectorref(2)^2)}$

$length1 = \sqrt{(vector1(1)^2 + vector1(2)^2)}$

Based on above equations, three angles are determined. Firstly, there is angle theta, θ which is the angle between the reference point and the starting point. Then angle beta, β is also defined between the starting point and the end point of the arc while angle gamma, γ is determined between the reference point and the end point of the arc. All these angles are illustrated in Figure B2.

```
% Angle between vector ref and vector 1
upperref1 =
vectorref(1)*vector1(1)+vectorref(2)*vector1(2);
bottomref1 = lengthref*length1;
theta = acos(upperref1/bottomref1);

% Angle between vector ref and vector 2
upperref2 =
vectorref(1)*vector2(1)+vectorref(2)*vector2(2);
bottomref2 = lengthref*length2;
beta = acos(upperref2/bottomref2);

% Angle between vector 1 and vector 2
upper = vector1(1)*vector2(1)+vector1(2)*vector2(2);
bottom = length1*length2;
alpha = acos(upper/bottom);

% This condition is to determine the points
if alpha == 0
    alpha = 360/180*pi;
end
```

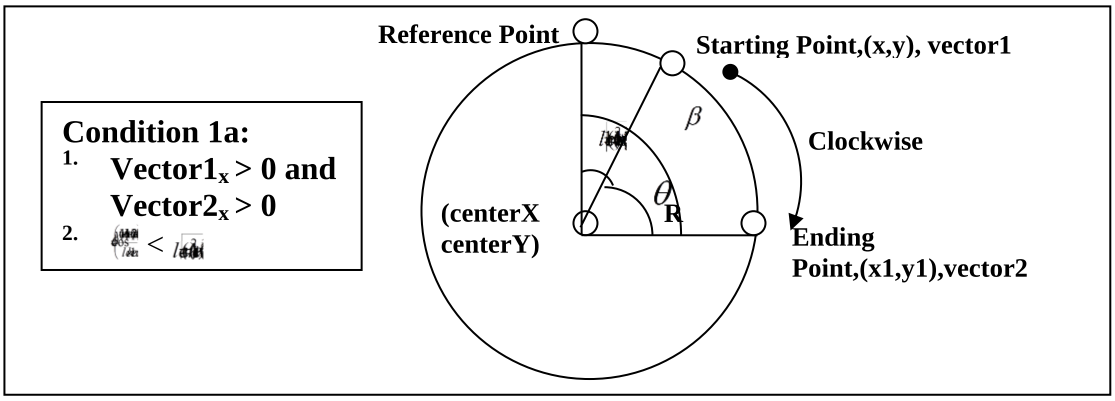
Condition 1a:
1. Vector1$_x$ > 0 and Vector2$_x$ > 0
2. [illegible] < [illegible]
Reference Point
Starting Point,(x,y), vector1
β
Clockwise
θ
R
(centerX centerY)
Ending Point,(x1,y1),vector2

Figure B2 Clockwise circular arc motion with angle of starting point θ smaller than angle of ending point β with respect to reference point

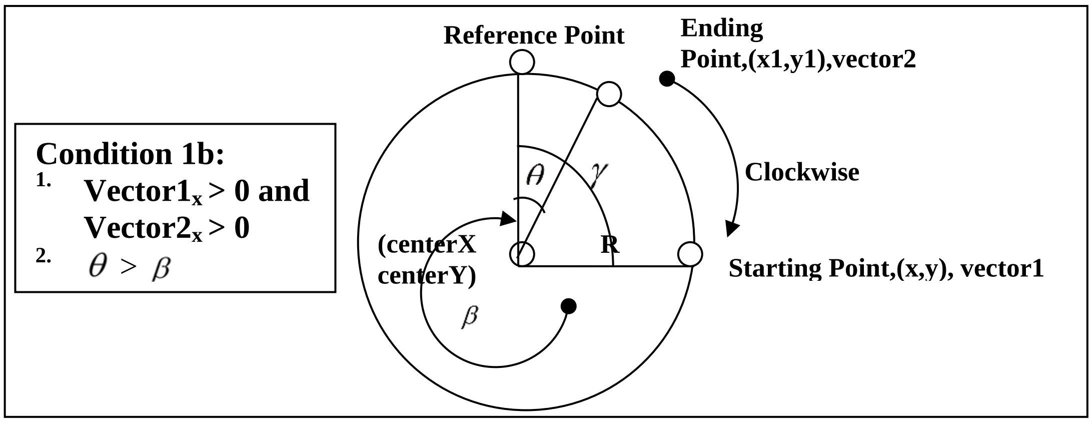

Figure B3 Clockwise circular arc motion with angle of ending point smaller than angle of starting point with referred to reference point

```
% condition 1a for the points
if (vector1(1) > 0 && vector2(1) > 0)
    if (theta < beta)
        % then the angle is theta + alpha
        startangle = theta;
        angle = alpha;
        max = determinemax(angle);
        for i = 1:max
            newx(i) =
centerX+R*sin(startangle+angle/max*i);
            newy(i) =
centerY+R*cos(startangle+angle/max*i);
        end
    end

% condition 1b

    if (theta > beta)
        % then the angle is 2*pi - alpha
       startangle = theta + beta;
       angle = 2*pi - alpha;
       max = determinemax(angle)
        for i = 1:max
            newx(i) =
centerX+R*sin(startangle+angle/max*i);
```

```
            newy(i) =
centerY+R*cos(startangle+angle/max*i);
        end
    end
end
```

The determination of the coordinates of the machining points can be derived based on the direction of rotation and the coordinates of the starting and ending points in the NC program as shown in Figures B2 and B3. Besides the mentioned condition, there are another two conditions which need to be considered such as the coordinates of the starting point and ending point. There is the possibility that the starting point will be on the right side of the reference point while the ending point at the left side as shown in Figure B4 or vice versa as shown in Figure B5.

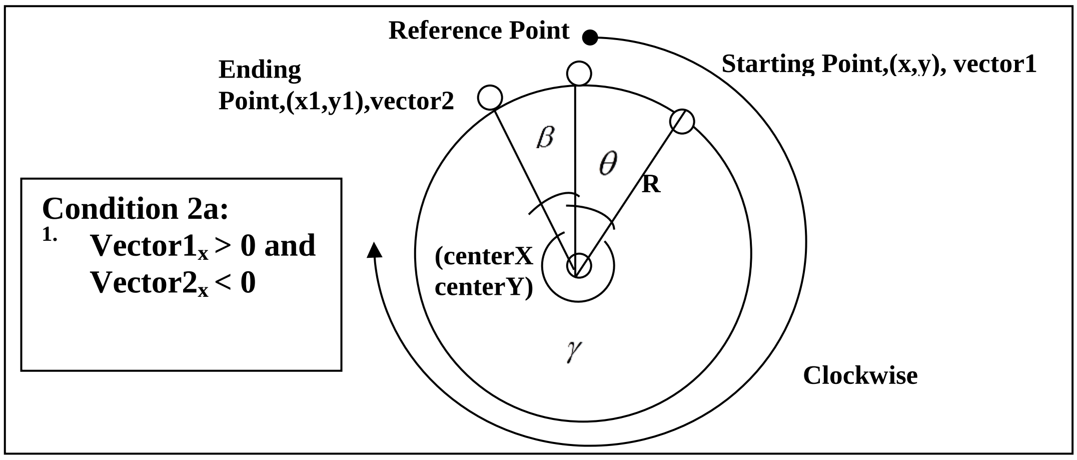
Reference Point
Ending Point,(x1,y1),vector2
Starting Point,(x,y), vector1
β
θ
R
Condition 2a:
1. Vector1$_x$ > 0 and Vector2$_x$ < 0
(centerX centerY)
γ
Clockwise

Figure B4 Clockwise circular arc motion with starting point at the right side and ending point at the left side of the reference point

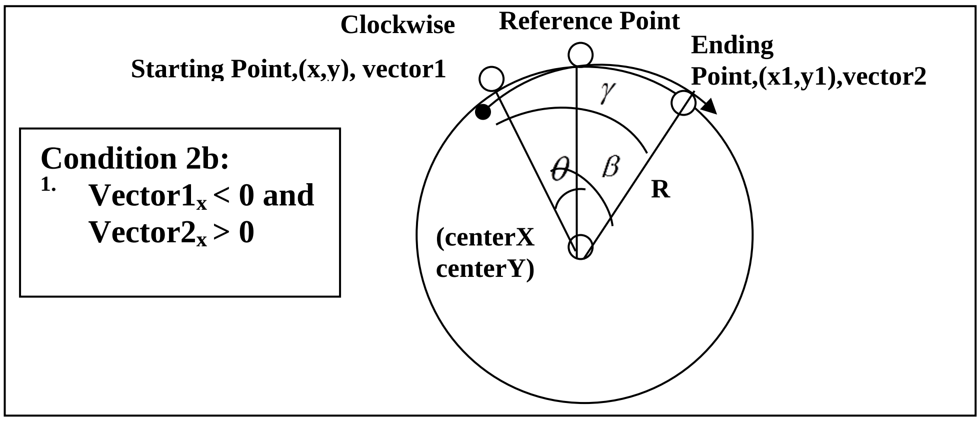
Clockwise
Reference Point
Starting Point,(x,y), vector1
Ending Point,(x1,y1),vector2
Condition 2b:
1. Vector1$_x$ < 0 and Vector2$_x$ > 0
γ
θ
β
R
(centerX centerY)

Figure B5 Clockwise circular arc motion with starting point at the left side and ending point at the right side of the reference point

Moreover, two more conditions would need to be considered when the coordinates of the machining points are determined. Firstly, if the starting and ending points are at the left side of the reference point, there is a possibility that the angle between the ending point and the reference point is larger than the angle between the starting point and reference point as shown in Figure B6 or vice versa in Figure B7. So by knowing the conditions, the corresponding coordinates of the machining point can be defined easily.

```
% condition 2a
if (vector1(1) > 0 && vector2(1) < 0)
       % then the angle is 2*pi - alpha
       startangle = theta;
       angle = 2*pi-theta-beta;
       max = determinemax(angle)
        for i = 1:max
            newx(i) =
centerX+R*sin(startangle+angle/max*i);
            newy(i) =
centerY+R*cos(startangle+angle/max*i);
        end
end
```

```
% condition 2b
if (vector1(1) < 0 && vector2(1) > 0)
       % then the angle is 2*pi - alpha
       startangle = 2*pi-theta;
       angle = theta+beta;
       max = determinemax(angle)
        for i = 1:max
            newx(i) =
centerX+R*sin(startangle+angle/max*i);
            newy(i) =
centerY+R*cos(startangle+angle/max*i);
        end
end
```

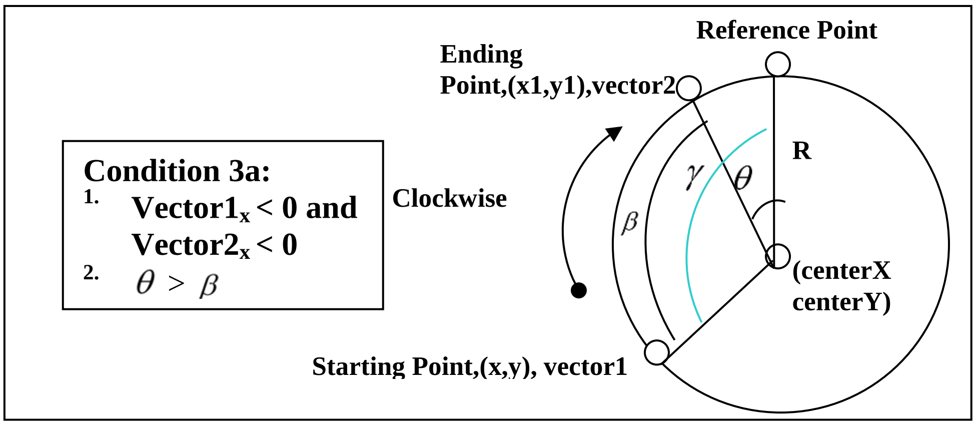

Figure B6 Clockwise circular arc motion with starting point and ending point at the left side of the reference point with angle theta larger than angle beta

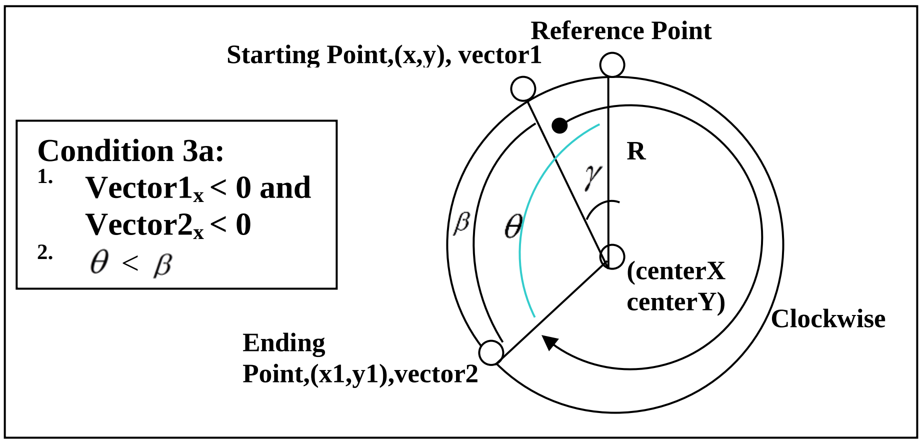

Figure B7 Clockwise circular arc motion with starting point and ending point at the left side of the reference point with angle theta smaller than angle beta

```
if (vector1(1) < 0 && vector2(1) < 0)
      % condition 3a
     if ( theta > beta)
            % then the angle is 2*pi - alpha
            startangle = 2*pi-theta;
            angle = alpha;
            max = determinemax(angle)
            for i = 1:max
                newx(i) =
centerX+R*sin(startangle+angle/max*i);
                newy(i) =
centerY+R*cos(startangle+angle/max*i);
            end
      end
     % condition 3b
      if (theta < beta)
          % then the angle is 2*pi - alpha
            startangle = 2*pi-alpha;
            angle = 2*pi-alpha;
            max = determinemax(angle)
            for i = 1:max
                newx(i) =
centerX+R*sin(startangle+angle/max*i);
                newy(i) =
centerY+R*cos(startangle+angle/max*i);
            end
      end
end
```

Another sub-function is written for the purpose of determining the resolution steps of the coordinates between the starting and ending points of the circular arc movement of the machining tool. Hence, by knowing the angle between the starting point and ending point, the resolution of the coordinate machining points will be increased according to the derived angle, for example if the angle is smaller than 90° then the resolution of the number of coordinates of the machining points will be 12.

```
% Extra function to determine the points along the path
function max = determinemax(angle)
if angle*180/pi <= 90
    max = 12
end
if angle*180/pi > 90 && angle*180/pi <= 180
    max = 18
end
if angle*180/pi > 180 && angle*180/pi <=270
    max = 24
end
if angle*180/pi > 270 && angle*180/pi <=360
    max = 30
end
```

In short, this algorithm can be used to categorize the resolution of the steps of all the machining coordinates by knowing the starting and ending points of the circular arc in the NC program. The same conditions and rules can also be applied to the tool movement in the NC program when it moves in an anticlockwise direction.

Appendix C: Sensors installation methods

Three methods are introduced to calibrate the accuracy of the Stewart Platform in this study. In addition, the calibration of the Epsilon wire sensor is also shown in the following section.

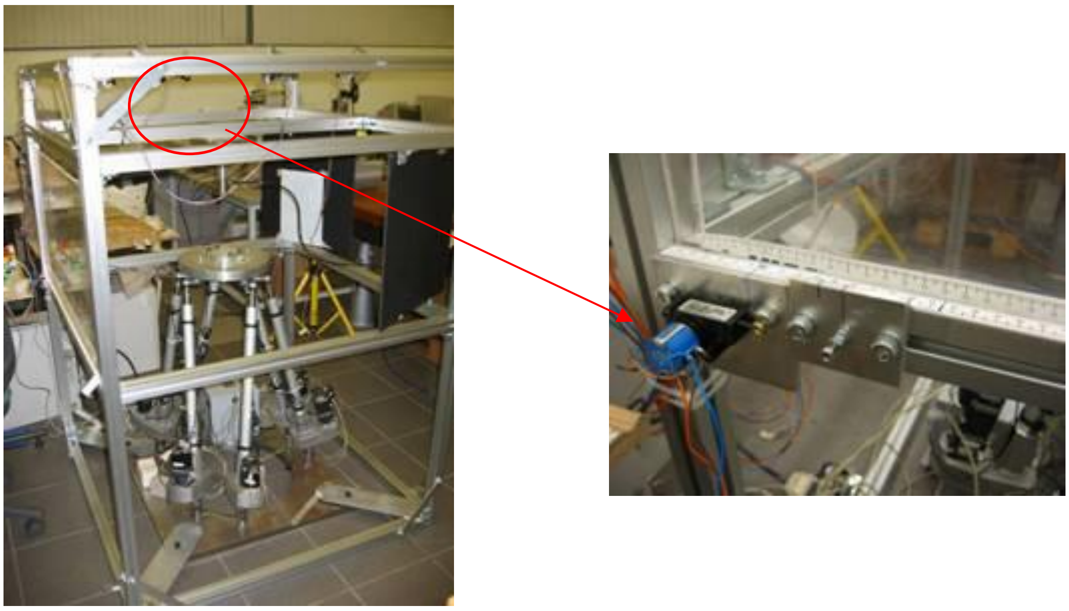

Figure C1 The developed Stewart Platform and the Epsilon wire sensor

C1.Calibration methods

Three calibration methods are developed to further verify the position and orientation errors of the platform and increase its accuracy. Three calibration methods, namely: Forward kinematics with Newton’s iteration, laser pointer calibration method and vector calibration method.

C1.1. Forward kinematic with Newton’s iteration

Inverse kinematics for the Stewart Platform can be formulated to determine the required length of the actuators by giving the pose of the platform with respect to the base. This is the simpler way to find the length of the actuator. Thus, by using inverse kinematics algorithms, the Stewart Platform can be manipulated to the desired position and orientation easily. However, forward kinematics is used to determine the pose of the platform in terms of translation and orientation motions with respect to its base by giving the actuator lengths. However, as shown in the literature studies, forward kinematics calculation in parallel kinematics manipulator is complex and the solution is not unique which might lead to a 40-pose solution. Therefore, numerical methods are applied to solve the problem of forward kinematics of the Stewart Platform.

One assumption is made so that all the joints of the platform or actuators on the base need not be in one plane. This assumption is useful if the joint coordinates are estimated after the manipulator is manufactured, and new, re-calibrated values are used for the forward kinematics. However, it is important to be noticed that the solution for forward kinematics is not unique. It is not necessary to have actuator length feedback if feature space feedback is used and the approximate position of the actuators is known. However, if the manipulator enters a singular position, the platform pose cannot be calculated with confidence by referring to the actuator lengths.

The wire sensors are installed on the frame and the end point of the sensors are attached to the edge of the mobile platform which are coincident with the ball joints location as shown in Figure C2. Hence while the platform is being manipulated, the position and orientation of the end-effector of the mobile platform can be determined through the known lengths of the wire sensors using the forward kinematics algorithm.

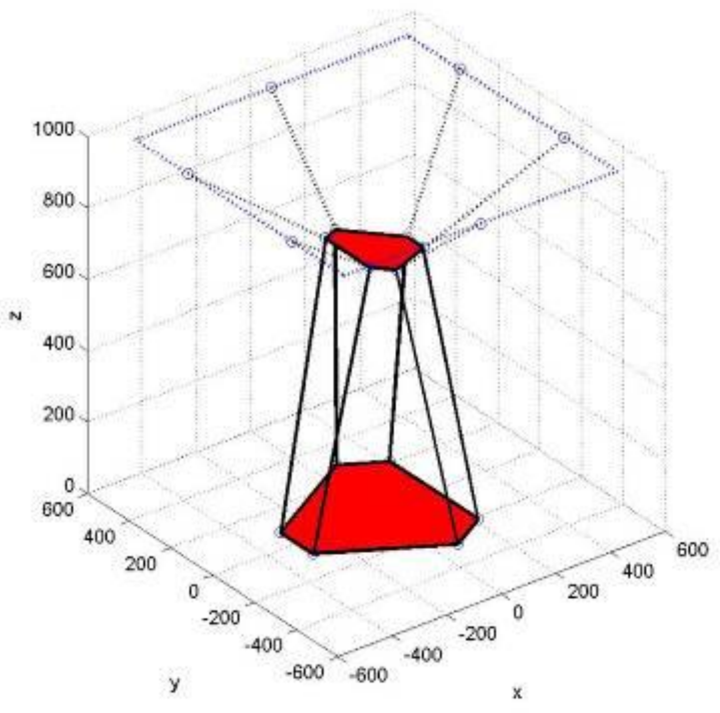

Figure C2 The MATLAB® simulation of the forward kinematics calibration system

C1.2. Laser pointer calibration method

It is time-consuming to calibrate the accuracy of the Stewart Platform by using forward kinematics due to the increment of the complexity of the solution, two alternative calibration methods are applied in the project.

As shown in Figure C3, by setting up two laser pointers orthogonally, the light source of the laser pointer is emitted onto two plane surfaces which are perpendicular to the light beam. By knowing the virtual point on the edge of the platform which is located along the straight line of the laser beam, the new position of the 2nd virtual point can be easily obtained by using inverse kinematics. Hence, by knowing the new virtual point and the origin point of the mobile platform as shown in Figure C3, the vector line can be retrieved.

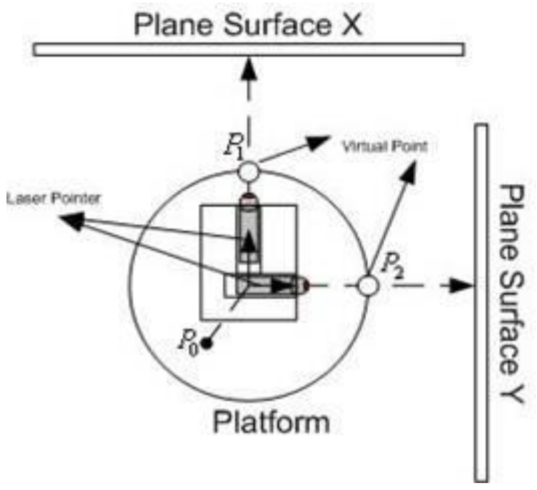

Figure C3 The laser pointer calibration system diagram

Basically, this calibration is to investigate the reflection of the laser pointer on the surface of the plane. The intersection of the laser line and a plane can be determined by defining a line parametrically in terms of two vector points **u** and **v** which are located along the emitted laser light as shown in the equation:

$$p\{u+\alpha(v-u)\}=0, \therefore \alpha=-\frac{pu}{p(v-u)} \tag{C1}$$

where

$u = p_1, v = p_1 - p_0$.

P is the plane vector of the plane surface X and surface Y. To define a plane, one would need to have three points in the same plane which are $\begin{bmatrix} Px_1 \\ Py_1 \\ Pz_1 \end{bmatrix}, \begin{bmatrix} Px_2 \\ Py_2 \\ Pz_2 \end{bmatrix}, \begin{bmatrix} Px_3 \\ Py_3 \\ Pz_3 \end{bmatrix}$ as shown in Figure C4 . These three points are located on the same plane of the plane surface X. Hence to obtain Plane [a b c d], the following equations are used:

$$\begin{bmatrix} a & b & c \end{bmatrix}^T = \begin{bmatrix} Px_1 - Px_2 \\ Py_1 - Py_2 \\ Pz_1 - Pz_2 \end{bmatrix} \times \begin{bmatrix} Px_1 - Px_3 \\ Py_1 - Py_3 \\ Pz_1 - Pz_3 \end{bmatrix} \tag{C2}$$

and $d = -[a \cdot Px_1 + b \cdot Py_1 + c \cdot Pz_1]$ (C3)

The cross product of the vectors must be linearly independent. Hence, three points must not lie in a straight line. Vectors **u** and **v** can be predefined using inverse kinematics by knowing the rotational and translation of the platform which is $q = \begin{bmatrix} x & y & z & \alpha & \beta & \gamma \end{bmatrix}^T$. Hence, by knowing all the parameters, α of equation (C4) can be solved. Next, the coordinate *Pnew* of the emitted laser light on the plane surface can be defined as shown in equation:

$$Pnew = u + \alpha(v - u)$$

(C4)

Comparatively, the laser point calibration method is faster than the forward kinematics method. It can act as a reference point to evaluate the positioning and rotation errors of the platform. By using the inverse kinematics method, a set of theoretical laser point locations at the plane surface can be collected through simulation, and compared with the actual location of the laser light emitted on the plane surface. Errors can be detected through the difference between the theoretical coordinate and actual coordinate of laser light emitted on the surface of the plane.

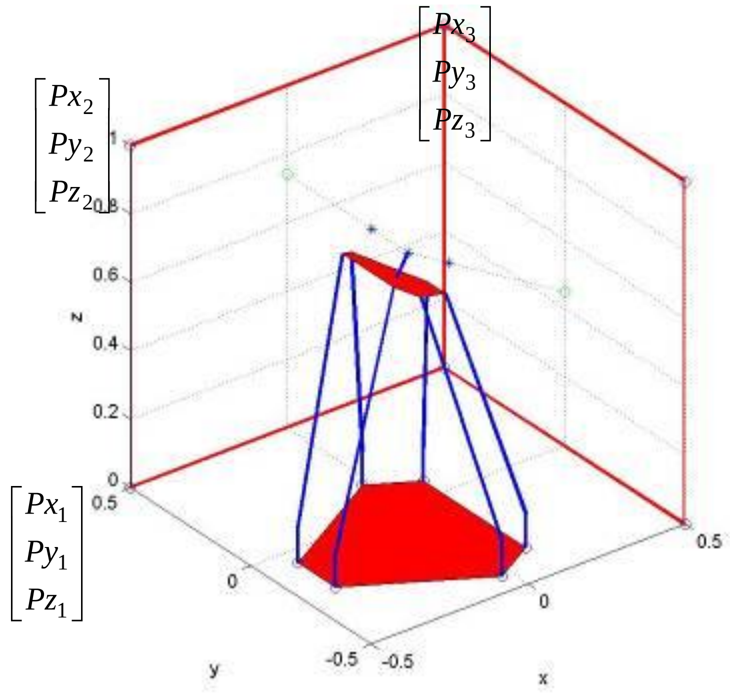
$\begin{bmatrix} Px_3 \\ Py_3 \\ Pz_3 \end{bmatrix}$
$\begin{bmatrix} Px_2 \\ Py_2 \\ Pz_2 \end{bmatrix}$
$\begin{bmatrix} Px_1 \\ Py_1 \\ Pz_1 \end{bmatrix}$
1
0.8
0.6
0.4
0.2
0
z
0.5
0
-0.5
y
-0.5
0
0.5
x

Figure C4 The MATLAB® simulation of the laser platform calibration system

C1.3. Vector Calibration methods

As the previous two methods need time to process the outcome of the calibration, the vector calibration method is able to obtain the calibration result immediately due to the simplicity of the calibration algorithm which involves only linear algebra. However, there are disadvantages of this calibration method compared to the previous two methods. The vector calibration method needs to apply three wire sensors to derive one point coordinate. The calibration of the orientation and position of the platform can be more reliable when nine wire sensors are installed if compared with the forward kinematics method which only needs six sensors. As shown in Figure C5, six locations of the wire sensors are predefined as $\begin{bmatrix} X_{bi} \\ Y_{bi} \\ Z_i \end{bmatrix}, where i = 1,2\ldots,6$. By knowing the length of the wire sensor, ℓ_i where i = 1, 2 …, 6, the coordinate of the point at the platform by equations (C5-C10) is shown in equations

$$\ell_1^{\ 2} = (X_1 - X_{b1})^2 + (Y_1 - Y_{b1})^2 + (Z_1 - Z_{b1})^2 \tag{C5}$$

$$\ell_2^{\ 2} = (X_1 - X_{b2})^2 + (Y_1 - Y_{b2})^2 + (Z_1 - Z_{b2})^2 \tag{C6}$$

$$\ell_3^{\ 2} = (X_1 - X_{b3})^2 + (Y_1 - Y_{b3})^2 + (Z_1 - Z_{b3})^2 \tag{C7}$$

$$\ell_4^{\ 2} = (X_2 - X_{b4})^2 + (Y_2 - Y_{b4})^2 + (Z_2 - Z_{b4})^2 \tag{C8}$$

$$\ell_5^{\ 2} = (X_2 - X_{b5})^2 + (Y_2 - Y_{b5})^2 + (Z_2 - Z_{b5})^2 \tag{C9}$$

$$\ell_6^{\ 2} = (X_2 - X_{b6})^2 + (Y_2 - Y_{b6})^2 + (Z_2 - Z_{b6})^2 \tag{C10}$$

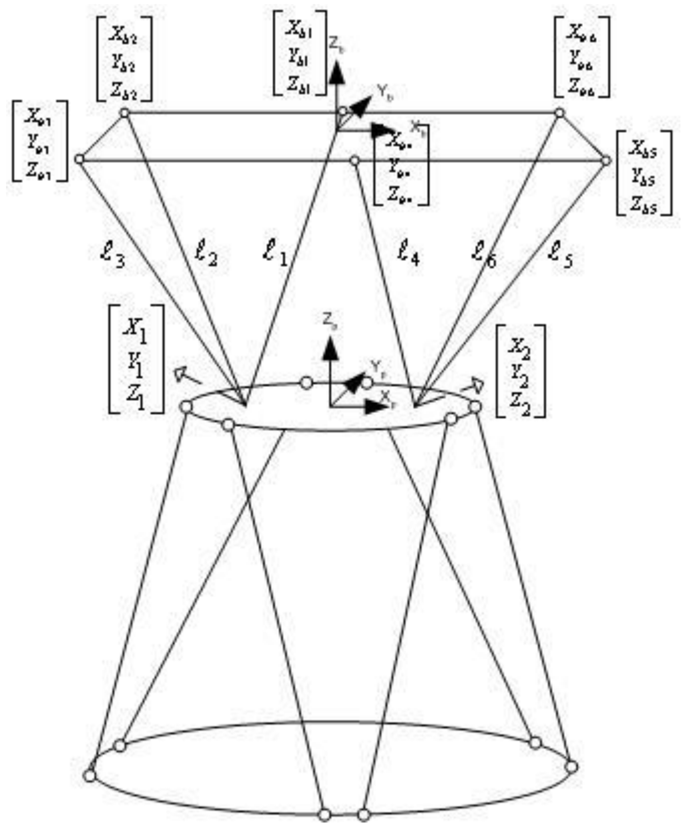

$\begin{bmatrix} X_{b2} \\ Y_{b2} \\ Z_{b2} \end{bmatrix}$
$\begin{bmatrix} X_{b1} \\ Y_{b1} \\ Z_{b1} \end{bmatrix}$
$\begin{bmatrix} X_{b6} \\ Y_{b6} \\ Z_{b6} \end{bmatrix}$
$\begin{bmatrix} X_{b3} \\ Y_{b3} \\ Z_{b3} \end{bmatrix}$
$\begin{bmatrix} X_{b4} \\ Y_{b4} \\ Z_{b4} \end{bmatrix}$
$\begin{bmatrix} X_{b5} \\ Y_{b5} \\ Z_{b5} \end{bmatrix}$
Z_b
Y_b
X_b
ℓ_3
ℓ_2
ℓ_1
ℓ_4
ℓ_6
ℓ_5
$\begin{bmatrix} X_1 \\ Y_1 \\ Z_1 \end{bmatrix}$
$\begin{bmatrix} X_2 \\ Y_2 \\ Z_2 \end{bmatrix}$
Z_p
Y_p
X_p

Figure C5 The wire sensor calibration system diagram

To simplify the calculation, the reference origin and datum are set at the top of the frame $X_bY_bZ_b$ hence all the $Z_{bi} = 0$, where i = 1,2,…6. Hence, the coordinates of the point can be solved through the equations below:

$$X_1 = \frac{(Y_{b3}-Y_{b2})C_1-(Y_{b2}-Y_{b1})C_2-\left[X_{b1}{}^2-X_{b2}{}^2+Y_{b1}{}^2-Y_{b2}{}^2\right](Y_{b3}-Y_{b2})+\left[X_{b2}{}^2-X_{b3}{}^2+Y_{b2}{}^2-Y_{b3}{}^2\right](Y_{b2}-Y_{b1})}{2(X_{b2}-X_{b1})(Y_{b3}-Y_{b2})-2(X_{b3}-X_{b2})(Y_{b2}-Y_{b1})} \quad \text{(C11)}$$

$$Y_1 = \frac{C_1-\left(X_{b1}{}^2-X_{b2}{}^2\right)-\left(Y_{b1}{}^2-Y_{b2}{}^2\right)-2(X_{b2}-X_{b1})\cdot X_1}{2(Y_{b2}-Y_{b1})} \quad \text{(C12)}$$

$$Z_1 = \sqrt{\ell_1{}^2-(X_1-X_{b1})^2-(Y_1-Y_{b1})^2} \quad \text{(C13)}$$

where $C_1 = \ell_1^{\ 2} - \ell_2^{\ 2}$, $C_2 = \ell_2^{\ 2} - \ell_3^{\ 2}$. Hence similarly, matrix $\begin{bmatrix} X_2 \\ Y_2 \\ Z_2 \end{bmatrix}$ can be obtained by using the same method of Equations (C11), (C12) and (C13). Therefore, by acquiring values from the three wire sensors, the position of the platform can be evaluated. However, it could only specify the position of the platform. The definition of the orientation of the platform can only be achieved when three vector points are defined on the surface of the platform. The coordinate of the vector points can be used to form a vector plane which allows the orientation of the platform to be read with respect to the reference plane. However, this configuration of the system requires at least nine sensors. Since only six wire sensors are available, an alternative method is applied to acquire the desired position and orientation. Six wires are attached to two points on the surface of the platform as shown in Figure C6. The locations of the points are predefined such that two of the points are of equal distance and aligned with the center point of the platform. Thus, the center of the platform $\begin{bmatrix} X_C \\ Y_C \\ Z_C \end{bmatrix}$ can be acquired by a simple equation in Equation (C14).

$$X_C = \frac{X_1 + X_2}{2}, Y_C = \frac{Y_1 + Y_2}{Y}, Z_C = \frac{Z_1 + Z_2}{2} \qquad \text{(C14)}$$

To determine the orientation of the platform, a geometric method is used to measure the angle of rotation of the platform, roll-pitch-yaw: α, β and γ as shown in Figure C6.

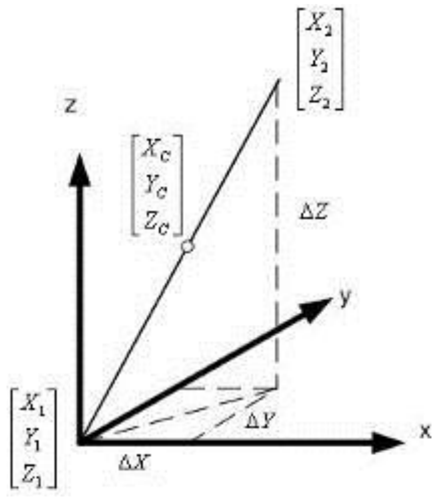

z
y
x
$\begin{bmatrix} X_2 \\ Y_2 \\ Z_2 \end{bmatrix}$
$\begin{bmatrix} X_c \\ Y_c \\ Z_c \end{bmatrix}$
$\begin{bmatrix} X_1 \\ Y_1 \\ Z_1 \end{bmatrix}$
ΔZ
ΔY
ΔX

Figure C6 Cartesian Coordinate of the vector points

$$Rot_Z : yaw, \gamma = \tan^{-1}\frac{\Delta Y}{\Delta X} = \tan^{-1}\frac{Y_2 - Y_1}{X_2 - X_1} \tag{C15}$$

$$Rot_Y : pitch, \beta = \tan^{-1}\frac{\Delta Z}{\Delta X} = \tan^{-1}\frac{Z_2 - Z_1}{X_2 - X_1} \tag{C16}$$

$$Rot_X : roll, \alpha = \tan^{-1}\frac{\Delta Z}{\Delta Y} = \tan^{-1}\frac{Z_2 - Z_1}{Y_2 - Y_1} \tag{C17}$$

In short, three methods are described in this section to calibrate the accuracy of the Stewart Platform. Among the three methods, the forward kinematics method can evaluate the errors of the platform effectively but it is very time consuming, due to the complexity of the algorithms. The laser pointer method can verify the error of the position of the platform quite easily, but it cannot be applied to the feedback system because it involves manual measurement. An image processing system is suggested to be implemented with the laser pointer system which can increase the accuracy of the calibration as well as the whole system can be automated and applied to the feedback system. The drawback of the image processing system is that it will increase the complexity and cost of the system. Lastly, the vector point calibration system can evaluate the error of the position swiftly and is able to perform excellent feedback. However, the cost will be increased due to the requirement of extra wire sensors. Furthermore, more wire sensors will also hinder the movement of the Stewart Platform. Hence, based on the availability of the wire sensors, the forward kinematics method is used accordingly to optimize the accuracy of the Stewart Platform.

C2.Calibration of the wire sensor

A multifunctional Data Acquisition card (DAQ) was purchased for the purpose of converting the analog outputs of the six wire sensors into digital signals which are fed to the computer. The model chosen is the PCI-6034E Low Cost Multifunction IO Board from National Instruments^{TM}... The verification of the accuracy of the wire sensor is done by configuring a simple setup as shown in Figure C7. The wire sensors are fixed on the holder plate; the steel wires of the sensors are then attached to the slider. Thus, by varying the length of the wires by moving the slider according to the distance indicating by the measuring tape, a voltage difference can be detected by a multimeter.

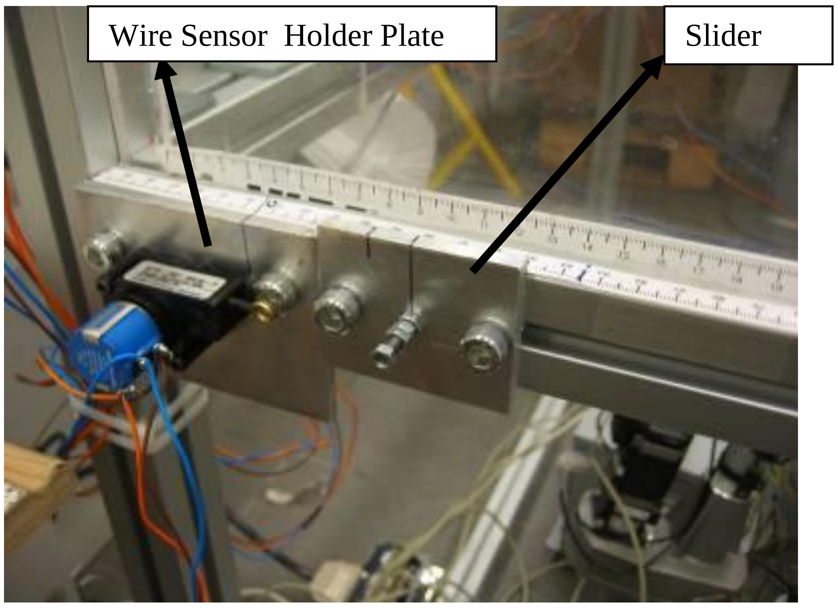

Figure C7 The calibration setup for wire sensor

Many problems were encountered during the communication between the wire sensors and the DAQ card. There are problems, such as the issues of offset, settling time and gain problem to justify the accuracy of the wire sensors. Hence, the experiment was first conducted by comparing two pools of data which are collected from the wire sensors. A pool of the data is collected through a multimeter; and another one is collected by the computer through the DAQ card. The wire sensors are the WPS-750-MK30-P Draw-wire displacement Sensors from Micro-Epsilon^{TM} which convert displacement into signals that are input into the data acquisition card. The wire sensors can travel 750 mm and the sensitivity of the sensor is 1.279mV/V/mm and the deviation $\leq 0.10\,\%$. The excitation voltage is 10 V. Hence, a theoretical data can be calculated based on the characteristics of the wire sensor by supplying 5 V of Voltage. Next, the result is compared with the results from the multi-meter to verify the zero errors of the wire sensors as shown in Figure C8.

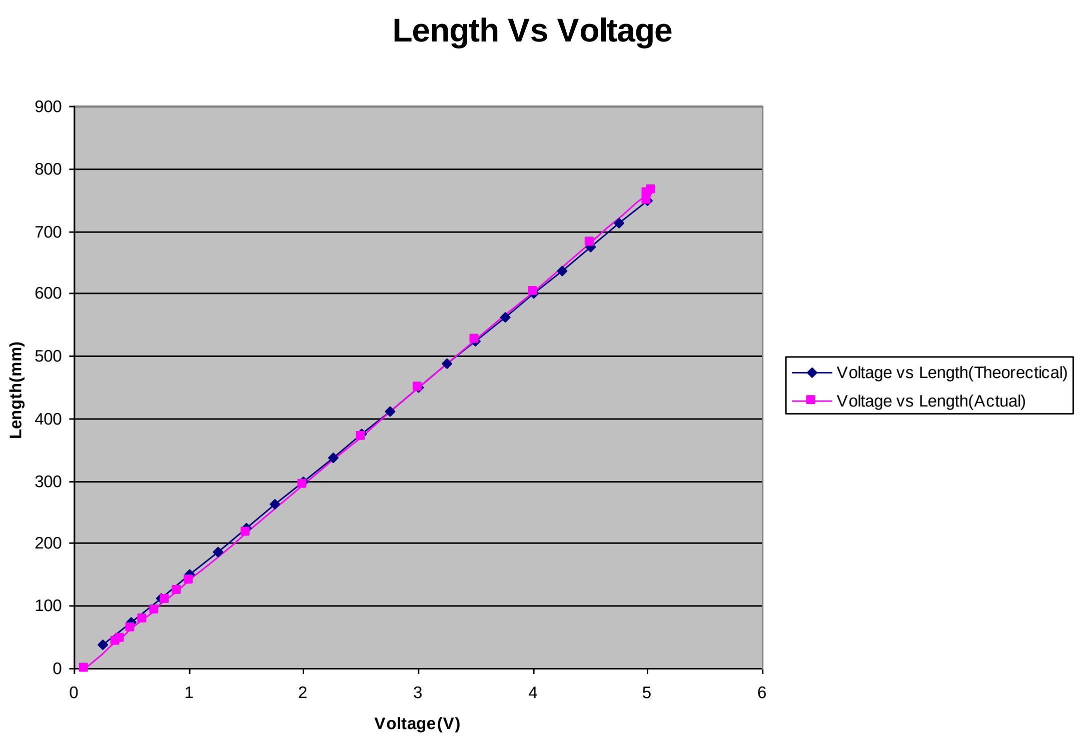

Figure C8 Graph of Comparison between theoretical data and actual data from Multimeter

From Figure C8, it is noticed that the error between the actual and theoretical data of wire sensor is minor. It is observed that there is still some offset at the start of the measurement. The offset problem might be caused by the settling time or the delay of the signal transfer from the card to the computer. However, the data collected from the multimeter can be used as a reference data to verify of the accuracy of the acquired data from the computer. By using Labview to acquire the data of the wire sensor, an estimated offset of 0.5 V was discovered as shown in Figure C9. From the graph, the results of the Labview data are affected by the improper gain setting and sampling rate.

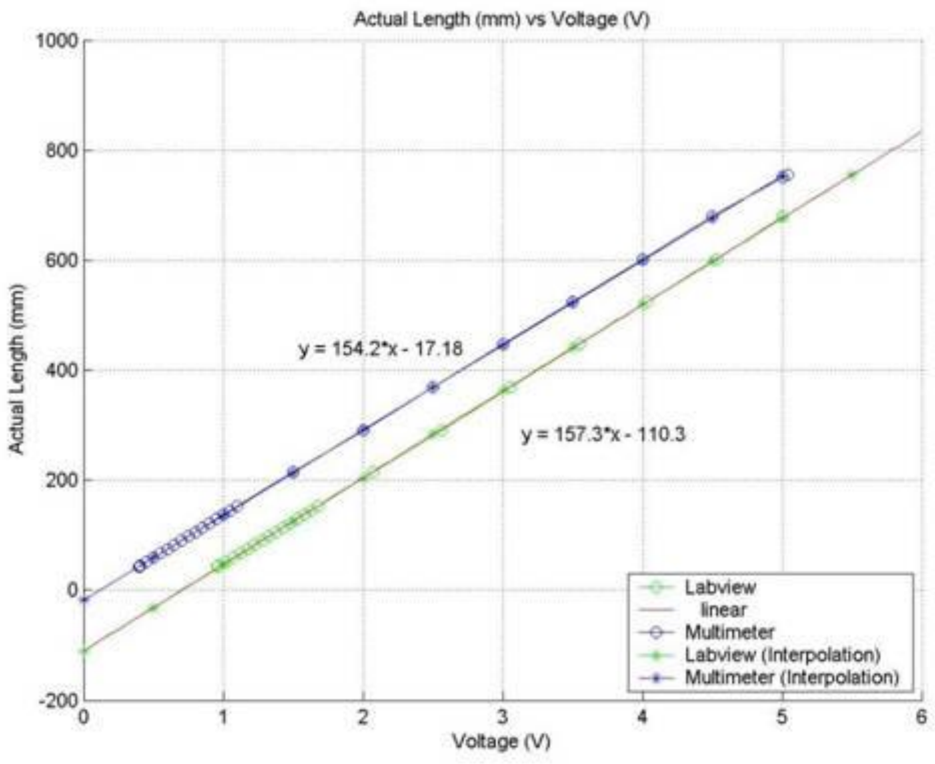

Figure C9 Graph of Actual Length vs Voltage of the wire sensor

Thus, based on the data collected, a Visual C++ programming using the library of NIDAQ software is completed to read the data of the wire sensor. An interface as shown in Figure C10 is developed to read the value of the wire sensors. The acquired result is satisfactory and the error between the multimeter and the DAQ is limited to 0.1V. The value acquiring algorithm is developed based on the Sampling Theorem. This is because the entire signal collected from the wire sensor is moving in a sinusoidal wave form as shown in Figure C11. It shows a sampled waveform and its corresponding signal vector. When the waveform is sampled, its amplitude is measured and recorded at different times. Hence, these different times are equally spaced in the time domain. The interval between samples is called the sampling interval or time step. In Figure 12, the time step is

$\Delta t \equiv T = 10ms$. Thus, to read an average value of the wire sensor, an averaging method is used.

$$\overline{V} = \frac{\sum_{T=1}^{500} V(T)}{T} \tag{C18}$$

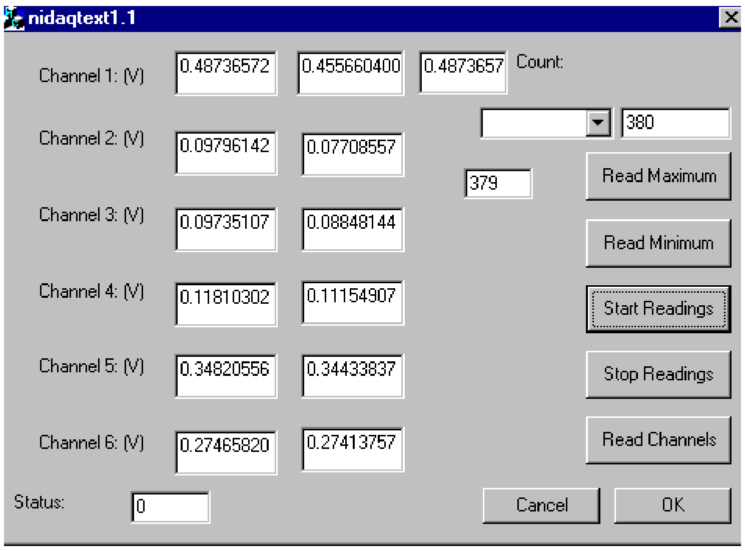
nidaqtext1.1

Channel 1: (V)	0.48736572	0.455660400	0.4873657	Count:
Channel 2: (V)	0.09796142	0.07708557	379	380
Channel 3: (V)	0.09735107	0.08848144		
Channel 4: (V)	0.11810302	0.11154907		
Channel 5: (V)	0.34820556	0.34433837		
Channel 6: (V)	0.27465820	0.27413757		
Status:	0			

Figure C10 Wire sensor interface

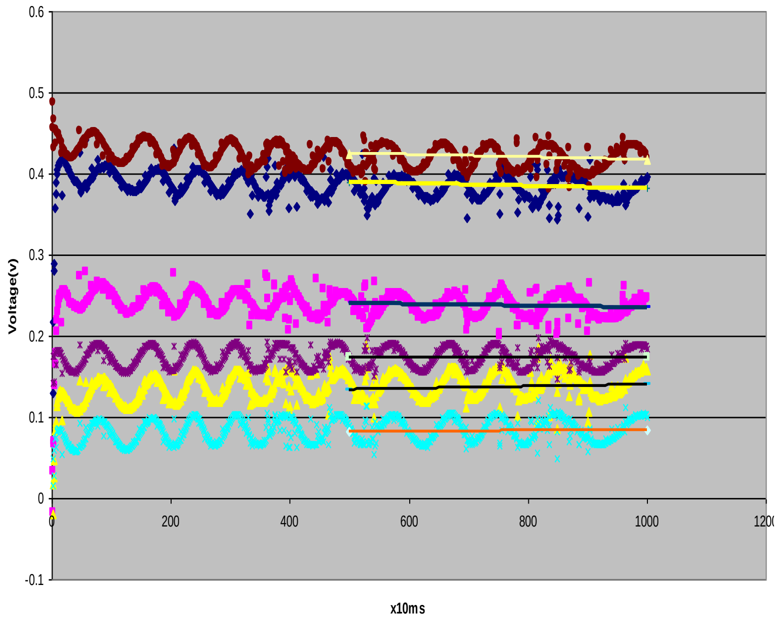

Figure C11 The Sampled Wave Signal of the wire sensors

Hence, by reading the average value, a constant value of the wire sensor can be obtained as a straight line as shown in Figure C11. After the averaging of the data, the wire sensors are calibrated and can be used in the calibration systems mentioned in the previous section to verify the position and orientation of the Stewart Platform.

Appendix D: Image processing

A basic image processing method has been developed to calibrate the accuracy of the motion of the Stewart Platform in Cartesian workspace. The Stewart Platform is programmed to move along the workpiece while probing the center of the respective circular patterns as shown in Figure D1. The calibration steps of the workpiece are evaluated in the following sections.

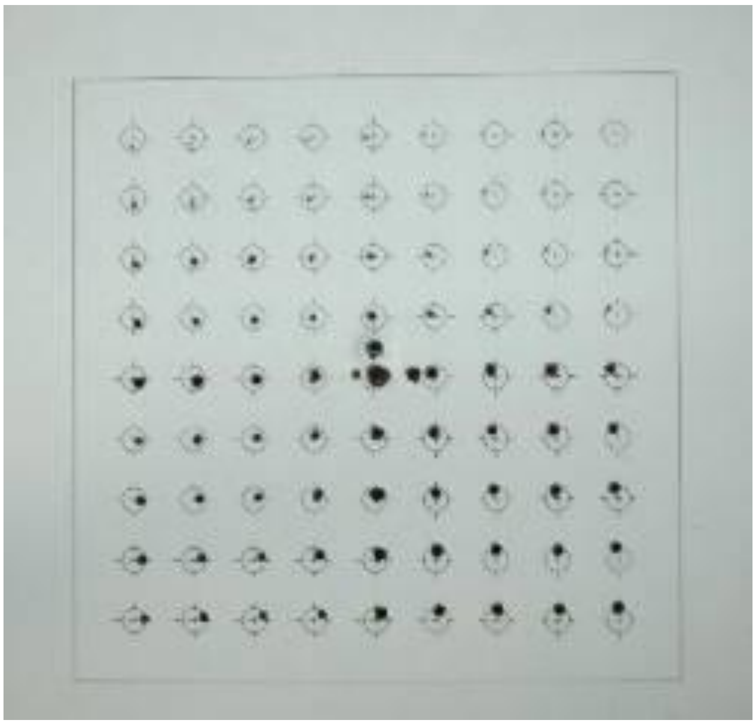

Figure D1 The original image with marked points

Firstly, the original image goes through an image processing of turning it into a black and white image as shown in Figure D2.

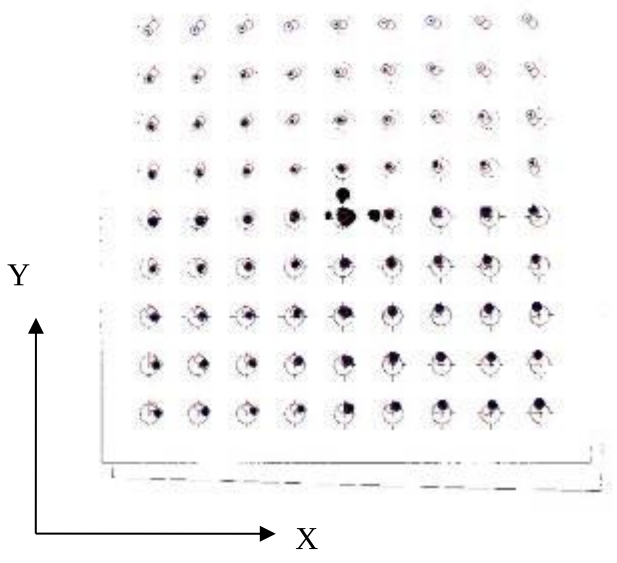

Figure D2 Black and white image

Next, the edge of the image is highlighted. The highlighted line will be used to determine the rotational angle error of the work piece with respect to the horizontal level along the X-axis. Hence, after modifying the Stewart Platform with the rotational angle, all the printed points in the image will be in line horizontally.

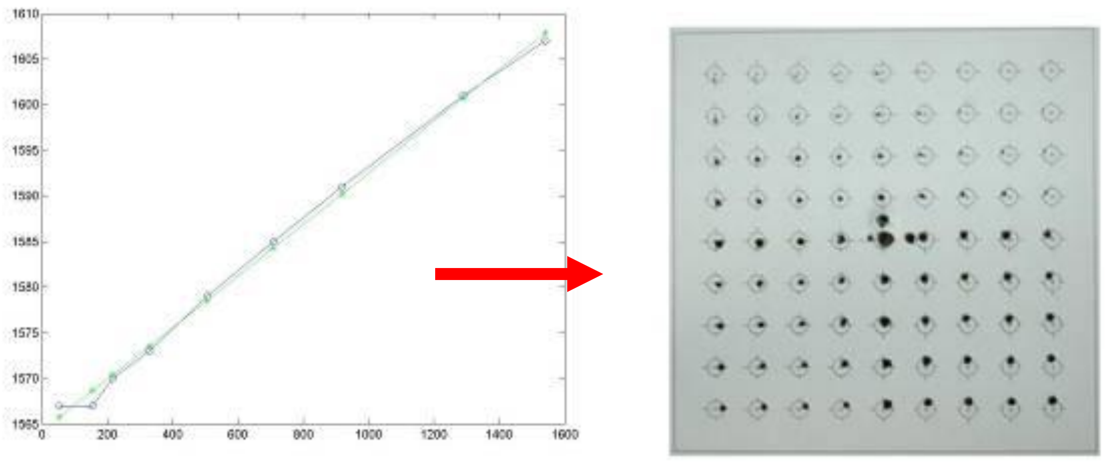

Figure D3 the Image is rotated into the position so that it is in line with the horizontal level

After the image is rotated into the horizontal level, all the printed center points are highlighted in red. Next, the same image will be highlighted with the blue dots for the calibrated points which were marked by the pen during the machining process.

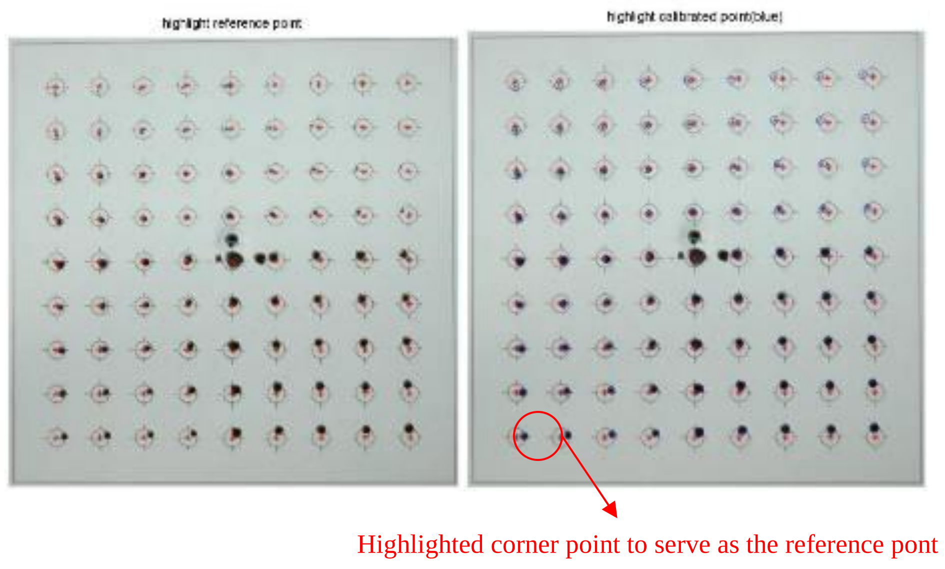
highlight reference point
highlight calibrated point(blue)
Highlighted corner point to serve as the reference pont

Figure D4 Calibrated points of the image in terms of red color for the printed point and blue color highlighted dots for the points marked by the pen

One point is highlighted at the lower left corner to be served as the reference point as shown in Figure D4. With respect to the reference point, two matrices of the coordinate of the marked point (blue) and printed point (red) are determined. Based on the coordinates of the points, it is realized that the points are slightly tilted in certain angles around the Z-axis with respect to the center point in the graph. Hence, another line is plotted by choosing a series of points with reference to the marked point in the middle of the graph and compared with the printed points of the graph as shown in Figure D5.

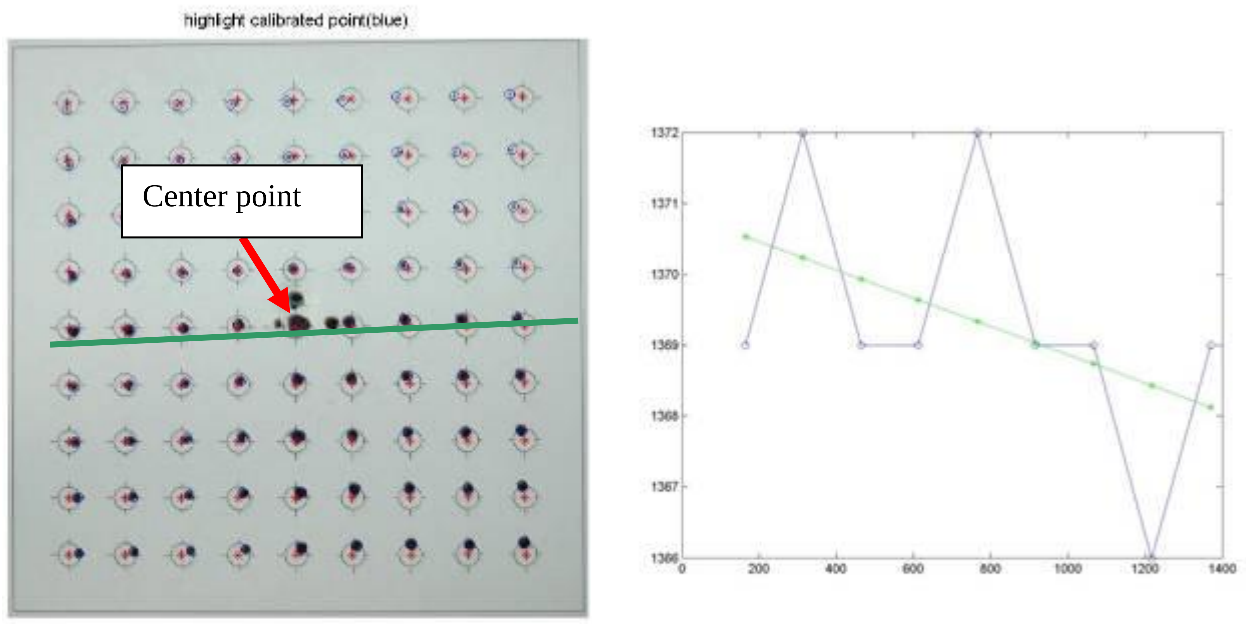

Figure D5 the tilted line (in green) plotted with respected to the marked points in the middle of the graph

After simple geometry calculation, it is found that the all the marked points on the workpiece are tilted approximately -1.811 deg with respect to the center point of the workpiece. Hence, another set of the coordinates is generated based on the rotation angle of -1.811 deg with respect to the Z-axis. As a result, three sets of coordinate points were collected which are the original printed points (red), the marked points (blue) and the modification points by rotating the marked points around the Z-axis with respect to the middle point of the workpiece (green). All the coordinates are shown in Figure D6.

From the view of the image of Figure D6, one can see that the error of the coordinate of the points was reduced when the points were rotated to the positions as shown in the green spot.

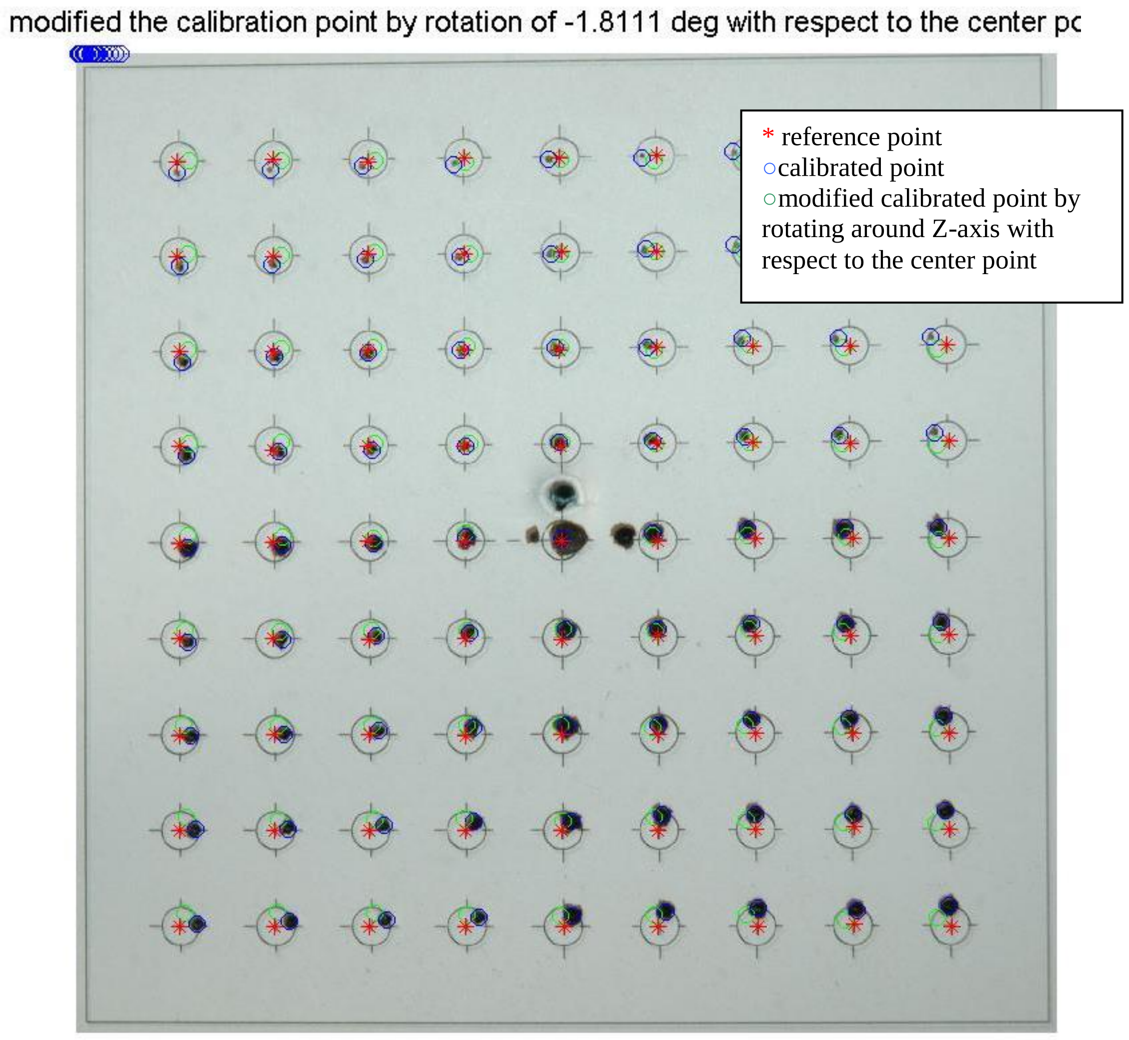

Figure D6a All three sets of coordinates of the Printed Points (Red), Marked Points (Blue) and Modified Points (Green)

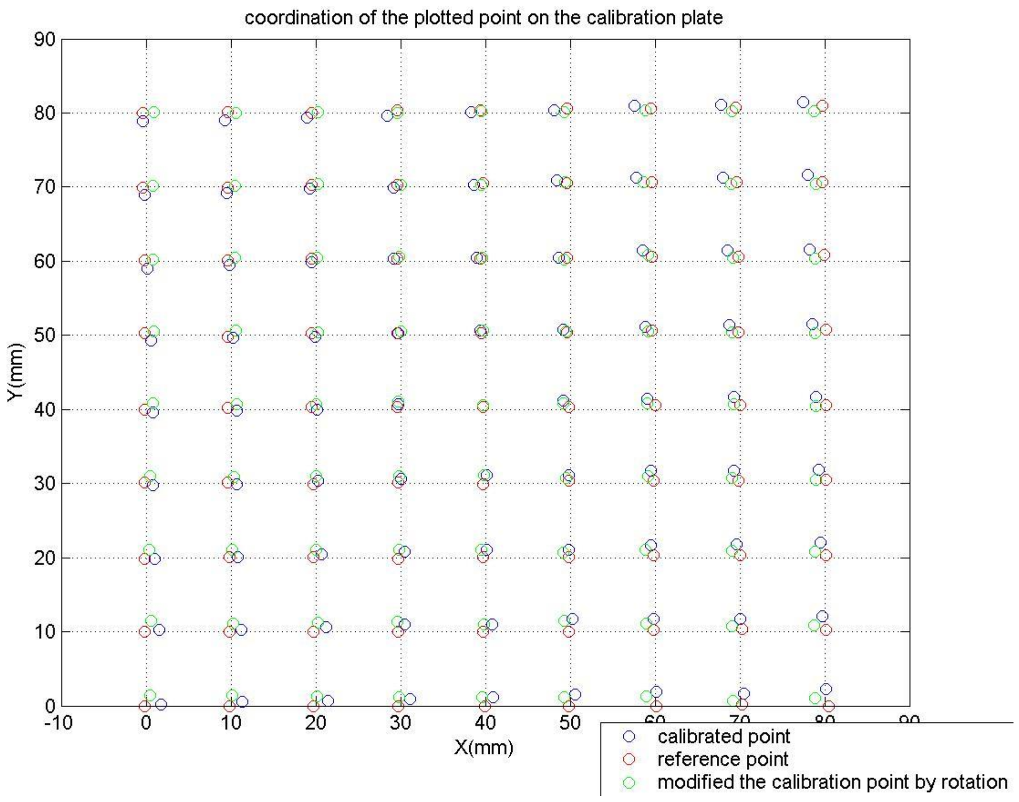

Figure D6b All three sets of coordinates without background image

All the magnitudes of the coordinate errors of the points are plotted in the graph and analyzed along the X-axis as shown in Figure D7. Two set of error values are plotted which are the coordinates of the marked points with respect to the printed points (blue) and the coordinates of the modified points with respect to the printed points (red). After the comparison, it is shown that before the modification of the points, the marked points have an average X-axis error of 0.79 mm. However, if all the marked points are rotated by -1.8 deg, the modified calibrated point errors will have a better accuracy with respect to the printed points. The position errors along the X-axis can be reduced to 0.62 mm.

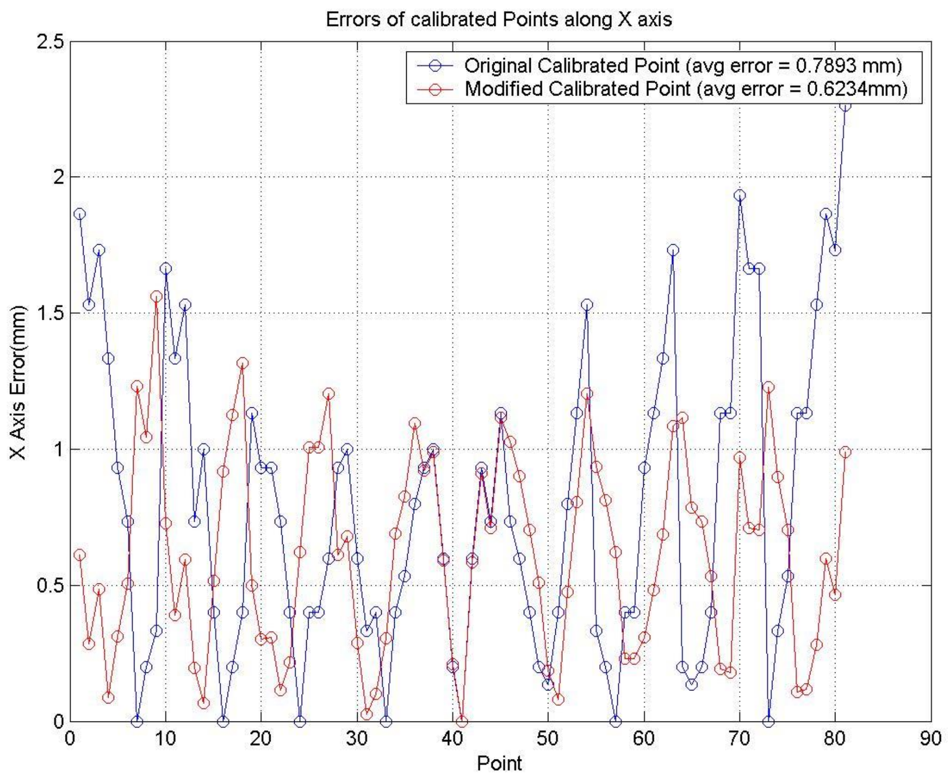

Figure D7 the errors of calibrated points along the X-axis

Furthermore, the same analysis is done on the coordinates of the points in terms of the Y-axis. The values of the errors are shown in Figure D8. The distance error between the marked points to the printed points (blue) along the Y-axis is 0.75 mm. However, if the coordinates of the marked points are able to be rotated -1.8 deg, the positioning errors along the Y-axis can be reduced to 0.58 mm.

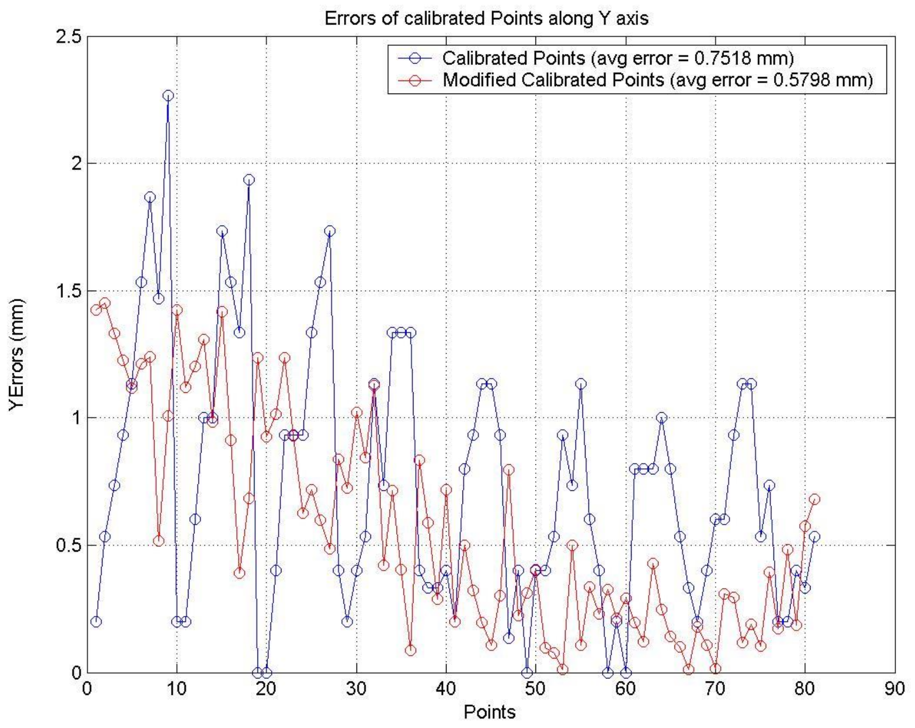

Figure D8 the errors of calibrated points along the Y-axis

Instead of measuring the coordinates of the marked points with respect to the reference point, another calibration method is used by measuring the distance between the two adjacent marked points which is 10 mm apart. From the data collected, it is found that the average distance of the two adjacent calibrated points along the X-axis is 9.78 mm and the average distance of two adjacent points along the Y-axis is 9.87 mm. The results of the distances between the adjacent points are shown in Figure D9. Hence, it can be concluded that the accuracy between the two adjacent points is higher than the coordinates of the points with respect to the reference point. From Figure D9(a), it can be seen that the marker points nearer to the center point will have higher accuracy but when they are further away from the center point, the errors become larger, and the coordinates of the marked points are smaller than the actual printed points with respect to the center point.

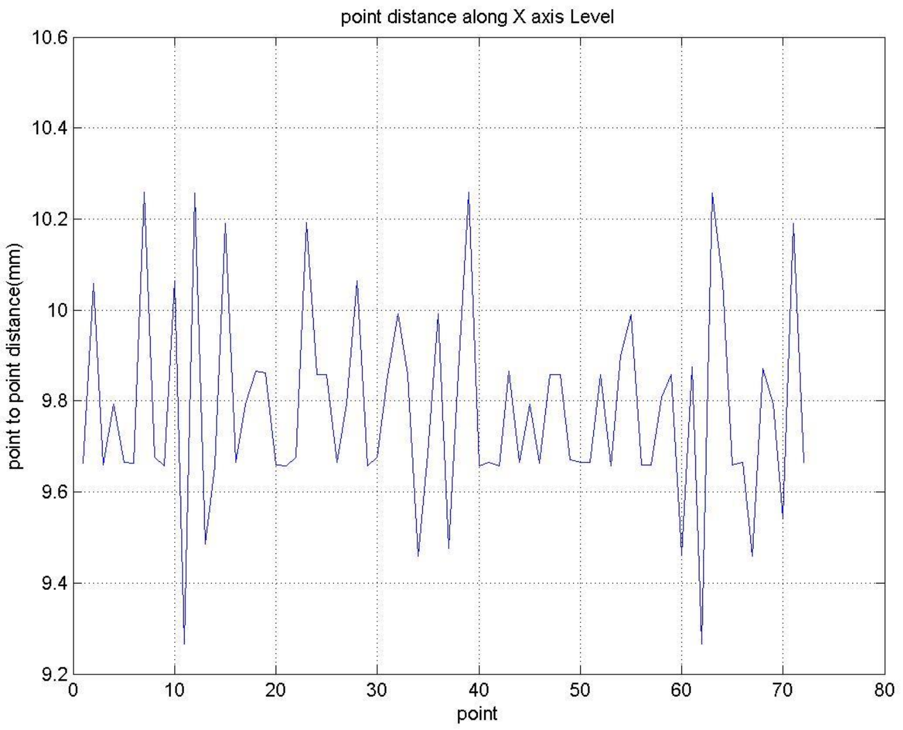

Figure D9(a) the distance between two adjacent points along the X-axis

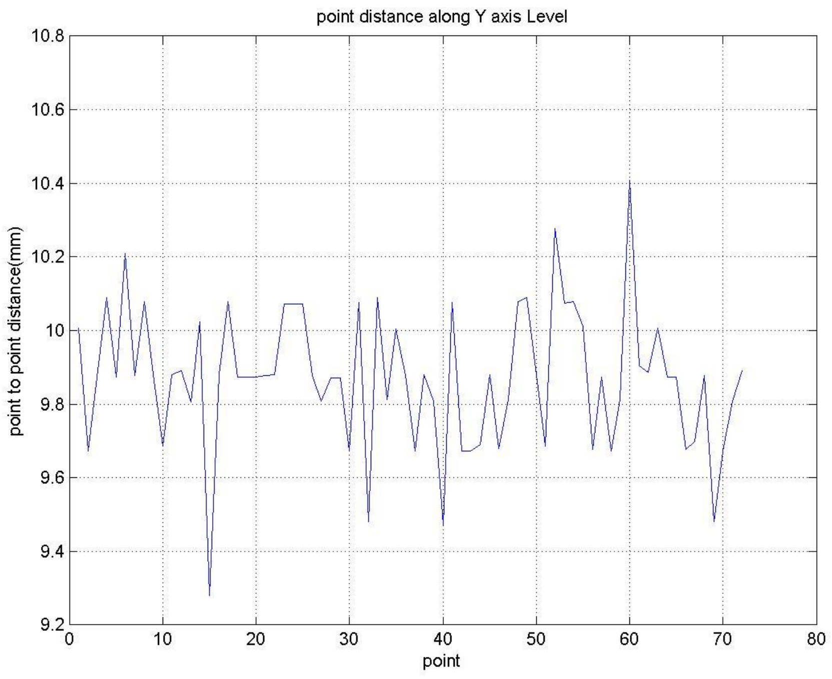

Figure D9(b) the distance between two adjacent points along the Y-axis

One of the sources of error is each distance error between the two adjacent points is approximately 0.2 mm. Hence, through the analysis, it is found that the Stewart Platform is not moving in a pure straight line from one point to another even though the platform is manipulated to move along the X-axis as shown by the blue line in Figure D10.

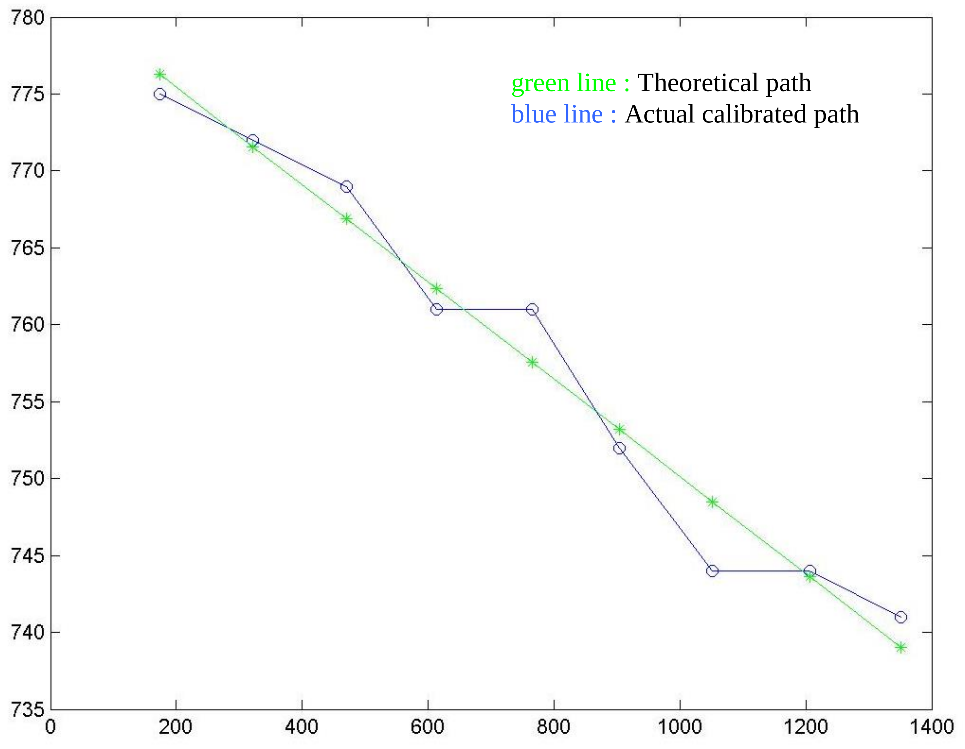

Figure D10 The unevenness of the points motion even though it is moving in the X-direction

In short, another error is the physical set up of the Stewart Platform. From the analysis of the calibration results of the Stewart Platform, minor errors of assembling the Stewart Platform have caused deviations in the manipulation of the Stewart Platform such as the platform has been installed with a tilted angle of -1.8 deg around the Z-axis and the surface of the platform is uneven.

Thus, to solve the physical errors of the Stewart Platform, one method can be applied is to dismantle and assemble the platform again but a comprehensive calibration method must be figured out so that the Stewart Platform can be reassembled in a more accurate manner. An alternative method is to compensate the error by modifying the parameters using software.

The Calibration Experiment

The purpose of this calibration experiment is to fine tune the accuracy of the Stewart Platform by using the parameters obtained through the analysis of the processed images. Firstly, the Stewart Platform was turned around the Z-axis by -1.8 deg. Then the Stewart Platform is turned around rotation about the Y-axis by -0.5 deg.

After the sensors are verified and rounded to 0.15 mm resolution, all the wire sensors are installed along the actuators. First of all, by performing the calibration of single actuator several times, such as every 100,000 counts of the motor pulse, it moves 145.62 mm – 138.01 mm = 7.61 mm. Hence, a coefficient of 100000/7.61 is used for the stroke of the Stewart Platform during the calculation from distance movement to the count of steps of the actuator. As a result, by assuming a different reachable distance for the actuator to move in 100,000 counts, a graph of errors is plotted based on the calibrated length with the reference length is shown in Figure D11.

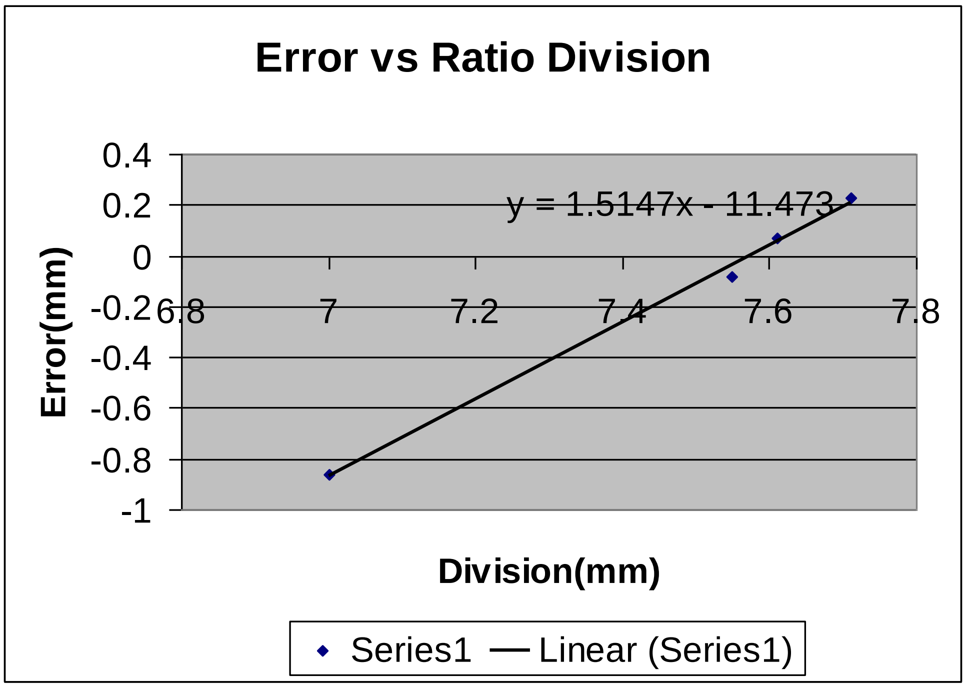

Figure D11 The corresponding error resulting from the ratio of actuator movement over the counter of 100,000 steps from the controller

An equation is obtained from the line plotted: y = 1.5147x - 11.473 where y is the displacement in mm and x is the counter step of the motor. Hence to obtain a zero error, the approximate ratio division should be 7.574 mm displacement equal to 100,000 counts of the stepper motor.

Sample Calculation:

If the ratio changes to division of 7.5744 mm:

Calibrated Length = 147.79 mm – 138.01 mm = 9.78 mm
m_XAxis = 130023
m_XAxis = Stroke*(100000000/7.574437);
130023 = Stroke *100000000/7.574437
Stroke = 130023 *7.574337 /100000000 = 0.009848 m
Stroke Error from calibration = 9.848 mm (computed) – 9.78 mm (calibrated) = 0.068 mm

In conclusion, it is quite hard to reach exactly the same computed value of 9.848 mm since the stroke is measured by the wire sensors with the resolution of 0.15 mm. When it reaches the end position, it fluctuates between 147.79 mm and 147.94 mm. If the average is taken, it would be 147.865 mm. If this value minus 138.01 mm, then it will equal to 9.855 mm which is almost the same as 9.848 mm with an error of 0.007 mm which would make the calibrated results quite satisfactory.

When the Stewart Platform is in the homing position, the wire sensors of the actuators show the values in Table D1.

Table D1 Difference of displacement value of each actuator corresponding to 100,000 counts of pulse of the stepper motor

	X-axis (mm)	Y-axis (mm)	Z-axis (mm)	T axis (mm)	U axis (mm)
Homing Position	123.74	145.49	129 .65	142.63	136.61
Displacement after counter of 100000	131.18	152.79	137.09	150.07	143.90
Difference	7.44	7.3	7.44	7.44	7.29

Calibration of the Z-axis

A Z-axis position sensor is assembled as shown in Figure D12. Basically the principle of this device is to serve as a function similar to a LVDT. The device is designed to be moving freely along the Z-axis, so that the end point of the free end is attached to the wire sensor. The end point touches the surface of the platform and moves freely along the platform while reading the movement of the platform. Hence, when the platform is moving in a planar motion, the wire sensor of this system can detect the unevenness of motion of the platform along the Z-axis.

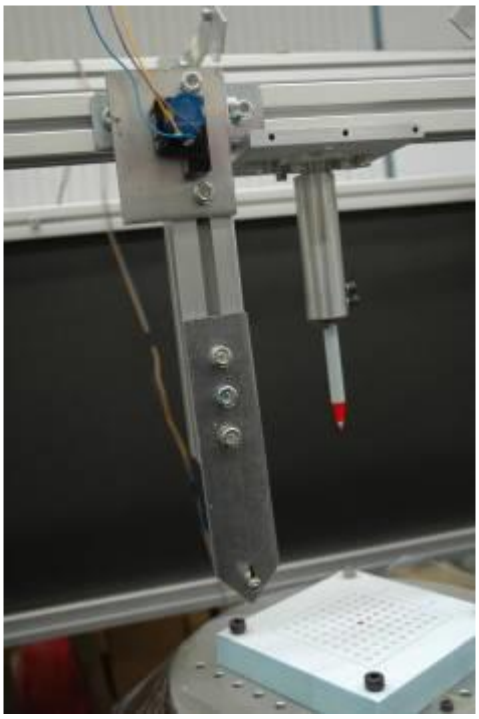
Figure D12 The LVDT-like device

All the wire sensors are installed along the actuators but the last one is installed on top of the platform to be used as a LVDT. Compared to the reference actuation of 7.57 mm for 100,000 counts, there is an average error of 0.188 mm. The error is affected by the resolution of the sensors of 0.15 mm. To calibrate the position accuracy of the Stewart Platform while moving along the Z-axis, the LVDT-like sensor is used. A series of readings is shown in Table D2.

Table D2 Error of motion along the Z-axis

Z position (m)	Z Difference (m) (a)	Sensor Reading (m)	Reading Difference (m) (b)	Error (a) – (b)
0.8666	0	0.25313	0	0
0.8766	0.01	0.24321	0.009920	0.00008
0.8866	0.02	0.23313	0.002	0
0.8966	0.03	0.22320	0.029930	0.000070
0.9166	0.05	0.20319	0.049940	0.000060
			Average Error	0.000042

After recalibration of the actuators and the ratio of movement of the actuator corresponding to the count of the motor, the accuracy has increased significantly. Compared to the previous result, the error of the Stewart Platform moving along the Z-axis has been reduced to an average of 0.000042 m or 0.042 mm. However, more calibration experiments are needed to verify the accuracy. Furthermore, the accuracy is calibrated based on point-to-point motion only without considering the motion along the X- and Y-axes.

Calibration of the X- and Y-axes

An X-Y planar calibration is performed on the calibrated Stewart Platform and the calibration result is shown in Figure D13.

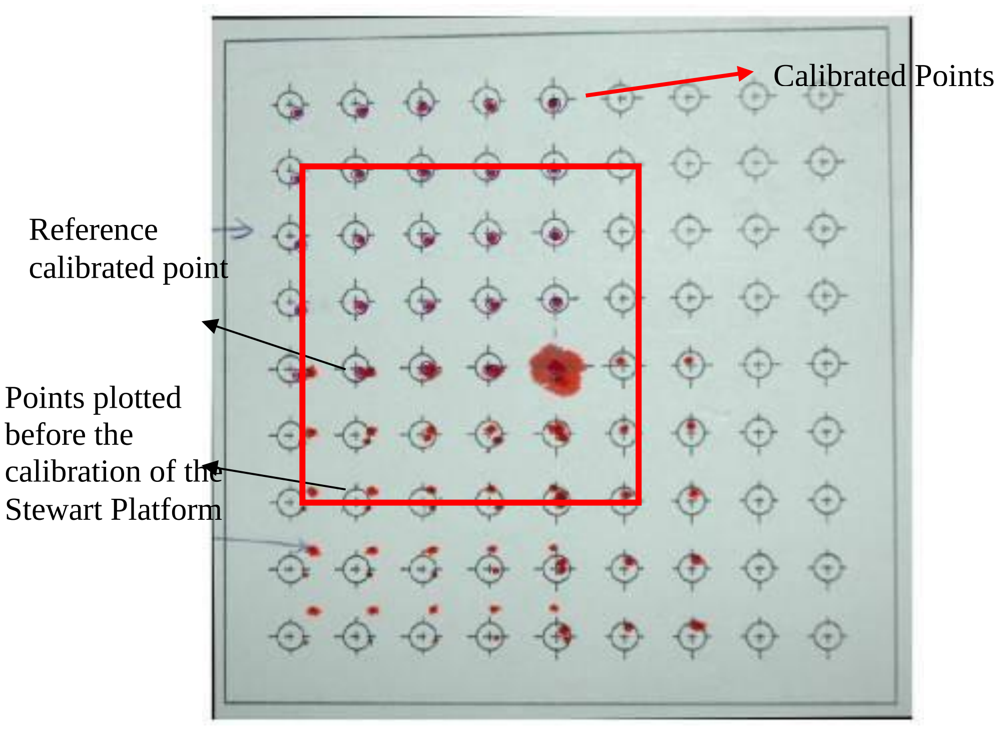
Calibrated Points
Reference calibrated point
Points plotted before the calibration of the Stewart Platform

Figure D13 Calibrated Workpiece

Using a simple image processing algorithm written in MATLAB®, all the points in the red square as shown in Figure D13 are verified in terms of coordinates with respect to the reference calibrated point. Since the distance of the adjacent points is 10 mm, it is able to compare the coordinate of each point and determine their accuracy. The coordinates of each point are shown in Table D3.

Table D3 Coordinate of the calibrated Points

X(mm) Calibrated	X(mm) Original	Error(mm)	Y(mm)	Y(mm) Original	Error(mm)
0.12	0.00	0.12	0.00	0.00	0.00
8.94	10.00	-1.06	0.25	0.00	0.25
18.75	20.00	-1.25	0.63	0.00	0.63
28.57	30.00	-1.43	0.50	0.00	0.50
38.13	40.00	-1.87	0.63	0.00	0.63
0.50	0.00	0.50	10.14	10.00	0.14
9.19	10.00	-0.81	10.14	10.00	0.14
19.37	20.00	-0.63	10.26	10.00	0.26
28.94	30.00	-1.06	10.14	10.00	0.14
38.25	40.00	-1.75	10.26	10.00	0.26
0.50	0.00	0.50	19.90	20.00	-0.10
9.44	10.00	-0.56	20.40	20.00	0.40
19.37	20.00	-0.63	20.15	20.00	0.15
28.69	30.00	-1.31	20.15	20.00	0.15
38.50	40.00	-1.50	20.40	20.00	0.40
0.25	0.00	0.25	29.79	30.00	-0.21
9.44	10.00	-0.56	30.16	30.00	0.16
19.13	20.00	-0.87	30.16	30.00	0.16
29.31	30.00	-0.69	30.04	30.00	0.04
38.50	40.00	-1.50	30.16	30.00	0.16
0.50	0.00	0.50	39.68	40.00	-0.32
10.06	10.00	0.06	39.68	40.00	-0.32
19.00	20.00	-1.00	40.30	40.00	0.30
29.31	30.00	-0.69	39.80	40.00	-0.20
38.50	40.00	-1.50	40.05	40.00	0.05
	Avg Error	-0.75		Avg Error	0.15

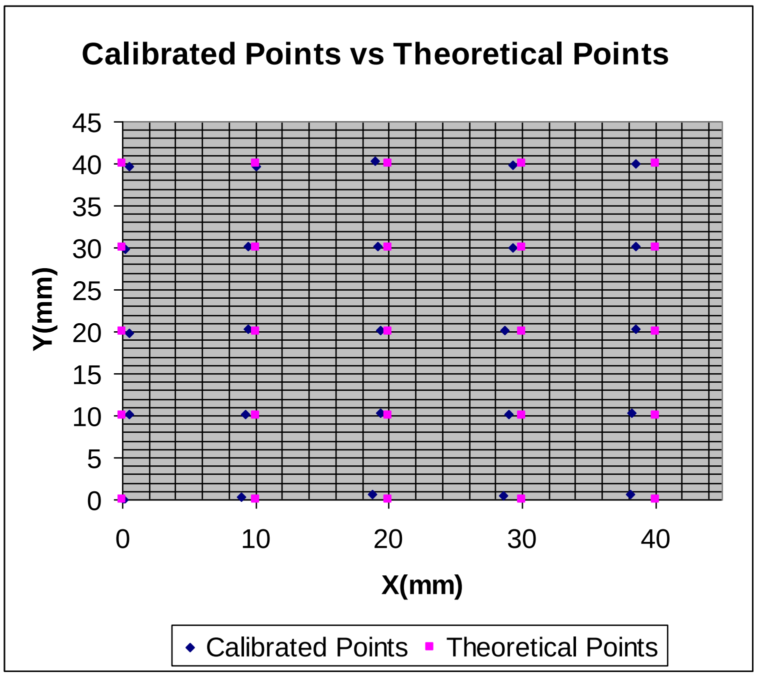

Figure D14 The comparison of coordinates between the actual calibrated points and the theoretical points

From Table D4 and from Figure D14, the calibration results are better than the results in the previous calibration. However, there is still an error of 0.7 mm along the X-axis but the error along the Y-axis is reduced drastically to 0.15 mm. However, more calibration tests are needed to further improve the accuracy of the X-Y plane motion.

Appendix E: Interval time calculation

Firstly, the Stewart Platform is manipulated to move from 0.8 m to 0.81 m along the Z-axis, which is a 0.01 m movement difference or motion of 1cm. The steps sent to the controller in terms of counter pulse of the motor are 326327 (0.8 m) to 464988 (0.81 m). This pulse will control the displacement of the actuator. Thus, the total movement is 464988 – 326327 = 138661 steps, and the setup of velocity and acceleration of the actuators are 50000 steps/s and the acceleration is 500000 steps/s^2 with respect to the stepper motor. Below is the sample calculation of the time interval.

$$
\begin{aligned}
&s = 138661 step \\
&u = 0 \\
&v = 50000 step / s \\
&a = 500000 step / s^2 \\
&v = u + at \\
&u : initial\_velocity \\
&v : final\_velocity \\
&s = vt \\
&\therefore t = \frac{s}{v} = \frac{138661}{50000} = 2.77s(assume\_initial\_u = v)
\end{aligned}
$$

Since the initial velocity is 0 m/s, the acceleration is needed to be considered in the calculation.

$$v = u + at$$
$$\therefore v = at, \because u = 0$$
$$t = \frac{v}{a} = \frac{50000}{500000} = 0.1s$$
$$\therefore s = vt$$
$$\therefore s = (u + at)t$$
$$\therefore s = ut + at^2$$
$$\therefore s = at^2 = 500000 \times 0.1^2 = 5000$$
$$s_a = 5000 \times 2 = 10000$$
$$s_f = s - s_a = 138661 - 10000 = 128661$$
$$\because s_f = vt$$
$$\therefore t = \frac{s_f}{v} = \frac{128661}{50000} = 2.57322s$$
$$\therefore t_{total} = 2.57322 + 0.1 + 0.1 = 2.7732s$$

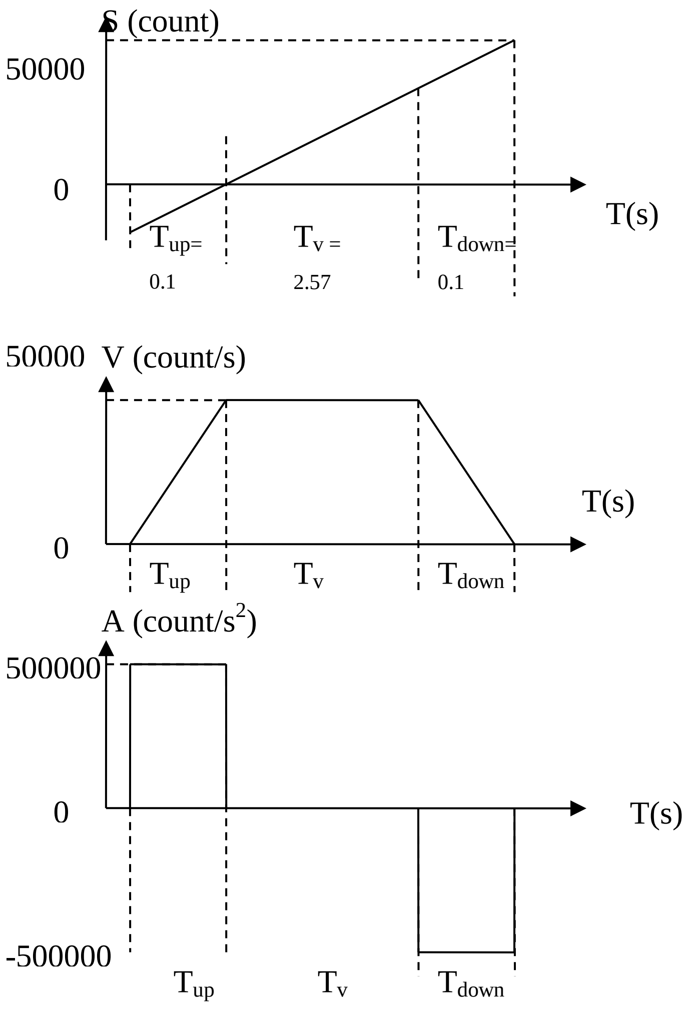

Figure E1 Distance, Velocity and Acceleration Diagram

Even though according to calculation, the time needed for the actuator to move to the final destination is 2.77s but in the actual manipulation of the platform there is a time delay due to friction and inertia.

The time interval is the key control of communication between the CPU and the controller. There is problem of jamming of actuators during manipulation corresponding to the trajectory path. It is because signals sent to the Stewart Platform are sent constantly in the interval time of 100 ms. The Stewart Platform cannot reach the destination in 100 ms before the following signal is updated to the controller. In the long run, there are more commands accumulated in the controller card before the actuator can execute all of them immediately. Until certain time, the controller card will be jammed due to the overwhelming amount of data stored. Hence a more comprehensive algorithm is needed to improve the communication between the PC and the controller card.

Therefore, the solution is to vary the time interval with respect to the travel distance so that when the travel distance is long, the time interval will become longer corresponding to the travel distance. Similarly, when the travel distance is shorter, the interval time will be shortened. Alternatively, another method is to adjust the velocity of the respective actuator based on travel distance. When the travel distance is very far away, the velocity will be increased so that the actuator will move within the limitation of the travel time.

Table E1 Previous data collected by manually moving the Stewart Platform

S1	S2	S3	S4	S5	S6	Time Interval(S)
1451561	1478117	1463124	1527877	1532208	1440899	1993
1452290	1452290	1452290	1452290	1452290	1452290	8
326326	326326	326326	326326	326326	495722	36
464987	464987	464987	464987	464987	466228	19
0	0	0	0	0	0	2364
326326	326326	326326	326326	326326	326326	13
49336	49336	49336	49336	49336	49336	17
326326	326326	326326	326326	326326	326326	11
49336	49336	49336	49336	49336	49336	14
1438353	1438353	1438353	1438353	1438353	1438353	36
1437327	1437327	1436571	1441181	1441181	1436571	2

Table E2 The time calculation when the velocity is 50000 step/sec and the acceleration is 500000 step/sec^2

Travel Position of the Legs	Travel Distance	Time Interval(Actual)	Time Interval(Calculated)
326326	326326	12	6.62652
603754	277428	10	5.64856
1438353	834599	22	16.79198

A small program has been written for the calculation of the interval time with different travel distance, velocity and acceleration. After much consideration, it is realized that the time interval between the commands might not be able to control by using only “Ontimer”, a function in Visual C++ to control the time trigger. Another programming code is to use “Sleep”, which is a function in Visual C++ to make the program rest until the predefined time is reached. After testing with the command of “Sleep”, the speed of the signal transferred from the CPU to the controller card can be controlled, but the problem is that further command will not be sent by the CPU until the previous command line sent to the controller card has been executed. Hence, the clock timer of the interface will pause for the time defined in "Sleep" and the updating of the feedback position will be further delayed.

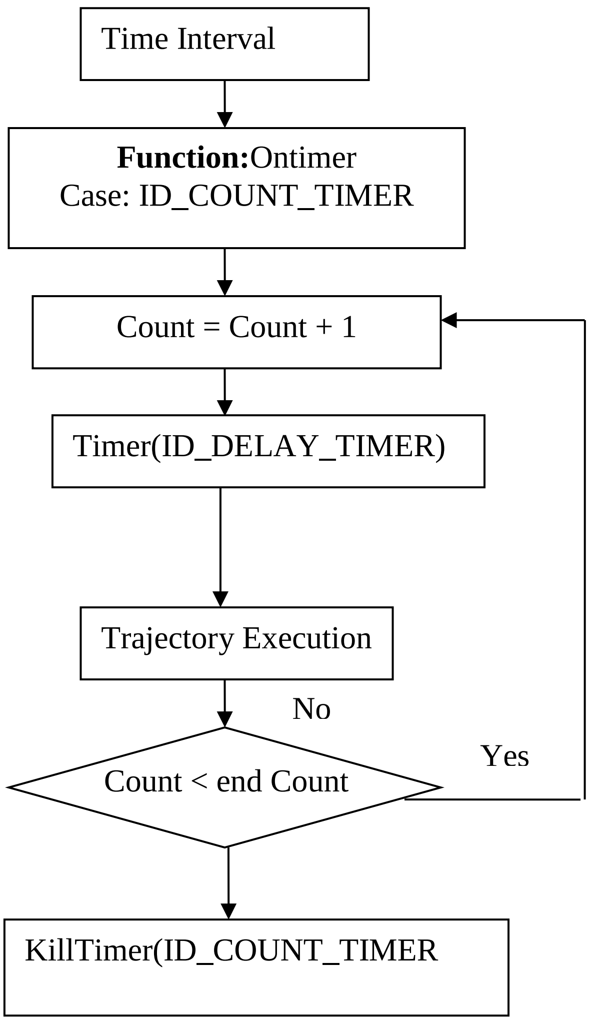

Figure E2 Flow chart of the interval time control

So an ID_DELAY_TIMER can be added but there is a problem to obtain the time interval. There are two ways to obtain the interval time; one is referred to the position of the Platform and another method is referred to the position of the actuator. Since the velocity and acceleration are determined with reference to the actuator, it is suggested that the time interval is defined by the longest distance traveled among the six actuators. So a function must be written to decide which one has the longest travel distance.

After the implementation of the above-mentioned method in the developed software program of the Stewart Platform, it is proven that the previous jamming error which is caused by the insufficient time interval can now be solved. Hence by controlling the given time interval correctly, the Stewart Platform can now run more than 300 lines of trajectory path command. The capability of the Stewart Platform to execute more than 300 lines of command helps to improve the potential of Stewart Platform to be used in machining processes.